ON GEOMETRICALLY-EXACT SANDWICH STRUCTURES

By

HUI DENG

A DISSERTATION PRESENTED TO THE GRADUATE SCHOOL
OF UNIVERSITY OF FLORIDA IN PARTIAL FULFILLMENT
OF THE REQUIREMENTS FOR THE DEGREE OF
DOCTOR OF PHILOSOPHY

UNIVERSITY OF FLORIDA

1997

ACKNOWLEDGEMENTS

I would like to express my gratitude to my committee chairman, Professor Loc Vu-Quoc, for his supervision and guidance. His enthusiasm and resourcefulness were a crucial foundation for this work. I feel I have gained tremendously from his mathematical insight and have learned several other skills via his instruction.

I am grateful to Professors I.K. Ebcioglu, N.D. Cristescu, B.V Sankar and Marc Hoit for serving on my committee and carefully reviewing the thesis. Their comments were invaluable.

Many thanks go to my colleagues Vinay Srinivas, Lee Lesburg, Xiang Zhang and Brian Fuller for helping me on the various aspects of UNIX and the DECstations. Their friendship has also been the driving force in my graduate work. Specially, I would like to express my gratitude to Xiangguang Tan for his valuable input of the illustrating figures for our newly developed theory and for his help in running ABAQUS to compare our numerical results.

This research was supported by a grant from the National Science Foundation and from the SRAP program of the Florida Space Grant Consortium. This support is gratefully acknowledged.

TABLE OF CONTENTS

Page

ACKNOWLEDGEMENTS ii

ABSTRACT vi

PART I: SANDWICH BEAMS AND 1-D PLATES

1 INTRODUCTION 2

2 EQUILIBRIUM EQUATIONS 8
- 2.1 Strong Form 8
- 2.2 Stress Power 11

3 GALERKIN PROJECTION 13
- 3.1 Weak Form 13
- 3.2 Linearization of Weak Form 17
- 3.3 Projection: Galerkin Finite Element 21

4 NUMERICAL EXAMPLES 24
- 4.1 Verification of FE Implementation with Single-Layer Beam . . . 24
- 4.2 Sandwich Beam with Identical Layers 25
  - 4.2.1 Normal moment distribution 26
  - 4.2.2 Assigned moment on core layer only 29
  - 4.2.3 Assigned axial force on core layer 30
  - 4.2.4 Reduced equations of equilibrium 32
  - 4.2.5 Assigned transverse force 33
  - 4.2.6 Roll-up maneuver with normal moment distribution 36
  - 4.2.7 Roll-up maneuvers: Saint-Venant principle 38
    - 4.2.7.1 Long beam 38
    - 4.2.7.2 Short beam 41
- 4.3 Two-layer Beams 48
  - 4.3.1 Case without ply drop-off 48
  - 4.3.2 Case with ply drop-off 50
    - 4.3.2.1 Assigned transverse force 50
    - 4.3.2.2 Roll-up maneuver 53
- 4.4 Ideal Sandwich Beams 65

4.4.1 Heuer's theory for sandwich beams 66

5 DYNAMIC ANALYSIS: EQUATIONS OF MOTION 72

6 FINITE ELEMENT IMPLEMENTATION 75
6.1 Weak Form of Kinetic Energy 75
6.2 Time Stepping Scheme: Newmark Algorithm 79
6.3 Linearization and Tangent Operator 80
6.4 Tangent Inertia Operator 81
6.5 Tangent Stiffness Operator 85
6.6 Spatial Discretization: Galerkin Finite Element 87

7 NUMERICAL EXAMPLES 90
7.1 Sandwich Frame with Ply Drop-offs 90
7.2 Comparison of Sandwich Beam Having Three Identical Layers with Equivalent Single-layer Beam 97
7.2.1 Vibrational frequencies 97
7.2.2 Harmonic response of cantilever beam with three identical layers 100
7.2.3 Cantilever sandwich beam with three identical layers under impact force 102
7.3 Ideal Sandwich Beam 104
7.3.1 Comparison of frequencies 104
7.3.2 Simply supported ideal sandwich beam with overhangs . . 108
7.3.3 Ideal sandwich frame subject to tip impact force 109
7.4 Free-free Sandwich Beam Undergoing Large Overall Motion . . . 129
7.4.1 Free-free single-layer beam and sandwich beam with identical layers 129
7.4.2 Free-free ideal sandwich beam 131
7.5 Spin-up Maneuver 137

PART II: SANDWICH SHELLS

8 INTRODUCTION 153

9 ON THE ALGEBRA OF TWO-POINT TENSORS AND THEIR APPLICATIONS 156
9.1 Introduction 156
9.2 Pull-back of Covector Fields in Terms of the Adjoint of a Tangent Map 158
9.3 Application to Piola-Kirchhoff Stress Tensors 160

10 KINEMATICS OF DEFORMATION 163
10.1 Basic Kinematic Assumptions and Configurations 163

10.2 Important Kinematic Quantities 167

11 EQUATIONS OF MOTION 173
11.1 Power of Contact Forces/Couples 173
11.2 Power of Assigned Forces/Couples 179
11.3 Rate of Kinetic Energy 180
11.4 Equations of Motion for Sandwich Shells 184
11.5 Angular Velocity/Acceleration of Director Field 191

12 LINEARIZED EQUATIONS OF MOTION 193
12.1 Alternative Equations of Motion 193
12.2 Equations of Motion for Symmetric Sandwich Shells 195
12.3 Classical Results for Symmetric Sandwich Plates 197

13 STRAIN MEASURES AND CONSTITUTIVE LAWS 203
13.1 Constitutive Restriction 203
13.2 Alternative Form for the Balance of Angular Momentum 204
13.3 Effective Stress Resultants 206
13.4 Reduced Stress Power and Conjugate Strain Measures 209
13.5 Constitutive Relations 213

14 CLOSURE 214

REFERENCES 216
BIOGRAPHICAL SKETCH

Abstract of Dissertation Presented to the Graduate School of the University of Florida in
Partial Fulfillment of the Requirement for the Degree of Doctor of Philosophy

ON GEOMETRICALLY-EXACT SANDWICH STRUCTURES

By

HUI DENG

August 1997

Chairman: Dr. Loc Vu-Quoc

Major Department: Aerospace Engineering, Mechanics and Engineering Science

This work has two parts: 1) On the geometrically-exact sandwich beams/1-d plates and 2) On the geometrically-exact sandwich shells.

Most recent formulations in regard to sandwich structures have incorporated the geometric nonlinearity as high-order deformation, and are not suitable for problems that include the large overall motion. On the other hand, formulations proposed for analyzing large overall motion of sandwich structures in general bypass the kinematic description of the deformation in different layers to use the classical single-layer Euler-Bernoulli beam theory, which cannot describe a relative thick sandwich structure exactly.

In the first part of this work, a Galerkin projection of the equations of motion for a recent theory of geometrically-exact sandwich beams that allow finite rotations and shear deformation in each layer is presented. The continuity of the displacement across the layers is exactly satisfied. The resulting finite element formulation can accommodate large deformation. The number of layers is variable, with layer lengths and thicknesses not required to be the same, thus allowing the modeling of sandwich structures with ply drop-offs. Extensive numerical examples are presented which underline the salient features of the formulation. Saint-Venant principle is demonstrated for very short sandwich beams. Numerical examples also including sandwich structures with ply drop-offs, free flying and spin-up maneuver of sandwich beams are presented to illustrate the applicability and versatility of the proposed formulation.

Classical treatments of shells are all cast in terms of the complex differential geometric object such as the covariant derivatives, the Riemann connections or the Christoffel symbols. In dealing with sandwich shell the situation get even complex due to the complexity of the sandwich shells itself. To avoid these complexities, efforts have been made on a numerical scheme called degenerated solid approach. In the degenerated solid approach, numerical integrations are made through out the thickness of the shell which have reduced the fully 3-dimensional equations of motion to 2-dimensional equations of motion. While this scheme avoids the complexity of the classical theory of sandwich shells, it suffers more expense due to numerical intergrations through the thickness of the shell. Further more, there is no mathematical analysis to the degenerated solid approach in its numerical integrations through the thickness.

The geometrically-exact theory provides a simpler way in dealing with the the dynamics of fully nonlinear structures. Thus in the second part, following the similar procedures as the works on geometrically-exact sandwich beams and one-dimensional plates , we present a geometrically-exact sandwich shell theory, entirely in terms of stress resultants which accommodates finite deformations in membrane, bending, and transverse shear. The motion of the shell are referred directly to the inertial frame; the transverse fiber of the sandwich shell has a motion identical to that of a chain of three rigid links connected by revolute joints. An important approximated theory is developed from the general nonlinear equations, the classical linear theory is recovered by the consistent linearization.

The weak form of the fully-nonlinear resultant equations of motions are derived. The

weak form is then linearized exactly. The linearized weak form of the equations of motions are used in the Newton-Raphson iterative solution procedure, which leads to quadratic convergence rate in the solution procedure. The traditional finite element projection is used in both the static and dynamic cases. To avoid shear locking, selective reduced integration is used.

PART I.

ON GEOMETRICALLY-EXACT SANDWICH BEAMS AND 1-D PLATES

CHAPTER 1
INTRODUCTION

A description of extensive use of multilayer structures in engineering and various approaches to their theoretical and computational formulation can be found in review papers such as Thompson [1987], Chia [1988], Reddy [1989], Yu [1989], etc., to name a few. Laminated composite structures, initially developed for use in the aerospace industry, have played an increasingly important role in robotics and machine systems that require high operating speed. More recently, considerable attention has been given to a class of smart structures with embedded piezoelectric[1] layers as sensors and actuators (see, e.g., Motovilovets [1985], Evseichik [1989], Tzou [1989], Lee [1990]) or interferometric optical fiber sensors (see, e.g., Sirkis [1993]) for monitoring the strain level and for vibration control. Large overall motion of multilayer structures can be found in robot arms or space structures with embedded sensors/actuators. Yet another example of multilayer structures can be found in the damping of structural vibration by the use of viscoelastic constrained layers (e.g., Mantena [1991], Rao, Sankar and Sun [1992], Alberts [1993], Dubbelday [1993], Rao [1993]).

Particularly for sandwich structures, which have had extensive use in aerospace engineering, an account of the classical formulations is given in Plantema [1966]. Application of sandwich construction to reduce noise has been considered in the automotive industry (Schreffler [1993]). The reader can consult Lakes and Elms [1993] for a recent study of sandwich structures with negative Poisson's ratio foam core[2] destined to withstand better damages produced by low-energy impacts on light-aircraft fuselages. A survey of the wide range of applications of sandwich structures (e.g., helicopter rotor blades, propeller blades, etc.) and related design issues are provided in, e.g., Edwards [1991]. In early formulations of sandwich structures, the bending stiffness of the core layer was often neglected; only shear was accounted for. The transverse shear effects of the outer layers were first considered in Yu [1959*a*], who was also the first to employ the hypothesis of continuous piecewise linear deformed sandwich cross section (Toledano and Murakami [1987]). Most formulations so far have incorporated the geometric nonlinearity as higher-order deformation (see the review paper by Chia [1988]), and are not suitable for problems that include the large overall motion such as the slider-crank mechanism or the four-bar linkage systems. On the other hand, formulations proposed for studying the large overall motion of laminated composite structures in general bypass the kinematic description of the deformation in different layers to use the classical single-layer Euler-Bernoulli beam theory, and make use of a constitutive law which is a weighted average of the constitutive laws of the layers (see, e.g., Thompson [1987]). However, it should be noted that a rigorous approach to obtain effective properties of multilayer structures is via homogenization methods as done in Milgrom [1989].

---

[1] The reader can consult Dökmeci [1990] for a theory of single-layer shells with piezoelectric materials.

[2] Some biomaterials have negative Poisson's ratios. More recently, there has been considerable effort in designing, analyzing, and manufacturing materials with negative Poisson's ratio for various engineering applications (e.g., Sigmund [1994]). For a survey on materials with negative Poisson's ratios, see, e.g.,

We review here recent developments on the theory of geometrically-exact multilayer beams, also applicable to 1-D plates, accounting for bending stiffness and shear deformation in all layers (see Vu-Quoc and Ebcioğlu [1995]). Some additional results are also presented. Each layer can have arbitrary thickness, with no a priori assumption made on the distribution of mass over the layer cross section. The deformed cross section is piecewise linear, and admits finite rotations in the layer cross sections. The continuity of the displacement field at the layer interfaces is enforced. The motion of a typical cross section is that of a planar *multibody system* consisted of three rigid links, connected to

---

Lakes [1987].

each other by hinges, and moving in a plane *without* any a priori restriction on the magnitude of motion—see, e.g., Kamman and Huston [1984] for the dynamic formulation of a chain of rigid links. With the kinematics of its deformation described by exact, fully nonlinear expressions, the formulation of this multi-rigid/flexible-body system can be employed to model problems involving large deformation in very flexible multilayer structures, and/or large overall motion as typified by the large rotation maneuvers of flexible composite robot arms or satellite appendages with embedded layers of sensors and actuators. The formulation of single-layer beams can be found in Simo and Vu-Quoc [1986*a*], with examples of complex motion in Simo and Vu-Quoc [1986*b*]. Geometrically-exact formulation has proved to be versatile in a wide range of applications (see Simo [1985], Simo and Vu-Quoc [1986*c*], Simo and Vu-Quoc [1988], Simo and Vu-Quoc [1991]); a comprehensive account of this development can be found in Vu-Quoc [1986].

With the dynamics of motion referred directly to the inertial frame—bypassing the need for a floating reference frame as employed, e.g., in Thompson and Sung [1986]—the equations of motion are derived from the balance of (1) the rate of kinetic energy and power of contact forces/couples and (2) the power of assigned forces/couples. The development of the expression for the power of contact forces/couples for a sandwich beam begins with a sum of the powers of separate individual layers. The rate of fully nonlinear strain measures in each layer is that of a single-layer beam as given in Simo and Vu-Quoc [1986*a*]. The kinematic constraints of the motion of the cross section (chain of rigid links) are then incorporated into the sum of powers, whose expression is written in terms of five[3] principal unknown kinematic quantities: Two translations and three rotations. Expression for the rate of kinetic energy for this multibody system in terms of the five unknown kinematic quantities is also derived.

---

[3] We are considering here the case of sandwich (3-layer) structures; the case of structures with arbitrary number of layers is presented in future publications.

The resulting equations of motion are fully nonlinear. Of particular interest is the case where the core layer admits finite rotation (thus large deformation and/or large overall motion), but rotations in the outer layers are infinitesimal *relative* to the finite core-layer rotation. Such case can be found in flexible multilayer structures performing large overall motion (but not large deformation), e.g., robot arms. For this case, nonlinear approximated equations of motion for multilayer beams/1-D plates are consistently deduced from the fully nonlinear equations. Finally, we obtain the linear equations of motion in the case where all rotations are infinitesimal, and of the same order. Further reduction of the linear equations by assuming equal outer-layer rotations leads to results obtained by Yu [1959*a*] for sandwich beams/1-D plates, but the present theory is more general in that we do not make the a priori assumption of zero axial motion as employed in Yu [1959*a*].

For the static case, the starting point for the development of the Galerkin projection of the governing equations is the nonlinear weak form based on the stress power, from which expressions of fully nonlinear strain measures are obtained (see Vu-Quoc and Deng [1995*b*]). A linearization of this nonlinear weak form is performed for use in the solution for the kinematic quantities via Newton's method. The result of this linearization is a symmetric tangent stiffness operator, which is composed of a geometric part and a material part. Linear and quadratic finite element functions are chosen to form a basis for the Galerkin projection of the linearized equilibrium equations into a finite-dimensional subspace of trial solutions. The tangent stiffness matrix is symmetric, and is evaluated using uniformly reduced integration in all layers to avoid shear locking. There are several ways to assign the boundary conditions in the present theory, e.g., while a clamped boundary condition can be represented by only one way in a single-layer beam (one rotation), it can be represented by six different ways in a sandwich beam (three different rotations). The same can be said for the assignment of applied moments.

For the dynamics case, the Newmark time-stepping algorithm is used to make the time discretization. The time discretized equations of motion are then linearized using the same procedure as in the static case. The result of this linearization is an unsymmetric tangent operator, which is composed of a tangent geometric stiffness operator, a tangent material stiffness operator and a tangent inertia operator. The tangent geometric and material stiffness operators are symmetric as stated above, whereas the tangent inertia operator is unsymmetric, thus making the total dynamic tangent stiffness of the sandwich beam unsymmetric Vu-Quoc and Deng [1995*a*]. Linear and quadratic finite element basis functions are chosen to form a basis for the Galerkin projection of the linearized equations of motion into a finite-dimensional space of trial solutions. The symmetric tangent stiffness matrix is evaluated using uniformly reduced integration in all layers to avoid shear locking, while the unsymmetric tangent inertia operator is integrated exactly.

It should be noted, however, that the present theory is *not* only restricted to the topology of sandwich beams/1-D plates with three layers as stated above; the theory is in fact valid for a structure having a variable number of layers from one to three. Extension of the present theory to beams with arbitrary number of layers is given in Vu-Quoc and Ebcioğlu [1996]. Clearly, there are only three unknown kinematic quantities for a single-layer structure, four for a two-layer structure, and five for a three-layer structure. The equations of motion for a single-layer beam/1-D plate reduce exactly to those found in Simo and Vu-Quoc [1986*a*]. In addition to the variable number of layers allowed in the formulation, the length of each layer can be arbitrary; such is the case of an important class of multilayer structures having *ply drop-off*.

Extensive numerical examples, with comparison to single-layer beams, are given to illustrate the salient features of the present formulation. In particular, the important case of multilayer beams with ply drop-offs, under large deformation, is presented. Unlike single-layer beams, the sandwich beam in the present formulation can be used to illustrate clearly the Saint-Venant principle, as shown in the examples. The computed solution of a sandwich beam in a roll-up maneuver under normal distribution of moments at beam tip is identical to the exact solution. For the dynamic case, we also present sandwich beams under large overall motion (such as free-flying motion and spin-up maneuver), with the results compared to those of the single-layer beam.

CHAPTER 2
EQUILIBRIUM EQUATIONS

2.1. Strong Form

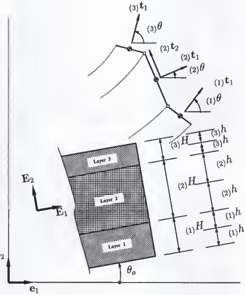

Figure 2.1. *Sandwich beam/1-D plate:* Section profile. Layer thickness. Basis vectors: $_{(1)}\mathbf{t}_2$ and $_{(3)}\mathbf{t}_2$ are not drawn.

The profile of a sandwich beam and its deformed cross section is depicted in Figure 2.1 where the layers are numbered (1), (2), (3) from bottom to top. As already mentioned, the present theory is valid for layers with unequal length, as occurred in beams with ply drop-offs. In our finite element formulation, we allow the number of layers within an element to be variable, while keeping the length of all layers in the same element equal. Since our focus is the development of the expressions for the element matrices, we will henceforth consider the case where all layers have equal length L, without loss of generality. Beams with ply drop-offs are modelled by assembling elements with different numbers of layers. Thus let $\mathcal{L} :=]0, L[$ be the domain of the space variable S, on which the equilibrium equations are defined. The thickness of layer (ℓ)—for $\ell = 1, 2, 3$—is denoted by ${}_{(\ell)}H := 2\ {}_{(\ell)}h$.

The deformation map ${}_{(2)}\boldsymbol{\Phi}_0 \colon \mathcal{L} \rightarrow \mathrm{R}^2$ of the centroidal line of the core layer (2), chosen to be the reference layer, is given by[4]

$$
{}_{(2)}\boldsymbol{\Phi}_0(S) = S\mathbf{E}_1 + \mathbf{u}(S)\ , \quad \mathbf{E}_1 = \cos\theta_o \mathbf{e}_1 + \sin\theta_o \mathbf{e}_2\ , \quad \mathbf{u}(S) = u^\alpha(S)\mathbf{e}_\alpha\ , \tag{2.1}
$$

where $S \in \mathcal{L}$ is the material coordinate, $\mathbf{E}_1$ the material basis vector along the undeformed beam, $\{\mathbf{e}_1, \mathbf{e}_2\}$ the spatial basis vectors, and $\mathbf{u} = u^\alpha \mathbf{e}_\alpha$ the displacement vector of the material point $S\mathbf{E}_1$ (see also Vu-Quoc and Li [1995]). With $\{\ {}_{(\ell)}\mathbf{t}_1,\ {}_{(\ell)}\mathbf{t}_2\}$ designating the basis vectors attached to a cross section of layer (ℓ) as shown in Figure 2.1, then the deformation maps of centroidal line for layers (1) and (3) can be expressed in terms of ${}_{(2)}\boldsymbol{\Phi}_0$ as follows

$$
\begin{aligned}
{}_{(1)}\boldsymbol{\Phi}_0 &= {}_{(2)}\boldsymbol{\Phi}_0 - {}_{(1)}h\ {}_{(1)}\mathbf{t}_2 - {}_{(2)}h\ {}_{(2)}\mathbf{t}_2\ , \\
{}_{(3)}\boldsymbol{\Phi}_0 &= {}_{(2)}\boldsymbol{\Phi}_0 + {}_{(2)}h\ {}_{(2)}\mathbf{t}_2 + {}_{(3)}h\ {}_{(3)}\mathbf{t}_2\ ,
\end{aligned} \tag{2.2}
$$

so that the displacement is continuous at the layer interfaces. The spatial strain measure ${}_{(\ell)}\boldsymbol{\gamma} = {}_{(\ell)}\gamma^\alpha \mathbf{e}_\alpha$ in layer (ℓ) is given by

$$
{}_{(\ell)}\boldsymbol{\gamma} := \frac{\partial\ {}_{(\ell)}\boldsymbol{\Phi}_0}{\partial S} - {}_{(\ell)}\mathbf{t}_1 \tag{2.3}
$$

The resultant contact force ${}_{(\ell)}\mathbf{n} = {}_{(\ell)}n^\alpha \mathbf{e}_\alpha$ is related to the spatial strain ${}_{(\ell)}\boldsymbol{\gamma}$ by

$$
{}_{(\ell)}\mathbf{n} = {}_{(\ell)}\boldsymbol{\Lambda}\bullet\ {}_{(\ell)}\mathcal{C}\bullet\ {}_{(\ell)}\boldsymbol{\Lambda}^T\bullet\ {}_{(\ell)}\boldsymbol{\gamma}\ , \tag{2.4}
$$

---

[4] Summation convention on repeated indices is implied, with Greek letters taking values in $\{1, 2\}$.

where ${}_{(\ell)}\boldsymbol{\Lambda} = {}_{(\ell)}\Lambda^{\alpha}_{\beta}\mathbf{e}_{\alpha} \otimes \mathbf{e}^{\beta}$ is the rotation tensor defined as follows

$$ {}_{(\ell)}\mathbf{t}_{\alpha} = {}_{(\ell)}\boldsymbol{\Lambda}\boldsymbol{\cdot}\mathbf{E}_{\alpha}\,, \qquad \left[{}_{(\ell)}\Lambda^{\alpha}_{\beta}\right] := \begin{bmatrix} \cos\, {}_{(\ell)}\theta & -\sin\, {}_{(\ell)}\theta \\ \sin\, {}_{(\ell)}\theta & \cos\, {}_{(\ell)}\theta \end{bmatrix}\,, \tag{2.5} $$

with ${}_{(\ell)}\theta$ being the rotation angle of layer (ℓ) cross section, and ${}_{(\ell)}\boldsymbol{C} = {}_{(\ell)}C^{\alpha}_{\beta}\mathbf{e}_{\alpha} \otimes \mathbf{e}^{\beta}$ the tensor of elastic moduli whose matrix of components is

$$ \left[{}_{(\ell)}C^{i}_{j}\right] := \begin{bmatrix} {}_{(\ell)}EA & 0 \\ 0 & {}_{(\ell)}GA_{s} \end{bmatrix}\,, \tag{2.6} $$

where ${}_{(\ell)}EA$ and ${}_{(\ell)}GA_{s}$ are the axial and shear stiffness coefficients of layer (ℓ). The resultant contact couple ${}_{(\ell)}m$ of layer (ℓ) and the curvature ${}_{(\ell)}\theta_{,S}$ are related through

$$ {}_{(\ell)}m = {}_{(\ell)}EI\ {}_{(\ell)}\theta_{,S}\ . \tag{2.7} $$

Thus, for a sandwich beam, the five unknown kinematic quantities are gathered in $\Phi\colon \mathcal{L} \to \mathrm{R}^5$ such that

$$ \Phi(S) := \left\{u^1,\ u^2,\ {}_{(1)}\theta,\ {}_{(2)}\theta,\ {}_{(3)}\theta\right\}^{T}\Big|_{(S)}\ . \tag{2.8} $$

The contact force ${}_{(\ell)}\mathbf{n}$ is related to the kinematic quantities in a nonlinear fashion via (2.1)–(2.4). Further, let

$$ \hat{\mathbf{n}} := \sum_{\ell=1}^{3} {}_{(\ell)}\mathbf{n}\,, \tag{2.9} $$

denote the total resultant contact force for all layers, and $\bar{\hat{\mathbf{n}}}\colon \mathcal{L} \to \mathrm{R}^2$ the total assigned resultant force distributed along the centroidal line of the reference layer. For layer (ℓ), the assigned couple is denoted by ${}_{(\ell)}\bar{\boldsymbol{m}}\colon \mathcal{L} \to \mathrm{R}$. The relationship between ${}_{(\ell)}\bar{\boldsymbol{m}}$ and the resultant contact couple ${}_{(\ell)}m$ will be seen in the expressions for the boundary conditions (2.11) below.

We recall below the equation of equilibrium of geometrically-exact sandwich beams, derived in Vu-Quoc and Ebcioğlu [1995]

$$\boxed{\begin{aligned} & \hat{\mathbf{n}}_{,S} + \overline{\hat{\mathbf{n}}} && = 0\,, \\ {}_{(1)}m_{,S} + \left[{}_{(2)}\boldsymbol{\Phi}_{0,S} \times {}_{(1)}\mathbf{n} \right] \cdot \mathbf{e}_3 \; & + {}_{(1)}h \left({}_{(1)}\mathbf{n} \cdot {}_{(1)}\mathbf{t}_1 \right)_{,S} && \\ & + {}_{(2)}h \; {}_{(2)}\theta_{,S} \left({}_{(1)}\mathbf{n} \cdot {}_{(2)}\mathbf{t}_2 \right) + {}_{(1)}\bar{\boldsymbol{m}} && = 0\,, \\ {}_{(2)}m_{,S} + \left[{}_{(2)}\boldsymbol{\Phi}_{0,S} \times {}_{(2)}\mathbf{n} \right] \cdot \mathbf{e}_3 \; & + {}_{(2)}h \left({}_{(1)}\mathbf{n}_{,S} - {}_{(3)}\mathbf{n}_{,S} \right) \cdot {}_{(2)}\mathbf{t}_1 + {}_{(2)}\bar{\boldsymbol{m}} && = 0\,, \\ {}_{(3)}m_{,S} + \left[{}_{(2)}\boldsymbol{\Phi}_{0,S} \times {}_{(3)}\mathbf{n} \right] \cdot \mathbf{e}_3 \; & - {}_{(3)}h \left({}_{(3)}\mathbf{n} \cdot {}_{(3)}\mathbf{t}_1 \right)_{,S} && \\ & - {}_{(2)}h \; {}_{(2)}\theta_{,S} \left({}_{(3)}\mathbf{n} \cdot {}_{(2)}\mathbf{t}_2 \right) + {}_{(3)}\bar{\boldsymbol{m}} && = 0\,. \end{aligned}} \tag{2.10}$$

Let $\{\overline{\mathbf{u}},\ {}_{(1)}\bar{\theta},\ {}_{(2)}\bar{\theta},\ {}_{(3)}\bar{\theta}\}$ represent the assigned displacement and the assigned rotations, respectively. The boundary conditions at $S = 0$ and $S = L$ are then stated as follows

$$\boxed{\begin{array}{llll} \text{Either} & \mathbf{u} = \overline{\mathbf{u}} & \text{or} & \hat{\mathbf{n}} = \overline{\overline{\hat{\mathbf{n}}}}\,, \\ \text{"} & {}_{(1)}\theta = {}_{(1)}\bar{\theta} & \text{"} & {}_{(1)}m + {}_{(1)}h \left({}_{(1)}\mathbf{n} \cdot {}_{(1)}\mathbf{t}_1 \right) = {}_{(1)}\bar{\bar{\boldsymbol{m}}}\,, \\ \text{"} & {}_{(2)}\theta = {}_{(2)}\bar{\theta} & \text{"} & {}_{(2)}m + {}_{(2)}h \left({}_{(1)}\mathbf{n} - {}_{(3)}\mathbf{n} \right) \cdot {}_{(2)}\mathbf{t}_1 = {}_{(2)}\bar{\bar{\boldsymbol{m}}}\,, \\ \text{"} & {}_{(3)}\theta = {}_{(3)}\bar{\theta} & \text{"} & {}_{(3)}m - {}_{(3)}h \left({}_{(3)}\mathbf{n} \cdot {}_{(3)}\mathbf{t}_1 \right) = {}_{(3)}\bar{\bar{\boldsymbol{m}}}\,, \end{array}} \tag{2.11}$$

where $\overline{\overline{\hat{\mathbf{n}}}}$ is the concentrated forces, and ${}_{(\ell)}\bar{\bar{\boldsymbol{m}}}$ the concentrated couples, at the boundaries.

2.2. Stress Power

The above equations of equilibrium and boundary conditions (2.10)–(2.11) can be shown to derive from the balance of the mechanical powers (see Vu-Quoc and Ebcioğlu

[1995])

$$\boxed{\mathcal{P}_c = \mathcal{P}_a \,,} \tag{2.12}$$

for all admissible velocities[5] $\dot{u}^1$, $\dot{u}^2$, ${}_{(1)}\dot{\theta}$, ${}_{(2)}\dot{\theta}$, ${}_{(3)}\dot{\theta}$, where $\mathcal{P}_c$ is the power of contact forces/couples

$$\boxed{\mathcal{P}_c := \sum_{\ell=1}^{3} {}_{(\ell)}\mathcal{P}_c \,, \quad \text{and } {}_{(\ell)}\mathcal{P}_c := \int_{\mathfrak{L}} \left[{}_{(\ell)}\mathbf{n} \cdot {}_{(\ell)}\overset{[\ell]}{\gamma} + {}_{(\ell)}m \; {}_{(\ell)}\dot{\theta}_{,S} \right] dS \,,} \tag{2.13}$$

and $\mathcal{P}_a$ is the power of assigned forces/couples

$$\boxed{\mathcal{P}_a := \int_{\mathfrak{L}} \left\{ \bar{\bar{\mathbf{n}}} \cdot \dot{\mathbf{u}} + \sum_{\ell=1}^{3} {}_{(\ell)}\bar{m} \; {}_{(\ell)}\dot{\theta} \right\} dS + \left[\bar{\bar{\bar{\mathbf{n}}}} \cdot \dot{\mathbf{u}} + \sum_{\ell=1}^{3} {}_{(\ell)}\bar{\bar{m}} \; {}_{(\ell)}\dot{\theta} \right]_{S=0}^{S=L} .} \tag{2.14}$$

In (2.13)–(2.14), the overhead dot "$\bullet$" designates time differentiation, whereas the overhead symbol "$^{[\ell]}$" designates the time differentiation of a vector quantity, say, $\mathbf{v}$, expressed in the cross-section basis $\{ {}_{(\ell)}\mathbf{t}_1, \; {}_{(\ell)}\mathbf{t}_2 \}$ of layer (ℓ) while keeping *this* basis *fixed*; we have

$$ {}_{(\ell)}\overset{[\ell]}{\mathbf{t}}_\alpha \equiv 0 \,, \quad \text{and } \mathbf{v} = v^\alpha \; {}_{(\ell)}\mathbf{t}_\alpha \Longrightarrow \overset{[\ell]}{\mathbf{v}} := \dot{v}^\alpha \; {}_{(\ell)}\mathbf{t}_\alpha \,. \tag{2.15}$$

---

[5] Consider the dynamics case, where all kinematic quantities are time dependent.

CHAPTER 3
GALERKIN PROJECTION

We now develop the operator expressions for the weak form of the equilibrium equations based on the balance of power in Section 2.2. These expressions will be linearized, and subsequently used in a Galerkin projection for the solution process.

3.1. Weak Form

Let $\mathbf{w}\colon \mathcal{L} \rightarrow \mathrm{R}^5$ be the weighting functions corresponding to the five kinematic quantities in (2.8)

$$\mathbf{w} := \left\{ v^1,\ v^2,\ {}_{(1)}\varphi,\ {}_{(2)}\varphi,\ {}_{(3)}\varphi \right\}^T , \tag{3.1}$$

instead of velocities in (2.13). Gathered in ${}_{(\ell)}\mathbf{f}_c\colon \mathcal{L} \times \mathrm{R}_+ \rightarrow \mathrm{R}^3$ such that

$$ {}_{(\ell)}\mathbf{f}_c := \left\{ {}_{(\ell)}n^1,\ {}_{(\ell)}n^2,\ {}_{(\ell)}m \right\}^T . \tag{3.2}$$

are the contact forces/couple for layer (ℓ). Since the core layer (2) is the reference layer based on which the deformation of all layers is referred to, we focus our attention on this layer first. Based on the expression for ${}_{(\ell)}\mathcal{P}_c$ in $(2.13)_2$, the weak form for the contact forces/couple in layer (2) can be written as

$$ {}_{(2)}G_c(\boldsymbol{\Phi}, \mathbf{w}) := \int\limits_{\mathfrak{L}} \left[\, {}_{(2)}\mathbf{n} \bullet {}_{(2)}\overset{[2]}{\boldsymbol{\gamma}} + {}_{(2)}m \; {}_{(2)}\varphi_{,S} \right] dS , \tag{3.3}$$

where, in terms of the weighting functions (3.1),

$$ {}_{(2)}\overset{[2]}{\boldsymbol{\gamma}} = \left[v^1{}_{,S} + \left(\sin\theta_o + u^2{}_{,S} \right) \, {}_{(2)}\varphi \right] \mathbf{e}_1 + \left[v^2{}_{,S} - \left(\cos\theta_o + u^1{}_{,S} \right) \, {}_{(2)}\varphi \right] \mathbf{e}_2 , \tag{3.4}$$

is the expression for the variation of the strain ${}_{(2)}\gamma$ by virtue of (2.15), (2.3), (2.1), and (2.5) (see Vu-Quoc and Ebcioğlu [1995]).[6] Using (3.2) and (3.4), the integrand in (3.3) can be rearranged in matrix form as follows

$$\boxed{{}_{(2)}G_c(\boldsymbol{\Phi}, \mathbf{w}) = \int_{\mathfrak{L}} \Big[{}_{(2)}\boldsymbol{\Xi}(\boldsymbol{\Phi})\mathbf{w} \Big] \cdot {}_{(2)}\mathbf{f}_c(\boldsymbol{\Phi}) \, dS \, ,} \tag{3.5}$$

where

$${}_{(2)}\boldsymbol{\Xi}(\boldsymbol{\Phi}) := \begin{bmatrix} \dfrac{d}{dS} & 0 & 0 & {}_{(2)}\Xi_1 & 0 \\ 0 & \dfrac{d}{dS} & 0 & {}_{(2)}\Xi_2 & 0 \\ 0 & 0 & 0 & \dfrac{d}{dS} & 0 \end{bmatrix}_{3\times 5} , \tag{3.6}$$

and

$${}_{(2)}\Xi_1 \;:=\; +\Big[\sin\theta_o + u^2_{,S}\Big] \, , \tag{3.7}$$

$${}_{(2)}\Xi_2 \;:=\; -\Big[\cos\theta_o + u^1_{,S}\Big] \, . \tag{3.8}$$

The stress power ${}_{(1)}\mathcal{P}_c$ for layer (1) as given in $(2.13)_2$ can be rewritten as a weak form

$${}_{(1)}G_c(\boldsymbol{\Phi}, \mathbf{w}) := \int_{\mathfrak{L}} \Big[{}_{(1)}\mathbf{n} \cdot {}_{(1)}\overset{[1]}{\boldsymbol{\gamma}} + {}_{(1)}m \; {}_{(1)}\varphi_{,S} \Big] \, dS \, , \tag{3.9}$$

where, in terms of the weighting functions (3.1),

$$\begin{aligned} {}_{(1)}\overset{[1]}{\boldsymbol{\gamma}} \;=\; & \Big[v^1{}_{,S} + \Big(\sin\theta_o + u^2{}_{,S}\Big) \; {}_{(1)}\varphi\Big] \, \mathbf{e}_1 + \Big[v^2{}_{,S} - \Big(\cos\theta_o + u^1{}_{,S}\Big) \; {}_{(1)}\varphi\Big] \, \mathbf{e}_2 \\ & + {}_{(1)}h \; {}_{(1)}\varphi_{,S} \; {}_{(1)}\mathbf{t}_1 + {}_{(2)}h \; {}_{(2)}\varphi_{,S} \; {}_{(2)}\mathbf{t}_1 + {}_{(2)}h \; {}_{(2)}\theta_{,S} \Big[{}_{(2)}\varphi - {}_{(1)}\varphi \Big] \; {}_{(2)}\mathbf{t}_2 , \end{aligned} \tag{3.10}$$

is the expression for the variation of the strain ${}_{(1)}\gamma$ by virtue of (2.15), (2.3), $(2.2)_1$, and (2.5). Rearranging (3.9) in matrix form with the aid of (3.2) and (3.10), we obtain

$$\boxed{{}_{(1)}G_c(\boldsymbol{\Phi}, \mathbf{w}) = \int_{\mathfrak{L}} \Big[{}_{(1)}\boldsymbol{\Xi}(\boldsymbol{\Phi})\mathbf{w} \Big] \cdot {}_{(1)}\mathbf{f}_c(\boldsymbol{\Phi}) \, dS \, ,} \tag{3.11}$$

---

[6] Recall that $\{u^1, u^2\}$ are the components of $\mathbf{u}$ along the basis vectors $\{\mathbf{e}_1, \mathbf{e}_2\}$. In fact, (3.4) is more general than the corresponding expression (3.8) in Vu-Quoc and Ebcioğlu [1995], where $\theta_o = 0$; we are following here the formulation in Vu-Quoc and Li [1995].

where

$$
{}_{(1)}\boldsymbol{\Xi}(\boldsymbol{\Phi}) := \begin{bmatrix} \dfrac{d}{dS} & 0 & {}_{(1)}\Xi_1 & {}_{(1)}\Xi_3 & 0 \\ 0 & \dfrac{d}{dS} & {}_{(1)}\Xi_2 & {}_{(1)}\Xi_4 & 0 \\ 0 & 0 & \dfrac{d}{dS} & 0 & 0 \end{bmatrix}_{3\times 5} , \tag{3.12}
$$

in which the elements ${}_{(1)}\Xi_i$, for $i = 1, \ldots, 4$, have the following expressions

$$
{}_{(1)}\Xi_1 \ := \ \underbrace{+\left[\sin\theta_o + u^2{}_{,S}\right]} + {}_{(1)}h \cos\ {}_{(1)}\theta \frac{d}{dS} + {}_{(2)}h\ {}_{(2)}\theta_{,S} \sin\ {}_{(2)}\theta \ , \tag{3.13}
$$

$$
{}_{(1)}\Xi_2 \ := \ \underbrace{-\left[\cos\theta_o + u^1{}_{,S}\right]} + {}_{(1)}h \sin\ {}_{(1)}\theta \frac{d}{dS} - {}_{(2)}h\ {}_{(2)}\theta_{,S} \cos\ {}_{(2)}\theta \ , \tag{3.14}
$$

$$
{}_{(1)}\Xi_3 \ := \ {}_{(2)}h \cos\ {}_{(2)}\theta \frac{d}{dS} - {}_{(2)}h\ {}_{(2)}\theta_{,S} \sin\ {}_{(2)}\theta \ , \tag{3.15}
$$

$$
{}_{(1)}\Xi_4 \ := \ {}_{(2)}h \sin\ {}_{(2)}\theta \frac{d}{dS} + {}_{(2)}h\ {}_{(2)}\theta_{,S} \cos\ {}_{(2)}\theta \ . \tag{3.16}
$$

Similarly, we have for layer (3) the weak form

$$
{}_{(3)}G_c(\boldsymbol{\Phi}, \mathbf{w}) := \int_{\mathfrak{L}} \left[\ {}_{(3)}\mathbf{n} \cdot {}_{(3)}\overset{[3]}{\boldsymbol{\gamma}} + {}_{(3)}m\ {}_{(3)}\varphi\right] dS \ , \tag{3.17}
$$

in which the variation of the strain ${}_{(3)}\boldsymbol{\gamma}$ is given by

$$
\begin{aligned}
{}_{(3)}\overset{[3]}{\boldsymbol{\gamma}} \ = \ & \left[v^1 + \left(\sin\theta_o + u^2{}_{,S}\right)\ {}_{(3)}\varphi\right]\mathbf{e}_1 + \left[v^2 - \left(\cos\theta_o + u^1{}_{,S}\right)\ {}_{(3)}\varphi\right]\mathbf{e}_2 \\
& - {}_{(3)}h\ {}_{(3)}\varphi_{,S}\ {}_{(3)}\mathbf{t}_1 - {}_{(2)}h\ {}_{(2)}\varphi_{,S}\ {}_{(2)}\mathbf{t}_1 - {}_{(2)}h\ {}_{(2)}\theta_{,S}\left[\ {}_{(2)}\varphi - {}_{(3)}\varphi\right]\ {}_{(2)}\mathbf{t}_2 \ .
\end{aligned} \tag{3.18}
$$

Expression (3.18) is the counterpart of (3.10) for layer (3). In matrix form,

$$
\boxed{{}_{(3)}G_c(\boldsymbol{\Phi}, \mathbf{w}) = \int_{\mathfrak{L}} \left[\ {}_{(3)}\boldsymbol{\Xi}(\boldsymbol{\Phi})\mathbf{w}\right] \cdot {}_{(3)}\mathbf{f}_c(\boldsymbol{\Phi})\ dS \ .} \tag{3.19}
$$

where

$$
{}_{(3)}\boldsymbol{\Xi}(\boldsymbol{\Phi}) := \begin{bmatrix} \dfrac{d}{dS} & 0 & 0 & {}_{(3)}\Xi_3 & {}_{(3)}\Xi_1 \\ 0 & \dfrac{d}{dS} & 0 & {}_{(3)}\Xi_4 & {}_{(3)}\Xi_2 \\ 0 & 0 & 0 & 0 & \dfrac{d}{dS} \end{bmatrix}_{3\times 5} , \tag{3.20}
$$

in which the elements ${}_{(3)}\Xi_i$, for $i = 1, \ldots, 4$, have the following expressions

$$ {}_{(3)}\Xi_1 := \underbrace{+\left[\sin\theta_o + u^2{,}_S\right]} - {}_{(2)}h\ {}_{(2)}\theta{,}_S \sin\ {}_{(2)}\theta - {}_{(3)}h \cos\ {}_{(3)}\theta \frac{d}{dS}\,, \tag{3.21} $$

$$ {}_{(3)}\Xi_2 := \underbrace{-\left[\cos\theta_o + u^1{,}_S\right]} + {}_{(2)}h\ {}_{(2)}\theta{,}_S \cos\ {}_{(2)}\theta - {}_{(3)}h \sin\ {}_{(3)}\theta \frac{d}{dS}\,, \tag{3.22} $$

$$ {}_{(3)}\Xi_3 := {}_{(2)}h\ {}_{(2)}\theta{,}_S \sin\ {}_{(2)}\theta - {}_{(2)}h \cos\ {}_{(2)}\theta \frac{d}{dS}\,, \tag{3.23} $$

$$ {}_{(3)}\Xi_4 := -\ {}_{(2)}h\ {}_{(2)}\theta{,}_S \cos\ {}_{(2)}\theta - {}_{(2)}h \sin\ {}_{(2)}\theta \frac{d}{dS}\,. \tag{3.24} $$

It can be seen from (3.7), (3.13), and (3.21) that there is a common part between the matrix elements ${}_{(\ell)}\Xi_1$, for $\ell = 1, 2, 3$, as indicated by the underbraces; similarly for ${}_{(\ell)}\Xi_2$ in (3.8), (3.14), and (3.22). Notice that the matrix elements ${}_{(\ell)}\Xi_1$ and ${}_{(\ell)}\Xi_2$ are in the same column corresponding to the rotation ${}_{(\ell)}\theta$, and above the differential operator d/dS. The total weak form of contact forces/couples for a geometrically-exact sandwich beam is then given by

$$ \boxed{G_c(\mathbf{\Phi}, \mathbf{w}) = \sum_{\ell=1}^{3} {}_{(\ell)}G_c(\mathbf{\Phi}, \mathbf{w})\,.} \tag{3.25} $$

Gathered in $\overline{\mathcal{F}}: \mathcal{L} \rightarrow \mathrm{R}^5$ are the assigned forces/couples

$$ \overline{\mathcal{F}} := \left\{\overline{n}^1,\ \overline{n}^2,\ {}_{(1)}\overline{\mathcal{M}},\ {}_{(2)}\overline{\mathcal{M}},\ {}_{(3)}\overline{\mathcal{M}}\right\}^T\,. \tag{3.26} $$

The weak form for assigned forces/couples is as follows

$$ \boxed{G_a(\mathbf{w}) = \int_{\mathfrak{L}} \overline{\mathcal{F}} \bullet \mathbf{w}\, dS + \left[\overline{\mathcal{F}} \bullet \mathbf{w}\right]_{S=0}^{S=L}\,.} \tag{3.27} $$

Let $\mathcal{V}$ designate the set of admissible weighting functions (see Hughes [1987]). The weak form of the geometrically-exact multilayer beam problem is to

$$ \boxed{\begin{array}{l} \text{Find } \Phi \text{ such that} \\ \qquad G_c(\mathbf{\Phi}, \mathbf{w}) = G_a(\mathbf{w})\,, \quad \forall \mathbf{w} \in \mathcal{V}\,. \end{array}} \tag{3.28} $$

3.2. Linearization of Weak Form

Define the residual

$$G(\Phi, \mathbf{w}) := G_c(\mathbf{\Phi}, \mathbf{w}) - G_a(\mathbf{w}) , \tag{3.29}$$

and consider the incremental formula for the solution

$$\Phi_\epsilon^{(i+1)} := \Phi^{(i)} + \epsilon \Delta \Phi^{(i+1)} , \tag{3.30}$$

where $\Phi^{(i+1)}$ and $\Phi^{(i)}$ are the values of Φ at iterations $(i+1)$ and (i), respectively, of the solution process by Newton's method, and $\Delta\Phi^{(i+1)}$ the incremental value. The linearization of the weak form $G(\Phi, \mathbf{w})$ at $\Phi = \Phi^{(i)}$ can be written as

$$L\left[G(\Phi^{(i)}, \mathbf{w})\right] = G(\Phi^{(i)}, \mathbf{w}) + DG(\Phi^{(i)}, \mathbf{w}) \boldsymbol{\cdot} \Delta\Phi^{(i+1)} , \tag{3.31}$$

where the tangent stiffness operator $DG(\Phi^{(i)}, \mathbf{w})$ is computed as the directional derivative (with respect to Φ) of G_c by virtue (3.29)

$$DG(\Phi^{(i)}, \mathbf{w}) \boldsymbol{\cdot} \Delta\Phi^{(i+1)} = DG_c(\Phi^{(i)}, \mathbf{w}) \boldsymbol{\cdot} \Delta\Phi^{(i+1)} = \frac{d}{d\epsilon} G_c(\Phi_\epsilon^{(i+1)}, \mathbf{w}) \bigg|_{\epsilon=0} . \tag{3.32}$$

Then, using (3.25), we can write the tangent stiffness operator as the sum of the contribution from each layer

$$\boxed{DG(\Phi^{(i)}, \mathbf{w}) = \sum_{\ell=1}^{3} D_{\ (\ell)} G_c(\Phi^{(i)}, \mathbf{w}) ,} \tag{3.33}$$

keeping in mind the decomposition

$$\boxed{D_{\ (\ell)} G_c = \left[D^g + D^m\right]_{\ (\ell)} G_c ,} \tag{3.34}$$

where D^g is the differential operator that gives rise to the tangent geometric stiffness, and D^m the tangent material stiffness.

In the present section, it is more convenient to use matrix of components of tensors. Define the material properities matrix

$$ {}_{(\ell)}\boldsymbol{\mathcal{C}} := \begin{bmatrix} {}_{(\ell)}EA & 0 & 0 \\ 0 & {}_{(\ell)}GA_s & 0 \\ 0 & 0 & {}_{(\ell)}EI \end{bmatrix}_{3\times 3} , \qquad (3.35) $$

and the rotation matrix

$$ {}_{(\ell)}\boldsymbol{\Lambda} := \begin{bmatrix} \cos {}_{(\ell)}\theta & -\sin {}_{(\ell)}\theta & 0 \\ \sin {}_{(\ell)}\theta & \cos {}_{(\ell)}\theta & 0 \\ 0 & 0 & 1 \end{bmatrix}_{3\times 3} . \qquad (3.36) $$

Also let the material contact forces/couple ${}_{(\ell)}\mathbf{F}_c$ be defined as follows

$$ {}_{(\ell)}\mathbf{F}_c := {}_{(\ell)}\boldsymbol{\Lambda}^T \, {}_{(\ell)}\mathbf{f}_c \, , \quad \text{or } {}_{(\ell)}\mathbf{f}_c = {}_{(\ell)}\boldsymbol{\Lambda} \, {}_{(\ell)}\mathbf{F}_c \, , \qquad (3.37) $$

where the spatial contact forces/couple ${}_{(\ell)}\mathbf{f}_c$ was defined in (3.2). Expression $(3.37)_2$ is to be used in the expressions for ${}_{(\ell)}G_c$ in (3.5), (3.11), (3.19). For each layer, the tangent geometric stiffness is obtained from the linearization of the operators ${}_{(\ell)}\boldsymbol{\Xi}$ and ${}_{(\ell)}\boldsymbol{\Lambda}$ at $\Phi^{(i)}$, while keeping the material contact forces/couple ${}_{(\ell)}\mathbf{F}_c$ fixed. On the other hand, the tangent material stiffness is obtained from the linearization of ${}_{(\ell)}\mathbf{F}_c$ at $\Phi^{(i)}$

$$ D \, {}_{(\ell)}\mathbf{F}_c(\Phi^{(i)}) \cdot \Delta\Phi^{(i+1)} = {}_{(\ell)}\boldsymbol{\mathcal{C}} \, {}_{(\ell)}\boldsymbol{\Lambda}^{(i)^T} \, {}_{(\ell)}\boldsymbol{\Xi}(\Phi^{(i)}) \cdot \Delta\Phi^{(i+1)} \, . \qquad (3.38) $$

The contribution of layer (2) to the total tangent geometric stiffness is then

$$ \boxed{ D^g \, {}_{(2)}G_c(\Phi^{(i)}, \mathbf{w}) \cdot \Delta\Phi^{(i+1)} = \int_{\mathfrak{L}} \left[{}_{(2)}\boldsymbol{\Upsilon}\mathbf{w} \right] \cdot \left[{}_{(2)}\mathbf{B}(\Phi^{(i)}) \, {}_{(2)}\boldsymbol{\Upsilon}\Delta\Phi^{(i+1)} \right] dS \, . } \qquad (3.39) $$

where

$$ {}_{(2)}\boldsymbol{\Upsilon} := \begin{bmatrix} d/dS & 0 & 0 & 0 & 0 \\ 0 & d/dS & 0 & 0 & 0 \\ 0 & 0 & 0 & 0 & 0 \\ 0 & 0 & 0 & 1 & 0 \\ 0 & 0 & 0 & 0 & 0 \end{bmatrix}_{5\times 5} , \qquad (3.40) $$

$$
{}_{(2)}\mathbf{B}(\Phi) := \begin{bmatrix} 0 & 0 & 0 & -\,{}_{(2)}n^2 & 0 \\ 0 & 0 & 0 & {}_{(2)}n^1 & 0 \\ 0 & 0 & 0 & 0 & 0 \\ -\,{}_{(2)}n^2 & {}_{(2)}n^1 & 0 & -\,{}_{(2)}\mathbf{n}\cdot\,{}_{(2)}\mathbf{\Phi}_{,S} & 0 \\ 0 & 0 & 0 & 0 & 0 \end{bmatrix}_{5\times 5} , \tag{3.41}
$$

with

$$
{}_{(2)}\mathbf{n}\cdot\,{}_{(2)}\mathbf{\Phi}_{,S} = {}_{(2)}n^1\,\left(\cos\theta_o + u^1_{,S}\right) + {}_{(2)}n^2\left(\sin\theta_o + u^2_{,S}\right) , \tag{3.42}
$$

by virtue of (2.4) and (2.1).

The contribution of layers (1) and (3) to the total tangent geometric stiffness can be collectively expressed by

$$
\boxed{\begin{aligned} & D^g\ {}_{(\ell)}G_c(\Phi^{(i)}, \mathbf{w})\cdot\Delta\Phi^{(i+1)} \\ & \quad = \int_{\mathfrak{L}} \Big\{\Big[\,{}_{(\ell)}\Upsilon_1\mathbf{w}\Big]\cdot\,{}_{(\ell)}\mathbf{B}_1(\Phi^{(i)})\ {}_{(\ell)}\Upsilon_1 + \Big[\,{}_{(\ell)}\Upsilon_2\mathbf{w}\Big]\cdot\,{}_{(\ell)}\mathbf{B}_2(\Phi^{(i)})\ {}_{(\ell)}\Upsilon_2\Big\}\cdot\Delta\Phi^{(i+1)}dS\,, \end{aligned}}
$$

(3.43)

for $\ell = 1, 3$. For layer (1), we obtain the following expressions

$$
{}_{(1)}\Upsilon_1 := \begin{bmatrix} d/dS & 0 & 0 & 0 & 0 \\ 0 & d/dS & 0 & 0 & 0 \\ 0 & 0 & 1 & 0 & 0 \\ 0 & 0 & 0 & 0 & 0 \\ 0 & 0 & 0 & 0 & 0 \end{bmatrix}_{5\times 5} , \tag{3.44}
$$

$$
{}_{(1)}\mathbf{B}_1(\Phi) := \begin{bmatrix} 0 & 0 & -\,{}_{(1)}n^2 & 0 & 0 \\ 0 & 0 & {}_{(1)}n^1 & 0 & 0 \\ -\,{}_{(1)}n^2 & {}_{(1)}n^1 & -\,{}_{(1)}\mathbf{n}\cdot\,{}_{(2)}\mathbf{\Phi}_{,S} & 0 & 0 \\ 0 & 0 & 0 & 0 & 0 \\ 0 & 0 & 0 & 0 & 0 \end{bmatrix}_{5\times 5} , \tag{3.45}
$$

with ${}_{(1)}\mathbf{n}\cdot\,{}_{(2)}\mathbf{\Phi}_{,S}$ having an expansion similar to (3.42), and

$$
{}_{(1)}\Upsilon_2 := \begin{bmatrix} 0 & 0 & 0 & 0 & 0 \\ 0 & 0 & -1 & 1 & 0 \\ 0 & 0 & 1 & -1 & 0 \\ 0 & 0 & 0 & d/dS & 0 \\ 0 & 0 & 0 & 0 & 0 \end{bmatrix}_{5\times 5} , \tag{3.46}
$$

$${}_{(1)}\mathbf{B}_2(\Phi) := \begin{bmatrix} 0 & 0 & 0 & 0 & 0 \\ 0 & 0 & 0 & {}_{(2)}h \cos\, {}_{(2)}\theta\, {}_{(1)}n^2 & 0 \\ 0 & 0 & {}_{(1)}\beta_2 & {}_{(2)}h \sin\, {}_{(2)}\theta\, {}_{(1)}n^1 & 0 \\ 0 & {}_{(2)}h \cos\, {}_{(2)}\theta\, {}_{(1)}n^2 & {}_{(2)}h \sin\, {}_{(2)}\theta\, {}_{(1)}n^1 & 0 & 0 \\ 0 & 0 & 0 & 0 & 0 \end{bmatrix}_{5\times 5} , \tag{3.47}$$

with

$${}_{(1)}\beta_2 := -\, {}_{(2)}h\, {}_{(2)}\theta_{,S}\; {}_{(1)}\mathbf{n}^{\bullet}\, {}_{(2)}\mathbf{t}_1 = -\, {}_{(2)}h\, {}_{(2)}\theta_{,S} \left[{}_{(1)}n^1 \cos\, {}_{(2)}\theta + {}_{(1)}n^2 \sin\, {}_{(2)}\theta \right] . \tag{3.48}$$

For layer (3), we obtain

$${}_{(3)}\boldsymbol{\Upsilon}_1 := \begin{bmatrix} d/dS & 0 & 0 & 0 & 0 \\ 0 & d/dS & 0 & 0 & 0 \\ 0 & 0 & 0 & 0 & 0 \\ 0 & 0 & 0 & 0 & 0 \\ 0 & 0 & 0 & 0 & 1 \end{bmatrix}_{5\times 5} , \tag{3.49}$$

$${}_{(3)}\mathbf{B}_1(\Phi) := \begin{bmatrix} 0 & 0 & 0 & 0 & -\, {}_{(3)}n^2 \\ 0 & 0 & 0 & 0 & {}_{(3)}n^1 \\ 0 & 0 & 0 & 0 & 0 \\ 0 & 0 & 0 & 0 & 0 \\ -\, {}_{(3)}n^2 & {}_{(3)}n^1 & 0 & 0 & -\, {}_{(3)}\mathbf{n}^{\bullet}\, {}_{(2)}\boldsymbol{\Phi}_{,S} \end{bmatrix}_{5\times 5} , \tag{3.50}$$

with ${}_{(3)}\mathbf{n}^{\bullet}\, {}_{(2)}\boldsymbol{\Phi}_{,S}$ having an expansion similar to (3.42), and

$${}_{(3)}\boldsymbol{\Upsilon}_2 := \begin{bmatrix} 0 & 0 & 0 & 0 & 0 \\ 0 & 0 & 0 & 0 & 0 \\ 0 & 0 & 0 & -1 & 1 \\ 0 & 0 & 0 & d/dS & 0 \\ 0 & 0 & 0 & 1 & -1 \end{bmatrix}_{5\times 5} , \tag{3.51}$$

$${}_{(3)}\mathbf{B}_2(\Phi) := \begin{bmatrix} 0 & 0 & 0 & 0 & 0 \\ 0 & 0 & 0 & 0 & 0 \\ 0 & 0 & 0 & {}_{(2)}h \cos\, {}_{(2)}\theta\, {}_{(3)}n^2 & 0 \\ 0 & 0 & {}_{(2)}h \cos\, {}_{(2)}\theta\, {}_{(3)}n^2 & 0 & {}_{(2)}h \sin\, {}_{(2)}\theta\, {}_{(3)}n^1 \\ 0 & 0 & 0 & {}_{(2)}h \sin\, {}_{(2)}\theta\, {}_{(3)}n^1 & {}_{(3)}\beta_2 \end{bmatrix}_{5\times 5} , \tag{3.52}$$

with

$${}_{(3)}\beta_2 := {}_{(2)}h\, {}_{(2)}\theta_{,S}\; {}_{(3)}\mathbf{n}^{\bullet}\, {}_{(2)}\mathbf{t}_1 = {}_{(2)}h\, {}_{(2)}\theta_{,S} \left[{}_{(3)}n^1 \cos\, {}_{(2)}\theta + {}_{(3)}n^2 \sin\, {}_{(2)}\theta \right] . \tag{3.53}$$

Recall from (3.39) and (3.43) that the matrices ${}_{(2)}\mathbf{B}$, ${}_{(1)}\mathbf{B}_{\alpha}$, and ${}_{(3)}\mathbf{B}_{\alpha}$ (for $\alpha = 1, 2$) are to be evaluated at $\Phi = \Phi^{(i)}$, and so are the quantities in (3.41), (3.42), and in (3.45), (3.47), (3.48), and in (3.50), (3.52), (3.53).

The total tangent *material* stiffness has the following contribution from layer (ℓ)

$$\boxed{D^m \, {}_{(\ell)}G_c(\Phi^{(i)}, \mathbf{w}) \cdot \Delta\Phi^{(i+1)} = \int_{\mathfrak{L}} \left[{}_{(\ell)}\Xi(\Phi^{(i)})\mathbf{w} \right] \cdot {}_{(\ell)}\mathbf{\Lambda}^{(i)} \, {}_{(\ell)}\boldsymbol{\mathcal{C}} \, {}_{(\ell)}\mathbf{\Lambda}^{(i)^T} \, {}_{(\ell)}\Xi(\Phi^{(i)})\Delta\Phi^{(i)} dS \, ,} \tag{3.54}$$

where the expressions for ${}_{(\ell)}\Xi(\Phi^{(i)})$ are given in (3.6), (3.12) and (3.20).

Finally, the total tangent stiffness operator is obtained by combining (3.33), (3.34), (3.39), (3.43), and (3.54). It is noted that the total tangent stiffness operator is symmetric since each of its constituents is. The increment $\Delta\Phi^{(i+1)}$ is solved for by setting the linearized weak form (3.31) to zero, and thus

$$\boxed{\Delta\Phi^{(i+1)} = -\left[DG(\Phi^{(i)}, \mathbf{w})\right]^{-1} \cdot G(\Phi^{(i)}, \mathbf{w}) \, , \quad \forall \mathbf{w} \in \mathcal{V} \, .} \tag{3.55}$$

3.3. Projection: Galerkin Finite Element

Following the standard classical finite element discretization, we divide the domain $[0, L]$ of the beam into N subintervals, with $(N+1)$ being the total number of nodes, i.e.,

$$[0, L] = \bigcup_{A=1}^{N} \left[X_A^1, \, X_{A+1}^1 \right] , \tag{3.56}$$

where $0 = X_1^1 < X_2^1 < ... < X_{N+1}^1 = L$.

Let $N^A \colon \mathcal{L} \rightarrow \mathrm{R}$ be a function in the space of weighting functions $\mathcal{V}$, and consider a family of independent functions $\left\{ N^A, \; A = 1, ..., n \right\} \subset \mathcal{V}$, such that

$$\mathcal{V}^h = span \left\{ N^A, \; A = 1, ..., n \right\} \subset \mathcal{V}, \tag{3.57}$$

is a finite dimensional subspace of $\mathcal{V}$ (see e.g., Hughes [1987]). Consider the following approximations $\Delta\mathbf{\Phi}^h(S) \in \mathcal{V}^h$ and $\mathbf{w}^h \in \mathcal{V}^h$ of $\Delta\Phi(S) \in \mathcal{V}$ and of $\mathbf{w} \in \mathcal{V}$, respectively[7]

$$\Delta\Phi(S) \approx \Delta\Phi^h(S) = \sum_{J=1}^{n} \mathbf{d}_J N_J(S) \in \mathrm{R}^{5\times 1}\,, \quad \mathbf{w}(S) \approx \mathbf{w}^h(S) = \sum_{I=1}^{n} \mathbf{c}_I N_I(S) \in \mathrm{R}^{5\times 1}\,, \tag{3.58}$$

with $\mathbf{d}_J,\ \mathbf{c}_I \in \mathrm{R}^{5\times 1}$. The matrix equation resulting from the restriction of (3.55) from $\mathcal{V}$ to $\mathcal{V}^h \subset \mathcal{V}$ takes the form[8]

$$\mathbf{d} = -\mathbf{K}^{-1}\mathbf{r} \in \mathrm{R}^{5n\times 1}\,, \tag{3.59}$$

where $\mathbf{d} := \{\mathbf{d}_J\} \in \mathrm{R}^{5n\times 1}$ is the matrix of incremental (generalized) displacement, $\mathbf{K} \in \mathrm{R}^{5n\times 5n}$ the tangent stiffness matrix, and $\mathbf{r} \in \mathrm{R}^{5n\times 1}$ the residual matrix. The tangent stiffness matrix is obtained by

$$\boxed{\mathbf{K} = \sum_{\ell=1}^{3} \left[\, {}_{(\ell)}\mathbf{K}^g + {}_{(\ell)}\mathbf{K}^m \right] \in \mathrm{R}^{5n\times 5n}\,,} \tag{3.60}$$

where ${}_{(\ell)}\mathbf{K}^g = \left[\, {}_{(\ell)}\mathbf{K}^g_{IJ} \right]$ and ${}_{(\ell)}\mathbf{K}^m = \left[\, {}_{(\ell)}\mathbf{K}^m_{IJ} \right]$ are, respectively, the tangent geometric stiffness matrix and the tangent material stiffness matrix of layer (ℓ). Let $\mathfrak{I}_n$ be a unit matrix, i.e.,

$$\mathfrak{I}_n := Diag\,[1, \ldots, 1] \in \mathrm{R}^{n\times n}\,. \tag{3.61}$$

From (3.39) and (3.43), we obtain respectively the tangent geometric stiffness matrices of layer (2)

$$\boxed{{}_{(2)}\mathbf{K}^g_{IJ} = \int_{\mathfrak{L}} \left\{ {}_{(2)}\boldsymbol{\Upsilon}\,[N_I \mathfrak{I}_5] \right\}^T \left\{ {}_{(2)}\mathbf{B}(\Phi)\ {}_{(2)}\boldsymbol{\Upsilon}\,[N_J \mathfrak{I}_5] \right\} dS \in \mathrm{R}^{5\times 5}\,,} \tag{3.62}$$

---

[7] The dimension 5 in (3.58) comes from the definitions of Φ in (2.8) and of $\mathbf{w}$ in (3.1) for sandwich beams. It is recalled, however, that since the number of layers in a finite element can vary between 1 and 3, the number of degrees of freedom per node varies between 3 and 5.

[8] We omit the superscripts $(i+1)$ and (i) to keep the exposition clear. Thus, in the context of Newton's method, the argument Φ in the formulae in Section 3.3 should be read as $\Phi^{(i)}$.

and of layers $\ell = 1, 3$

$$\boxed{\begin{aligned} {}_{(\ell)}\mathbf{K}^{g}_{IJ} = \int\limits_{\mathfrak{L}} & \Big(\Big\{ {}_{(\ell)}\boldsymbol{\Upsilon}_1 \, [N_I \mathfrak{I}_5] \Big\}^T \, {}_{(\ell)}\mathbf{B}_1(\Phi) \, {}_{(\ell)}\boldsymbol{\Upsilon}_1 \\ & + \Big\{ {}_{(\ell)}\boldsymbol{\Upsilon}_2 \, [N_I \mathfrak{I}_5] \Big\}^T \, {}_{(\ell)}\mathbf{B}_2(\Phi) \, {}_{(\ell)}\boldsymbol{\Upsilon}_2 \Big) \, [N_J \mathfrak{I}_5] \, dS \in \mathrm{R}^{5\times 5} \, . \end{aligned}} \tag{3.63}$$

The tangent material stiffness matrix is obtained from (3.54) to yield

$$\boxed{{}_{(\ell)}\mathbf{K}^{m}_{IJ} = \int\limits_{\mathfrak{L}} \Big\{ {}_{(\ell)}\Xi(\Phi) \, [N_I \mathfrak{I}_5] \Big\}^T \, {}_{(\ell)}\boldsymbol{\Lambda} \, {}_{(\ell)}\boldsymbol{\mathcal{C}} \, {}_{(\ell)}\boldsymbol{\Lambda}^T \, {}_{(\ell)}\Xi(\Phi) \, [N_J \mathfrak{I}_5] \, dS \in \mathrm{R}^{5\times 5} \, .} \tag{3.64}$$

Finally, the residual matrix $\mathbf{r} = \{\mathbf{r}_I\} \in \mathrm{R}^{5n\times 1}$ in (3.59) is obtained from (3.29) to yield

$$\boxed{\mathbf{r}_I = \sum_{\ell=1}^{3} {}_{(\ell)}\mathbf{F}_I - \overline{\mathbf{F}}_I \in \mathrm{R}^{5\times 1} \, ,} \tag{3.65}$$

where the internal (generalized) force ${}_{(\ell)}\mathbf{F}_I$ of layer (ℓ) is computed from (3.5), (3.11), or (3.19) so that

$$\boxed{{}_{(\ell)}\mathbf{F}_I = \int\limits_{\mathfrak{L}} \Big\{ {}_{(\ell)}\Xi(\Phi) \, [N_I \mathfrak{I}_5] \Big\}^T \, {}_{(\ell)}\mathbf{f}_c(\Phi) \, dS \in \mathrm{R}^{5\times 1} \, ,} \tag{3.66}$$

and the assigned (generalized) force $\overline{\mathbf{F}}_I$ is computed from (3.27) so that

$$\boxed{\overline{\mathbf{F}}_I = \int\limits_{\mathfrak{L}} N_I \overline{\boldsymbol{\mathcal{F}}} dS + \big[N_I \overline{\boldsymbol{\mathcal{F}}} \big]_{S=0}^{S=L} \in \mathrm{R}^{5\times 1} \, .} \tag{3.67}$$

CHAPTER 4
NUMERICAL EXAMPLES

The finite-element formulation for geometrically-exact sandwich beams presented in Section 3.3 has been implemented in the Finite Element Analysis Program (FEAP), developed by R.L. Taylor (see Zienkiewicz and Taylor [1989]), and run on a DEC 5000 with the Ultrix 4.2 operating system. The finite element basis functions used in the examples in this section are linear or quadratic. To avoid shear locking, uniform reduced integration is used to evaluate the tangent stiffness matrix (3.60) and the residual matrix (3.65).

4.1. Verification of FE Implementation with Single-Layer Beam

To check the correctness of the formulation and the implementation, we consider the case where the outer layers of the sandwich beam element are nonexistent, and compare the results to those from a single-layer beam theory: The results must be identically the same for the implementation to be correct. To do so, we simply set the material constants of the outer layers of sandwich beam elements to zero. We select the following material constants

$$ {}_{(\ell)}EA = 0, \ \ {}_{(\ell)}GA_s = 0, \ {}_{(\ell)}EI = 0, \text{ for } \ell = 1, 3 \, , \tag{4.1} $$

$$ {}_{(2)}EA = 2, \ \ {}_{(2)}GA_s = 2, \ {}_{(2)}EI = 2 \, . \tag{4.2} $$

Consider a cantilever beam of length $L = 1$, and having the above material constants. Linear basis functions are used for the discretization. Two loading tests are performed. In the first test, 5 linear sandwich beam elements are used, and the beam is subjected to a transverse tip load of $P = 0.1$. A transverse tip displacement of 0.067 is obtained, and corresponds exactly to the theoretical results using linear Timoshenko beam theory. In the second loading test, we subject the cantilever beam to a pure bending by applying a moment of $M = 12.566 \approx 4\pi$ at the beam tip to force the beam to roll up into an exact circle (see Vu-Quoc [1986]). In this case, the beam tip is displaced to coincide exactly with the clamped end, with a displacement having a component of -1 along the beam length, a zero transverse component, and a rotation of $2\pi\ rad$; the numerical results are very close to the exact results:[9]

u^1	u^2	${}_{(2)}\theta$
−1.00003	2.92110E−09	6.28300

Figure 4.1 depicts the deformed shape as a pentagon because linear elements are used; the nodes lie exactly on the circle circumscribing the pentagon. Convergence to the deformed shape shown is obtained in 2 iterations; the same rate of convergence was obtained for single-layer beams in Simo and Vu-Quoc [1986*b*] and Vu-Quoc [1986]. It should be noted, however, that such rapid rate of convergence is obtained only when we set ${}_{(\ell)}EA = {}_{(\ell)}GA_s = {}_{(\ell)}EI$ as in (4.2). In other words, with $EA \neq GA_s \neq EI$, a higher number of iterations to convergence is expected. Indeed, with the material properties $EA = 5$, $GA_s = 1$, $EI = 2$, we need 8 iterations to converge, but the converged result is identical to the case where ${}_{(\ell)}EA = {}_{(\ell)}GA_s = {}_{(\ell)}EI$ as in (4.2) above. We now have demonstrated that the present sandwich-beam element contains the single-layer beam element as a particular case.

4.2. Sandwich Beam with Identical Layers

Consider a cantilever sandwich beam with three identical layers subjected to assigned end moments as shown in Figure 4.2. Thus let ${}_{(\ell)}EA = EA$, ${}_{(\ell)}GA_s = GA_s$,

---

[9] All rotations are given in radians.

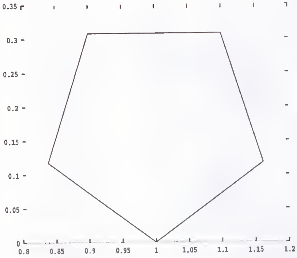

Figure 4.1. *Verification of FE implementation.* "Sandwich" beam having only core layer (2), with layers (1) and (3) inexistent. Roll-up maneuver. Comparison with single-layer beam.

${}_{(\ell)}EI = EI$, for $\ell = 1, 2, 3$. The cantilever boundary conditions at $S = 0$ are

$$u^1(0) = u^2(0) = {}_{(1)}\theta(0) = {}_{(2)}\theta(0) = {}_{(3)}\theta(0) = 0 \,. \tag{4.3}$$

4.2.1. Normal moment distribution

A sandwich beam will behave as a single-layer beam when the rotations in the three layers are constrained to be the same so that the overall beam cross section remains plane in the deformed configuration, i.e.,

$${}_{(1)}\theta = {}_{(2)}\theta = {}_{(3)}\theta = \theta \,. \tag{4.4}$$

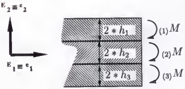

Figure 4.2. *Sandwich beam with identical layers.* Assigned layer moments at beam tip.

In a force-driven problem, the above constraint is not applied explicitly, but an appropriate distribution of assigned layer moments must be applied to keep the layer rotations to be the same as in (4.4). To find such moment distribution, we begin by computing the tangent material stiffness matrix of a cantilever sandwich beam with one *linear* element according to (3.64). There are thus five dof's at the beam tip. Let $\theta_o = 0$ so that ${}_{(\ell)}\Lambda = \mathfrak{I}_3$, for $\ell = 1, 2, 3$.[10] Thus, since

$$\Delta\mathbf{\Phi}(S) = \mathbf{d}N(S) \in \mathrm{R}^{5\times 1}\,, \quad \mathbf{w}(S) = \mathbf{c}N(S) \in \mathrm{R}^{5\times 1}\,, \tag{4.5}$$

where $\mathbf{d} \in \mathrm{R}^{5\times 1}$ contains the two displacement components and three layer rotations at the beam tip in the same order as in (2.8), and $N(\cdot)$ is a *linear* basis function. The tangent material stiffness matrix (3.64) becomes

$$\mathbf{K}^m = \sum_{\ell=1}^{3} \int_{\mathfrak{L}} \left\{ {}_{(\ell)}\Xi(\mathbf{\Phi})\,[N\mathfrak{I}_5] \right\}^T {}_{(\ell)}\boldsymbol{\mathcal{C}}\; {}_{(\ell)}\Xi(\mathbf{\Phi}) N\mathfrak{I}_5 \, dS \tag{4.6}$$

$$= \int_{\mathfrak{L}} \begin{bmatrix} 3EA\,(N_{,S})^2 & 0 & EAh\,(N_{,S})^2 & 0 & -EAh\,(N_{,S})^2 \\ 0 & 3GA_s\,(N_{,S})^2 & -GA_sNN_{,S} & -GA_sNN_{,S} & -GA_sNN_{,S} \\ EAh\,(N_{,S})^2 & -GA_sNN_{,S} & K_{33} & EAh^2\,(N_{,S})^2 & 0 \\ 0 & -GA_sNN_{,S} & EAh^2\,(N_{,S})^2 & K_{44} & EAh^2\,(N_{,S})^2 \\ -EAh\,(N_{,S})^2 & -GA_sNN_{,S} & 0 & EAh^2\,(N_{,S})^2 & K_{55} \end{bmatrix}_{5\times 5} dS\,, \tag{4.7}$$

---

[10] See (3.61) for the definition of $\mathfrak{I}_3$. Here, we can ignore the superscript (i) related to Newton's iterative solution process.

where

$$K_{33} = K_{55} \;\; := EAh^2 \left(N_{,S}\right)^2 + GA_s N^2 + EI \left(N_{,S}\right)^2 \,, \tag{4.8}$$

$$K_{44} \;\; := 2EAh^2 \left(N_{,S}\right)^2 + GA_s N^2 + EI \left(N_{,S}\right)^2 \,. \tag{4.9}$$

We assume the beam has unit width, then

$$EAh^2 = 2Eh^3, \quad EI = \frac{2}{3}Eh^3. \tag{4.10}$$

Let the tip forces and moments be gathered in

$$\mathbf{F} = \left\{F^1,\ F^2,\ {}_{(1)}M,\ {}_{(2)}M,\ {}_{(3)}M\right\}^T = \mathbf{K}^m\mathbf{d}\,. \tag{4.11}$$

For pure bending problems, such as the roll-up maneuver presented in Figure 4.1, shear deformation is absent. Thus to find the distribution of moments that replicates the conditions of pure bending in single-layer beams, we set tip displacements to zero (as if the tip is simply-supported) and the layer rotations at the beam tip to be the same as in (4.4), i.e.,

$$\mathbf{d} = \{0,\ 0,\ \theta,\ \theta,\ \theta\}^T \,. \tag{4.12}$$

Consider the beam element as having *unit length.* Then from (4.7), (4.10) and (4.11) with $GA_S = 0$, we have the following moment distribution that makes the sandwich beam behaving as a single-layer beam

$${}_{(1)}M = {}_{(3)}M \;\; = \frac{14}{3}Eh^3\theta\,, \tag{4.13}$$

$${}_{(2)}M \;\; = \frac{26}{3}Eh^3\theta\,. \tag{4.14}$$

Such moment distribution is referred to as the *normal* moment distribution *for sandwich beam with three identical layers.* It can be verified that

$${}_{(1)}M + {}_{(2)}M + {}_{(3)}M = E\frac{(6h)^3}{12}\theta = EI_{total}\theta\,, \tag{4.15}$$

i.e., the sandwich beam with the moment distribution (4.13), and (4.14) has the same bending stiffness as the single-layer beam. The normal moment distribution will be used in the roll-up of cantilever sandwich beams presented below.

Remark 4.1. If we assume that $GA_S = 0$, and make use of (4.4) and (4.7), then the equations in (4.11) that are related to the moments can be written as

$$\int_{\mathfrak{L}} (N,_S)^2 \, dS \begin{bmatrix} EAh^2 + EI & EAh^2 & 0 \\ EAh^2 & 2EAh^2 + EI & EAh^2 \\ 0 & EAh^2 & EAh^2 + EI \end{bmatrix}_{3\times 3} \begin{Bmatrix} \theta \\ \theta \\ \theta \end{Bmatrix} = \begin{Bmatrix} {}_{(1)}M \\ {}_{(2)}M \\ {}_{(3)}M \end{Bmatrix}, \tag{4.16}$$

i.e., the item $\int_{\mathfrak{L}} (N,_S)^2 \, dS$ can be extracted out as a common factor. By using (4.10) in (4.16), we can conclude that the normal distribution of moment

$${}_{(1)}M : \ {}_{(2)}M : \ {}_{(3)}M := 7 : 13 : 7 \tag{4.17}$$

is not depend on the choice of the shape function N. ∎

4.2.2. Assigned moment on core layer only

For the same linear sandwich beam with one end clamped and one end simply

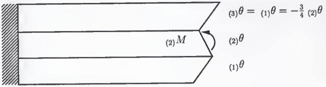

${}_{(3)}\theta = {}_{(1)}\theta = -\frac{3}{4}\,{}_{(2)}\theta$
${}_{(2)}M$
${}_{(2)}\theta$
${}_{(1)}\theta$

Figure 4.3. *Sandwich beam with identical layers.* Moment assigned to core layer only, and distribution of layer rotations in the *linear* case.

supported as in Section 4.2.1, consider now the case where only the moment assigned on the core layer (2) exists, i.e.,

$${}_{(1)}M = 0, \ {}_{(2)}M \neq 0, \ {}_{(3)}M = 0 \, . \tag{4.18}$$

Then from (4.11), we obtain the following layer rotations

$${}_{(1)}\theta = {}_{(3)}\theta = -\frac{9}{20}\frac{{}_{(2)}M}{Eh^3}, \tag{4.19}$$

$${}_{(2)}\theta = \frac{3}{5}\frac{{}_{(2)}M}{Eh^3}, \tag{4.20}$$

as shown in Figure 4.3. The computer implementation has been verified against the above analytical results.

4.2.3. Assigned axial force on core layer

Consider now a cantilever sandwich beam having identical layers with half-layer thickness $h = 0.001$, and with equal length $L = 1$. The beam is subjected to an assigned axial force $F^1 = 3$ at the tip (all other components of $\mathbf{F}$ in (4.11) are zero); the force acts on the centroidal line of the core layer by virtue of the formulation of the present theory. The material properties are

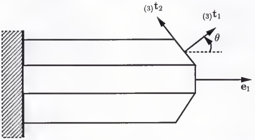

Figure 4.4. *Sandwich beam with identical layers.* Applied axial force at core layer. Deformed shape.

$$_{(\ell)}EA = 2, \quad _{(\ell)}GA_s = 2, \quad _{(\ell)}EI = 2 \,, \text{ for } \ell = 1, 2, 3 \,. \tag{4.21}$$

The beam is discretized using 5 linear elements. The displacements and rotations at the beam tip are given below.

$u^1(1)$	$u^2(1)$	$_{(1)}\theta(1)$	$_{(2)}\theta(1)$	$_{(3)}\theta(1)$
5.00000E−01	−7.91110E−21	−3.44091E−04	−6.15256E−21	3.44091E−04

It is observed from the numerical results that the axial displacement is the same as that in an equivalent single-layer beam with axial stiffness $3EA = 6$ (i.e., $\frac{F^1}{3EA} = 0.5$), while the two outer layers have non-zero, symmetric rotations. Such observation can be explained by looking at the first equation of (4.11), at $S = 1$

$$F^1 = 3EA\,(N_{,S})^2\,u^1(1) + EAh\,(N_{,S})^2\left[\,{}_{(1)}\theta(1) - {}_{(3)}\theta(1)\right] , \tag{4.22}$$

obtained with the aid of (4.7). In (4.22), it can be seen that the contribution of the outer rotations ${}_{(1)}\theta$ and ${}_{(3)}\theta$ (values from the table above) to the axial force $F^1 = 3$ is of order

$$EAh\,(N_{,S})^2\;{}_{(1)}\theta \approx (2)(0.002)(1)(3\times 10^{-4}) = \mathcal{O}(10^{-6}) , \tag{4.23}$$

and is thus negligible in front of the contribution of the axial displacement u^1 (value from the table above) of order

$$3EA\,(N_{,S})^2\,u^1(1) \approx (3)(2)(1)^2(0.5) = 3 . \tag{4.24}$$

When the outer layer rotations are not small, or when the beam is thick, the axial displacement will not be the same as that in an equivalent single layer beam, as shown below. Let the beam now have a thickness parameter of $h = 0.05$ (i.e., 50 times thicker than in the above example), and with the same material properties as in (4.21). The displacements and rotations at the beam tip are now

$u^1(1)$	$u^2(1)$	${}_{(1)}\theta(1)$	${}_{(2)}\theta(1)$	${}_{(3)}\theta(1)$
5.00545E−01	7.80458E−20	−1.71837E−02	1.73529E−19	1.71837E−02

Furthermore, if we increase the depth of the beam by another 10 times, i.e., $h = 0.5$, we obtain the following results

$u^1(1)$	$u^2(1)$	${}_{(1)}\theta(1)$	${}_{(2)}\theta(1)$	${}_{(3)}\theta(1)$
5.48942E−01	2.03216E−18	−1.54095E−01	1.09290E−18	1.54095E−01

It can be seen clearly that the axial tip displacement $u^1(1)$ of the sandwich beam is not the same as that of a single-layer beam with an equivalent axial stiffness, due to the coupling between $u^1(1)$ and the outer-layer rotations ${}_{(\ell)}\theta$, for $\ell = 1, 3$, as shown in Figure 4.4. This coupling becomes important as the beam thickness increases as shown in the numerical results above.

4.2.4. Reduced equations of equilibrium

We now develop the reduced nonlinear equations of equilibrium for a sandwich beam under tip axial loading. By symmetry of the problem, we have only *two* unknown kinematic quantities, the axial displacement u^1 and the outer-layer rotation ${}_{(1)}\theta = -\ {}_{(3)}\theta$, since $u^2 = \ {}_{(2)}\theta = 0$. Hence the 5 equilibrium equations are reduced to 2 equations for u^1 and ${}_{(3)}\theta$.

The reduced equations of equilibrium for this particular case are as follows: From the first equation in (2.1), and since $\mathbf{E}_1 = \mathbf{e}_1$ and $u^2 = 0$, we obtain

$$ {}_{(2)}\mathbf{\Phi}_0(S) = (S + u^1)\mathbf{e}_1 \ . \qquad (4.25)$$

Also since ${}_{(2)}\mathbf{t}_1 = \mathbf{e}_1$ and ${}_{(2)}\mathbf{t}_2 = \mathbf{e}_2$, and using (2.5) and (2.2), we obtain

$$ {}_{(3)}\mathbf{\Phi}_0 = \left(S + u^1{}_{,S} - h \sin\ {}_{(3)}\theta\right)\mathbf{e}_1 + h\left(1 + \cos\ {}_{(3)}\theta\right)\mathbf{e}_2 \ . \qquad (4.26)$$

Now from (2.3), it follows that

$$ {}_{(3)}\boldsymbol{\gamma} = \left(1 + u_{,S} - h\ {}_{(3)}\theta_{,S} \cos\ {}_{(3)}\theta - \cos\ {}_{(3)}\theta\right)\mathbf{e}_1 - \sin\ {}_{(3)}\theta \left(1 + h\ {}_{(3)}\theta_{,S}\right)\mathbf{e}_2 \ , \qquad (4.27)$$

which then yields the expression

$$ {}_{(3)}\mathbf{n} = 2\left(1 + u_{,S} - h\ {}_{(3)}\theta_{,S} \cos\ {}_{(3)}\theta - \cos\ {}_{(3)}\theta\right)\mathbf{e}_1 - 2\sin\ {}_{(3)}\theta \left(1 + h\ {}_{(3)}\theta_{,S}\right)\mathbf{e}_2 \ , \qquad (4.28)$$

by virtue of relation (2.4) and the material properties (4.21). Similarly, the resultant contact force for the layer (1) takes the form

$$ {}_{(1)}\mathbf{n} = 2\left(1 + u_{,S} - h\ {}_{(3)}\theta_{,S} \cos\ {}_{(3)}\theta - \cos\ {}_{(3)}\theta\right)\mathbf{e}_1 + 2\sin\ {}_{(3)}\theta \left(1 + h\ {}_{(3)}\theta_{,S}\right)\mathbf{e}_2 \ . \qquad (4.29)$$

It is easy to see from (4.25) that

$$ {}_{(2)}\mathbf{n} = 2u,_S \, \mathbf{e}_1 \; . \tag{4.30}$$

Now from first equation in (2.10), we obtain the equilibrium equation for the axial force

$$\boxed{6u,_S + 4\left(1-\cos\,{}_{(3)}\theta\right) - 4h\,{}_{(3)}\theta,_S \cos\,{}_{(3)}\theta = 3\,,} \tag{4.31}$$

while the fourth equation in (2.10) yields the equation of equilibrium for the outer-layer moment

$$\boxed{\left(1+h^2\right)\,{}_{(3)}\theta,_{SS} - hu,_{SS}\cos\,{}_{(3)}\theta - 2\left(1+u,_S\right)\sin\,{}_{(3)}\theta = 0\,.} \tag{4.32}$$

The boundary conditions are given as follows

$$\boxed{\begin{array}{lll} \text{At S} = 0, & u^1(0) = 0\,, & {}_{(3)}\theta(0) = 0\,, \\ \text{At S} = 1, & u^1,_S(1) = \dfrac{F^1}{EA} = 0.5\,, & {}_{(3)}\theta,_S(1) = 0\,. \end{array}} \tag{4.33}$$

An analytical solution to problem (4.31)–(4.33) can be developed using an iterative procedure as follows. First assume that u^1 is the same as the axial displacement u^1_0 of a linear single-layer beam, and replace this solution in (4.32) to obtain an equation for ${}_{(3)}\theta_0$. Then solve for ${}_{(3)}\theta_0$, which is then replaced into (4.31) to solve for a more accurate solution for u^1_1. And so on so forth.

4.2.5. Assigned transverse force

Consider now a cantilever sandwich beam having identical layers with $h = 0.5$, and with equal length $L = 200$. The beam is subjected to an assigned transverse force $F^2 = 0.3$ at the tip (all other components of $\mathbf{F}$ in (4.11) are zero); the force acts on the centroidal line of the core layer. The material properties are

$$ {}_{(\ell)}EA = 240,000, \;\; {}_{(\ell)}GA_s = 200,000, \;\; {}_{(\ell)}EI = 20,000\;, \text{ for } \ell = 1,2,3\,. \tag{4.34}$$

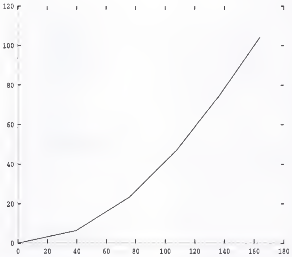

Figure 4.5. *Sandwich beam with identical layers.* Assigned transverse force at beam tip. Large deformation.

The beam is discretized using 5 linear elements. With the above properties and assigned force, the deformation is small. The transverse displacement of the beam tip of an equivalent single-layer Euler-Bernoulli beam with bending stiffness $EI = 20,000 \times 27$ is 1.48148, whereas the computed value is 1.44678 (or a relative error of 2.4%). The layer rotations at the tip are

${}_{(1)}\theta$	${}_{(2)}\theta$	${}_{(3)}\theta$
0.0111114	0.0111108	0.0111114

It can be observed that even though the layer rotations are not perfectly equal (the relative error is very small), the outer-layer rotations are equal. The assumption of equal outer-layer rotations is often made to simplify the formulation (less number of unknowns) as in Yu [1959*a*]. Thus, a long sandwich beam behaves similarly to a single-layer beam; the local effects due to the presence of the layers are negligible, and this can be explained by Saint-Venant's principle. Such will not be the case for short beams as will be illustrated below.

The above results are for small deformation. We now increase the assigned transverse force to $F^2 = 30$ to produce large deformation in the sandwich beam. The displacements and layer rotations at the tip are

u^1	u^2	${}_{(1)}\theta$	${}_{(2)}\theta$	${}_{(3)}\theta$
−36.0783	104.181	0.839639	0.839592	0.839658

The above results are close to those obtained from an equivalent single-layer geometrically-exact beam with material properties

$$EA = 240,000 \times 3, \; GA_s = 200,000 \times 3, \; EI = 20,000 \times 27 \qquad (4.35)$$

as given below

u^1	u^2	θ
−36.0781	104.180	0.839623

The deformed shape is shown in Figure 4.5. For both cases (sandwich beam and single-layer beam), it takes 12 iterations in the Newton solution process to converge to the solution as shown in the table below.

Iteration Number	Euclidean Norm of Residual
0	0.3000000E+02
1	0.6055829E+07
2	0.8571570E+05
3	0.1340028E+05
4	0.1449196E+04
5	0.2375566E+05
6	0.3230652E+03
7	0.4572836E+04
8	0.1172864E+03
9	0.2590801E+04
10	0.4400550E+01
11	0.3232107E+01
12	0.7529341E−04

4.2.6. Roll-up maneuver with normal moment distribution

We now apply the *normal* moment distribution for a cantilever sandwich beam with the following ratio ${}_{(1)}M\colon\ {}_{(2)}M\colon\ {}_{(3)}M = 7\colon 13\colon 7$ as derived in Section 4.2.1 (see (4.13)–(4.14) and (4.17) in Remark 4.1).

Remark 4.2. In fact, it can be shown easily that the ratio (4.17) is independent of the shape function used and of the beam length, as see in Vu-Quoc and Deng [1995*a*]. ▮

The layer half-thickness is chosen to be

$$h = 0.01732 \approx 0.01\sqrt{3}\,. \tag{4.36}$$

The material properties are as follows

$${}_{(\ell)}EA = 2,000,000,\ \ {}_{(\ell)}GA_s = 2,000,000,\ \ {}_{(\ell)}EI = 200\,,\ \text{for}\ \ell = 1,2,3\,, \tag{4.37}$$

thus making the total bending stiffness equivalent to a single-layer beam to be

$$EI_{total} = 27EI = 5,400\,. \tag{4.38}$$

The beam is discretized using 5 linear sandwich elements. A cantilever beam subjected to assigned moment M at the free end will undergo pure bending; the deformed shape will be that of an arc of a circle of radius

$$R = \frac{EI_{total}}{M}\,, \tag{4.39}$$

depending on the magnitude of the assigned moment. Thus to have the beam of length $L = 1$ rolled up into one full circle, the radius will be

$$R = \frac{L}{2\pi}\,, \tag{4.40}$$

and the desired total moment will be

$$M = EI_{total}\frac{2\pi}{L} . \tag{4.41}$$

Thus using the ratio (4.17), the distribution of the total moment M over three layers of the sandwich beam is

$$_{(1)}M = {}_{(3)}M \;\; = \tfrac{7}{27}M = 8,796.46 , \tag{4.42}$$

$$_{(2)}M \;\; = \tfrac{13}{27}M = 16,336.28 . \tag{4.43}$$

It takes 2 iteractions to converge to reach the final deformed shape (i.e., the full circle), with the convergence results shown in the table below.

Iteration Number	Euclidean Norm of Residual
0	0.2053363E+05
1	0.4412925E+08
2	0.3051970E−02

The tip displacements of the sandwich beam are

u^1	u^2	$_{(1)}\theta$	$_{(2)}\theta$	$_{(3)}\theta$
−0.999999	−2.15292E−09	6.28319	6.28319	6.28319

Note that the beam tip moved back to coincide with the cantilever end, with a horizontal displacement of 1 and a vertical displacement zero,[11] and the cross section rotates by 6.28319 ≈ $2\pi \; rad$. Using an equivalent single-layer beam with the same bending stiffness as in (4.38), and the same total assigned moment as in (4.41), the converged tip displacements and rotation, obtained with 2 iterations as in Simo and Vu-Quoc [1986*b*], are given below

u^1	u^2	θ
−1.00000	1.25011E−15	6.28319

---

[11] There are round-off errors.

The deformed shape (a pentagon), given in Figure 4.1, is exactly the same as that of the single-layer beam. Despite the presence of three layers in the sandwich beam and the more complex system of equations, the rate of convergence is the same as that of the single-layer beam.

4.2.7. Roll-up maneuvers: Saint-Venant principle

We now solve a series of roll-up maneuver problems with different distribution of moments, the results of which will provide an illustration of Saint-Venant principle. The material properties and half layer-thickness selected are

$$EA = 2,000,000,\ GA_s = 700,000,\ EI = 200,\ h = 0.01732051 = 0.01\sqrt{3}\,. \quad (4.44)$$

4.2.7.1. Long beam

First, a long sandwich beam with $L = 10$ is considered. Appropriate moments will be assigned at the beam tip so that the sandwich beam is rolled up into a full circle. The total thickness of the beam

$$6h \approx 0.104 \quad (4.45)$$

is very *small* compared to the radius of the circle of the deformed shape

$$R = \frac{L}{2\pi} = 1.592\,. \quad (4.46)$$

In this case, the distribution of the total assigned tip moment among the layers has negligible effects on the deformed shape; in other words, Saint-Venant principle cannot be illustrated with this choice of geometry. To obtain a smoother figure of the circular deformed shape, we use 40 linear sandwich elements.[12] Three calculations are performed with three different moment distributions having the same resultant $M = 3,392.92$ computed using (4.41): (i) normal distribution, (ii) concentrated moment on core layer ${}_{(2)}M = M$, (iii)

---

[12] Recall the pentagonal deformed shape in Figure 4.1, obtained with 5 linear elements.

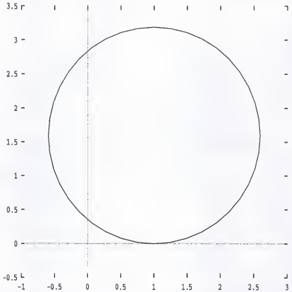

Figure 4.6. *Sandwich beam with identical layers.* Roll-up maneuver. Beam length $L = 10$, total thickness $6h = 0.104$. Results for 3 moment distributions: (i) normal, (ii) ${}_{(2)}M = M$, (iii) ${}_{(3)}M = M$.

concentrated moment on top layer ${}_{(3)}M = M$. We do not have the same rapid convergence (i.e., 2 iterations with 1 loading step) as obtained in Section 4.1. The full load M, in all three cases, is divided into 10 steps with an increment of $\frac{M}{10}$. For each loading step, the computation takes an average about 12 iterations to converge. The convergence results in terms of residual norm for the $10th$ load step for the 3 cases of moment distribution are

Iteration number vs. residual norm
Normal moment distribution; 10th load step

Iteration Number	Euclidean Norm of Residual
0	0.2053363E+03
1	0.1173036E+07
2	0.5707052E+05
3	0.1648645E+06
4	0.3985817E+04
5	0.1866985E+06
6	0.9028812E+03
7	0.3409209E+04
8	0.1437554E+01
9	0.2722030E+03
10	0.4444039E−02
11	0.4325145E−02

given below.

Iteration number vs. residual norm
Moment on layer (2); 10th load step

Iteration Number	Euclidean Norm of Residual
0	0.3392920E+03
1	0.1171357E+07
2	0.5670319E+05
3	0.1631370E+06
4	0.3996060E+04
5	0.1838174E+06
6	0.8672319E+03
7	0.2959335E+04
8	0.1338442E+01
9	0.2029514E+03
10	0.3593026E−02
11	0.2375995E−02

Iteration number vs. residual norm
Moment on layer (3); 10th load step

Iteration Number	Euclidean Norm of Residual
0	0.3392920E+03
1	0.1181360E+07
2	0.5766325E+05
3	0.1776548E+06
4	0.3906623E+04
5	0.2101669E+06
6	0.1228777E+04
7	0.1146405E+05
8	0.3287691E+01
9	0.2549532E+04
10	0.1278831E−01
11	0.9167536E−01
12	0.9660165E−07

The deformed shape is depicted in Figure 4.6. The displacements and layer rotations at the beam tip are[13]

${}_{(\ell)}M = M$	Displacements & Rotations				
$\ell =$	u^1	u^2	${}_{(1)}\theta$	${}_{(2)}\theta$	${}_{(3)}\theta$
normal	−9.99999	−2.38251E−10	6.28319	6.28319	6.28319
2	−9.99998	5.31921E−04	6.18130	6.39316	6.18127
3	−9.99882	5.36146E−04	6.27634	6.18246	6.47592

It should be noted that the convergence rate is influenced by the magnitude of the shear stiffness. In the above example, if we increase the shear stiffness to $GA_s = 1,200,000$ (as used in the next example for short beams), then it will take an average of 10 iterations to converge.

4.2.7.2. Short beam

Next, to illustrate the effects of non-normal moment distributions and therefore Saint-Venant principle, we consider a beam with *unit* length $L = 1$, i.e., the beam is now

---

[13] where "ℓ =normal" means normal distribution of moments in the sense of (4.42)–(4.43).

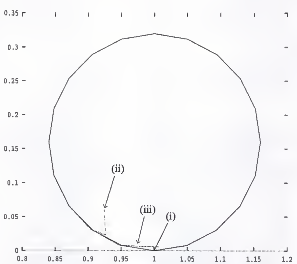

Figure 4.7. *Sandwich beam with identical layers.* Roll-up maneuver. Beam length $L = 1$, total thickness $6h = 0.104$. Saint-Venant principle. Effects of moment distributions at beam tip: (i) normal, (ii) ${}_{(2)}M = M$, (iii) ${}_{(3)}M = M$.

ten times shorter than the one in Section 4.2.7.1, with material properties[14]

$$EA = 2,000,000,\ GA_s = 1,200,000,\ EI = 200,\ h = 0.01732051 = 0.01\sqrt{3}\,. \tag{4.47}$$

The beam will be subjected to an assigned moment that would make a single-layer beam roll up into a full circle of radius

$$R = \frac{L}{2\pi} = 0.1592\,, \tag{4.48}$$

which is of the same order as the total beam thickness of $6h = 0.104$. For such a short beam, remarkable effects due to different non-normal moment distributions will be clearly seen in the deformation near the beam tip. Again, three types of moment distributions as used in Section 4.2.7.1 are studied. The beam is discretized using 20 linear elements. For all cases of moment distributions, we use 10 load steps of equal increments to reach the full moment $M = 33929.20$ computed by using (4.38) and (4.41); each load step takes about 5 iterations to converge. Recall that in the previous case of a long beam, each load step takes about 12 iterations to converge; the reason is because in the present example, we use a higher value of shear stiffness (almost twice). Indeed, for the roll up problems, convergence is achieved faster for beams with higher shear stiffness. The displacements and layer rotations at the beam tip are now given for three cases of moment distribution

---

[14] Note that only the value for GA_s is different from the one in (4.44).

${}_{(\ell)}M = M$	Displacements & Rotations				
$\ell =$	u^1	u^2	${}_{(1)}\theta$	${}_{(2)}\theta$	${}_{(3)}\theta$
normal	-0.999999	$-1.93779\text{E}{-09}$	6.28319	6.28319	6.28319
2	-1.07561	$6.01950\text{E}{-02}$	7.47542	8.82463	1.67826
3	-0.993617	$5.77551\text{E}{-03}$	6.23661	5.80239	7.33838

The deformed shapes corresponding to the three moment distributions are given in Figure 4.7, where the effects of non-normal distribution can be seen near the beam tip. However, such effects diminish rapidly as one moves away from the beam tip, and the three deformed shapes merge into one. This observation is consistent with Saint-Venant principle. The case with concentrated moment applied at the core layer yields the most prominent effects at the beam tip (see Figure 4.7). In the next example, we will use a discretization with a refined mesh near the beam tip to obtain a better deformed shape, and plot the layer rotations versus the axial coordinate S to show the occurrence of a bifurcation near the tip.

Next, we consider an even shorter beam with $L = 0.75$, keeping the same value of layer half thickness $h = 0.01\sqrt{3}$, thus decreasing the radius of the full circle of deformed shape to

$$R = \frac{L}{2\pi} = 0.1194 \,, \tag{4.49}$$

which is very close to the total beam thickness $6h = 0.104$. The total moment needed to roll the beam into a complete circle is now $M = 45,230.8$. The idea here is to see how far we can push the aspect ratio of the beam and still can perform the analysis. The

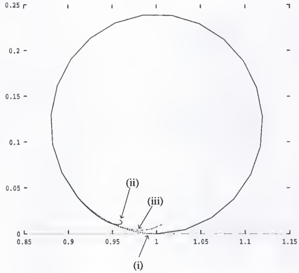

Figure 4.8. *Sandwich beam with identical layers.* Roll-up Maneuver. Beam length $L = 0.75$, total thickness $6h = 0.104$. Saint-Venant principle. Effects of moment distributions at beam tip: (i) normal distribution, (ii) ${}_{(2)}M = M$, applied moment on the layer (2), (iii) ${}_{(3)}M = M$, applied moment on the layer (3).

effects of Saint-Venant principle should be even stronger for shorter beams. The same three types of moment distribution as in Section 4.2.7.1 are assigned to the beam tip. As mentioned above, to obtain better accuracy and deformed shape near the beam tip in the case of concentrated moment applied at the core layer, the beam is discretized as follows: For $S \in [1, 1.65]$, a uniform discretization with 20 linear elements is used, and for $S \in [1.65, 1.75]$, a uniform discretization with 10 linear elements is used. Below are the convergence rate results for the last ($10th$) load step for the three cases of moment distribution; as noted, convergence is obtained in 5 iterations

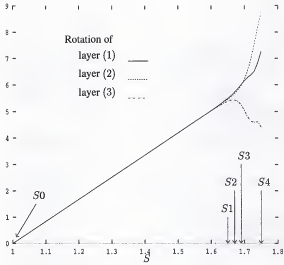

Figure 4.9. *Shorter sandwich beam with identical layers.* Roll-up Maneuver. Beam length $L = 0.75$, total thickness $6h = 0.104$. Concentrated moment assigned to core layer ${}_{(2)}M = M$. Bifurcation of layer rotations. Clamped end at $S = 1$ free end at $S = 1.75$.

Iteration number vs. residual norm
Normal moment distribution; 10th load step

Iteration Number	Euclidean Norm of Residual
0	0.2737817E+04
1	0.1224504E+07
2	0.1334027E+05
3	0.2294266E+04
4	0.3810224E+01
5	0.5732329E−02

Iteration number vs. residual norm
Moment on layer (2); 10th load step

Iteration Number	Euclidean Norm of Residual
0	0.4523892E+04
1	0.1719565E+07
2	0.2948932E+05
3	0.9726053E+04
4	0.3945345E+02
5	0.1903428E−01

Iteration number vs. residual norm
Moment on layer (3); 10th load step

Iteration Number	Euclidean Norm of Residual
0	0.4523892E+04
1	0.1734447E+07
2	0.9843020E+04
3	0.3006222E+04
4	0.2156821E+01
5	0.3720495E−02

We obtain the following displacements and layer rotations

${}_{(\ell)}M = M$	Displacements & Rotations				
$\ell =$	u^1	u^2	${}_{(1)}\theta$	${}_{(2)}\theta$	${}_{(3)}\theta$
normal	−0.750248	1.10700E−04	6.28319	6.28319	6.28319
2	−0.791437	1.50488E−02	7.25595	8.76131	4.40996
3	−0.744060	9.93078E−03	6.12431	5.96892	7.44478

The deformed shapes corresponding to each moment distribution is given in Figure 4.8. For the case of concentrated moment assigned at the core ${}_{(2)}M = M$, the bifurcation in the layer rotations can be seen clearly in Figure 4.9. In the interval $[1, 1.65]$, the three layer rotations take on very close values, i.e., the overall cross section remain close to a plane. From $S = 1.65$ on, i.e., near the beam tip, the three layer rotations begin to diverge sharply from each other. The outer layer rotations are also very different from each other as seen in Figure 4.10.

When the concentrated moment is applied on the lower layer (1), a singularity will develop at a certain magnitude of the applied moment, and thus will prevent numerical convergence and further deformation in the beam. The magnitude of the applied moment is increased from zero in increments of $\Delta\ {}_{(1)}M = 0.1M$, where $M = 45,230.8$ is the moment employed in the roll-up of the sandwich beam, for the first two steps, and from then on in increment of $\Delta\ {}_{(1)}M = 0.001M$ until non-convergence occurs at ${}_{(1)}M = 0.233M$ due to the development of the singularity in the deformed shapes (see Figure 4.11) as mentioned above. At ${}_{(1)}M = 0.232M$, i.e., just before the occurrence of the non-convergence, the convergence behavior is given in the table below.

Iteration Number	Euclidean Norm of Residual
0	0.4523892E+02
1	0.1591907E+04
2	0.8555221E+02
3	0.1244564E+01
4	0.1896584E−03

Figure 4.11 shows the deformed shape of the sandwich beam, from which we can see that the free tip of layer (1), where the applied moment is exerted, has been seriously distorted, and the distortion reduces quickly as one moves away from the free tip. The bifurcation in the layer rotations can be seen clearly in Figure 4.12, which is similar to Figure 4.9. In the interval $[1, 1.65]$, the three layer rotations take on very close values, i.e., the overall cross section remain close to a plane. From $S = 1.65$ on, i.e., near the free tip, the three layer rotations begin to diverge sharply from each other. A zoom-in plot of the tip of the deformed beam is given in Figure 4.13, where the two sandwich beam elements close to the beam tip are shown. It can be seen in Figure 4.13 that the bottom layer (1) is seriously distorted: Its cross section, initially perpendicular to its top fiber, now aligns with its deformed top fiber (which is the interface between layer (1) and layer (2)), such singularity in the deformed shape accounts for the non-convergence of the numerical solution for the next load step of ${}_{(1)}M = 0.233M$ as shown in the table

below.

Iteration Number	Euclidean Norm of Residual
0	0.4523892E+02
1	0.4877053E+04
2	0.5849041E+06
3	0.8682607E+05
⋮	⋮
18	0.2293493E+05
19	0.3882698E+04
20	0.3574932E+04

4.3. Two-layer Beams

An example of application of the present formulation to the important class of multilayer structures with ply drop-offs is now presented. A two-layer beam used in this section is depicted in Figure 4.20, where the top layer is shorter than the bottom layer by half, creating a ply drop-off. There is thus a sharp discontinuity in the cross section in the middle of the beam. The present example illustrates both the variability of the number of layers in the present multilayer beam element (since elements with two layers and elements with one layer are used to modeled the beam), and the ability to accommodate ply drop-offs naturally. The case with small deformation is analyzed in Zinno and Barbero [1994]. The following material properties are selected[15]

$$E = 29,000,\ \nu = 0.294,\ \chi = \frac{5}{6}\,, \tag{4.50}$$

for both layers, i.e.,

$${}_{(\ell)}EA = 14,500,\ \ {}_{(\ell)}GA_s = 5,602.8,\ \ {}_{(\ell)}EI = 302.1\,. \tag{4.51}$$

The beam has a length of $L = 5$, and a half-layer thickness $h = 0.25$.

4.3.1. Case without ply drop-off

To verify the modeling, we consider first the case without ply drop-off for which exact solution for small deformation exists. Thus, for now, the two layers have equal length $L = 5$. A transverse force $F^2 = 1$ is applied at the beam tip. Using the linear Timoshenko beam theory for an equivalent *single*-layer beam, we obtain a tip displacement of

---

[15] Young's modulus E, Poisson's ratio ν, shear coefficient χ such that $A_s = \chi A$.

$$u^2(L) = \frac{F^2 L^3}{3EI} + \frac{F^2 L}{GA_s} = 0.017775 \,, \tag{4.52}$$

as compared to a value of 0.01750 obtained in Zinno and Barbero [1994]. The two-layer beam is modeled using 20 linear sandwich-beam elements with core layers having zero height ($h = 0$) and zero material properties. In this case, with the core layer (2) having zero height, the top fiber of layer (1) coincides with the bottom fiber of layer (3); the deformation of the two-layer beam thus modelled is described by the top fiber of layer (1), together with the 2 layer rotations. The computed transverse tip displacement is 0.017766, i.e., a relative error of 0.05% compared to the equivalent single-layer Timoshenko beam, and 1.52% compared to Zinno and Barbero [1994]. The deformed shape is shown in Figure 4.15.

Remark 4.3. That there are three ways to model a two-layer beam using the proposed sandwich-beam element is yet another aspect of the versatility of the present formulation. Setting the height and the material properties of the core layer (2) to zero as done above is only one way: see Figure 4.14. One could conceivably do the same to layer (1) or to layer (3), i.e., setting the height and material properties to zero: see Figure 4.16 and Figure 4.17. But then when we consider the assigned force, these three ways of modelling actually correspond to three different loading conditions: Recall that by expressing the deformed centroidal lines of all layers relative to that of the core layer (2), the assigned force is always acted on the centroidal line of the core layer. Hence, as noted above, when layer (2) is inexistent, the assigned force is applied at the top fiber of layer (1), which coincides with the bottom fiber of layer (3). When layer (1) or layer (3) is inexistent, the assigned force is applied at the centroidal line of layer (2): See Figure 4.16 for the case where the drop-off occurs in layer (2). ■

4.3.2. Case with ply drop-off

Consider now the beam with a ply drop-off as shown in Figure 4.20. We will consider two loading cases: (i) Assigned transverse force at beam tip, and (ii) assigned tip moment.

4.3.2.1. Assigned transverse force

Again, a transverse force $F^2 = 1$ is applied at the tip. The displacement obtained from the use of the linear Timoshenko beam with *symmetric* ply the drop-off as shown in Figure 4.18 will serve as a reference for comparison. Unlike the multilayer theory, all sections in the linear Timoshenko beam, including the one at the symmetric drop-off, remain plane after deformation. The transverse tip displacement W_t of the linear Timoshenko beam is then given by

$$\begin{aligned} W_t &= W_d + \theta_d \bullet L_2 + W_r \\ &= \underbrace{\left[\frac{F^2(L_2)^3}{3EL_2} + \frac{F^2L_1(L_2)^2}{2EL_2} + \frac{F^2L_2}{GA_{s2}}\right]}_{W_d} + \underbrace{\left(\frac{F^2(L_2)^2}{2EL_2} + \frac{F^2L_1L_2}{EL_2} + \frac{F^2}{GA_{s2}}\right)}_{\theta_d} \bullet L_2 \\ &\quad + \underbrace{\left[\frac{F^2(L_1)^3}{3EL_1} + \frac{F^2L_1}{GA_{s1}}\right]}_{W_r} = 0.03393\,, \end{aligned} \tag{4.53}$$

where W_d and θ_d are respectively the transverse displacement and section rotation at the symmetric drop-off point, and W_r the transverse tip displacement relative to the drop-off point, $F^2 = 1$ the transverse tip force, and all other quantities are as explained in Figure 4.18. The finite element formulation for small-deformation multilayer structures by Zinno and Barbero [1994] yields a computed transverse displacement of 0.034846 for the two-layer beam with a ply drop-off at mid-span as shown in Figure 4.20. Using our formulation, we now model the beam in Figure 4.20 using 20 linear sandwich-beam elements with the layer (2) inexistent (as explained above), and with layer (3) removed from midspan ($S = 2.5$) to the beam tip ($S = 5$). The computed tip displacement, for our formulation and with the mentioned modeling of the ply drop-off, is 0.0354247. Figure 4.19 shows the comparison of the deformed shape of the beam with a ply drop-off with the deformed shape of the beam without the ply drop-off.

Remark 4.4. Unlike Remark 4.3 for beam *with* a ply drop-off, there are only *two* ways to model two-layer beams with a ply drop-off using the present sandwich-beam elements (see Figures 4.20 and 4.21). If the two-layer beam with a ply drop-off were modelled using layers (2) and (3), with layer (1) inexistent, and with layer (3) shorter than layer (2) by half (see Figure 4.21), then the transverse force F^2 at the beam tip would be applied on the centroidal line of layer (2). Note that point of application of the transverse force F^2 in Figure 4.20 is different from that in Figure 4.21. The eccentricity in Figure 4.20 will result in an assigned moment to the centroid of layer (1) as the beam deforms, in addition to the assigned force F^2, and therefore a larger transverse displacement. Indeed, using the modelling of the beam as described in Figure 4.21 (without eccentricity), we obtain a computed tip displacement of 0.0353380, which is smaller than the tip displacement of 0.0354247 obtained above.

Now if the two-layer beam with a ply drop-off were modelled using layers (1) and (2), with layer (3) inexistent, and with layer (2) shorter than layer (1) by half[16] (see Figure 4.22), then the transverse force F^2 at the beam tip is applied, not anywhere within layer (1), but on the extended centroidal line of layer (2). Such modelling leaves $(2.10)_3$ meaningless, i.e.,

$$_{(2)}h \; _{(1)}\mathbf{n}_{,S} \cdot {}_{(2)}\mathbf{t}_1 = 0 \; , \tag{4.54}$$

---

[16] By setting the material properties of layer (2) to zero, but leaving the thickness unchanged.

since for the ply drop-off part of layer (2) ($S \in [\frac{L}{2}, L]$), the applied moment ${}_{(2)}\overline{\boldsymbol{m}}$, the resultant force ${}_{(2)}\mathbf{n}$, and the moment ${}_{(2)}m_{,S}$ for layer (2), and the resultant force[17] ${}_{(3)}\mathbf{n}$ are all zero. Hence ${}_{(2)}h \neq 0$ is impossible for (4.54) to be satisfied. One way to overcome this problem is to set ${}_{(2)}h = 0$ for $S \in [\frac{L}{2}, L]$, i.e., after the drop-off point, thus making the top fiber of layer (1) a reference line within this portion. In this case, the overall reference line is no longer a straight line, but a discontinuous, piecewise constant line, because the reference line for $S \in [0, \frac{L}{2}]$ is the centroidal line of layer (2), while the reference line for $S \in [\frac{L}{2}, L]$ is the top fiber of layer (1). ∎

In summary, we now compare our results to those obtained using (i) the linear Timoshenko beam theory (Figure (4.18) with symmetric discontinuous variation of cross section as depicted in Figure (4.18)), and using (ii) the Zinno and Barbero [1994] formulation, and this for each geometry of the beam. For the two-layer beam *without* a ply drop-off, our results differ from the linear Timoshenko theory by 0.05%, and from Zinno and Barbero [1994] by 1.52%. For the two-layer beam *with* a ply drop-off, our results differ from the linear Timoshenko theory by 4.22%, and from Zinno and Barbero [1994] by 1.63%. The above comparison suggests that the Zinno and Barbero [1994] formulation is not accurate for the beam without a ply drop-off. On the other hand, for the beam with a ply drop-off, the results using the Timoshenko theory are clearly erroneous since the non-symmetry in the ply drop-off cannot be modelled, and also since the cross section at the drop-off point remains plane (i.e., cannot develop a hinge). As a consequence, the beam modelled using the linear Timoshenko theory is stiffer than our beam model. The same can be said for the Zinno and Barbero [1994] formulation, since the error between our results and Zinno and Barbero [1994]'s is only 1.63%.

Thus far, a unit transverse force $F^2 = 1$ is applied at the beam tip. To produce large deformation in the beam, the assigned force is increased to $F^2 = 100$. Shown in the table below are the computed results using the present sandwich-beam elements; compared to those obtained from using the single-layer geometrically-exact beam (i.e., nonlinear Timoshenko theory) to model beams with symmetric discontinuous variation of cross section[18] (see Figure 4.18):

---

[17] Because layer (3) is inexistent.

Beam	u^1	u^2	${}_{(1)}\theta$
Sandwich	-0.798692	-2.45561	-1.14239
Single-layer	-0.769361	-2.16970	-0.979568

As explained in Remark 4.3, the displacements u^1 and u^2 in the above table are those of the top fiber of layer (1), and the rotation ${}_{(1)}\theta$ is that of layer (1) cross section. Similar to the small deformation case, the (nonlinear) Timoshenko theory produces a stiffer model yielding smaller displacements.

4.3.2.2. Roll-up maneuver

We now consider a roll-up of the same two-layer beam with ply a drop-off modelled as in Figure 4.20, as used in Section 4.3.2.1, by assigning the moment ${}_{(1)}M$ at the tip of layer (1) with increasing magnitude. The loading is divided into 10 steps with equal increments of $m = 80.983$ for the moment ${}_{(1)}M$, such that at the 10th load step we have

$$ {}_{(1)}M = \frac{2\pi E I_1}{L_1} = 10 \times 80.983 \,, \tag{4.55} $$

which is the magnitude of the tip moment to make the thin half of the beam rolled into one full circle (see (4.41) in Section 4.2.6). The deformed shape is shown in Figure 4.23, where it can be seen that the thin half of the two-layer beam (i.e., layer (1)) is rolled up into a full circle, whereas the thicker half deformed into an arc of a circle. A zoom-in plot of the deformed beam in the neighborhood of the ply drop-off point is given in Figure 4.24, where the cross section at the drop-off point shows clearly a hinge. The cross section before the drop-off point also develops a hinge. For a beam with equal layers under assigned moment at its tip, there is no shear force at mid-span, and the cross section there remains plane (i.e., there is no hinge; see also Figure 4.10).[19] On the other hand, in the present example, shear force is introduced due to the ply drop-off. Figure 4.24 also shows a significant shear distortion in the bottom layer, just before the drop-off point. The typical convergence behavior is as described in the table below for the 10th load step.

---

[18] As in the linear Timoshenko beam, the cross section in the nonlinear Timoshenko beam at the drop-off point remains plane after deformation, and cannot develop a hinge. Thus, this is a single-layer beam with varying cross section.

Iteration number vs. residual norm
Moment on layer (3); 10th load step

Iteration Number	Euclidean Norm of Residual
0	0.8098300E+02
1	0.2856593E+04
2	0.1774659E+02
3	0.1678655E+01
4	0.1607245E−03

---

[19] Away from the beam tip, there is no Saint-Venant effect, and therefore the cross section must remain plane.

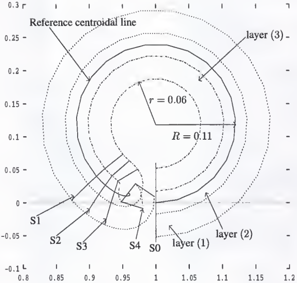

Figure 4.10. *Sandwich beam with identical layers.* Roll-up Maneuver. Beam length $L = 0.75$, total thickness $6h = 0.104$. Concentrated moment assigned to core layer ${}_{(2)}M = M$. $S0$ is the cross-section at the clamped end ($S = 1$); $S1$ is the cross-section at $S = 1.65$; $S2$ is the cross-section at $S = 1.67$; $S3$ is the cross-section at $S = 1.69$; $S4$ is the cross-section at $S = 1.75$(beam tip).

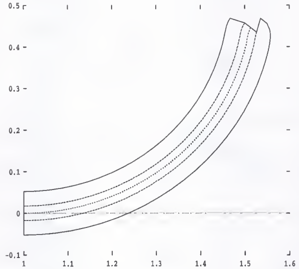

Figure 4.11. *Shorter sandwich beam with identical layers.* Beam length $L = 0.75$, total thickness $6h = 0.104$. Clamped end at $S = 1$, free end at $S = 1.75$. Concentrated moment assigned on layer (1), ${}_{(1)}M = 0.232 \cdot M$. Deformed shape. Solid line: beam boundary. Dashed line: layer interfaces. Dotted line: reference centroidal line.

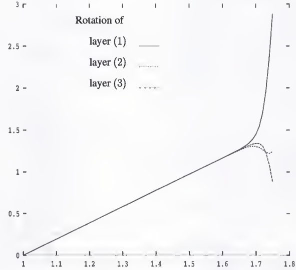

Figure 4.12. *Shorter sandwich beam with identical layers.* Beam length $L = 0.75$, total thickness $6h = 0.104$. Clamped end at $S = 1$, free end at $S = 1.75$. Concentrated moment assigned on layer (1), ${}_{(1)}M = 0.232 \cdot M$. Bifurcation of layer rotations.

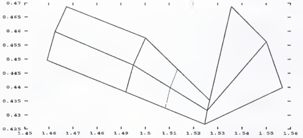

Figure 4.13. *Shorter sandwich beam with identical layers.* Beam length $L = 0.75$, total thickness $6h = 0.104$. Clamped end at $S = 1$, free end at $S = 1.75$. Concentrated moment assigned on layer (1), ${}_{(1)}M = 0.232 \cdot M$. Zoom-in figure of the two elements at the free tip. Top three quadrilaterals are the three layers in the first element at the free tip; bottom three quadrilaterals are the three layers in the second element from the free tip; the dotted line represents the reference centroidal line.

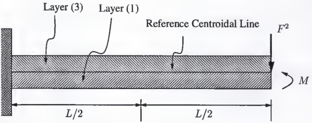

Figure 4.14. *Two-layer beam.* Without ply drop-off. Reference centroidal line is top fiber of layer (1).

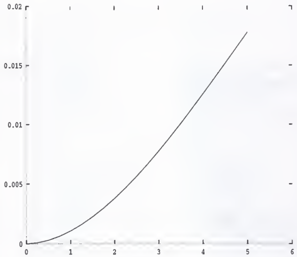

Figure 4.15. *Two-layer beam.* Without ply drop-off. Deformed shape.

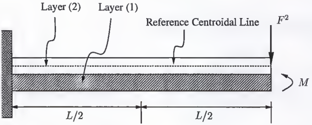

Figure 4.16. *Two-layer beam.* Without ply drop-off. Layer (3) Inexistent. Reference centroidal line is centroidal line of layer (2).

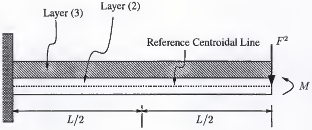

Figure 4.17. *Two layer beam.* Without ply drop-off. Reference centroidal line is centroidal line of layer (2).

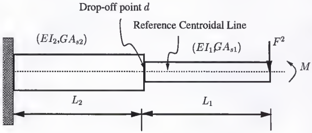

Figure 4.18. *Linear Timoshenko beam with symmetric discontinuous variation of cross section.* Model used to calculate theoretical results for comparison.

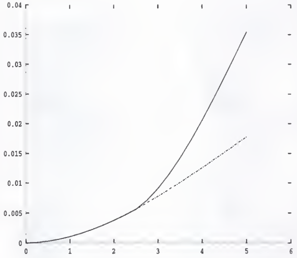

Figure 4.19. *Two-layer beam.* Deformed shape. Solid line: With a ply drop-off at mid-span. Dotted line: Without the ply drop-off.

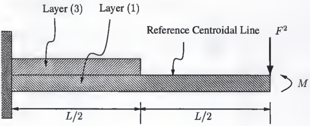

Figure 4.20. *Two-layer beam.* With a ply drop-off. Long layer (1), inexistent layer (2), short layer (3). Reference centroidal line is top fiber of layer (1).

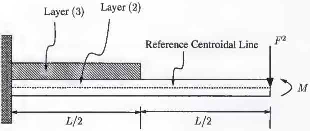

Figure 4.21. *Two layer beam.* With a ply drop-off. Inexistent layer (1), long layer (2), short layer (3). Reference centroidal line is centroidal line of layer (2).

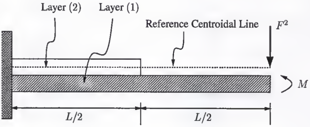

Figure 4.22. *Two layer beam.* With a ply drop-off. Long layer (1), short layer (2), inexistent layer (3). Reference centroidal line is centroidal line of layer (2).

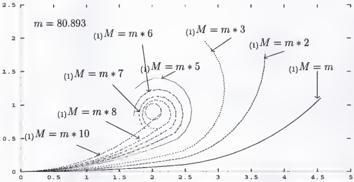

Figure 4.23. *Two-layer beam.* With a ply drop-off. Roll-up maneuver. Applied moment at the tip of layer (1). The thinner part of the beam form a full circle when $_{(1)}M = m * 10$.

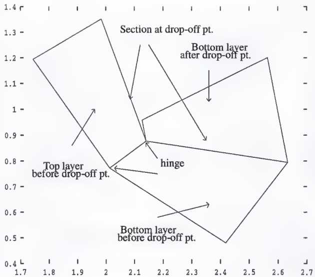

Figure 4.24. *Two-layer beam.* With a ply drop-off. Roll-up maneuver. Zoom-in figure with one beam element before, and one beam element after the drop-off point. Deformation.

4.4. Ideal Sandwich Beams

We now consider the sometimes-called *ideal* sandwich beam, with symmetrical cross section having a soft core layer, together with very thin, but axially very stiff, outer layers (see Sayir and Koller [1986]). Such thin and stiff outer layers are expected to allow primarily shear deformation in the sandwich beam, since they prevent bending by means of membrane deformation almost completely. Consider a simply-supported ideal sandwich beam, with overhangs, shown in Figure 4.25. Let $L = 10$ and let a concentrated force $F^2 = -30$ be applied at mid-span, i.e., at $S = L$. Also consider the cross section of the beam to be of unit width. The material properties used are as follows

$$\chi = \frac{A_s}{A} = 1 \, , \nu = 0.25 \, , \tag{4.56}$$

$$_{(1)}E = \ _{(3)}E = 4 * 10^5, \ \ _{(1)}h = \ _{(3)}h = 0.025 \, , \tag{4.57}$$

$$_{(2)}E = 10^3, \ \ _{(2)}h = 0.5 \, , \tag{4.58}$$

which imply the following elastic moduli for the three layers

$$_{(1)}EA = \ _{(3)}EA = 20,000 \, , \tag{4.59}$$

$$_{(1)}EI = \ _{(3)}EI = 4.1667 \, , \tag{4.60}$$

$$_{(1)}GA_s = \ _{(3)}GA_s = 8,000 \, , \tag{4.61}$$

$$_{(2)}EA = 1,000, \ \ _{(2)}EI = 83.33, \ \ _{(2)}GA_s = 400 \, . \tag{4.62}$$

A uniform discretization of 20 linear sandwich beam elements yields a transverse deflection at mid-span to be $u^2(L) = -0.773186$.

Remark 4.5. The coefficient χ in $(4.56)_1$ is the Timoshenko shear coefficient for each layer; see Heuer [1992], p.3, which refers to Yu [1959*b*] for a proper selection of χ for sandwich plates. ▮

4.4.1. Heuer's theory for sandwich beams

Next, we calculate the deflection of the sandwich beam using the theory developed in Heuer [1992], which essentially yields a linear Timoshenko beam equivalent to the sandwich beam. Let H be the total half-thickness of the beam defined as

$$H := \sum_{\ell=1}^{3} {}_{(\ell)}h \, . \tag{4.63}$$

Heuer [1992] derives the following equation of equilibrium[20]

$$\mathcal{E}\mathcal{I}_{total} u^2{}_{,SSSS} = \overline{\overline{n}}^2 - s\mathcal{E}\mathcal{I}_{total}\overline{\overline{n}}^2{}_{,SS} \ , \tag{4.64}$$

where we $\mathcal{E}\mathcal{I}_{total}$ is the equivalent bending stiffness, u^2 the transverse deflection, s the "shear tracer" coefficient,[21] and $\overline{\overline{n}}^2$ the distributed transverse load.

Remark 4.6. The second term of the right-hand side in (4.64) is in fact the correction to the deflection of the Euler-Bernoulli beam theory due to shear deformation. This remark can be seen easily from the governing equations of the Timoshenko beam. Recall the equations of equilibrium for beams (Euler-Bernoulli or Timoshenko) are

$$\frac{dV}{dS} = -\overline{n} \, , \quad \frac{dM}{dS} = -V \, , \tag{4.65}$$

where V is the shear force, $\overline{n}$ the transverse distributed force, and M the moment. The constitutive laws for the Timoshenko beam are

$$V = GA_s \left(\frac{du}{dS} - \theta \right) \, , \quad M = EI \frac{d\theta}{dS} \, , \tag{4.66}$$

where u is the transverse displacement, and θ the rotation of the cross section. From (4.65) and $(4.66)_2$, we have

$$EI\theta_{,SSS} = \overline{n} \, . \tag{4.67}$$

---

[20] See Equation (16) in Heuer [1992].

[21] See Heuer [1992], p.5.

Now using $(4.65)_1$, $(4.66)_1$, and (4.67), we obtain

$$EIu_{,ssss} = \overline{n} - \frac{EI}{GA_s}\overline{n}_{,ss} \; . \tag{4.68}$$

A comparison of (4.64) to (4.68) clearly explain the meaning of the second term of the right-hand side as stated above. ∎

Let ${}_{(\ell)}b$ be the width of layer (ℓ). Following Heuer [1992][22] the equivalent bending stiffness $\mathcal{EI}_{total}$ is given by

$$\mathcal{EI}_{total} = \frac{{}_{(2)}E \; {}_{(2)}b(2H)^3\epsilon}{12} = 11,116.7 \, , \tag{4.69}$$

where

$$\epsilon := \left[1 - \left(\frac{{}_{(2)}h}{H}\right)^3\right] \frac{{}_{(1)}E}{{}_{(2)}E} \frac{{}_{(1)}b}{{}_{(2)}b} + \left(\frac{{}_{(2)}h}{H}\right)^3 = 100.225 \, . \tag{4.70}$$

Remark 4.7. *Equivalent Euler-Bernoulli beam.* To verify the bending stiffness $\mathcal{EI}_{total}$ obtained in (4.69), we compute the equivalent total bending stiffness using the Euler-Bernoulli theory:

$$EI_{total} = 2 \; {}_{(1)}E \int\limits_{0.5}^{0.55} x^2 dx + \; {}_{(2)}E \int\limits_{-0.5}^{0.5} x^2 dx = 11,116.66 \, . \tag{4.71}$$

Comparing (4.71) and (4.69), it can be seen that $\mathcal{EI}_{total} \equiv EI_{total}$. The transverse tip deflection according the Euler-Bernoulli theory is then

$$u^2(L) = \frac{FL^3}{6EI_{total}} = 0.44978 \, . \tag{4.72}$$

∎

The shear tracer coefficient s is given by[23]

$$s = \frac{\psi}{\epsilon \; {}_{(2)}G \; {}_{(2)}b(2H)} \, , \tag{4.73}$$

---

[22] See Equations (17) in Heuer [1992].

[23] See Heuer [1992], p.5, Equation $(22)_2$.

where ϵ had been defined in (4.70), and

$$\psi := \frac{1}{\chi^2\left[\tilde{b}\left(1-\tilde{h}\right)+\tilde{h}\right]}\left\{\tilde{E}\tilde{b}\left[\frac{3}{2}\left(\tilde{h}-\tilde{h}^3\right)+\frac{1}{\tilde{G}}\left(1-\frac{3}{2}\tilde{h}+\frac{1}{2}\tilde{h}^3\right)\right]+\tilde{h}^3\right\} = \frac{95.6}{\chi^2} \tag{4.74}$$

$$\tilde{h} := \frac{{}_{(2)}h}{H}\,, \quad \tilde{b} := \frac{{}_{(1)}b}{{}_{(2)}b}\,, \quad \tilde{E} := \frac{{}_{(1)}E}{{}_{(2)}E}\,, \quad \tilde{G} := \frac{{}_{(1)}G}{{}_{(2)}G}\,. \tag{4.75}$$

Remark 4.8. The shear tracer coefficient s as defined in (4.73) in Heuer [1992] has the same dimension as the inverse of the shear modulus GA_s of an equivalent single-layer Timoshenko beam. In fact, by comparing (4.64) to (4.68), one can immediately see that

$$s = \frac{1}{GA_s}\,. \tag{4.76}$$

∎

Remark 4.9. The solution of the linear equation (4.68) can be easily obtained for the problem in Figure 4.25 by decomposing the displacement u into

$$u = u^{(i)} + u^{(ii)}\,, \tag{4.77}$$

such that

$$EIu^{(i)}{}_{,SSSS} = \overline{n}\,, \quad u^{(ii)}{}_{,SS} = -\frac{1}{GA_s}\overline{n}\,, \tag{4.78}$$

to obtain mid-span deflection

$$u(L) = \frac{\overline{n}L^3}{6EI} + \frac{\overline{n}L}{2GA_s}\,. \tag{4.79}$$

Thus for the solution according to Heuer [1992]'s theory, we use (4.79) with $\mathcal{EI}_{total}$ instead of EI, and s instead of $1/GA_s$. ∎

For the present problem, $\overline{\tilde{n}}^2 = F^2\delta(S-L)$. Thus with $\chi = 1$ as stated in $(4.56)_1$, so that $s = 0.0021678$, the mid-span transverse deflection is computed using (4.79) to yield $u^2(L) = -0.77497$. So the computed mid-span deflection using our sandwich beam elements (i.e., $u^2(L) = -0.773186$) is smaller than that from Heuer's theory by 0.23%.

Remark 4.10. If one uses the geometrically-exact single-layer beam theory (nonlinear Timoshenko beam) with the equivalent material properties EA and GA_s obtained by naively summing the material properties of each layer, i.e.,[24]

$$EA = \sum_{\ell=1}^{3} {}_{(\ell)}EA = 41,000\,, \quad GA_s = \sum_{\ell=1}^{3} {}_{(\ell)}GA_s = 16,400\,, \quad EI = EI_{total} = 11,116.67\,, \tag{4.80}$$

then a mid-span deflection of $u^2(L) = -0.453498$ is obtained. Such small deflection, as compared to the one by the present sandwich beam theory and the one by Heuer's theory, demonstrates the result of a complex coupling between axial, shear, and bending deformations in sandwich beams. In a sense, Heuer' theory accounts for this coupling through the shear tracer coefficient s. ∎

Remark 4.11. To show clearly the difference in behavior between sandwich beams and single-layer beams, as demonstrated in experiments (Sayir and Koller [1986]), we increase the magnitude of the assigned force to $F^2 = -210$. The same material properties as in (4.80) are used. The deformed shapes are shown in Figure 4.26, where it can be seen that the overhangs of the sandwich beam do not rise up as high as those of the equivalent single-layer beam. In addition, there is a clear break in the beam slope at the supports when using the proposed sandwich beam formulation. Such behavior of sandwich beams is corroborated by experiments (Sayir and Koller [1986]). ∎

---

[24] EI is as computed in (4.71) or in (4.69).

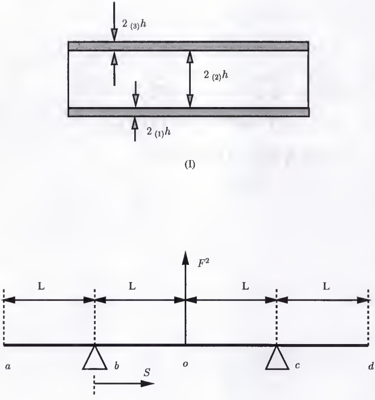

Figure 4.25. *Ideal sandwich beam.* (I) Profile: Soft core layer, thin and axially stiff outer layers. (II) Simply-supported beam with overhangs: Loading at mid-span; origin of coordinate S at support b.

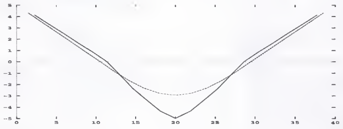

Figure 4.26. *Ideal sandwich beam.* Simply-supported beam with overhangs. Deformed shape. Comparison with geometrically-exact single-layer beam (dotted line).

CHAPTER 5
DYNAMIC ANALYSIS: EQUATIONS OF MOTION

Let ${}_{(\ell)}\mathfrak{A}$ be the interval of the X^2 coordinate corresponding to the cross section of layer (ℓ), and ${}_{(\ell)}\Omega = \mathcal{L} \times {}_{(\ell)}\mathfrak{A}$ be the domain of layer (ℓ) (see Figure 2.1 for details). We now define for layer (ℓ) the following mass quantities

$$ {}_{(\ell)}A_\rho^k := \int\limits_{{}_{(\ell)}\mathfrak{A}} {}_{(\ell)}\rho \left(X^2\right)^k dX^2 , \quad \text{for } k = 0, 1, 2, \tag{5.1} $$

where ${}_{(\ell)}\rho$ is the mass density of the material in layer (ℓ), and ${}_{(\ell)}A_\rho^0$ is the mass per unit length, ${}_{(\ell)}A_\rho^1$ the mass first moment per unit length and ${}_{(\ell)}A_\rho^2$ the mass moment of inertia per unit length, all for layer (ℓ). The kinetic energy $\mathcal{K}$ and its time derivative can be written as

$$ \mathcal{K} := \frac{1}{2}\sum_{\ell=1}^{3} \int\limits_{{}_{(\ell)}\Omega} {}_{(\ell)}\rho \; {}_{(\ell)}\dot{\mathbf{\Phi}} \cdot {}_{(\ell)}\dot{\mathbf{\Phi}} d\Omega \quad \Longrightarrow \quad \frac{d}{dt}\mathcal{K} = \sum_{\ell=1}^{3} \int\limits_{{}_{(\ell)}\Omega} {}_{(\ell)}\rho \; {}_{(\ell)}\ddot{\mathbf{\Phi}} \cdot {}_{(\ell)}\dot{\mathbf{\Phi}} d\Omega . \tag{5.2} $$

Using (2.1), (2.2) and their time derivatives, the time derivative of the kinetic energy $(5.2)_2$ can be expressed as

$$ \frac{d}{dt}\mathcal{K} = \int\limits_{\mathfrak{L}} \left[\mathbf{f} \cdot \dot{\mathbf{u}} + \sum_{\ell=1}^{3} {}_{(\ell)}C \; {}_{(\ell)}\dot{\theta} \right] dS, \tag{5.3} $$

with the total inertia force $\mathbf{f}$ expressed as

$$ \begin{aligned} \mathbf{f} \;=\;& \left(\sum_{\ell=1}^{3} {}_{(\ell)}A_\rho^0 \right) \ddot{\mathbf{u}} + \left[{}_{(2)}h \; {}_{(1)}A_\rho^0 + {}_{(1)}A_\rho^1 \right] {}_{(1)}\ddot{\mathbf{t}}_2 \\ & + \left[- {}_{(2)}h \; {}_{(1)}A_\rho^0 + {}_{(2)}A_\rho^1 + {}_{(2)}h \; {}_{(3)}A_\rho^0 \right] {}_{(2)}\ddot{\mathbf{t}}_2 - \left[{}_{(2)}h \; {}_{(3)}A_\rho^0 - {}_{(3)}A_\rho^1 \right] {}_{(3)}\ddot{\mathbf{t}}_2 , \end{aligned} \tag{5.4} $$

and the inertia couple ${}_{(\ell)}C$, for $\ell = 1, 2, 3$, as

$$ \begin{aligned} {}_{(1)}C \;=\;& \left[\left({}_{(2)}h \right)^2 {}_{(1)}A_\rho^0 + 2 \, {}_{(2)}h \; {}_{(1)}A_\rho^1 + {}_{(1)}A_\rho^2 \right] {}_{(1)}\ddot{\theta} \\ & - \left[{}_{(2)}h \; {}_{(1)}A_\rho^0 + {}_{(1)}A_\rho^1 \right] \left(\ddot{\mathbf{u}} - {}_{(2)}h \; {}_{(2)}\ddot{\mathbf{t}}_2 \right) \cdot {}_{(1)}\mathbf{t}_1 , \end{aligned} \tag{5.5} $$

$$\begin{aligned}
{}_{(2)}C \;=\;& \left[\left({}_{(2)}h\right)^2 {}_{(1)}A^0_\rho + {}_{(2)}A^2_\rho + \left({}_{(2)}h\right)^2 {}_{(3)}A^0_\rho\right] {}_{(2)}\ddot{\theta} \\
&+ \left[{}_{(2)}h\, {}_{(1)}A^0_\rho - {}_{(2)}A^1_\rho - {}_{(2)}h\, {}_{(3)}A^0_\rho\right] \left(\ddot{\mathbf{u}} \cdot {}_{(2)}\mathbf{t}_1\right) \\
&+ {}_{(2)}h \left[{}_{(2)}h\, {}_{(1)}A^0_\rho + {}_{(1)}A^1_\rho\right] \left({}_{(1)}\ddot{\mathbf{t}}_2 \cdot {}_{(2)}\mathbf{t}_1\right) \\
&+ {}_{(2)}h \left[{}_{(2)}h\, {}_{(3)}A^0_\rho - {}_{(3)}A^1_\rho\right] \left({}_{(3)}\ddot{\mathbf{t}}_2 \cdot {}_{(2)}\mathbf{t}_1\right),
\end{aligned} \tag{5.6}$$

$$\begin{aligned}
{}_{(3)}C \;=\;& \left[\left({}_{(2)}h\right)^2 {}_{(3)}A^0_\rho - 2\, {}_{(2)}h\, {}_{(3)}A^1_\rho + {}_{(3)}A^2_\rho\right] {}_{(3)}\ddot{\theta} \\
&+ \left[{}_{(2)}h\, {}_{(3)}A^0_\rho - {}_{(3)}A^1_\rho\right] \left(\ddot{\mathbf{u}} + {}_{(2)}h\, {}_{(2)}\ddot{\mathbf{t}}_2\right) \cdot {}_{(3)}\mathbf{t}_1.
\end{aligned} \tag{5.7}$$

Remark 5.1. The quantity ${}_{(\ell)}\ddot{\mathbf{t}}_2$ in (5.4)–(5.7) is related to the five principal unknowns (2.8) as follows. From (2.5), we obtain the time derivatives of the section basis vector ${}_{(\ell)}\dot{\mathbf{t}}_2$ as

$${}_{(\ell)}\dot{\mathbf{t}}_2 = -\, {}_{(\ell)}\dot{\theta}\, {}_{(\ell)}\mathbf{t}_1 \quad\Longrightarrow\quad {}_{(\ell)}\ddot{\mathbf{t}}_2 = -\left[{}_{(\ell)}\ddot{\theta}\, {}_{(\ell)}\mathbf{t}_1 + \left({}_{(\ell)}\dot{\theta}\right)^2 {}_{(\ell)}\mathbf{t}_2\right], \tag{5.8}$$

thus the total inertia force $\mathbf{f}$ and the inertia couple ${}_{(\ell)}C$, for $\ell = 1, 2, 3$, can be expressed in the five principal unknowns (2.8). ∎

From the balance of the power of contact forces/couples (2.13), the power of assigned forces/couples (2.14) and the sum of the time rate of kinetic energy (5.3)

$$\frac{d}{dt}\mathcal{K} + \mathcal{P}_c = \mathcal{P}_a, \tag{5.9}$$

we obtain the following equations of motion for sandwich beam (Vu-Quoc and Ebcioğlu [1995])

$$\boxed{\begin{array}{lll}
 & \hat{\mathbf{n}}_{,S} + \bar{\hat{\mathbf{n}}} & = \mathbf{f}, \\
{}_{(1)}m_{,S} + \left[\, {}_{(2)}\boldsymbol{\Phi}_{0,S} \times {}_{(1)}\mathbf{n} \right] \bullet \mathbf{e}_3 & + {}_{(1)}h \left({}_{(1)}\mathbf{n} \bullet {}_{(1)}\mathbf{t}_1 \right)_{,S} & \\
 & + {}_{(2)}h \, {}_{(2)}\theta_{,S} \left({}_{(1)}\mathbf{n} \bullet {}_{(2)}\mathbf{t}_2 \right) + {}_{(1)}\bar{\boldsymbol{m}} & = {}_{(1)}C, \\
{}_{(2)}m_{,S} + \left[\, {}_{(2)}\boldsymbol{\Phi}_{0,S} \times {}_{(2)}\mathbf{n} \right] \bullet \mathbf{e}_3 & + {}_{(2)}h \left({}_{(1)}\mathbf{n}_{,S} - {}_{(3)}\mathbf{n}_{,S} \right) \bullet {}_{(2)}\mathbf{t}_1 + {}_{(2)}\bar{\boldsymbol{m}} & = {}_{(2)}C, \\
{}_{(3)}m_{,S} + \left[\, {}_{(2)}\boldsymbol{\Phi}_{0,S} \times {}_{(3)}\mathbf{n} \right] \bullet \mathbf{e}_3 & - {}_{(2)}h \, {}_{(2)}\theta_{,S} \left({}_{(3)}\mathbf{n} \bullet {}_{(2)}\mathbf{t}_2 \right) & \\
 & - {}_{(3)}h \left({}_{(3)}\mathbf{n} \bullet {}_{(3)}\mathbf{t}_1 \right)_{,S} + {}_{(3)}\bar{\boldsymbol{m}} & = {}_{(3)}C,
\end{array}} \tag{5.10}$$

where $(5.10)_1$ is the balance of linear momentum, and $(5.10)_2$–$(5.10)_4$ the balance of angular momentum for each of the three layers.

The boundary conditions at $S = 0$ and $S = L$ are given by

$$\boxed{\begin{array}{llllrl}
\text{Either} & \mathbf{u} & = \bar{\mathbf{u}} & \text{or} & \hat{\mathbf{n}} & = \bar{\hat{\mathbf{n}}}, \\
\text{"} & {}_{(1)}\theta & = {}_{(1)}\bar{\theta} & \text{"} & {}_{(1)}m + {}_{(1)}h \left({}_{(1)}\mathbf{n} \bullet {}_{(1)}\mathbf{t}_1 \right) & = {}_{(1)}\bar{\boldsymbol{m}}, \\
\text{"} & {}_{(2)}\theta & = {}_{(2)}\bar{\theta} & \text{"} & {}_{(2)}m + {}_{(2)}h \left({}_{(1)}\mathbf{n} - {}_{(3)}\mathbf{n} \right) \bullet {}_{(2)}\mathbf{t}_1 & = {}_{(2)}\bar{\boldsymbol{m}}, \\
\text{"} & {}_{(3)}\theta & = {}_{(3)}\bar{\theta} & \text{"} & {}_{(3)}m - {}_{(3)}h \left({}_{(3)}\mathbf{n} \bullet {}_{(3)}\mathbf{t}_1 \right) & = {}_{(3)}\bar{\boldsymbol{m}},
\end{array}} \tag{5.11}$$

which is the same as (2.11). The detailed derivation of (5.10)–(2.11) can be found in Vu-Quoc and Ebcioğlu [1995].

CHAPTER 6
FINITE ELEMENT IMPLEMENTATION

We now develop the weak form of the equation of motion presented at the end of Chapter 5. This weak form will then be linearized and subsequently used in a Galerkin projection for the iterative solution process.

6.1. Weak Form of Kinetic Energy

We now develop the expression for the nonlinear weak form of the equations of motion based on the balance of power (2.12). This weak form will be linearized, and subsequently used in a Galerkin projection for the iterative solution process. The static weak for is already given in Section(3.1), thus here we only give the dynamic weak for that comes from the kinetic energy. To simplify the presentation, we rewrite the expression for the inertia forces (5.4) in matrix form as follows

$$\mathbf{f}_I := \left\{ f^1 \, , \, f^2 \, , 0 \, , 0 \, , 0 \right\}^T , \tag{6.1}$$

and the expression for the inertia couples (5.5)–(5.7) in matrix form as

$$\mathbf{C}_I := \left\{ 0 \, , 0 \, , \, {}_{(1)}C \, , \, {}_{(2)}C \, , \, {}_{(3)}C \right\}^T . \tag{6.2}$$

We gather the inertia forces/couples into the following array

$$\boldsymbol{\mathcal{F}}_I := \left\{ f^1, \; f^2, \; {}_{(1)}C, \; {}_{(2)}C, \; {}_{(3)}C \right\}^T . \tag{6.3}$$

From (5.3), we obtain the weak form of the inertia forces/couples as

$$G_I(\boldsymbol{\Phi}, \mathbf{w}) = \int_{\mathfrak{L}} \boldsymbol{\mathcal{F}}_I \boldsymbol{\cdot} \mathbf{w} dS . \tag{6.4}$$

Again, to simplify the presentation, we define the following arrays for displacements, velocities and accelerations

$$\mathbf{d} := \left\{ u^1, u^2,\ {}_{(1)}\theta,\ {}_{(2)}\theta,\ {}_{(3)}\theta \right\}^T, \quad \mathbf{v} := \dot{\mathbf{d}}, \quad \mathbf{a} := \ddot{\mathbf{d}}, \tag{6.5}$$

and define $\mathbf{v}^{<2>}$ as

$$\mathbf{v}^{<2>} := \left\{ (\dot{u}^1)^2,\ (\dot{u}^2)^2,\ (\ {}_{(1)}\dot{\theta})^2,\ (\ {}_{(2)}\dot{\theta})^2,\ (\ {}_{(3)}\dot{\theta})^2 \right\}^T. \tag{6.6}$$

Remark 6.1. The items related to $\mathbf{v}^{<2>}$ come from the second time derivative of the basis vector ${}_{(\ell)}\mathbf{t}_2$ as given in (5.8). Note that in the expressions for the inertia forces (6.1) and for the inertia couples (6.2) in terms of the kinematic quantities (2.8), only $(\ {}_{(1)}\dot{\theta})^2$, $(\ {}_{(2)}\dot{\theta})^2$ and $(\ {}_{(3)}\dot{\theta})^2$ are needed, while the quantities $(\dot{u}^1)^2$ and $(\dot{u}^2)^2$ are *not* needed. This observation can be clearly understood by noting that the first and second columns of the matrices of $\mathbf{M}_2$ and $\mathbf{M}_4$ in (6.9) and in (6.12), respectively, are zero. ∎

Using (5.4) and the expression for the basis vector (2.5) and the second time derivative of the basis vector (5.8), we can rewrite the expression for the inertia forces given in (6.1) as follows

$$\mathbf{f}_I := \left\{ f^1,\ f^2, 0, 0, 0 \right\}^T = \mathbf{M}_1\mathbf{a} + \mathbf{M}_2\mathbf{v}^{<2>}, \tag{6.7}$$

where the matrices $\mathbf{M}_1$ and $\mathbf{M}_2$ are defined as

$$\mathbf{M}_1 := \begin{bmatrix} \sum_{\ell=1}^{3}\ {}_{(\ell)}A_\rho^0 & 0 & -\Pi_1 \cos\ {}_{(1)}\theta & -\Pi_2 \cos\ {}_{(2)}\theta & -\Pi_3 \cos\ {}_{(3)}\theta \\ 0 & \sum_{\ell=1}^{3}\ {}_{(\ell)}A_\rho^0 & -\Pi_1 \sin\ {}_{(1)}\theta & -\Pi_2 \sin\ {}_{(2)}\theta & -\Pi_3 \sin\ {}_{(3)}\theta \\ 0 & 0 & 0 & 0 & 0 \\ 0 & 0 & 0 & 0 & 0 \\ 0 & 0 & 0 & 0 & 0 \end{bmatrix}_{5\times5}, \tag{6.8}$$

$$\mathbf{M}_2 := \begin{bmatrix} 0 & 0 & \Pi_1 \sin\ {}_{(1)}\theta & \Pi_2 \sin\ {}_{(2)}\theta & \Pi_3 \sin\ {}_{(3)}\theta \\ 0 & 0 & -\Pi_1 \cos\ {}_{(1)}\theta & -\Pi_2 \cos\ {}_{(2)}\theta & -\Pi_3 \cos\ {}_{(3)}\theta \\ 0 & 0 & 0 & 0 & 0 \\ 0 & 0 & 0 & 0 & 0 \\ 0 & 0 & 0 & 0 & 0 \end{bmatrix}_{5\times5}, \tag{6.9}$$

where the coefficients Π_1, Π_2 and Π_3 are functions of the material constants (see (6.14)–(6.16)). Using the similar method as in getting the matrix form of the inertia force, we obtain the following matrix form for the inertia couples in (6.2) as

$$\mathbf{C}_I = \mathbf{M}_3\mathbf{a} + \mathbf{M}_4\mathbf{v}^{<2>}, \tag{6.10}$$

in which $\mathbf{v}^{<2>}$ is defined in (6.6), and the matrices $\mathbf{M}_3$ and $\mathbf{M}_4$ are given by

$$\mathbf{M}_3 := \begin{bmatrix} 0 & 0 & 0 & 0 & 0 \\ 0 & 0 & 0 & 0 & 0 \\ -\Pi_1 \cos {}_{(1)}\theta & -\Pi_1 \sin {}_{(1)}\theta & \Pi_4 & -\Pi_6 \cos\psi_{21} & 0 \\ -\Pi_2 \cos {}_{(2)}\theta & -\Pi_2 \sin {}_{(2)}\theta & -\Pi_6 \cos\psi_{21} & \Pi_5 & -\Pi_7 \cos\psi_{23} \\ -\Pi_3 \sin {}_{(3)}\theta & -\Pi_3 \cos {}_{(3)}\theta & 0 & -\Pi_7 \cos\psi_{23} & \Pi_8 \end{bmatrix}_{5\times5}, \tag{6.11}$$

$$\mathbf{M}_4 := \begin{bmatrix} 0 & 0 & 0 & 0 & 0 \\ 0 & 0 & 0 & 0 & 0 \\ 0 & 0 & 0 & \Pi_6 \sin\psi_{21} & 0 \\ 0 & 0 & -\Pi_6 \sin\psi_{21} & 0 & -\Pi_7 \sin\psi_{23} \\ 0 & 0 & 0 & \Pi_7 \sin\psi_{23} & 0 \end{bmatrix}_{5\times5}, \tag{6.12}$$

where

$$\psi_{ij} := {}_{(i)}\theta - {}_{(j)}\theta. \tag{6.13}$$

The constants employed in (6.8), (6.9), (6.11) and (6.12) above are defined as follows

$$\Pi_1 := {}_{(2)}h \, {}_{(1)}A_\rho^0 + {}_{(1)}A_\rho^1, \tag{6.14}$$

$$\Pi_2 := -{}_{(2)}h \, {}_{(1)}A_\rho^0 + {}_{(2)}A_\rho^1 + {}_{(2)}h \, {}_{(3)}A_\rho^0, \tag{6.15}$$

$$\Pi_3 := -{}_{(2)}h \, {}_{(3)}A_\rho^0 + {}_{(3)}A_\rho^1, \tag{6.16}$$

$$\Pi_4 := \left({}_{(2)}h\right)^2 {}_{(1)}A_\rho^0 + 2\, {}_{(2)}h \, {}_{(1)}A_\rho^1 + {}_{(1)}A_\rho^2, \tag{6.17}$$

$$\Pi_5 := \left({}_{(2)}h\right)^2 {}_{(1)}A_\rho^0 + \left({}_{(2)}h\right)^2 {}_{(3)}A_\rho^0 + {}_{(2)}A_\rho^2, \tag{6.18}$$

$$\Pi_6 := \left({}_{(2)}h \, {}_{(1)}A_\rho^0 + {}_{(1)}A_\rho^1\right) \bullet {}_{(2)}h, \tag{6.19}$$

$$\Pi_7 := \left(+ {}_{(2)}h \, {}_{(3)}A_\rho^0 - {}_{(3)}A_\rho^1\right) \bullet {}_{(2)}h, \tag{6.20}$$

$$\Pi_8 \;:=\; \left({}_{(2)}h\right)^2 \, {}_{(3)}A^0_\rho - 2\, {}_{(2)}h\, {}_{(3)}A^1_\rho + {}_{(3)}A^2_\rho . \tag{6.21}$$

With the following definition of the matrices $\mathbf{M}_a$ and $\mathbf{M}_v$

$$\mathbf{M}_a := \mathbf{M}_1 + \mathbf{M}_3 =$$
$$\begin{bmatrix} \sum_{\ell=1}^3 {}_{(\ell)}A^0_\rho & 0 & -\Pi_1 \cos {}_{(1)}\theta & -\Pi_2 \cos {}_{(2)}\theta & -\Pi_3 \cos {}_{(3)}\theta \\ 0 & \sum_{\ell=1}^3 {}_{(\ell)}A^0_\rho & -\Pi_1 \sin {}_{(1)}\theta & -\Pi_2 \sin {}_{(2)}\theta & -\Pi_3 \sin {}_{(3)}\theta \\ -\Pi_1 \cos {}_{(1)}\theta & -\Pi_1 \sin {}_{(1)}\theta & \Pi_4 & -\Pi_6 \cos \psi_{21} & 0 \\ -\Pi_2 \cos {}_{(2)}\theta & -\Pi_2 \sin {}_{(2)}\theta & -\Pi_6 \cos \psi_{21} & \Pi_5 & -\Pi_7 \cos \psi_{23} \\ -\Pi_3 \cos {}_{(3)}\theta & -\Pi_3 \sin {}_{(3)}\theta & 0 & -\Pi_7 \cos \psi_{23} & \Pi_8 \end{bmatrix}_{5\times 5} , \tag{6.22}$$

$$\mathbf{M}_v := \mathbf{M}_2 + \mathbf{M}_4 = \begin{bmatrix} 0 & 0 & \Pi_1 \sin {}_{(1)}\theta & \Pi_2 \sin {}_{(2)}\theta & \Pi_3 \sin {}_{(3)}\theta \\ 0 & 0 & -\Pi_1 \cos {}_{(1)}\theta & -\Pi_2 \cos {}_{(2)}\theta & -\Pi_3 \cos {}_{(3)}\theta \\ 0 & 0 & 0 & \Pi_6 \sin \psi_{21} & 0 \\ 0 & 0 & -\Pi_6 \sin \psi_{21} & 0 & -\Pi_7 \sin \psi_{23} \\ 0 & 0 & 0 & \Pi_7 \sin \psi_{23} & 0 \end{bmatrix}_{5\times 5} , \tag{6.23}$$

the combined array of inertia forces/couples $\mathcal{F}_I$ defined in (6.3) can be expressed simply as

$$\mathcal{F}_I = \mathbf{M}_a \mathbf{a} + \mathbf{M}_v \mathbf{v}^{<2>} . \tag{6.24}$$

Now, the weak form of the equations of motion of sandwich beams, when inertia effects are taken into account, can be written as

$$G_{dyn}(\mathbf{\Phi}, \mathbf{w}) := G_I(\mathbf{\Phi}, \mathbf{w}) + G_c(\mathbf{\Phi}, \mathbf{w}) - G_a(\mathbf{\Phi}, \mathbf{w}), \tag{6.25}$$

where $G_I(\mathbf{\Phi}, \mathbf{w})$, $G_c(\mathbf{\Phi}, \mathbf{w})$ and $G_a(\mathbf{\Phi}, \mathbf{w})$ are given in (6.4), (3.27) and (3.25), respectively.

Let $\mathcal{V}$ designate the set of admissible weighting functions (see, e.g., Hughes [1987]). The weak form for the equations of motion for geometrically-exact sandwich beams is to

$$\boxed{\begin{array}{l} \text{Find } \mathbf{\Phi} \text{ such that} \\ \qquad G_c(\mathbf{\Phi}, \mathbf{w}) + G_I(\mathbf{\Phi}, \mathbf{w}) - G_a(\mathbf{\Phi}, \mathbf{w}) = 0, \quad \forall \mathbf{w} \in \mathcal{V}. \end{array}} \tag{6.26}$$

Remark 6.2. For a single-layer beam, i.e., when only the core layer exists, all terms related to layer (1) and layer (3) are zero, thus $\Pi_1 = \Pi_3 = \Pi_4 = \Pi_6 = \Pi_7 = \Pi_8 = 0$; and $\Pi_2 = {}_{(2)}A^1_\rho$, $\Pi_5 = {}_{(2)}A^2_\rho$. In addition, if the mass distribution is symmetric with respect to the centroidal line of the core layer, then $\Pi_2 = 0$. Thus $\mathbf{M}_a$ reduces to $diag\left[\, {}_{(2)}A^0_\rho,\ {}_{(2)}A^0_\rho,\ 0,\ {}_{(2)}A^2_\rho,\ 0\right]$, and $\mathbf{M}_v$ reduces to a zero matrix; this result is identical to the one obtained for single-layer beams as in Vu-Quoc [1986]. See also Simo and Vu-Quoc [1986*c*] for the similar expression for 3–D case. It is also important to remember that $\mathbf{M}_v$ is the only unsymmetric matrix here. ∎

6.2. Time Stepping Scheme: Newmark Algorithm

Let the displacement field

$$\mathbf{\Phi}_n(S) := \left\{u^1(S,t_n),\ u^2(S,t_n),\ {}_{(1)}\theta(S,t_n),\ {}_{(2)}\theta(S,t_n),\ {}_{(3)}\theta(S,t_n)\right\}^T \tag{6.27}$$

denote the solution $\mathbf{\Phi}(S,t)$ at time $t = t_n$. Also let $\mathbf{v}_n := \dot{\mathbf{\Phi}}(S,t_n)$ and $\mathbf{a}_n := \ddot{\mathbf{\Phi}}(S,t_n)$ be the velocity and the acceleration at time t_n.

Assuming that $(\ \mathbf{\Phi}_n, \mathbf{v}_n, \mathbf{a}_n)$ satisfy the weak form (6.25) of the equations of motion at time t_n, that is

$$G_{dyn}(\ \mathbf{\Phi}_n, \mathbf{w}) = G_I(\ \mathbf{\Phi}_n, \mathbf{w}) + G_c(\ \mathbf{\Phi}_n, \mathbf{w}) - G_a(\ \mathbf{\Phi}_n, \mathbf{w}) = 0, \qquad \forall \mathbf{w} \in \mathcal{V}, \tag{6.28}$$

with

$$G_I(\ \mathbf{\Phi}_n, \mathbf{w}) = \int_{\mathfrak{L}} (\ \mathbf{M}_a\mathbf{a}_n +\ \mathbf{M}_v\mathbf{v}_n^{<2>})\boldsymbol{\cdot}\mathbf{w}dS, \tag{6.29}$$

where

$$\mathbf{v}_n^{<2>} = \left\{(\dot{u}^1(S,t_n))^2,\ (\dot{u}^2(S,t_n))^2,\ (\ {}_{(1)}\dot{\theta}(S,t_n))^2,\ (\ {}_{(2)}\dot{\theta}(S,t_n))^2,\ (\ {}_{(3)}\dot{\theta}(S,t_n))^2\right\}^T. \tag{6.30}$$

We want to obtain the solution $(\mathbf{\Phi}_{n+1}, \mathbf{v}_{n+1}, \mathbf{a}_{n+1})$ at time t_{n+1}, such that

$$G_{dyn}(\ \mathbf{\Phi}_{n+1}, \mathbf{w}) = G_I(\ \mathbf{\Phi}_{n+1}, \mathbf{w}) + G_c(\ \mathbf{\Phi}_{n+1}, \mathbf{w}) - G_a(\ \mathbf{\Phi}_{n+1}, \mathbf{w}) = 0, \qquad \forall \mathbf{w} \in \mathcal{V}, \tag{6.31}$$

with

$$G_I(\ \mathbf{\Phi}_{n+1}, \mathbf{w}) = \int_{\mathfrak{L}} (\ \mathbf{M}_a \mathbf{a}_{n+1} + \ \mathbf{M}_v \mathbf{v}_{n+1}^{<2>}) \cdot \mathbf{w} dS, \tag{6.32}$$

where $\mathbf{v}_{n+1}^{<2>}$ is defined for $t = t_{n+1}$ similar to $\mathbf{v}_n^{<2>}$ for $t = t_n$ in (6.30) above.

The Newmark time-stepping algorithm defines the relationship between the two values $(\mathbf{\Phi}_n, \mathbf{v}_n, \mathbf{a}_n)$ and $(\mathbf{\Phi}_{n+1}, \mathbf{v}_{n+1}, \mathbf{a}_{n+1})$ of the solution at time t_n and t_{n+1}, respectively, according to

$$\mathbf{a}_{n+1} = \frac{\mathbf{\Phi}_{n+1} - \mathbf{\Phi}_n}{h^2 \beta} - \frac{\mathbf{v}_n}{h\beta} - \frac{\tau - \beta}{\beta} \mathbf{a}_n, \tag{6.33}$$

$$\mathbf{v}_{n+1} = \mathbf{v}_n + h \left[(1 - \tau) \mathbf{a}_n + \tau \mathbf{a}_{n+1} \right], \tag{6.34}$$

where $h := t_{n+1} - t_n$ is the time step size, and (β, τ) the parameters for the Newmark algorithm. Note that $\beta = 0.25$ and $\tau = 0.5$ corresponds to the trapezoidal rule, which guarantees unconditional stability and second order accuracy. Substituting (6.33) and (6.34) into (6.31), we obtain a nonlinear equation in the unknown $\mathbf{\Phi}_{n+1}$, which can then be solved for by using Newton's iterative method. Once $\mathbf{\Phi}_{n+1}$ is obtained, $(\mathbf{v}_{n+1}, \mathbf{a}_{n+1})$ can be computed using (6.33)–(6.34), the next iteration is then ready to be carried out.

6.3. Linearization and Tangent Operator

The first step in using the Newton's iterative scheme is to linearize the nonlinear equation (6.28); to do so, let us define the incremental solution at time t_{n+1} as

$$\Delta \mathbf{\Phi}_{n+1}(S) := \tag{6.35}$$

$$\left\{ \Delta u^1(S, t_{n+1}), \Delta u^2(S, t_{n+1}), \Delta\ {}_{(1)}\theta(S, t_{n+1}), \Delta\ {}_{(2)}\theta(S, t_{n+1}), \Delta\ {}_{(3)}\theta(S, t_{n+1}) \right\}^T, \tag{6.36}$$

and the perturbed configuration

$$\mathbf{\Phi}_{n+1}^{(i+\varepsilon)} = \mathbf{\Phi}_{n+1}^{(i)} + \varepsilon \Delta \mathbf{\Phi}_{n+1}^{(i)}, \tag{6.37}$$

where ε is a scalar quantity. The superscript (i) here designates the *ith* iteration in Newton's iterative solution method in searching for the unknown mapping $\mathbf{\Phi}_{n+1}$. The initial guess for the (n+1)*th* time increment is chosen to be

$$\begin{gathered} \mathbf{\Phi}_{n+1}^{(0)} = \mathbf{\Phi}_n, \\ \mathbf{a}_{n+1}^{(0)} = \frac{\mathbf{\Phi}_{n+1}^{(0)} - \mathbf{\Phi}_n}{h^2 \beta} - \frac{\mathbf{v}_n}{h\beta} - \frac{\tau - \beta}{\beta} \mathbf{a}_n, \\ \mathbf{v}_{n+1}^{(0)} = \mathbf{v}_n + h \left[(1-\tau) \mathbf{a}_n + \tau \mathbf{a}_{n+1}^{(0)} \right], \end{gathered} \tag{6.38}$$

where $\mathbf{\Phi}_n$, $\mathbf{v}_n$ and $\mathbf{a}_n$ designate the converged solution for the n*th* time increment. The linearization of the weak form $G_{dyn}(\mathbf{\Phi}, \mathbf{w})$ at $\mathbf{\Phi}_{n+1}^{(i)}$ can be written as

$$L \left[G_{dyn}(\mathbf{\Phi}_{n+1}^{(i)}, \mathbf{w}) \right] = G_{dyn}(\mathbf{\Phi}_{n+1}^{(i)}, \mathbf{w}) + \mathcal{D} G_{dyn}(\mathbf{\Phi}_{n+1}^{(i)}, \mathbf{w}) \cdot \Delta \mathbf{\Phi}_{n+1}^{(i+1)}, \tag{6.39}$$

where $G_{dyn}(\mathbf{\Phi}_{n+1}^{(i)}, \mathbf{w})$ is the dynamic residual at the configuration $\mathbf{\Phi}_{n+1}^{(i)}$. The linear operator $\mathcal{D} G_{dyn}(\mathbf{\Phi}_{n+1}^{(i)}, \mathbf{w})$ is obtained by taking the directional derivative of $G_{dyn}(\mathbf{\Phi}_{n+1}^{(i)}, \mathbf{w})$ at $\mathbf{\Phi}_{n+1}^{(i)}$ as follows

$$\mathcal{D} G_{dyn}(\mathbf{\Phi}_{n+1}^{(i)}, \mathbf{w}) \cdot \Delta \mathbf{\Phi}_{n+1}^{(i)} = \frac{d}{d\varepsilon} G_{dyn}(\mathbf{\Phi}_{n+1}^{(i+\varepsilon)}, \mathbf{w}) \bigg|_{\varepsilon = 0} . \tag{6.40}$$

Next, we will derive the linearization of each part of the weak form G_{dyn} given in (6.25).

6.4. Tangent Inertia Operator

First, we will obtain the linearization of the weak form of the inertia operator G_I given in (6.4) and (6.24). For a clear presentation of the linearization process, we will treat separately the two terms of the weak form of the inertia operator G_I: The acceleration term

$$G_{Ia}(\mathbf{\Phi}_{n+1}^{(i)}, \mathbf{w}) := \int_{\mathcal{L}} \left[\mathbf{M}_a \left(\mathbf{\Phi}_{n+1}^{(i)} \right) \mathbf{a}_{n+1}^{(i)} \right] \cdot \mathbf{w} dS, \tag{6.41}$$

and the velocity term

$$G_{Iv}(\mathbf{\Phi}_{n+1}^{(i)},\mathbf{w}) := \int\limits_{\mathfrak{L}} \left[\, \mathbf{M}_v\left(\mathbf{\Phi}_{n+1}^{(i)}\right) \mathbf{v}_{n+1}^{(i)<2>} \right] \bullet \mathbf{w}\, dS, \tag{6.42}$$

where $\mathbf{v}_{n+1}^{(i)<2>}$ is defined similar to $\mathbf{v}_n^{<2>}$ in (6.30), but with velocity $\mathbf{v}_{n+1}^{(i)}$, instead of velocity $\mathbf{v}_n$. The linearization of G_{Ia} goes as follows

$$\mathcal{D}G_{Ia}\left(\mathbf{\Phi}_{n+1}^{(i)},\mathbf{w}\right) \bullet \Delta\mathbf{\Phi}_{n+1}^{(i)} = \frac{d}{d\varepsilon} G_{Ia}\left(\mathbf{\Phi}_{n+1}^{(i+\varepsilon)},\mathbf{w}\right)\bigg|_{\varepsilon=0}$$

$$= \int\limits_{\mathfrak{L}} \left[\, \mathbf{M}_a\left(\mathbf{\Phi}_{n+1}^{(i)}\right) \frac{d}{d\varepsilon}\mathbf{a}_{n+1}^{(i+\varepsilon)}\bigg|_{\varepsilon=0} \right] \bullet \mathbf{w}\, dS + \int\limits_{\mathfrak{L}} \left[\frac{d}{d\varepsilon}\, \mathbf{M}_a(\mathbf{\Phi}_{n+1}^{(i+\varepsilon)})\bigg|_{\varepsilon=0} \mathbf{a}_{n+1}^{(i)} \right] \bullet \mathbf{w}\, dS. \tag{6.43}$$

Using the Newmark algorithm (6.33), we have

$$\mathbf{a}_{n+1}^{(i+\varepsilon)} = \frac{\mathbf{\Phi}_{n+1}^{(i+\varepsilon)} - \mathbf{\Phi}_n}{h^2\beta} - \frac{\mathbf{v}_n}{h\beta} - \frac{\tau-\beta}{\beta}\mathbf{a}_n, \tag{6.44}$$

and thus by virtue of (6.37)

$$\frac{d}{d\varepsilon}\, \mathbf{a}_{n+1}^{(i+\varepsilon)}\bigg|_{\varepsilon=0} = \frac{1}{h^2\beta}\Delta\mathbf{\Phi}_{n+1}^{(i)}. \tag{6.45}$$

Further, after some reorganization to pull the increment $\mathbf{\Phi}_{n+1}^{(i)}$ out as a common factor, we obtain

$$\frac{d}{d\varepsilon}\; \mathbf{M}_a\left(\mathbf{\Phi}_{n+1}^{(i+\varepsilon)}\right)\bigg|_{\varepsilon=0} \mathbf{a}_{n+1}^{(i)} = \mathbf{M}_b\left(\mathbf{\Phi}_{n+1}^{(i)}, \mathbf{a}_{n+1}^{(i)}\right) \Delta\mathbf{\Phi}_{n+1}^{(i)}, \tag{6.46}$$

where the matrix $\mathbf{M}_b\left(\mathbf{\Phi}_{n+1}^{(i)}, \mathbf{a}_{n+1}^{(i)}\right)$ takes the form[25]

$$\mathbf{M}_b\left(\mathbf{\Phi},\mathbf{a}\right) := \begin{bmatrix} 0 & 0 & \Pi_1\ {}_{(1)}\ddot{\theta}\sin\ {}_{(1)}\theta & \Pi_2\ {}_{(2)}\ddot{\theta}\sin\ {}_{(2)}\theta & \Pi_3\ {}_{(3)}\ddot{\theta}\sin\ {}_{(3)}\theta \\ 0 & 0 & -\Pi_1\ {}_{(1)}\ddot{\theta}\cos\ {}_{(1)}\theta & -\Pi_2\ {}_{(2)}\ddot{\theta}\cos\ {}_{(2)}\theta & -\Pi_3\ {}_{(3)}\ddot{\theta}\cos\ {}_{(3)}\theta \\ 0 & 0 & \Upsilon_1 & \Pi_6\ {}_{(2)}\ddot{\theta}\sin\psi_{21} & 0 \\ 0 & 0 & -\Pi_6\ {}_{(1)}\ddot{\theta}\sin\psi_{21} & \Upsilon_2 & -\Pi_7\ {}_{(3)}\ddot{\theta}\sin\psi_{23} \\ 0 & 0 & 0 & \Pi_7\ {}_{(2)}\ddot{\theta}\sin\psi_{23} & \Upsilon_3 \end{bmatrix}_{5\times5}, \tag{6.47}$$

---

[25] While the subscript "$_a$" in $\mathbf{M}_a$ is mnemonic for "acceleration", the subscript "$_b$" in $\mathbf{M}_b$ is chosen arbitrary.

with Υ_1, Υ_2 and Υ_3 defined as

$$\Upsilon_1 := \Pi_1 \ddot{u}_0{}^1 \sin {}_{(1)}\theta - \Pi_1 \ddot{u}_0{}^2 \cos {}_{(1)}\theta - \Pi_6 \, {}_{(2)}\ddot{\theta} \sin \psi_{21}, \tag{6.48}$$

$$\Upsilon_2 := \Pi_2 \ddot{u}_0{}^1 \sin {}_{(2)}\theta - \Pi_2 \ddot{u}_0{}^2 \cos {}_{(2)}\theta + \Pi_6 \, {}_{(1)}\ddot{\theta} \sin \psi_{21} + \Pi_7 \, {}_{(3)}\ddot{\theta} \sin \psi_{23}, \tag{6.49}$$

$$\Upsilon_3 := \Pi_3 \ddot{u}_0{}^1 \sin {}_{(3)}\theta - \Pi_3 \ddot{u}_0{}^2 \cos {}_{(3)}\theta - \Pi_7 \, {}_{(2)}\ddot{\theta} \sin \psi_{23}, \tag{6.50}$$

where $\psi_{2\ell} := {}_{(2)}\theta - {}_{(\ell)}\theta$ as in (6.13). Finally, the linearization of G_{Ia} is obtained as follows

$$\mathcal{D}G_{Ia}\left(\mathbf{\Phi}_{n+1}^{(i)}, \mathbf{w}\right) \cdot \Delta\mathbf{\Phi}_{n+1}^{(i)} = \int_{\mathfrak{L}} \left\{ \left[\frac{1}{h^2\beta} \mathbf{M}_a \left(\mathbf{\Phi}_{n+1}^{(i)}\right) + \mathbf{M}_b \left(\mathbf{\Phi}_{n+1}^{(i)}, \mathbf{a}_{n+1}^{(i)}\right) \right] \Delta\mathbf{\Phi}_{n+1}^{(i)} \right\} \cdot \mathbf{w} dS. \tag{6.51}$$

Remark 6.3. For a single-layer beam, as noted in Remark 6.2, $\Pi_1 = \Pi_3 = \Pi_4 = \Pi_6 = \Pi_7 = \Pi_8 = 0$, while $\Pi_2 = {}_{(2)}A_\rho^1$, $\Pi_5 = {}_{(2)}A_\rho^2$, thus $\Upsilon_1 = \Upsilon_3 = 0$, $\Upsilon_2 = \Pi_2 \ddot{u}_0{}^1 \sin {}_{(2)}\theta - \Pi_2 \ddot{u}_0{}^2 \cos {}_{(2)}\theta$. The only nonzero entries in the matrix $\mathbf{M}_b$ are in the fourth column, which is identical to that obtained for the single-layer beam case.

▮

We now consider the linearization of the velocity term G_{Iv} in (6.42) of the weak form of the inertia operator. Similar to (6.43),

$$\begin{aligned} \mathcal{D}G_{Iv}\left(\mathbf{\Phi}_{n+1}^{(i)}, \mathbf{w}\right) \cdot \Delta\mathbf{\Phi}_{n+1}^{(i)} &= \frac{d}{d\varepsilon} G_{Iv}\left(\mathbf{\Phi}_{n+1}^{(i+\varepsilon)}, \mathbf{w}\right)\bigg|_{\varepsilon=0} \\ &= \int_{\mathfrak{L}} \left[\mathbf{M}_v\left(\mathbf{\Phi}_{n+1}^{(i)}\right) \frac{d}{d\varepsilon} \mathbf{v}_{n+1}^{(i+\varepsilon)<2>}\bigg|_{\varepsilon=0} \right] \cdot \mathbf{w} dS + \int_{\mathfrak{L}} \left[\frac{d}{d\varepsilon} \mathbf{M}_v(\mathbf{\Phi}_{n+1}^{(i+\varepsilon)})\bigg|_{\varepsilon=0} \mathbf{v}_{n+1}^{(i)<2>} \right] \cdot \mathbf{w} dS, \end{aligned} \tag{6.52}$$

where $\mathbf{v}_{n+1}^{(i+\varepsilon)<2>}$ is defined similar to $\mathbf{v}_{n+1}^{(i)<2>}$, but using the velocity $\mathbf{v}_{n+1}^{(i+\varepsilon)}$ instead of the velocity $\mathbf{v}_{n+1}^{(i)}$. After some reorganization to pull the increment $\Delta\mathbf{\Phi}_{n+1}^{(i)}$ out as a common factor, we obtain

$$\frac{d}{d\varepsilon}\,\mathbf{M}_v(\mathbf{\Phi}^{(i+\varepsilon)}_{n+1})\bigg|_{\varepsilon=0}\,\mathbf{v}^{(i)<2>}_{n+1} = \mathbf{M}_u\left(\mathbf{\Phi}^{(i)}_{n+1},\,\mathbf{v}^{(i)<2>}_{n+1}\right)\Delta\mathbf{\Phi}^{(i)}_{n+1}, \tag{6.53}$$

where

$$\mathbf{M}_u\left(\mathbf{\Phi},\,\mathbf{v}^{<2>}\right)$$
$$= \begin{bmatrix} 0 & 0 & \Pi_1\left({}_{(1)}\dot{\theta}\right)^2\cos\,{}_{(1)}\theta & \Pi_2\left({}_{(2)}\dot{\theta}\right)^2\cos\,{}_{(2)}\theta & \Pi_3\left({}_{(3)}\dot{\theta}\right)^2\cos\,{}_{(3)}\theta \\ 0 & 0 & \Pi_1\left({}_{(1)}\dot{\theta}\right)^2\sin\,{}_{(1)}\theta & \Pi_2\left({}_{(2)}\dot{\theta}\right)^2\sin\,{}_{(2)}\theta & \Pi_3\left({}_{(3)}\dot{\theta}\right)^2\sin\,{}_{(3)}\theta \\ 0 & 0 & -\,\Pi_6\left({}_{(2)}\dot{\theta}\right)^2\cos\psi_{21} & \Pi_6\left({}_{(2)}\dot{\theta}\right)^2\cos\psi_{21} & 0 \\ 0 & 0 & \Pi_6\left({}_{(1)}\dot{\theta}\right)^2\cos\psi_{21} & \Upsilon_4 & \Pi_7\left({}_{(3)}\dot{\theta}\right)^2\cos\psi_{23} \\ 0 & 0 & 0 & \Pi_7\left({}_{(2)}\dot{\theta}\right)^2\cos\psi_{23} & -\,\Pi_7\left({}_{(2)}\dot{\theta}\right)^2\cos\psi_{23} \end{bmatrix}_{5\times5}, \tag{6.54}$$

with

$$\Upsilon_4 := -\,\Pi_6\left({}_{(2)}\dot{\theta}\right)^2\cos\psi_{21} -\,\Pi_7\left({}_{(3)}\dot{\theta}\right)^2\cos\psi_{23}. \tag{6.55}$$

Using the Newmark algorithm (6.34), we have

$$\mathbf{v}^{(i+\varepsilon)}_{n+1} = \mathbf{v}_n + h\left[(1-\tau)\mathbf{a}_n + \tau\mathbf{a}^{(i+\varepsilon)}_{n+1}\right], \tag{6.56}$$

and thus by virtue of (6.45)

$$\frac{d}{d\varepsilon}\mathbf{v}^{(i+\varepsilon)<2>}_{n+1}\bigg|_{\varepsilon=0} = 2Diag\left(\mathbf{v}^{(i)}_{n+1}\right)\frac{d}{d\varepsilon}\mathbf{v}^{(i+\varepsilon)}_{n+1}\bigg|_{\varepsilon=0} = 2Diag\left(\mathbf{v}^{(i)}_{n+1}\right)\frac{\tau}{h\beta}\Delta\mathbf{\Phi}^{(i)}_{n+1}, \tag{6.57}$$

where $Diag\left(\mathbf{v}^{(i)}_{n+1}\right)$ is the diagonal matrix with the components of $\mathbf{v}^{(i)}_{n+1}$ as diagonal coefficients, Finally the linearization of G_{Iv} is obtained as follows

$$\mathcal{D}G_{Iv}\left(\mathbf{\Phi}^{(i)}_{n+1},\mathbf{w}\right)\bullet\Delta\mathbf{\Phi}^{(i)}_{n+1}$$
$$= \int_{\mathfrak{L}}\left\{\left[\,\mathbf{M}_u + \frac{2\tau}{h\beta}\,\mathbf{M}_v Diag\left(\mathbf{v}^{(i)}_{n+1}\right)\right]\bullet\Delta\mathbf{\Phi}^{(i)}_{n+1}\right\}\bullet\mathbf{w}dS. \tag{6.58}$$

Remark 6.4. Similar to Remark 6.3, for a single-layer beam having only the core layer (2), the only nonzero entries in the matrix $\mathbf{M}_u$ in (6.54) are in the fourth column, which corresponds to the rotation of the core layer (2); thus the tangent initia operator is identical to that obtained for single-layer beam case. ∎

Combining (6.51) and (6.58), the total tangent inertia operator can be written as

$$\mathcal{D}G_I\left(\mathbf{\Phi}_{n+1}^{(i)}, \mathbf{w}\right) = \mathcal{D}G_{Ia}\left(\mathbf{\Phi}_{n+1}^{(i)}, \mathbf{w}\right) + \mathcal{D}G_{Iv}\left(\mathbf{\Phi}_{n+1}^{(i)}, \mathbf{w}\right). \tag{6.59}$$

6.5. Tangent Stiffness Operator

We now rewrite the tangent stiffness operator from the contact power (3.25) at time t_{n+1}. For each layer, the tangent material stiffness is obtained from the linearization of ${}_{(\ell)}\mathbf{F}_c$ at $\mathbf{\Phi}_{n+1}^{(i)}$

$$\mathcal{D}\ {}_{(\ell)}\mathbf{F}_c(\mathbf{\Phi}_{n+1}^{(i)}) \boldsymbol{\cdot} \Delta\mathbf{\Phi}_{n+1}^{(i)} = {}_{(\ell)}\boldsymbol{\mathcal{C}}\left({}_{(\ell)}\mathbf{\Lambda}^{(i)}\right)^T {}_{(\ell)}\Xi(\mathbf{\Phi}_{n+1}^{(i)}) \boldsymbol{\cdot} \Delta\mathbf{\Phi}_{n+1}^{(i)}\,. \tag{6.60}$$

Thus, the tangent material stiffness operator for layer (ℓ) can be written as

$$\begin{aligned} &{}_{(\ell)}\mathcal{D}_M G_{dyn}\left(\mathbf{\Phi}_{n+1}^{(i)}, \mathbf{w}\right) \boldsymbol{\cdot} \Delta\mathbf{\Phi}_{n+1}^{(i)} \\ &\quad = \int_{\mathfrak{L}} {}_{(\ell)}\Xi(\mathbf{\Phi})\mathbf{w} \boldsymbol{\cdot}\ {}_{(\ell)}\mathbf{\Lambda}\ {}_{(\ell)}\boldsymbol{\mathcal{C}}\ {}_{(\ell)}\mathbf{\Lambda}^T\ {}_{(\ell)}\Xi(\mathbf{\Phi})\Delta\mathbf{\Phi}_{n+1}^{(i)} dS\,. \end{aligned} \tag{6.61}$$

The tangent geometric stiffness is, on the other hand, obtained from the linearization of the operators ${}_{(\ell)}\Xi$ and ${}_{(\ell)}\mathbf{\Lambda}$ at $\mathbf{\Phi}_{n+1}^{(i)}$, while keeping the material contact forces/couple ${}_{(\ell)}\mathbf{F}_c$ fixed. As given in the static part, we write the tangent geometric stiffness at time t_{n+1} as follows

$${}_{(2)}\mathcal{D}_G G_{dyn}\left(\mathbf{\Phi}_{n+1}^{(i)}, \mathbf{w}\right) \boldsymbol{\cdot} \Delta\mathbf{\Phi}_{n+1}^{(i)} = \int_{\mathfrak{L}} \left[{}_{(2)}\mathbf{\Upsilon}\mathbf{w}\right] \boldsymbol{\cdot} \left[{}_{(2)}\mathbf{B}\ {}_{(2)}\mathbf{\Upsilon} \boldsymbol{\cdot} \Delta\mathbf{\Phi}_{n+1}^{(i)}\right] dS\,, \tag{6.62}$$

$$
{}_{(\ell)}\mathcal{D}_G G_{dyn}\left(\mathbf{\Phi}_{n+1}^{(i)}, \mathbf{w}\right) \cdot \Delta\mathbf{\Phi}_{n+1}^{(i)}
$$

$$
= \int\limits_{\mathfrak{L}} \left[{}_{(\ell)}\mathbf{\Upsilon}_1 \mathbf{w} \cdot {}_{(\ell)}\mathbf{B}_1 \, {}_{(\ell)}\mathbf{\Upsilon}_1 + {}_{(\ell)}\mathbf{\Upsilon}_2 \mathbf{w} \cdot {}_{(\ell)}\mathbf{B}_2 \, {}_{(\ell)}\mathbf{\Upsilon}_2 \right] \cdot \Delta\mathbf{\Phi}_{n+1}^{(i)} dS \text{ , for } \ell = 1, 3, \quad (6.63)
$$

where the differential operators ${}_{(\ell)}\mathbf{\Upsilon}_1$ and ${}_{(\ell)}\mathbf{\Upsilon}_2$ and the matrices ${}_{(\ell)}\mathbf{B}_1$ and ${}_{(\ell)}\mathbf{B}_2$ are defined in Section (3.2).

Using (6.59), (6.61), (6.62) and (6.63), we finally obtain the tangent dynamic stiffness operator

$$
\mathcal{D}G_{dyn}\left(\mathbf{\Phi}_{n+1}^{(i)}, \mathbf{w}\right) \cdot \Delta\mathbf{\Phi}_{n+1}^{(i)} = \left(\mathcal{D}_I + \mathcal{D}_M + \mathcal{D}_G\right) G_{dyn}\left(\mathbf{\Phi}_{n+1}^{(i)}, \mathbf{w}\right) \cdot \Delta\mathbf{\Phi}_{n+1}^{(i)}, \quad (6.64)
$$

where

$$
\begin{aligned}
\mathcal{D}_I G_{dyn}\left(\mathbf{\Phi}_{n+1}^{(i)}, \mathbf{w}\right) &= \mathcal{D}G_I\left(\mathbf{\Phi}_{n+1}^{(i)}, \mathbf{w}\right), && (6.65)\\
\mathcal{D}_M G_{dyn}\left(\mathbf{\Phi}_{n+1}^{(i)}, \mathbf{w}\right) &= \sum_{\ell=1}^{3} \mathcal{D}_M \, {}_{(\ell)}G_c\left(\mathbf{\Phi}_{n+1}^{(i)}, \mathbf{w}\right), && (6.66)\\
\mathcal{D}_G G_{dyn}\left(\mathbf{\Phi}_{n+1}^{(i)}, \mathbf{w}\right) &= \sum_{\ell=1}^{3} \mathcal{D}_G \, {}_{(\ell)}G_c\left(\mathbf{\Phi}_{n+1}^{(i)}, \mathbf{w}\right), && (6.67)
\end{aligned}
$$

as given in (6.59), (6.61) and (3.39), (6.63)}, respectively.

The increment $\Delta\mathbf{\Phi}_{n+1}^{(i+1)}$ is solved for by setting the linearized weak form (6.39) to zero, and thus

$$
\boxed{\Delta\mathbf{\Phi}_{n+1}^{(i+1)} = -\left[\mathcal{D}G_{dyn}\left(\mathbf{\Phi}_{n+1}^{(i)}, \mathbf{w}\right)\right]^{-1} \cdot G_{dyn}\left(\mathbf{\Phi}_{n+1}^{(i)}, \mathbf{w}\right), \quad \forall \mathbf{w} \in \mathcal{V}.} \quad (6.68)
$$

Remark 6.5. In the static case, all tangent matrices are symmetric (Vu-Quoc and Deng [1995*b*]). But in the dynamic case, the tangent dynamic stiffness operator is not symmetric, since the tangent inertia operator (6.59) is not symmetric (see also Remark 6.2).

∎

6.6. Spatial Discretization: Galerkin Finite Element

Similar to the procedure in Section (3.3), the tangent dynamic stiffness matrix $\mathbf{K}$ is obtained as

$$\boxed{\mathbf{K} = \mathbf{K}_I + \sum_{\ell=1}^{3} \left[{}_{(\ell)}\mathbf{K}_M + {}_{(\ell)}\mathbf{K}_G \right] \in \mathrm{R}^{5n \times 5n},} \tag{6.69}$$

where $\mathbf{K}_I = \left[\mathbf{K}_I^{AB}\right]$ is the tangent inertia matrix for all three layers, while ${}_{(\ell)}\mathbf{K}_M = \left[{}_{(\ell)}\mathbf{K}_M^{AB}\right]$ and ${}_{(\ell)}\mathbf{K}_G = \left[{}_{(\ell)}\mathbf{K}_G^{AB}\right]$ are, respectively, the tangent material and geometric stiffness matrices.

By introducing (3.58) into (6.59), we obtain the following expression for the tangent inertia matrix $\mathbf{K}_I^{AB}$

$$\mathbf{K}_I^{AB} = \int\limits_{\mathfrak{L}} \left[\frac{1}{h^2 \beta} \mathbf{M}_a + \mathbf{M}_b + \mathbf{M}_u + \frac{2\tau}{h\beta} \mathbf{M}_v \bullet Diag\left(\mathbf{v}_{n+1}^{(i)}\right) \right] N^A N^B dS. \tag{6.70}$$

Let $\mathfrak{I}_n \in \mathrm{R}^{n \times n}$ be a unit matrix, i.e.,

$$\mathfrak{I}_n := Diag\left[1, \ldots, 1\right] \in \mathrm{R}^{n \times n}. \tag{6.71}$$

By introducing (3.58) into (6.61), we obtain the following expression for the tangent material stiffness matrix ${}_{(\ell)}\mathbf{K}_M^{AB}$ for layer (ℓ)

$${}_{(\ell)}\mathbf{K}_M^{AB} = \int\limits_{\mathfrak{L}} \left\{ {}_{(\ell)}\Xi(\Phi) \left[N^A \mathfrak{I}_5\right] \right\}^T {}_{(\ell)}\mathbf{\Lambda} \, {}_{(\ell)}\boldsymbol{\mathcal{C}} \, {}_{(\ell)}\mathbf{\Lambda}^T \, {}_{(\ell)}\Xi(\Phi) \left[N^B \mathfrak{I}_5\right] dS \in \mathrm{R}^{5 \times 5},$$

$$\text{for } \ell = 1, 2, 3. \tag{6.72}$$

Finally, by introducing (3.58) into (3.39) and (6.63), we obtain the following tangent geometric stiffness matrix for layer (2)

$${}_{(2)}\mathbf{K}_G^{AB} = \int\limits_{\mathfrak{L}} \left\{ {}_{(2)}\mathbf{\Upsilon} \left[N^A \mathfrak{I}_5\right] \right\}^T \left\{ {}_{(2)}\mathbf{B}(\Phi) \, {}_{(2)}\mathbf{\Upsilon} \left[N^B \mathfrak{I}_5\right] \right\} dS \in \mathrm{R}^{5 \times 5}, \tag{6.73}$$

and for layers (1) and (3)

$$
{}_{(\ell)}\mathbf{K}_G^{AB} = \int_{\mathfrak{L}} \Big(\left\{ {}_{(\ell)}\boldsymbol{\Upsilon}_1 \left[N^A \mathbf{\mathfrak{I}}_5 \right] \right\}^T {}_{(\ell)}\mathbf{B}_1(\Phi)\, {}_{(\ell)}\boldsymbol{\Upsilon}_1 + \left\{ {}_{(\ell)}\boldsymbol{\Upsilon}_2 \left[N^A \mathbf{\mathfrak{I}}_5 \right] \right\}^T {}_{(\ell)}\mathbf{B}_2(\Phi)\, {}_{(\ell)}\boldsymbol{\Upsilon}_2 \Big) \left[N^B \mathbf{\mathfrak{I}}_5 \right] dS \in \mathrm{R}^{5\times 5}, \ \text{for } \ell = 1, 3. \tag{6.74}
$$

Finally, the dynamic residual force $\mathbf{r} = \{\mathbf{r}^A\} \in \mathrm{R}^{5n\times 1}$ can be obtained from (6.28)

$$
\boxed{\mathbf{r}^A = \mathbf{F}^A - \overline{\mathbf{F}}^A \in \mathrm{R}^{5\times 1},} \tag{6.75}
$$

where the combined internal (generalized) force $\mathbf{F}^A := \sum_{\ell=1}^{3} {}_{(\ell)}\mathbf{F}^A$ for all the three layers is computed from (3.5), (3.11), (3.19) and (6.4), so that

$$
\mathbf{F}^A\left(\boldsymbol{\Phi}_{n+1}^{(i)}\right) = \int_{\mathfrak{L}} \left[N^A\, \mathbf{M}_a \mathbf{a}_{n+1}^{(i)} + N^A\, \mathbf{M}_v \mathbf{v}_{n+1}^{<2>} \right] dS + \sum_{l=1}^{3} \int_{\mathfrak{L}} \left\{ {}_{(\ell)}\Xi \left[N^A \mathbf{I}_3 \right] \right\}^T \cdot {}_{(\ell)}\mathbf{f}_c dS, \tag{6.76}
$$

and the assigned (generalized) force $\overline{\mathbf{F}}^A$ is computed from (3.27), so that

$$
\boxed{\overline{\mathbf{F}}^A = \int_{\mathfrak{L}} N^A \overline{\boldsymbol{\mathcal{F}}} dS + \left[N^A \overline{\boldsymbol{\mathcal{F}}} \right]_{S=0}^{S=L} \in \mathrm{R}^{5\times 1}.} \tag{6.77}
$$

Substituting the expression for the stiffness matrix $\mathbf{K}$ in (6.69) and the dynamic residual $\mathbf{r}$ in (6.75) into (3.59), we can solve for the new incremental displacement, which subsequently serves to update the configuration from $\boldsymbol{\Phi}_{n+1}^{(i)}$ to $\boldsymbol{\Phi}_{n+1}^{(i+1)}$. The procedure is repeated for the next time step, and so on so forth until convergence.

Remark 6.6. It should be noted that since we allow the overall free motion, the tangent stiffness matrix $[\mathbf{K}_M + \mathbf{K}_G]$ is only positive semi-definite, whereas, the tangent inertia matrix is *not* symmetric. The estimate of time step size maybe difficult for some problems, However, if the *initial* acceleration and velocity is zero, then from (6.47), (6.23) and (6.54), we have

$$\mathbf{M}_b = \mathbf{M}_u = 0, \quad \mathbf{M}_v Diag\left(\mathbf{v}\right) = 0, \tag{6.78}$$

and since $\mathbf{M}_a$ given in (6.22) is symmetric, the tangent inertia matrix $\mathbf{K}_I = \left[\mathbf{K}_I^{AB}\right]$ with $\mathbf{K}_I^{AB}$ given in (6.70) is symmetric. One can obtain the initial time step size by solving a symmetric eigenvalue problem. ∎

CHAPTER 7
NUMERICAL EXAMPLES

The finite element formulation for the dynamics of geometrically-exact sandwich beam presented in Section 6.6 has been implemented in the Finite Element Analysis Program (FEAP), developed by R.L. Taylor (see Zienkiewicz and Taylor [1989]), and run on a DEC 5000 with the Ultrix 4.2 operating system. The finite element basis functions used in the examples in this section are either linear or quadratic. To avoid shear locking, uniformly reduced integration is used to evaluate the tangent material stiffness matrix ${}_{(\ell)}\mathbf{K}_M$ and tangent geometric stiffness matrix ${}_{(\ell)}\mathbf{K}_G$ in (6.69) and the residual matrix (6.75), whereas the tangent inertia ${}_{(\ell)}\mathbf{K}_I$ in (6.69) is evaluated exactly.[26]

7.1. Sandwich Frame with Ply Drop-offs

We now apply the proposed formulation to an important class of multilayer structures with ply drop-offs. First, we concern with the static case. The sandwich frame in this example is shown in Figure 7.1. The two vertical beams of the frame have three parts: The lower part has three layers, the middle part two layers, and the upper part one layer. Such arrangement form sharp discontinuities in the vertical beam. The horizontal beam of the frame has only one layer. The present example illustrates the ability of the proposed formulation in dealing with ply drop-offs problems. The case of multilayer beams with ply drop-offs in small deformation is discussed in Zinno and Barbero [1994]. The material properties for all three layers selected for the present example are

$$E = 24,000,\ \nu = 0.2,\ \chi = 1, \tag{7.1}$$

---

[26] We must use macro command 'utan' to form the unsymmetric tangent stiffness matrix in FEAP.

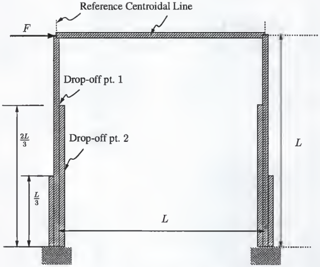

Figure 7.1. *Sandwich frame with ply drop-offs.* Applied horizontal force at the centroidal line of the top beam.

where E is youngs' modulus, ν the Poisson's ratio, and χ the shear correction coefficient. Also the half layer thickness is set to ${}_{(\ell)}h = 0.1$, for $\ell = 1, 2, 3$. The above data lead to the following elastic moduli of the beam layer

$$ {}_{(\ell)}EA = 4,800, \;\; {}_{(\ell)}GA_s = 2,000, \;\; {}_{(\ell)}EI = 16, \text{ for } \ell = 1, 2, 3. \qquad (7.2) $$

Both the two vertical beams and the horizontal beam have the same length $L = 10$; the ply drop-offs in the vertical beams occur at $L/3$ and $2L/3$ as shown in Figure 7.1.

First, to verify the modeling of the frame, we use uniform sandwich beams with three layers, and without ply drop-offs in the two vertical beams; the horizontal beam remains single layer. The result are compared to those of the same frame but with the

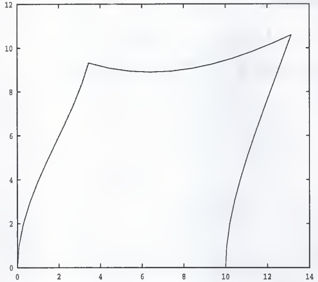

Figure 7.2. Deformed shapes of the sandwich frame *without* ply drop-offs (solid line) and the equivalent single-layer frame (dotted line). The difference in the two deformed shapes is hardly discernible.

two vertical (uniform sandwich) beams replaced by equivalent single-layer beams[27] with elastic moduli

$$EA = 14,400, \quad GA_s = 6,000, \quad EI = 432. \tag{7.3}$$

In the present example, the two vertical beams are uniformly discretized using 10 sandwich beam elements, whereas the horizontal beam is discretized using 10 (single-layer) beam elements. A horizontal force of magnitude $F = 20$ is applied at the upper left corner of the beam, along the centroidal line of the horizontal beam.

Table 7.1 summarizes the comparison of the generalized displacements at the point

---

[27] We refer the readers to Vu-Quoc and Deng [1995*b*] for the detail of the equivalent single-layer beam of a sandwich beam.

Table 7.1. Displacements at the point of application of the force of the sandwich frame *without* ply drop-offs and of the equivalent single-layer frame.

Disp.	Sandwich model	Equivalent model	Relative error
u^1	3.44288E+00	3.42967E+00	0.0038
u^2	−6.84398E−01	−6.79942E−01	0.0065
${}_{(1)}\theta$	−2.86020E−01	not available	not available
${}_{(2)}\theta$	−2.84562E−01	−2.85354E−01	−0.0028
${}_{(3)}\theta$	−2.84307E−01	not available	not available

of application of the force. Clearly, there is only one rotation in the equivalent single-layer frame. It can be seen from Table 7.1 that the present sandwich model yields almost the same results as those obtained using the equivalent single-layer model. The relative error is no more than 0.7%; such a small relative error can also be seen in Figure 7.2, from which one can hardly discern the difference between the deformed shape of the sandwich frame *without* ply drop-offs and that of the equivalent single-layer frame.

Second, we calculate the sandwich frame with ply drop-offs shown in Figure 7.1. Since the present frame is more flexible than the frame without ply drop-offs, we decrease the horizontal force to $F = 6$. All the two vertical beams and the horizontal beam are uniformly discretized using 12 sandwich elements. Note that the middle third of the two vertical beams is modeled using sandwich beams with 1 inexistent layer. The upper third of the two vertical beams and the horizontal beam are modeled using sandwich beams with inexistent top and bottom layers. The converged configuration of the frame is obtained after 4 time steps, and with an average of 26 iterations per time step to converge.

The same problem is also modeled using the equivalent single-layer beam *with* ply drop-offs represented by the discontinuities in the beam elastic moduli. A shortcoming of this model is that the ply drop-offs are necessarily symmetric, due to the existence of only a single layer in the model, as shows in Figure 7.3. The same number of elements as in the case of sandwich frame is used.

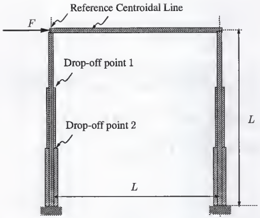

Figure 7.3. *Equivalent single-layer frame with symmetric ply drop-offs.*

The displacements at the drop-off point 2 (see Figure 7.1 and Figure 7.3) of the sandwich frame with unsymmetric drop-offs and of the equivalent single-layer frame with symmetric drop-offs are given in Table 7.2. A similar comparison for the point of application of the force is given in Table 7.3.

It can be seen from Table 7.2 and Table 7.3 that the difference is very large, with order ranging from 20% to 40%, except for the rotation of the core layer when compared to the only rotation of the equivalent single-layer frame. The reason for the large difference in the result is that hinges are not allowed in the cross section of the equivalent single-layer model (the cross section remains plane after deformation), thus making the single-layer model stiffer than the sandwich model. It should be noted that the equivalent single-layer beam is still stiffer than the sandwich beam with *symmetric* ply drop-offs, since the latter allows the formation of hinges, in particular, at the drop-offs points. In

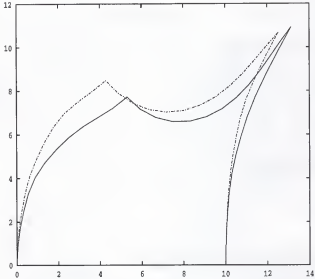

Figure 7.4. Deformed shapes of the sandwich frame with *unsymmetric* ply drop-offs (solid line) and of the equivalent single-layer frame with *symmetric* ply drop-offs (dotted line).

addition, the symmetric ply drop-offs renders the beam stiffer than the unsymmetric one, which cannot be modeled using the equivalent single-layer beam. The deformed shapes of the sandwich frame and of the equivalent single-layer frame are given in Figure 7.4, where one can easily see the difference.

We remove the static applied load $F = 6$ from the deformed positions shown in Figure 7.4 to let the frame undergo free vibration. The *nonlinear* vibrational period is estimated to be $T \approx 6.80$ for the sandwich frame with unsymmetric ply drop-offs and $T \approx 6.10$ for the equivalent single-layer frame with symmetric ply drop-offs (see Figure 7.5). Figure 7.6 shows the deformed shapes of both the sandwich beam model and the equivalent single-layer beam model at different time step, where $t = 6$ is the time when

Table 7.2. Displacements at the drop-off point 2 for the sandwich frame with *unsymmetric* ply drop-offs and for the equivalent single-layer frame with *symmetric* ply drop-offs.

Disp.	Sandwich model	equivalent model	Relative error
u^1	5.46323E−01	3.94658E−01	0.2776
u^2	−4.73368E−02	−2.95626E−02	−0.3755
$_{(1)}\theta$	−2.73068E−01	not available	not available
$_{(2)}\theta$	−3.09258E−01	−2.18808E−01	−0.2925
$_{(3)}\theta$	−3.10269E−01	not available	not available

Table 7.3. Displacements at point of application of the force for the sandwich frame with *unsymmetric* ply drop-offs and for the equivalent single-layer frame with *symmetric* ply drop-offs.

Disp.	Sandwich model	equivalent model	Relative error
u^1	5.30519E+00	4.28523E+00	0.1923
u^2	−2.28209E+00	−1.52320E+00	0.3325
$_{(1)}\theta$	not available	not available	not available
$_{(2)}\theta$	−8.41638E−01	−8.63334E−01	−0.0258
$_{(3)}\theta$	not available	not available	not available

the frame is released from the static load F and $t = 9.6$ is the approximate time when the sandwich frame reaches its maximum deformation. We should note that the period of this nonlinear vibration of the frame is different from the linear vibrational period of the frame $T_l = \frac{2\pi}{\omega}$, where ω is the natural frequency of the frame. The linear vibrational period is $T_l = 8.04881823$ for the sandwich frame with unsymmetric ply drop-offs and $T_s = 6.504199$ for the single-layer frame with symmetric ply drop-offs, which again shows that the single-layer model is stiffer than the sandwich model. Also, one should note that the deformed shape at $t = 9.6$ is not symmetric to the one at $t = 6$, since the latter is not a vibrational mode for the frame.

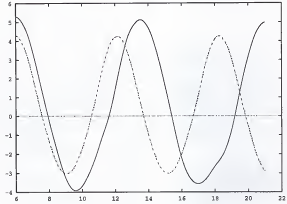

Figure 7.5. *Free vibration of the sandwich frame with unsymmetric ply drop-offs and the single-layer frame with symmetric ply drop-offs.* Time history of the horizontal displacement of the point of the applied force. At $t = 6$, the frame is released from the static load. Solid line: sandwich frame; dotted line: single-layer frame.

7.2. Comparison of Sandwich Beam Having Three Identical Layers with Equivalent Single-layer Be

The implementation of the tangent inertia and stiffness matrices of the proposed sandwich beam element has thus been verified in Section 7.1 , see also Vu-Quoc and Deng [1995*b*] for further validation. We now provide further verification of the implementation of the tangent inertia matrix of the proposed sandwich beam.

7.2.1. Vibrational frequencies

In the first model, a sandwich beam with three identical layers and length $L = 3$ as shown in Figure 7.7 is used. The following geometric and material properties are employed:

$$ {}_{(\ell)}h = 0.01, \quad {}_{(\ell)}A^0_\rho = 1, \quad {}_{(\ell)}EA = 60,000, \quad {}_{(\ell)}GA_s = 24,000, \quad {}_{(\ell)}EI = 2, \text{ for } \ell = 1, 2, 3, \tag{7.4} $$

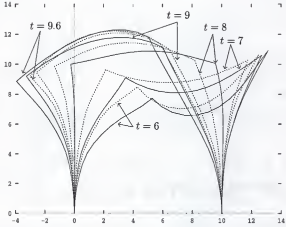

Figure 7.6. *Free vibration of the sandwich frame with unsymmetric ply drop-offs and the single-layer frame with symmetric ply drop-offs.* Deformed shapes at different time steps. At $t = 6$, the frame is released from the static load. Solid line: sandwich frame; dotted line: single-layer frame.

where we recall that ${}_{(\ell)}h = 0.01$ is the half layer thickness of layer (ℓ) and ${}_{(\ell)}A^0_\rho$ the mass per unit underformed length of layer (ℓ). In the second model, an equivalent single-layer beam is used, with the following mass per unit underformed length and material properties

$$A^0_\rho = 3, \quad EA = 180,000, \quad GA_s = 72,000, \quad EI = 54. \tag{7.5}$$

The equivalent axial and shear stiffness coefficients EA and GA_s are obtained by summing up the corresponding coefficients for the three layers of the sandwich beam, whereas the equivalent bending stiffness coefficient is obtained by using the assumption of plane section deformation (i.e., no hinge formation; in other words, the constraints ${}_{(1)}\theta = {}_{(2)}\theta = {}_{(3)}\theta$ are enforced), and $A^0_\rho = 3$ is obtained by summing up the mass per unit underformed length of each layer of the sandwich beam. The cantilever boundary conditions

Table 7.4. Comparison of the first four frequencies of the sandwich model vs. the equivalent single-layer model. Beam length $L = 3$.

Number of mode	Sandwich model	Single-layer model	Relative error
1	0.16582920E+01	0.16583236E+01	1.9055E−05
2	0.10465473E+02	0.10466863E+02	1.3280E−04
3	0.29700357E+02	0.29709793E+02	3.1761E−04
4	0.59435450E+02	0.59470526E+02	5.8980E−04

at $S = 0$ are

$$u^1(0) = u^2(0) = {}_{(1)}\theta(0) = {}_{(2)}\theta(0) = {}_{(3)}\theta(0) = 0, \tag{7.6}$$

for the sandwich model, and

$$u^1(0) = u^2(0) = \theta(0) = 0, \tag{7.7}$$

for the equivalent single-layer model, respectively.

Twenty linear elements are employed in both models to discretize uniformly the cantilever beam. Table 7.4 shows relatively small errors between the two models for the first four frequencies: less than 0.002% for the first mode, and less than 0.06% for the fourth mode. Such accuracy provides further confidence in the implementation of the tangent inertia matrix.

Next, we use the same parameters as in the previous example, but now with the beam length $L = 0.3$, i.e., a short beam. Table 7.5 shows the comparison of the first four frequencies of the sandwich model vs. the equivalent single-layer model.

Comparing the results presented in Table 7.4 and Table 7.5, it can be seen that the relative error in frequencies increases with the aspect ratio $\frac{h}{L}$, and that frequencies of the equivalent single-layer model are in general higher than those of the sandwich model, for the same vibrational mode. The reason for the above observation lies in the flexibility of the sandwich beam theory, in which hinges in the cross section are allowed to form,

Table 7.5. Comparison of the first four frequencies of the sandwich model vs. the equivalent single-layer model. Beam length $L = 0.3$.

Number of mode	Sandwich model	Single-layer model	Relative error
1	0.16261495E+03	0.16277602E+03	9.8952E−04
2	0.92656939E+03	0.93070401E+03	4.4425E−03
3	0.12764778E+04	0.12832095E+04	5.2460E−03
4	0.23298024E+04	0.23409991E+04	4.7829E−03

thus as the beam gets thicker, the error of the equivalent single-layer model relative to the sandwich model also increases.

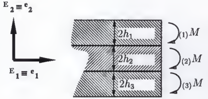

Figure 7.7. Sandwich beam with three identical layers. Assigned layer moments at beam tip.

7.2.2. Harmonic response of cantilever beam with three identical layers

We now consider the harmonic response of both the sandwich beam with three identical layers and the equivalent single-layer beam. Since the sandwich beam is made up of three identical layers, which have the same material properties, we expect that it will behave almost the same as the equivalent single-layer beam, except near the tip of the beam where the applied force or moment are exerted; there the rotations in the three layers will not be equal, and the assumption that plane section remains plane is not valid (i.e., the Saint-Venant principle, see Vu-Quoc and Deng [1995*b*] for more detail).

Here, we use the same material properties as given in (7.4) and the beam length

Table 7.6. Comparison of convergence rate of the sandwich model vs. the equivalent single-layer model in the first time step.

Number of iteration	Residual norm for sandwich model	Residual norm for single-layer model
0	0.5942987E+00	0.1657988E+00
1	0.1434455E−01	0.1517042E−02
2	0.8395247E−10	0.1341774E−09

Table 7.7. Comparison of convergence rate of the sandwich model vs. the equivalent single-layer model in the last time step.

Number of iteration	Residual norm for sandwich model	Residual norm for single-layer model
0	0.3080571E+04	0.3552385E+04
1	0.5163974E+03	0.6369403E+03
2	0.1231497E+03	0.2074593E+03
3	0.1674125E+01	0.2754551E+01
4	0.1203076E−01	0.7015308E−01
5	0.1657988E+00	0.3404278E−06
6	0.1520798E−02	converged
7	0.7809108E−10	converged

is $L = 3$. The cantilever boundary conditions at $S = 0$ is established by fixing all the 5 dof's as in (7.6). A force $F^2 = F \sin \omega t$ is applied at the tip of the cantilever beam with $F = 5$ and $\omega = 1.658292$, which is the first frequency of the beam as discussed in Subsection 7.2.1. The time step size chose is $\Delta t = 0.02$; the analysis is performed over 800 time steps. For the sandwich model, it takes about 2 iterations to converge at the beginning of the analysis and 7 iterations to converge in the last time step. The convergence study just mentioned is summarized in Table 7.6, from which it can be seen that the convergence behavior of the two models (sandwich and equivalent single-layer) is similar, despite the relative complexity of the sandwich model, even though towards the last time step in loading stage, a few more iterations are required for the sandwich model to converge (see Table 7.7).

Also, at $t = 16.0$, we obtain the tip displacements $u^1 = 0.7850670$, $u^2 = 2.7305944$ for the sandwich model, and $u^1 = 0.7778839$, $u^2 = 2.7333533$ for the equivalent single-layer model, the relative error for u^1 and u^2 are 0.92% and 0.1%, respectively. The time histories of the transverse displacements of both models are plotted in Figure 7.8, where one can hardly discern the difference between the two lines since the relative error is small as just mentioned.

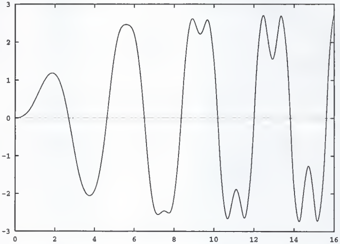

Figure 7.8. *Cantilever sandwich beam with three identical layers* subject to a harmonic force at beam tip. Time history of the transverse displacement u^2 at the beam tip. Solid line: sandwich model; dotted line: equivalent single-layer model.

7.2.3. Cantilever sandwich beam with three identical layers under impact force

Now consider the same beam as in Subsection 7.2.1, and the response to a transverse impact force applied at the free end of the beam. The beam is subjected to a tip load $F^2 = 400t$ for $t \in [0,\ 0.2]$, and undergoes free vibration for $t \in]0.2,\ 4]$. During

Table 7.8. Comparison of convergence rate of the sandwich model vs. the equivalent single-layer model in the last time step of the loading stage.

Number of iteration	Residual norm for sandwich model	Residual norm for single-layer model
0	0.1518376E+04	0.1538445E+04
1	0.1169280E+03	0.2019830E+03
2	0.1957944E−01	0.4496138E−01
3	0.1203561E−05	0.5679505E−04

the loading stage, we use the time step size $\Delta t = 0.10$, and during the free vibration stage $\Delta t = 0.02$. The time step size during the free vibration stage of the cantilever beam is smaller than that in the loading stage to capture the higher frequency contents in the vibration. The convergence study is summarized in Table 7.8, where it can be seen that the convergence rate is almost the same for the sandwich model and for the equivalent single-layer model: Both models require 3 iterations to converge during the last time step in the loading stage. And the same conclusion can be obtained for the free vibration stage.

The comparison of displacements at the beam tip at the last time step of the loading stage, i.e., at $t = 0.2$ are summarized in Table 7.9, from which we can see that the three rotations in the sandwich model are very close to the rotation in the equivalent single-layer model, because the beam is long and thin. The time histories of the transverse displacement u^2 at the beam tip are given in Figure 7.9; there the difference in the results between the sandwich model and the equivalent single-layer model is clearly discernible, with the maximum relative error 10.4% happened at $t \approx 1.24$. The time histories of the rotations are given in Figure 7.10; there the difference among the three rotations of the sandwich model is not discernible, but the difference between the rotations in the sandwich model and the rotation in the equivalent single-layer model can be clearly seen.

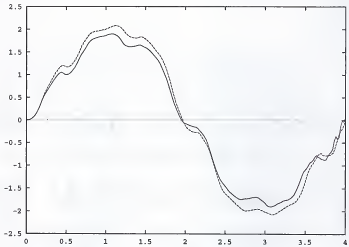

Figure 7.9. *Cantilever sandwich beam with three identical layers.* Assigned impact force at the beam tip, time history of the transverse displacement u^2. Solid line: equivalent single-layer model; dotted line: sandwich model.

7.3. Ideal Sandwich Beam

We now consider the so-called *ideal classical* sandwich beam shown in Figure 7.11. The beam has a symmetric cross section which has a soft core layer, together with very thin but stiff outer layers (see Sayir and Koller [1986]). Such thin and stiff outer layers are expected to allow primarily shear deformation in the sandwich beam, since they prevent bending by means of membrane force almost completely.

7.3.1. Comparison of frequencies

We now consider a simply supported ideal sandwich beam with overhangs, shown in Figure 7.12, with unit width and with the following geometric parameters

$$L = 10, \quad {}_{(1)}h = {}_{(3)}h = 0.025, \quad {}_{(2)}h = 0.5, \tag{7.8}$$

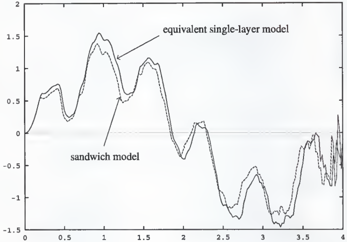

Figure 7.10. *Cantilever beam with three identical layers.* Assigned impact force at the beam tip, time history of the tip rotations. Solid line: equivalent single-layer model; dotted line: sandwich model (the different between the three rotations is hardly discernible).

The material properties used are as follows

$$\chi = \frac{A_s}{A} = 1, \quad \nu = 0.25, \tag{7.9}$$

$$_{(1)}E = {}_{(3)}E = 4 * 10^5, \quad {}_{(2)}E = 10^3. \tag{7.10}$$

(7.8)–(7.10) together yield the following elastic moduli for the three layers

$$_{(1)}EA = {}_{(3)}EA = 20,000, \tag{7.11}$$

$$_{(1)}EI = {}_{(3)}EI = 4.1667, \tag{7.12}$$

$$_{(1)}GA_s = {}_{(3)}GA_s = 8,000, \tag{7.13}$$

Table 7.9. Comparison of the displacements of the sandwich model vs. the equivalent single-layer model in the last time step of the loading stage.

Disp.	Sandwich model	Single-layer model	Relative error
u^1	− 0.106041	−0.108650	2.4%
u^2	0.453639	0.458377	1.03%
$_{(1)}\theta$	0.552368	not available	not available
$_{(2)}\theta$	0.552320	0.578036	4.44%
$_{(3)}\theta$	0.552368	not available	not available

Table 7.10. Comparison of the first four frequencies of the ideal sandwich model and of the equivalent single-layer model. Small core-layer shear stiffness.

Number of mode	Sandwich model	Single-layer model	Relative error
1	0.76712126D+00	0.83333678D+00	0.0795
2	0.10024876D+01	0.13713586D+01	0.2690
3	0.16309037D+01	0.28206429D+01	0.4218
4	0.34904063D+01	0.61831867D+01	0.4355

$$_{(2)}EA = 1{,}000, \quad _{(2)}EI = 83.33, \quad _{(2)}GA_s = 400. \tag{7.14}$$

Using the method described in Subsection 7.2.1, we obtain the following elastic moduli for the single-layer beam equivalent to the ideal sandwich beam

$$EA = 41{,}000, \; GA_s = 16{,}400, \; EI = 11{,}116.7. \tag{7.15}$$

We now can calculate and compare the frequencies to check if the equivalent single-layer model is accurate enough. Table 7.10 gives the comparison of the first four frequencies of the two models of the simply supported beam shown in Figure 7.12.

It can be seen from the results shown in Table 7.10, that the difference between the ideal sandwich beam and its equivalent single-layer beam is much larger than the difference between the sandwich beam with three identical layers and its equivalent single-layer beam, as mentioned in Subsection 7.2.1. The reason is that in the ideal sandwich beam,

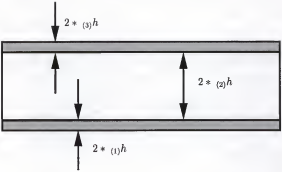

Figure 7.11. *Ideal sandwich beam.* Profile: Thick and soft core layer, thin and stiff outer layers.

the core layer is so soft that the two outer layer rotations are much different from the core layer rotation, thus making the plane cross-section assumption invalid (as can be seen later). So we know that the equivalent single-layer beam is not good enough to model the ideal sandwich beam.

Now, we change the shear stiffness of the core layer of the ideal sandwich beam to a large quantity (that means to force the two outer layer rotations to be the same as the core layer rotation), say, for example, ${}_{(2)}GA_s = 8,000$, while keeping unchanged the other material properties. The elastic moduli of the equivalent single-layer beam are the same as in (7.15) except for $GA_S = 24,000$. Table 7.11 shows the first four frequencies of the ideal sandwich model and of the equivalent single-layer model for the simply supported beam with overhangs. We can see from Table 7.11 that the difference between the sandwich model and its equivalent single-layer model has been reduced dramatically, in fact near zero for the first three frequencies, which means using equivalent single-layer model is accurate enough.

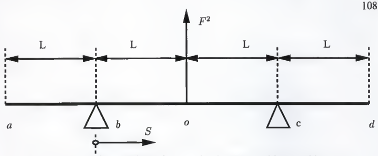

Figure 7.12. *Ideal sandwich beam.* Simply-supported beam with overhangs: Loading at the mid-span; the origin of coordinate S is at the support b.

Table 7.11. Comparison of the first four frequencies of the ideal sandwich model and of the equivalent single-layer model. Large core-layer shear stiffness.

Number of mode	Sandwich model	Single-layer model	Relative error
1	0.83306909E+00	0.83431282D+00	0.0015
2	0.13589369E+01	0.13789915D+01	0.0145
3	0.27811409E+01	0.28574081D+01	0.0267
4	0.69658177E+01	0.61840680D+01	−0.1263

7.3.2. Simply supported ideal sandwich beam with overhangs

Now consider the harmonic response of the simply supported ideal sandwich beam with two symmetric overhangs (see Figure 7.12), with the same material properties as given in (7.11) to (7.14) and the total beam length $4 * L = 40$. The beam is on a roller at point b, and is simply supported at point c. A transverse concentrated force $F^2 = 20\sin(\omega t)$ is applied at the center of the beam, with the excitation frequency $\omega = 0.76712126$ being the square root of the first eigenvalue as obtained in Table 7.10. The calculation was performed using time step size $\Delta t = 0.1$ and 2200 time steps. It takes an average of 2 iterations to converge both at the beginning and at the end of the loading. Note that the natural period of the linearized beam is $T = \dfrac{2\pi}{\omega} \approx \dfrac{2 * 3.1416}{0.7671} \approx 8.1908$ and thus the time step size $\Delta t \approx \dfrac{T}{80}$, that means that our formulation needs small time

Table 7.12. Convergence rate in the 1000*th* time step for the harmonic response of an ideal sandwich beam.

Number of iteration	Residual norm for sandwich beam
0	0.3534135E+03
1	0.3003966E+01
2	0.8976568E−05

step size to have good convergence properity for the large deformation. Table 7.12 shows the convergence obtained for the 1000*th* loading step.

Figure 7.13 shows the deformed shapes at various time stations. In sandwich beams, we note that there is a clear break in the slope of the beam at the support, i.e., the slope of the beam inside a support is different from the slope outside that support (in the overhang part); see Figure 7.14 for the deformed shape at $t = 1$. Such discontinuity in the beam slope exists in sandwich beams but not in single-layer beams; the reader is referred to Vu-Quoc and Deng [1995*b*] for an analysis and to Sayir and Koller [1986] for experimental evidence.

It can be seen from Figure 7.15 that at the beginning the vibration amplitude increases as time increases; such increase in amplitude is characteristic of beam vibration at resonance. However, as the amplitude increase, nonlinear effects set in, preventing further increase in amplitude; one observes instead a beat phenomena that follows. Such nonlinear vibration effects would be an interesting subject for an analytical study.

7.3.3. Ideal sandwich frame subject to tip impact force

To further demonstrate that the core-layer shear stiffness in an ideal sandwich beam is the main factor that makes the results depart from those obtained from the equivalent single-layer beam, we calculate the sandwich frame shown in Figure 7.16 with two different core-layer shear stiffnesses, and compare with the results obtained by using the

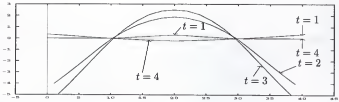

Figure 7.13. *Harmonic response of a simply supported ideal sandwich with overhangs.* Deformed shapes at $t = 1.0$, 2.0, 3.0, 4.0. Vertical displacement scaled up by two.

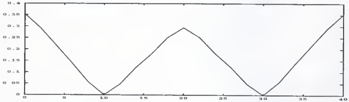

Figure 7.14. *Harmonic response of a simply supported ideal sandwich with overhangs.* Deformed shapes at $t = 1.0$. Vertical displacement scaled up by thirty. A clear break in the beam slope can be observed at the supports.

equivalent single-layer model. The impact force at the tip is $F = -1,000 * t$ for the time $0 \leq t \leq 0.5$, and $F = 0$ for $0.5 \leq t \leq 6$.

First, we consider a sandwich frame with large core-layer shear stiffness so that the results is expected to be close to that from an equivalent single-layer frame. The material properties are the same as in (7.11)–(7.14), except for the core-layer shear stiffness ${}_{(2)}GA_s = 20,000$ (which is much bigger than the previously used value of ${}_{(2)}GA_s = 400$, and thus making the layer rotations to be close to each other). The material properties of the equivalent single-layer are the same as in (7.15) except for the shear stiffness modulus of $GA_s = 36,000$. For both models, we use 20 uniformly distributed linear elements, and the time step size $\Delta t = 0.05$.

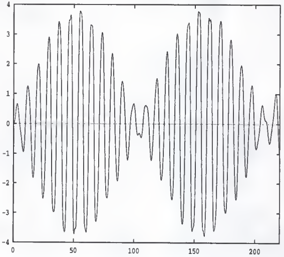

Figure 7.15. *Harmonic response of a simply supported ideal sandwich beam with overhangs.* Time history of transverse displacement u^2 at midspan.

From the time history of the tip displacements shown in Figure 7.17, and the deformed shapes shown in Figure 7.19, one can hardly discern the difference between the result of the sandwich frame and that of the equivalent single-layer frame, and from Figure 7.18, one can see that the layer rotations in the sandwich frame are almost the same, and are approximately equal to the rotation of the equivalent single-layer model. At the end of the loading, i.e., $t = 6$, we give the tip displacements in Table 7.13. The relative error between the results obtained from the two models are very small, meaning that for ideal sandwich beams with large core-layer shear stiffness, it more efficient to use the equivalent single-layer beams, which produce relatively accurate results as compared to the sandwich model, at a lower cost since there are 40% less degrees of freedom than in the sandwich model.

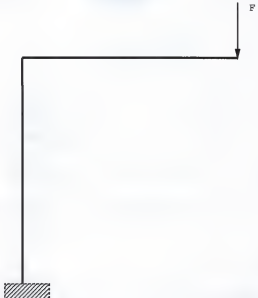

Figure 7.16. *Ideal sandwich frame.* All degrees of freedom fixed at the clamped end for all models. Response to impact force at the tip.

Second, we consider the ideal sandwich frame with the material properties as given in (7.11)-(7.14), subjected to the same loading force as used above. As one can see later in Figure 7.21 that there are high frequency vibrations for outer layer rotations, we choose the time step size as $\Delta t = 10^{-5}$, which is much smaller than the fundamental period $T = 10.13445$ of the ideal sandwich frame. The material properties of the equivalent single-layer beam are as given in (7.15). The time histories of the spatial coordinate (x^1, x^2) of the frame tip in the ideal sandwich model and in the equivalent single-layer model are given in Figure 7.20, where one can observe the large difference in the results of these models.

It can be seen clearly from Figure 7.21 that the rotation in the core layer (2) differs greatly from the rotations in the outer layers, thus making the assumption of plane deformed cross section invalid. It follows that there is a large difference in the results of

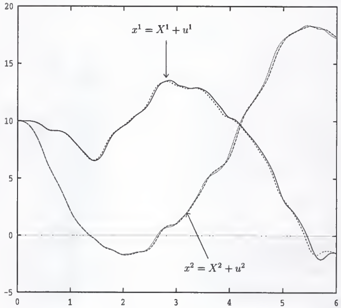

Figure 7.17. *Comparison of ideal sandwich frame with equivalent single-layer frame subject to impact force at tip.* Large core-layer shear stiffness ${}_{(2)}GA_s = 20,000$. Time history of axial displacement and transverse displacement at frame tip. Solid line: sandwich model; dotted line: equivalent single-layer model.

the ideal sandwich model with small core-layer stiffness and its equivalent single-layer model. Figure 7.22 depicts the deformed shapes of the two models at different times stations. At time $t = 3$ and $t = 5$, the deformed shapes of the two models differ from each other remarkably. Table 7.14 gives the tip displacements for the two models at $t = 3.0$.

In order to analyze the high frequency vibrations of the outer layer rotations shown in Figure 7.21 and the discontinuities in the slope of the ideal sandwich beam at certain time steps (e.g., $t = 1.0$) shown in Figure 7.22, we proceed our calculation by using a refined time step size from $t = 0.4$. Thus the time step size for the following analysis is

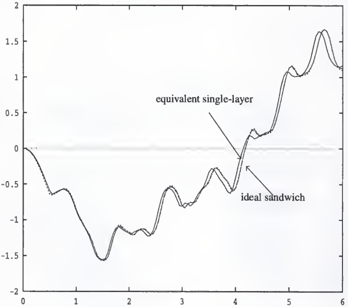

Figure 7.18. *Comparison of ideal sandwich frame with equivalent single-layer frame subjected to impact force at tip.* Large core-layer shear stiffness ${}_{(2)}GA_s = 20,000$. Time history of rotations at frame tip. Dotted lines: sandwich model (notice that one can hardly discern the difference between the three rotations); solid line: single-layer model.

$\Delta t = 10^{-5}$ for $0 \leq t < 0.4$, and $\Delta t = 2 \times 10^{-6}$ for $0.4 \leq t \leq 1.2$.

Figure 7.23 shows the zoom-in figure that corresponds to Figure 7.21 in time interval $0.4 \leq t \leq 1.2$, where one can see clearly the high frequency vibration of the outer layer rotations. Also from Figure 7.23 (and from Figure 7.21); it can be seen that the two outer layer rotations ${}_{(1)}\theta$ and ${}_{(3)}\theta$ are almost the same throughout the time interval except at the end of the loading stage when the rotation ${}_{(1)}\theta$ of layer (1) is little larger than rotation ${}_{(3)}\theta$ of layer (3). The same observation can also be made in the subsequent zoom-in figures for the deformed shape.

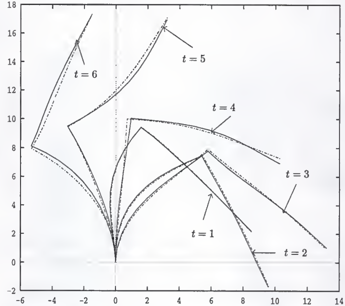

Figure 7.19. *Comparison of ideal sandwich frame with equivalent single-layer frame subject to impact force at tip.* Large core-layer shear stiffness ${}_{(2)}GA_s = 20,000$. Deformed shapes at different time steps. Solid lines: sandwich frame; dotted lines: equivalent single-layer frame.

An ideal sandwich beam is expected to display primarily shear deformation, with bending deformation resisted to a large extent by the membrane action of the two outer layers. Large shear deformations occur at the frame tip (where the concentrated load is applied—see Figure 7.24) and at the intersection between the vertical beam and the horizontal beam (Figure 7.25). Both Figure 7.24 and Figure 7.25 are taken at the end of the loading stage (i.e., just before the concentrated force at the frame is removed). The core layer (2) is weak in shear, and thus, because of the shear deformation, its section does not rotate as much as the centroidal line (see Figure 7.24); such shear deformation in layer (2) in turn generates shear deformation in the outer layers, making the overall

Table 7.13. Comparison of tip displacements for sandwich frame having large core-layer shear stiffness and for equivalent single-layer frame.

Disp.	Sandwich frame	Equivalent frame	Relative error
u^1	−1.15052E+01	−1.15495E+01	0.0038
u^2	7.33522E+00	7.23053E+00	−0.0145
$_{(1)}\theta$	1.09839E+00	not available	not available
$_{(2)}\theta$	1.12280E+00	1.16662E+00	0.0376
$_{(3)}\theta$	1.12610E+00	not available	not available

(broken) cross section of the sandwich frame at the tip depart clearly from a plane cross section. The magnitude of this section deformation diminishes, however, as one moves away from the frame tip (Figure 7.24). When the applied concentrated load is removed, the energy stored in the shear deformation of the frame cross section is released, causing the outer layer rotations to oscillate rapidly around the core-layer rotation, especially at the frame tip.

From Figure 7.24 and Figure 7.25, one can see that at the end of the loading stage ($t = 0.5$), large shear deformation occurs in the outer layers at the beam tip, where single load applied, and at the intersection of the vertical beam and horizontal beam. This sudden change in shear deformation diminishes when it moves away from the point where the single load applied on or the point of intersection. When one release the load from the frame tip, the energy stored in the form of shear energy is released, causing the two outer layer rotations to oscillate around the core layer rotation, especially at the point where the single load was on and the point of intersection. Just after the concentrated force is released, the deformed shapes of 4 elements at the frame tip and of 4 elements at the beam intersection are presented in Figure 7.26 and Figure 7.27. Comparing Figure 7.26 and Figure 7.27 with Figure 7.24 and Figure 7.25, one can observe the motion of shear waves moving away from the frame tip and from the beam intersection.

After the load is released from the frame, inertia still causes the frame to move

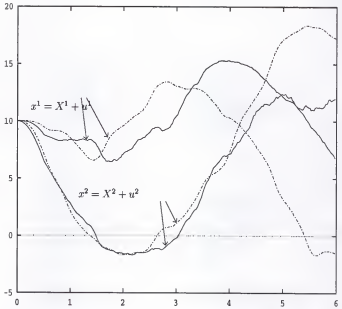

Figure 7.20. *Comparison of ideal sandwich frame with equivalent single-layer frame subjected to impact force at tip.* Small core-layer shear stiffness ${}_{(2)}GA_s = 400$. Time history of axial displacement and transverse displacement at frame tip. Solid lines: sandwich model; dotted lines: equivalent single-layer model.

down, and the transverse shear waves still propagate along the sandwich frame, causing the frame to deformed further. Figure 7.29 and Figure 7.28 show the zoom-in figures of portions of the deformed shape at time $t = 1$ (Figure 7.22); sharp discontinuities in the slope can be clearly observed, both at the frame tip (Figure 7.29) and in the upper portion of the vertical beam (Figure 7.28). From the deformed shapes at $t = 3$ and $t = 5$ shown in Figure 7.22, one can also see that there can be more than one points of discontinuities in the slope.

As we mentioned above, the natural frequency of the ideal sandwich beam differs

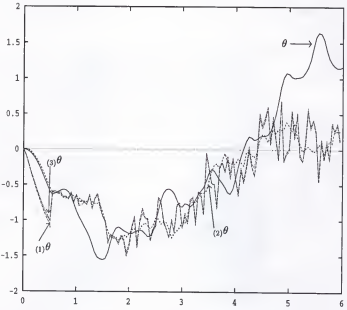

Figure 7.21. *Comparison of ideal sandwich frame with equivalent single-layer frame subjected to impact force at tip.* Small core-layer shear stiffness ${}_{(2)}GA_s = 400$. Time history of rotations at frame tip: Rotation θ of equivalent single-layer frame; and rotations ${}_{(1)}\theta$, ${}_{(2)}\theta$, ${}_{(3)}\theta$ of ideal sandwich frame.

largely from that of the equivalent single layer beam. The equivalent single layer beam is much stiffer than the ideal sandwich beam, since its cross section is constrained to remain straight after deformation. Hence the natural frequency of the equivalent single layer beam is much higher than that of the ideal sandwich beam. The dynamic behavior of sandwich beam is much different from that of the equivalent single-layer beam—Compare the deformed shape of the ideal sandwich frame with that of the equivalent single-layer frame at $t = 5$ in Figure 7.22.

The above results lead to the conclusion that an accurate dynamic analysis of ideal

Table 7.14. Tip displacements of ideal sandwich frame and of equivalent single-layer frame at $t = 3.0$.

disp.	Sandwich frame	equivalent frame
u^1	3.21173E−01	6.82583E−02
u^2	−1.04516E+01	−4.85042E−02
${}_{(1)}\theta$	−1.12154E+00	not available
${}_{(2)}\theta$	−1.07755E+00	−2.63593E−03
${}_{(3)}\theta$	−1.11227E+00	not available

sandwich beams with low shear stiffness in the core layer should be calculated using a formulation as presented herein, and not with equivalent single-layer beams.

To demonstrate further that the difference between the two models (sandwich and equivalent single-layer) as described above is essentially due to the case of ideal sandwich frame with soft shear stiffness in the core layer, we consider the case of sandwich frame with three identical layers. The material properties in each layer are as follows:

$${}_{(\ell)}EA = 120,000, \quad {}_{(\ell)}GA_s = 48,000, \quad {}_{(\ell)}EI = 100, \text{ for } \ell = 1, 2, 3. \tag{7.16}$$

The same spatial discretization of 20 uniformly distributed sandwich elements, and a time step size of $\Delta t = 0.001$ are used here. Notice that now the frame is much softer than the previous one, we divide the load magnitude by five, i.e., the impact force at the tip is $F = -200 * t$ for the time $0 \leq t \leq 0.5$, and $F = 0$ for $0.5 \leq t \leq 6$. The deformed shape at different time step is shown in Figure 7.30, from which one can see that the deformed shape at any time step takes a smooth shapes, which is different from the results for ideal sandwich beam as given in Figure 7.22.

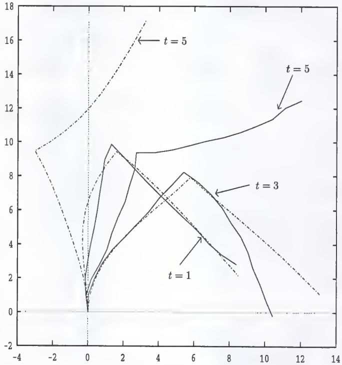

Figure 7.22. *Comparison of ideal sandwich frame with equivalent single-layer frame subjected to impact force at tip.* Small core-layer shear stiffness ${}_{(2)}GA_s = 400$. Deformed shapes at different time stations. Solid lines: sandwich model; dotted lines: equivalent single-layer model.

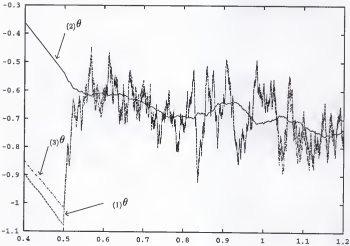

Figure 7.23. *Ideal sandwich frame subjected to impact force at tip.* Small core-layer shear stiffness $_{(2)}GA_s = 400$. Time history of layer rotations at frame tip in time interval $0.4 \leq t \leq 1.2$.

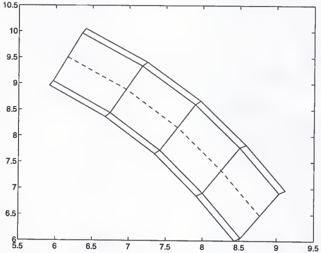

Figure 7.24. *Ideal sandwich frame subjected to impact force at tip.* Small core-layer shear stiffness ${}_{(2)}GA_s = 400$. Zoom-in figure of four elements at free tip at time $t = 0.5$. Solid lines: Layer boundaries and element boundaries; dash lines: Reference centroidal line.

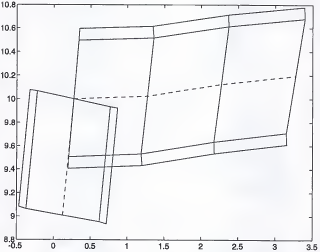

Figure 7.25. *Ideal sandwich frame subjected to impact force at tip.* Small core-layer shear stiffness ${}_{(2)}GA_s = 400$. Zoom-in figure of four elements at intersection of vertical beam and horizontal beam at time $t = 0.5$. Solid lines: Layer boundaries and element boundaries; dash lines: Reference centroidal line.

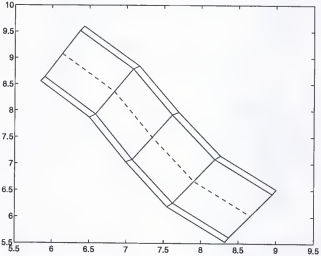

Figure 7.26. *Ideal sandwich frame subjected to impact force at tip*. Small core-layer shear stiffness ${}_{(2)}GA_s = 400$. Zoom-in figure of four elements at free tip at time $t = 0.56$. Solid lines: Layer boundaries and element boundaries; dash lines: Reference centroidal line.

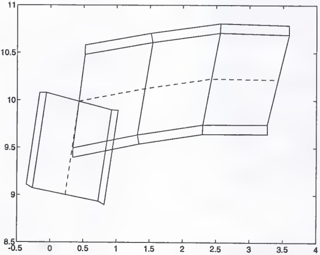

Figure 7.27. *Ideal sandwich frame subjected to impact force at tip.* Small core-layer shear stiffness ${}_{(2)}GA_s = 400$. Zoom-in figure of four elements at intersection of vertical beam and horizontal beam at time $t = 0.56$. Solid lines: Layer boundaries and element boundaries; dash lines: Reference centroidal line.

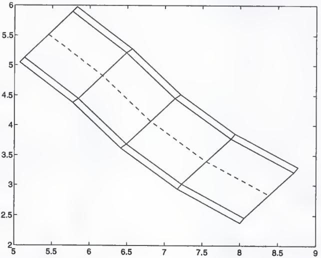

Figure 7.28. *Ideal sandwich frame subjected to impact force at tip.* Small core-layer shear stiffness ${}_{(2)}GA_s = 400$. Zoom-in figure of last four elements in vertical beam at time $t = 1.0$. Solid lines: Layer boundaries and element boundaries; dash lines: Reference centroidal line.

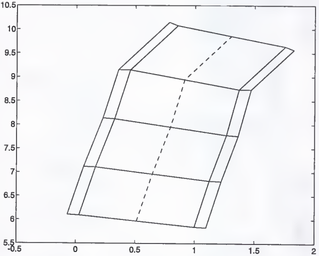

Figure 7.29. *Ideal sandwich frame subjected to impact force at tip*. Small core-layer shear stiffness ${}_{(2)}GA_s = 400$. Zoom-in figure of last four elements at vertical beam at time $t = 1.0$. Solid lines: Layer boundaries and element boundaries; dash lines: Reference centroidal line.

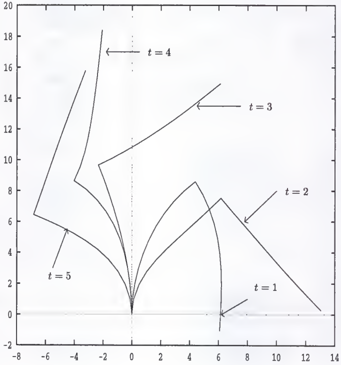

Figure 7.30. *Sandwich frame with three identical layers.* Assigned moment at tip of frame. Deformation shapes at different time steps.

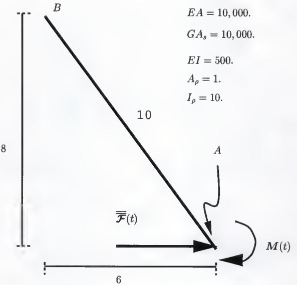

Figure 7.31. *Free-free ideal sandwich beam* undergoing large overall motion. Initial position and material properties.

7.4. Free-free Sandwich Beam Undergoing Large Overall Motion

In this section, we consider the free flight of a sandwich beam, the reader is referred to Simo and Vu-Quoc [1986*a*] for the similar problem for a single-layer beam.

7.4.1. Free-free single-layer beam and sandwich beam with identical layers

Shown in Figure 7.31 is a free-free beam, initially at an inclined position in the plane, together with the material properties of the beam. A spatially fixed force and a moment is applied at the lower tip of the beam (tip A), with the time history of the

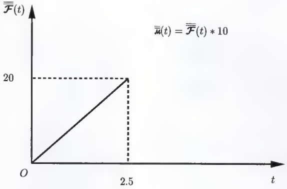

Figure 7.32. *Free flight of sandwich beam.* Time history of applied force and moment.

force and the moment given in Figure 7.32. The applied force produces a horizontal translational motion, while the combination of the force and the moment produces the tumbling motion. We analyze two cases: (i) Single-layer beam modeled using sandwich beam with only the core layer exist (i.e., without the outer layers), with material properties as shown in Figure 7.31, and with applied moment ${}_{(2)}\overline{\overline{\mathcal{M}}}(t) = \overline{\overline{\mathcal{M}}}(t)$ (see (7.32)), i.e., at the core layer only. (ii) Sandwich beam with three identical layers, whose equivalent single-layer beam[28] is the one in case (i) above, with the following geometric and material properties

$$
{}_{(\ell)}h = 0.129, \quad {}_{(\ell)}EA = 3333.33, \quad {}_{(\ell)}GA_s = 3333.33,
$$

$$
{}_{(\ell)}EI = 18.52, \quad {}_{(\ell)}A^0_\rho = 0.33, \quad \text{for } \ell = 1, 2, 3, \tag{7.17}
$$

and with the distribution of applied moments as ${}_{(1)}\overline{\overline{\mathcal{M}}}(t) : {}_{(2)}\overline{\overline{\mathcal{M}}}(t) : {}_{(3)}\overline{\overline{\mathcal{M}}}(t) = 21 : 38 : 21$, i.e., *nearly* normal distribution.[29] Thus ${}_{(1)}\bar{\bar{\boldsymbol{\mathcal{M}}}}(t) = {}_{(3)}\bar{\bar{\boldsymbol{\mathcal{M}}}}(t) = 21 * t$ and ${}_{(2)}\bar{\bar{\boldsymbol{\mathcal{M}}}}(t) = 38 * t$ in the loading stage $0 \leq t \leq 2.5$, and ${}_{(\ell)}\bar{\bar{\boldsymbol{\mathcal{M}}}}(t) = 0$ for $t > 2.5$.

---

[28] see Vu-Quoc and Deng [1995*b*] for the definition of the equivalent single-layer beam.

Both beams are discretized with 10 uniformly distributed linear elements. The time step size is $\Delta t = 0.1$, and 350 time steps are used to calculate the whole motion. The time histories of the lower tip of the beam for both models and for the equivalent single-layer model are shown in Figure 7.33. A sequence of snapshots of the deformed shapes during the loading stage, i.e., $t \in [0, 2.5]$, is given in Figure 7.34, while a sequence of snapshots of the deformed shapes throughout the time interval of analysis is given in Figure 7.35, both are similar to the results for single-layer beam presented in Simo and Vu-Quoc [1986*b*]. The results of the single-layer beam modeled using sandwich beam elements without outer layers are identical to those of the single-layer beam equivalent to the sandwich beam. In the present problem, the results of the three beam models (single-layer beam modeled with sandwich beam elements without outer layers, sandwich beam and equivalent single-layer beam) are very close to each other; one can hardly discern the difference. For this reason, we plot in Figure 7.35 only the deformed shapes of the single-layer beam modeled using only the core layer of sandwich elements. It is clear from the results that for the present problem, it more efficient to use the equivalent single-layer beam, since there are 40% percent less degrees of freedom than in the sandwich model.

7.4.2. Free-free ideal sandwich beam

We now consider a free-free *ideal* sandwich beam undergoing large overall motion to demonstrate the difference between an ideal sandwich model and its equivalent single-layer model. The beam takes the same initial position as shown in Figure 7.31, but with different material properties. The ideal sandwich beam is to be flexible to yield large

---

[29] Recall from Vu-Quoc and Deng [1995*b*] that the normal distribution of moment is ${}_{(1)}\bar{\bar{\boldsymbol{\mathcal{M}}}} : {}_{(2)}\bar{\bar{\boldsymbol{\mathcal{M}}}} : {}_{(3)}\bar{\bar{\boldsymbol{\mathcal{M}}}} = 7 : 13 : 7$.

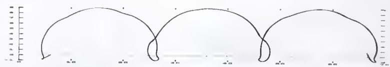

Figure 7.33. *Free-free sandwich beam.* (i) With only core layer. (ii) With three identical layers. Trace of the lower tip of the beam as compared to that of the equivalent single-layer model.

deformation; the following material properties are used

$$
\begin{aligned}
&{}_{(1)}EA = {}_{(3)}EA = 20,000, \\
&{}_{(1)}EI = {}_{(3)}EI = 4.1667, \\
&{}_{(1)}GA_s = {}_{(3)}GA_s = 8,000, \\
&{}_{(2)}EA = 8,000, \ {}_{(2)}EI = 666.667, \ {}_{(2)}GA_s = 8,000, \\
&{}_{(1)}\rho = {}_{(3)}\rho = 400, \ {}_{(2)}\rho = 20, \\
&{}_{(1)}h = {}_{(3)}h = 0.025, \ {}_{(2)}h = 0.5.
\end{aligned}
\tag{7.18}
$$

Thus the ideal sandwich beam used has soft and thick core layer, with hard and thin outer layers. The time history of the force is the same as in Figure 7.32, but we use the following distribution of the moment ${}_{(1)}\bar{\bar{\mathcal{M}}}(t) \,:\, {}_{(2)}\bar{\bar{\mathcal{M}}}(t) \,:\, {}_{(3)}\bar{\bar{\mathcal{M}}}(t) = 1 : 698 : 1$, because the outer layers themselves can support also bending moments. A similar calculation is performed with the equivalent single-layer model, which has the following material properties

$$
EA = 48,000, \ GA_s = 24,000, \ EI = 11,700, \ A_\rho = 60, \ I_\rho = 12.7. \tag{7.19}
$$

For both models we use 10 uniformly discretized linear elements. The motion of the beam during the loading stage is shown in Figure 7.36, in which the finite deformation in both models is clearly discernible, and the difference in the results of the equivalent

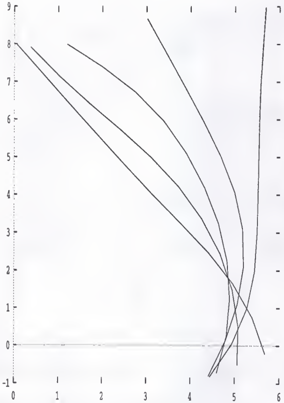

Figure 7.34. *Free-free sandwich beam.* Comparison of (i) sandwich model without outer layers, (ii) sandwich model with three identical layers, and (iii) equivalent single-layer model. Deformed shapes during the loading stage at $t = 0.5,\ 1.0,\ 1.5,\ 2.0,\ 2.5$. The difference in the results of the three models is not discernable.

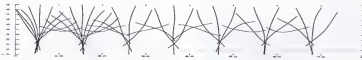

Figure 7.35. *Free-free sandwich beam.* With only core layer. Snapshots of deformed shapes at various time stations: At every 5 time increments till $t = 10$, and then at every 10 time increments till $t = 35$.

single-layer model and those of the sandwich model can be seen clearly. Time history of the lower tip A of both models is depicted in Figure 7.37, where one can also see clearly the difference in the results of the two models.

Remark 7.1. The core-layer shear stiffness is one of the most important factor in determining whether to use the equivalent single-layer model. If the core layer shear stiffness is very large, then the three layers will be forced to have close rotations, thus the beam will behave similarly to a single-layer beam. On the other hand, if the core-layer shear stiffness is very small, the rotations of the three layers can be so different that the assumption of plane cross-section becomes invalid; in this case the result of the sandwich beam will differ much from that of the equivalent single-layer beam. ∎

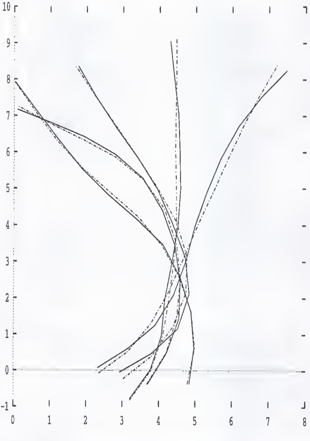

Figure 7.36. *Free-free ideal sandwich beam* undergoing large overall motion. Deformed shapes during the loading stage at time station $t = 0.5, 1.0, 1.5, 2.0, 2.5$. Solid lines: sandwich model; dotted lines: equivalent single-layer model.

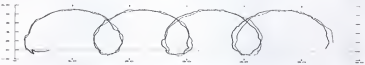

Figure 7.37. *Free-free ideal sandwich beam* undergoing large overall motion. Trace of lower beam tip (tip A). Solid lines: sandwich model, dotted lines: equivalent single-layer model.

7.5. Spin-up Maneuver

We now consider the re-positioning of a *flexible* beam rotating about a fixed axis passing through one end of the beam. The reader is referred to Simo and Vu-Quoc [1986*b*] and Vu-Quoc [1986] for the similar problem using a single-layer beam.

First, we consider a flexible robot arm subjected to a spin-up maneuver by prescribing the rotation of the hinged end of the beam as follows

$$\bar{\theta}(t) = \begin{cases} \dfrac{2}{5}\left[\dfrac{t^2}{2} + \left(\dfrac{15}{2\pi}\right)^2\left(\cos\dfrac{2\pi t}{15} - 1\right)\right] rad & 0 \le t \le 15\ sec, \\ (6t - 45)\, rad & t > 15\ sec. \end{cases} \tag{7.20}$$

This type of motion was first proposed by Kane, Ryan and Barnerjee [1987] to demonstrated that the conventional approach based on linear beam theories may lead to grossly inaccurate results. Thus one need to use higher order beam theories to deal with the centrifugal stiffening effects, even if the deformation remains small. The reader is referred to Kane *et al* and Simo and Vu-Quoc [1986*b*] for the single-layer beam case and for practical applications.

We now use a sandwich beam with three identical layers to model the single-layer beam given in Simo and Vu-Quoc [1986*b*], the material properties for the sandwich beam with length $L = 10$ is given as follows

$$_{(\ell)}EI = 518.5, \quad _{(\ell)}EA = 9.333 \times 10^6, \quad _{(\ell)}GA_s = 3.333 \times 10^6,$$
$$_{(\ell)}A_\rho^0 = 0.4, \quad _{(\ell)}h = 0.0129, \text{ for } \ell = 1, 2, 3. \tag{7.21}$$

Thus the material properties of the equivalent single-layer beam for the sandwich beam is exactly the same as that given in Simo and Vu-Quoc [1986*b*], i.e.,

$$EI = 14{,}000,\ EA = 2.8 \times 10^7,\ GA_s = 10^7,\ A_\rho^0 = 1.2, \tag{7.22}$$

where A_ρ^0 is the mass density per unit underformed length of the beam.

In the sandwich beam, the rotation of the core layer (2) at the hinged end is prescribed to follow the function in (7.20), while the rotations of the two outer layers remain free. In the equivalent single-layer beam, the rotation at the hinged end is prescribed to follow (7.20). The time step size is $\Delta t = 0.005$ for the accelerating stage $(0 \leq t < 15)$ and $\Delta t = 0.002$ for the steady rotation stage $(15 \leq t \leq 30)$. We use 10 uniformly distributed linear elements for both models.

The time histories of the relative displacements at the free tip for both sandwich model and single-layer model are given in Figure 7.39 and Figure 7.40. There the displacements is given relative to the shadow beam, which is a solid nondeformable beam hinged at the hinged end of the sandwich beam, and rotating with the prescribed rotation (7.20) (Figure 7.38).

From Figure 7.39 and Figure 7.40, one can see clearly that in the steady rotation stage (for $t \geq 15$), the displacements of the two models are almost the same, since the beam chosen here is a long beam, with the *length/thickness* ratio $10/(6 * 0.0129) \approx 130$. On the other hand, during the accelerating stage (for $0 \leq t < 15$), since the prescribed rotation is applied only to layer (2) of the sandwich beam, with the two outer layers remaining free; the cross section at the hinged end of the sandwich model is "broken" (i.e., hinges formed at the interlayer boundaries), thus making the relative deformation in the sandwich beam larger than that in the equivalent single-layer beam whose cross section at the hinged end is "constrained" to remain plane. The same explanation can be given to explain the larger layer rotations at the beam tip in the sandwich model compared to the smaller rotation at the beam tip in the equivalent single-layer model, during the accelerating stage (see Figure 7.41). The snapshots of the deformed shapes of both models are given in Figure 7.42, where one can see the difference in the results of the two models: We note that the deformed shapes of the sandwich beam lag behind those of the equivalent single-layer model; this observation is consistent with the explanation on the relative flexibility between those two models.

Let us consider another example with a different set of material properties, especially in the beam layer thickness, to demonstrate the case when the three layer rotations of the sandwich beam are largely different from each other. The material properties used here are

$$
\begin{aligned}
{}_{(\ell)}EA = 240,000, \;\; {}_{(\ell)}GA_s = 120,000, \;\; \text{for } \ell = 1,2,3, \\
{}_{(1)}EI = {}_{(3)}EI = 80, \;\; {}_{(2)}EI = 8,000, \;\; {}_{(1)}A_p^1 = {}_{(1)}A_p^3 = 0.2, \;\; {}_{(1)}A_p^2 = 0.6, \\
{}_{(1)}h = {}_{(3)}h = 0.01, \;\; {}_{(2)}h = 0.1. \quad (7.23)
\end{aligned}
$$

The beam is still relatively very thin, with the $length/thickness$ ratio $10/0.24 \approx 42$, but it is thick enough to demonstrate the difference between the three layer rotations, as will be seen shortly.

The beam is uniformly discretized with 10 linear elements, with a time step size of $\Delta t = 0.01$ during the accelerating stage $0 \leq t < 15$ and $\Delta t = 0.005$ during the steady rotation stage $15 \leq t \leq 30$. We employ three models to calculate, (i) assigned tip rotation for layer (1); (ii) assigned tip rotation for layer (2); (iii) assigned tip rotation for layer (3).

We can see from Figure 7.43 that in the accelerating stage, the relative axial displacement $\tilde{u}^1$ is smaller than that in the previous sandwich beam or equivalent single-layer beam case (see Figure 7.39), due to the larger bending stiffness of the present beam; but in the steady rotation stage, the relative axial displacement $\tilde{u}^1$ is much larger than that in Figure 7.39, because of the much smaller axial extension stiffness of the present beam. On the other hand, in the accelerating stage, the relative transverse displacement $\tilde{u}^2$ given in Figure 7.44 is smaller than that in Figure 7.40, because of the same reason as stated above; while in the steady rotation stage, the magnitude of vibration relative to the shadow beam is larger than that in Figure 7.40, even if the prescribed rotation is on the core layer

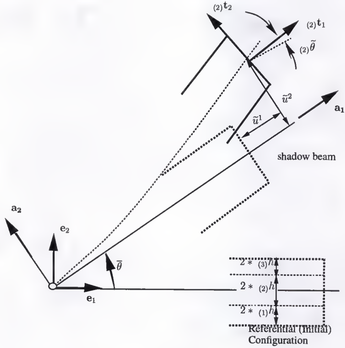

Figure 7.38. *Spin-up maneuver.* Initial underformed sandwich beam, shadow sandwich beam (layers not shown), and deformed sandwich beam (layers not shown).

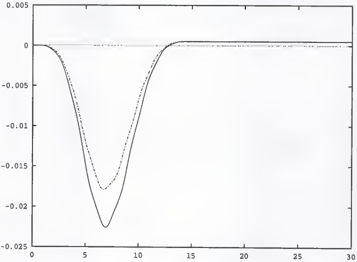

Figure 7.39. *Spin-up maneuver.* Comparison of sandwich model with three identical layers (with prescribed rotation on layer (2)) and equivalent single-layer model. Time history of relative axial displacement $\tilde{u}^1$. Solid line: sandwich model; dotted line: equivalent single-layer model.

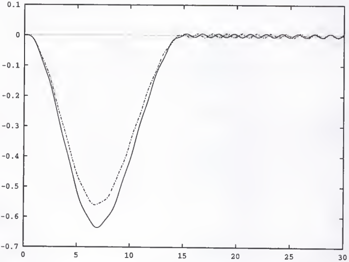

Figure 7.40. *Spin-up maneuver.* Comparison of sandwich model with three identical layers (with prescribed rotation on layer (2)) and equivalent single-layer model. Time history of relative transverse displacement $\widetilde{u}^2$. Solid line: sandwich model; dotted line: equivalent single-layer model.

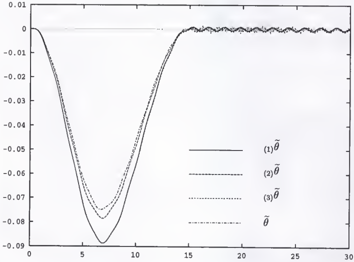

Figure 7.41. *Spin-up maneuver.* Comparison of sandwich model with three identical layers (with prescribed rotation on layer (2)) and equivalent single-layer model. Time history of tip rotations relative to prescribed rotation. $_{(\ell)}\tilde{\theta}$: relative rotation at tip of layer (ℓ) of sandwich model; $\tilde{\theta}$: relative rotation at tip of equivalent single-layer model.

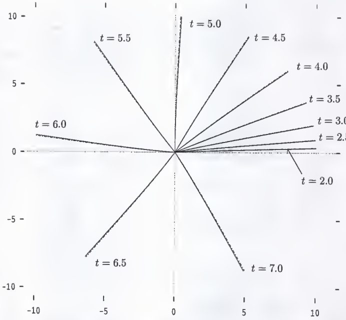

Figure 7.42. *Spin-up maneuver.* Snapshots of deformed shapes at various time stations ($t = 2.0,\ 2.5,\ 3.0,\ 3.5,\ 4.0,\ 4.5,\ 5.0,\ 5.5,\ 6.0,\ 6.5,\ 7.0$). Solid line: sandwich model with three identical layers and with prescribed core-layer rotation; dotted line: equivalent single-layer model.

(2) of the present sandwich beam, since the present sandwich beam is thicker than the previous one.

Let us consider the three layer rotations at the free tip of the beam for the three cases of prescribed rotation. The time history of the relative rotations are plotted in Figure 7.45, Figure 7.46 and Figure 7.47 for each case of prescribed rotation. First, let us consider the accelerating stage, when the prescribed rotation is on layer (1), i.e., ${}_{(1)}\theta(0,t) = \overline{\theta}(t)$ one can see from Figure 7.45, that the relative rotation at the tip of layer (1) does not depart far from zero, and returns to zero faster than the other two relative rotations. A similar observation can be made regarding the prescribed rotation on layer (3), as can be seen from Figure 7.47. When the prescribed rotation is on layer (2), the sandwich model behaves almost the same as the single-layer model, as can be seen from Figure 7.46; recall that in the present problem the beam is still relatively long.

Let us now consider the steady rotation stage, when the shadow beam is rotating at a constant angular velocity. When the prescribed rotation is on layer (1), we can see from Figure 7.45, that the rotation at the tip of layer (2) oscillates around that of the shadow beam. The rotation of layer (3) oscillates at the same frequency and magnitude around an angle lagging behind that of the shadow beam, while the rotation of layer (1) oscillates around an angle, ahead of that of the shadow beam, with basically the same frequency, but a much smaller amplitude. The reason is that the prescribed rotation is on layer (1), which makes the rotation of layer (1) a little larger than the rotation of layer (2) in the steady rotation stage. Being a reference layer, layer (2) has its rotation oscillate around that of the shadow beam in the steady rotation stage, while the rotation of layer (3) is lagging behind the rotation of layer (1) and layer (2). Also one should observe that there are some high frequencies in the rotation in Figure 7.45. A Similar observation can be made on Figure 7.46 and Figure 7.47 for prescribed rotation on layer (2) and layer (3), respectively.

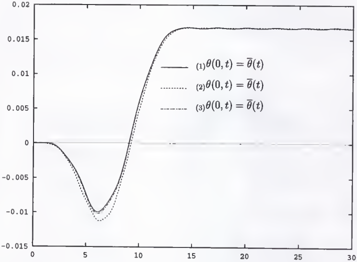

Figure 7.43. *Spin-up maneuver of ideal sandwich beam.* Comparison of relative axial displacement $\widetilde{u}^1$ for three ways of prescribed rotation at hinged end.

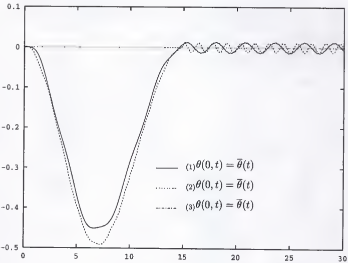

Figure 7.44. *Spin-up maneuver of ideal sandwich beam.* Comparison of relative transverse displacement for three ways of prescribed rotation. Difference between relative transverse displacement $\tilde{u}^2$ for prescribed rotation at hinged end $_{(1)}\theta(0,t) = \overline{\theta}(t)$ and for prescribed rotation $_{(3)}\theta(0,t) = \overline{\theta}(t)$ are not discernible.

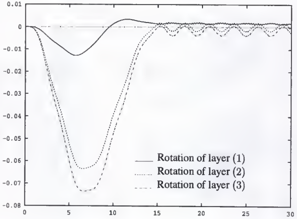

Figure 7.45. *Spin-up maneuver of ideal sandwich beam.* Prescribed rotation on layer (1): ${}_{(1)}\theta(0,t) = \bar{\theta}(t)$. Comparison of the relative rotations ${}_{(1)}\tilde{\theta}$, ${}_{(2)}\tilde{\theta}$ and ${}_{(3)}\tilde{\theta}$ at the free tip.

Finally, we consider an ideal sandwich beam under the spin-up maneuver. The material properties we used are as follows

$$
\begin{aligned}
{}_{(\ell)}EA = 4,800, \quad {}_{(\ell)}GA_s = 4,800, \quad {}_{(\ell)}EI = 4.0, \text{ for } \ell = 1, 3, \\
{}_{(2)}EA = 2,400, \quad {}_{(2)}GA_s = 2,400, \quad {}_{(2)}EI = 200, \\
{}_{(\ell)}A_\rho^0 = 0.6, \text{ for } \ell = 1,2,3, \quad {}_{(1)}h = {}_{(3)}h = 0.05, \quad {}_{(2)}h = 0.5.
\end{aligned}
\tag{7.24}
$$

Notice that the beam is 5 times thicker than the previous beam, and the material that forms the core layer (2) is much softer than that of layer (1) and layer (3); such choice of material properties is used to approximate the behavior of ideal sandwich beams.

Again we use 10 uniformly distributed linear elements, the same time step size and the same number of time steps to calculate the spin-up maneuver problem. The prescribed rotation for the present example is applied on the core layer (2) (notice that

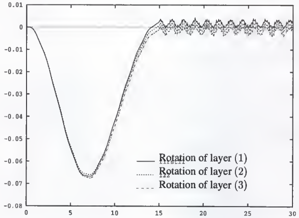

Figure 7.46. *Spin-up maneuver of ideal sandwich beam.* prescribed rotation on layer (2): ${}_{(2)}\theta(0,t) = \overline{\theta}(t)$. Comparison of the relative rotations ${}_{(1)}\widetilde{\theta}$, ${}_{(2)}\widetilde{\theta}$ and ${}_{(3)}\widetilde{\theta}$ at the free tip.

different results would be obtained if the prescribed rotation were applied on another layer as observed in the previous example above). The time history of the layer rotations at the beam tip is given in Figure 7.48, where one can see that the layer rotations clearly differ from each other in both the accelerating stage and the steady rotation stage.

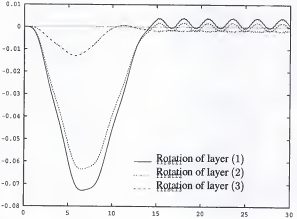

Figure 7.47. *Spin-up maneuver of ideal sandwich beam.* Prescribed rotation on layer (3): ${}_{(3)}\theta(0,t) = \overline{\theta}(t)$. Comparison of the relative rotations ${}_{(1)}\widetilde{\theta}$, ${}_{(2)}\widetilde{\theta}$ and ${}_{(3)}\widetilde{\theta}$ at the free tip.

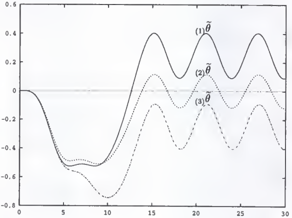

Figure 7.48. *Spin-up maneuver of* thick *ideal sandwich beam.* Prescribed rotation on layer (2): $_{(2)}\theta(0,t) = \overline{\theta}(t)$. Comparison of the relative rotations $_{(1)}\widetilde{\theta}$, $_{(2)}\widetilde{\theta}$ and $_{(3)}\widetilde{\theta}$ at the free tip.

PART II.

ON GEOMETRICALLY-EXACT SANDWICH SHELLS

CHAPTER 8
INTRODUCTION

The study of sandwich shells has been an area of increasing research interest due to the enormous usage of such structures in modern mechanical systems in aerospace, automotive, ship-building and other industries. Numerous papers have been published on this subject. A review of papers on sandwich shells published before 1965 can be found in Plantema [1966]. Later research on sandwich structures has been concentrating on accounting for more physical quantities in the model such as the transverse shear flexibility, the transverse normal strain, etc. The readers are referred to Noor and Burton [1989] and Noor, Burton and Bert [1996] and the references therein for the major contributions in this area. On the other hand, the dynamic modelling of the finitely deformable sandwich shells, especially when finite shear deformation is accounted for, is relatively unexplored.

The study on largely deformable single-layer shells, in a sense, can be divided into two major methodologies. One methodology, which has dominated the field for more than two decades, is the degenerated solid approach, in which the reduction to the resultant form is carried out numerically. We refer the readers to, e.g., Hughes [1987], Bathe [1996] for the comprehensive reviews, and also for Vu-Quoc and Mora [1989] and Vu-Quoc [1990*b*] for related issues. The other methodology is based on geometrically-exact formulations, pioneered first for beams by Simo and Vu-Quoc [1986*a*], Simo and Vu-Quoc [1986*b*], Simo and Vu-Quoc [1986*c*], Simo and Vu-Quoc [1988], Vu-Quoc and Li [1995] and then for shells by Simo and Fox [1989], Simo, Fox and Rifai [1989], Simo, Fox and Rifai [1990] and Simo, Rifai and Fox [1990]. In the geometrically-exact formulation, the reduction to the resultant form is carried out analytically, and thus leads to efficient numerical implementations and makes large-scale calculations possible.

Following the works on geometrically-exact sandwich beams and one-dimensional plates in Vu-Quoc and Ebcioğlu [1995] and Vu-Quoc and Deng [1995*b*], and the methodology in Simo and Fox [1989] in the formulation of the equations of motion for single-layer shells, we develop here the equations of motion for geometrically-exact sandwich shells, accounting for bending deformation, in-plane deformation, and shear deformation in each of the three layers. In the present theory, each layer can have arbitrary thickness, mass distribution, and different material properties. We adopt the single-director theory for each of the three layers, i.e., points that are originally located on a director must remain on the same director after deformation. The director, which is not extensible in the present formulation, must remain straight, but not necessary perpendicular to the neutral surface of the corresponding layer of the sandwich shell; thus shear deformations can be accounted for. The motion of a typical transverse fiber can best be viewed as a chain of three rigid links connected to each other by revolute joints. The continuity in displacements across the layer boundaries is exactly enforced.

With the dynamics of the motion referred directly to the inertial frame, the equations of motion of sandwich shells are derived from the balance of (1) the power of the contact forces/couples, (2) the rate of the kinetic energy and (3) the power of the assigned forces/couples. These equations of motion are entirely expressed in term of stress resultant and stress couples. The 12 principal unknowns, which describe the motion of the sandwich shell, are: Three displacements of the neutral surface of the reference layer, and three rotations for each of the three layers.

The resulting fully-nonlinear equations of motion are subsequently linearized, especially for symmetric sandwich shells. Further reduction of the linearized equations, by assuming equal outer layer rotations and by assuming that the sandwich shell surface is initially flat, leads to the results obtained in Yu [1959*a*] for the small deformable symmetric sandwich plates. The present theory is more general in that we deal with general sandwich shells, with no a priori assumptions in the symmetry of the sandwich shell and no zero in-plane motion as employed in Yu [1959*a*].

It is noted that we are not following the approach adopted in Green and Naghdi [1982] for small deformation theory of laminated composite plates, where the authors merely combined the layers, with each layer described by a theory for single-layer plates that they first developed.

CHAPTER 9
ON THE ALGEBRA OF TWO-POINT TENSORS AND THEIR APPLICATIONS

9.1. Introduction

Kollmann and Hackenberg [1993] gave a thorough discussion on the algebra of two-point tensors, and proposed a "new" definition of the transpose of two-point tensors, which led to a definition of the right Cauchy-Green tensor consistent with classical continuum mechanics. Basically, the definition of the transpose two-point tensors of Kollmann and Hackenberg [1993] does not involve metric tensor components, but only the interchange of the two basis tensors of order one (see Eq.(33) in Kollmann and Hackenberg [1993]). Here, we want to point out that the definition of the transpose of two-point tensors of Kollmann and Hackenberg [1993]) is well known in the mathematical literature, and is called the *adjoint* of two-point tensors. We provide also a short discussion on the use of the adjoint of two-point tensors in nonlinear continuum mechanics.[30]

Let $\mathcal{B}_o$ be the material (undeformed) configuration, $T_X\mathcal{B}_o$ the tangent space at $X \in \mathcal{B}_o$, and $T^*_X\mathcal{B}_o$ the contangent space at $X \in \mathcal{B}_o$. Similarly, let $\mathcal{B}_t$ the spatial (deformed) configuration, $T_x\mathcal{B}_t$ the tangent space at $x \in \mathcal{B}_t$, and $T^*_x\mathcal{B}_t$ the cotangent space at $x \in \mathcal{B}_t$. Let $\Phi\colon \mathcal{B}_o \to \mathcal{B}_t$ be the deformation map.

Definition 9.1. (Kollmann and Hackenberg [1993]) The transposition of a linear map $\mathcal{Q}\colon T_X\mathcal{B}_o \to T_x\mathcal{B}_t$ is a linear map of cotangent space $\mathcal{Q}^*\colon T^*_x\mathcal{B}_t \to T^*_X\mathcal{B}_o$, such that

$$\forall \boldsymbol{\alpha} \in T^*_x\mathcal{B}_t\,,\ \forall \mathbf{V} \in T_X\mathcal{B}_o\,,\ < \mathbf{V},\ \mathcal{Q}^*\boldsymbol{\alpha} >_X = < \mathcal{Q}\mathbf{V},\ \boldsymbol{\alpha} >_x, \tag{9.1}$$

---

[30] The convention of notation here is the same as that in Marsden and Hughes [1983].

$$\begin{tikzcd}
T^*\mathcal{B}_o & T^*\mathcal{B}_t \arrow[l, "T^*\Phi"'] \arrow[d, leftrightarrow, "dual"] \\
T\mathcal{B}_o \arrow[u, leftrightarrow, "dual"] \arrow[r, "T\Phi"] & T\mathcal{B}_t \\
\mathcal{B}_o \arrow[u, "\mathbf{V}"] \arrow[r, "\Phi"'] \arrow[uu, bend left=60, "\mathbf{A}"] & \mathcal{B}_t \arrow[u, "\mathbf{v}"'] \arrow[uu, bend right=60, "\alpha"']
\end{tikzcd}$$

Figure 9.1. $\mathbf{V}$ is a material vector field on $\mathcal{B}_o$, and $\mathbf{v}$ a spatial vector field on $\mathcal{B}_t$. $\mathbf{A}$ is a material covector field on $\mathcal{B}_o$, and α a spatial covector field on $\mathcal{B}_t$. $\Phi : \mathcal{B}_o \to \mathcal{B}_t$ is a deformation map, while $T\Phi : T\mathcal{B}_o \to \mathcal{B}_t$ is a tangent map, and $T^*\Phi : T^*\mathcal{B}_t \to T^*\mathcal{B}_o$ the adjoint of $T\Phi$.

where $< \cdot, \cdot >$ is the contraction[31] of a one-form with a vector. ∎

We refer the reader to Figure 9.1 for the relationship between the various spaces and mappings involved in Definition 9.1. The above definition is different from the definition of the transposition given in Marsden and Hughes [1983], as recalled below.

Definition 9.2. (Marsden and Hughes [1983], p.48) The transposition of a linear map $\mathcal{Q}$: $T_X\mathcal{B}_o \to T_x\mathcal{B}_t$ is a linear map $\mathcal{Q}^T$: $T_x\mathcal{B}_t \to T_X\mathcal{B}_o$, such that

$$\forall \mathbf{W} \in T_X\mathcal{B}_o \,, \mathbf{v} \in T_x\mathcal{B}_t \,, < \mathcal{Q}\mathbf{W}, \mathbf{v} >_x = < \mathbf{W},\ \mathcal{Q}^T\mathbf{v} >_X . \tag{9.2}$$

∎

Using Definition 9.1 of the transposition, Kollmann and Hackenberg [1993] derived some useful results related to two-point tensors; some of these results have a simpler form than those derived using Definition 9.2 (of the transposition) given in Marsden and Hughes [1983]. However, we have to mention here that Definition 9.1 for the transpose of two-point tensors is the same as the one for the *adjoint* of a linear map given in Crampin and Pirani [1988],[32] as recalled below.

---

[31] See Kollmann and Hackenberg [1993] or Marsden and Hughes [1983].

Definition 9.3. (Crampin and Pirani [1988], p.39) The adjoint of a linear map $\mathcal{Q}$: $T_X\mathcal{B}_o \to T_x\mathcal{B}_t$ is a linear map $\mathcal{Q}^*$: $T^*_x\mathcal{B}_t \to T^*_X\mathcal{B}_o$, such that

$$\forall \boldsymbol{\alpha} \in T^*_x\mathcal{B}_t\,,\ \forall \mathbf{V} \in T_X\mathcal{B}_o\,,\ <\mathbf{V},\ \mathcal{Q}^*\boldsymbol{\alpha}>_X = <\mathcal{Q}\mathbf{V},\ \boldsymbol{\alpha}>_x . \tag{9.3}$$

∎

In fact, in Vu-Quoc [1990*a*], we employ both Definitions 9.2 and Definitions 9.3, i.e., the transposition defined in Marsden and Hughes [1983], and the adjoint defined in Crampin and Pirani [1988], since both of these definitions have their applications in some widely used two-point tensors, such as the first Piola-Kirchhoff stress tensor, the right Cauchy-Green deformation tensor, the deformation gradient,[33] the two-point orthogonal tensor, etc. Below are some examples of the use of the adjoint of a tangent map.

9.2. Pull-back of Covector Fields in Terms of the Adjoint of a Tangent Map

From now on, we use the notation $\mathbf{F}^*$ and $\mathbf{F}^T$ for the *adjoint* and the *transposition* of a linear map $\mathbf{F}$, respectively. Each mathematical object employed below is explained in Figure 9.1.

Now, let $\{\mathbf{e}_a\}$ be a basis in $T_x\mathcal{B}_t$, and $\{\mathbf{E}_A\}$ a basis in $T_X\mathcal{B}_o$, their *dual* bases $\left\{\mathbf{e}^b\right\} \in T^*_x\mathcal{B}_t$ and $\left\{\mathbf{E}^B\right\} \in T^*_X\mathcal{B}_o$ can then be defined by the orthogonality condition $\mathbf{e}_a \bullet \mathbf{e}^b = \delta^b_a$ and $\mathbf{E}_A \bullet \mathbf{E}^B = \delta^B_A$, where the δ is the Kronecker delta.

---

[32] The adjoint of a linear map is also defined, e.g., in Chadwick [1976].

[33] There is a typesetting error in line 7, p.311 in Kollmann and Hackenberg [1993]: According to their definition, the transposition of the inverse transformation of the deformation gradient is $\mathbf{F}^{-T} : T^*_X\mathcal{B}_o \to T^*_x\mathcal{B}_t$ (and not $\mathbf{F}^{-T} := T^*_x\mathcal{B}_t \to T^*_X\mathcal{B}_o$).

Note that, for $\forall X \in \mathcal{B}_o$ and $\forall \mathbf{W} \in T\mathcal{B}_o$, the tangent map $T\Phi$ is defined as $T\Phi(X, \mathbf{W}) := (\Phi(X),\ \boldsymbol{\mathcal{D}}\Phi(X)\boldsymbol{\cdot}\mathbf{W})$, where $\Phi(X)$ is the base point, and $\boldsymbol{\mathcal{D}}\Phi(X)\boldsymbol{\cdot}\mathbf{W}$ is the vector part. The deformation gradient $\mathbf{F}$ corresponds to the vector part of the tangent map $T\Phi$ (see also Marsden and Hughes [1983], p.47), i.e.,

$$\mathbf{F} := \boldsymbol{\mathcal{D}}\Phi = \frac{\partial \Phi^a}{\partial X^A}\mathbf{e}_a \otimes \mathbf{E}^A\,. \tag{9.4}$$

Thus, according to Definition 9.3, the adjoint mapping $\mathbf{F}^* = [\boldsymbol{\mathcal{D}}\Phi]^*$ can be written as

$$\mathbf{F}^* := \boldsymbol{\mathcal{D}}^*\Phi = \frac{\partial \Phi^a}{\partial X^A}\mathbf{E}^A \otimes \mathbf{e}_a\,, \tag{9.5}$$

which is the same as the result obtained in Kollmann and Hackenberg [1993] (Theorem 3.1). Also, we have

$$\mathbf{F}^{-1} = \left(F^{-1}\right)^B_a \mathbf{E}_B \otimes \mathbf{e}^a\,. \tag{9.6}$$

Definition 9.4. The *pull-back* of a spatial covector field $\boldsymbol{\alpha}$ by Φ is a material covector field denoted by $\mathbf{A} := \Phi^*\boldsymbol{\alpha} = T^*\Phi \circ \boldsymbol{\alpha} \circ \Phi \colon \mathcal{B}_o \to T^*\mathcal{B}_o$, such that

$$< \Phi^*\boldsymbol{\alpha},\ \mathbf{W} >_X = < \boldsymbol{\alpha},\ \Phi_*\mathbf{W} >_{\mathbf{x}},\ \forall\, \mathbf{W} \in T\mathcal{B}_o\,, \tag{9.7}$$

where $\Phi_*\mathbf{W}$ is the push-forward of a material vector field $\mathbf{W}$, defined as $\Phi_*\mathbf{W} = \boldsymbol{\mathcal{D}}\Phi\boldsymbol{\cdot}\mathbf{W} = F^a_A W^A \mathbf{e}_a$, and $T^*\Phi$ is the adjoint of the tangent map $T\Phi$. ∎

The pull-back of the covector field $\boldsymbol{\alpha}$ by Φ, expressed in component form, can be written as

$$\mathbf{A} = \frac{\partial \Phi^a}{\partial X^A}\alpha_a \mathbf{E}^A\,. \tag{9.8}$$

Also, the push-forward of a material covector field can be expressed similarly as follows. Let $\mathbf{A} : \mathcal{B}_o \to T^*\mathcal{B}_o$ be a material covector field on $\mathcal{B}_o$, then the push-forward of $\mathbf{A}$ by Φ can be written as

$$\boldsymbol{\alpha} = \Phi_*\mathbf{A} = (T\Phi^{-1})^* \circ \mathbf{A} \circ \Phi^{-1}\,, \tag{9.9}$$

expressed in component form

$$\boldsymbol{\alpha} = (F^{-1})_a^B A_B \mathbf{e}^a \,, \tag{9.10}$$

where $(\mathbf{F}^{-1})^* = (\mathcal{D}(\Phi^{-1}))^*$, the vector part of $(T\Phi^{-1})^*$, is the adjoint of the inverse of the deformation gradient $\mathbf{F}$. Using (9.4)–(9.6), one can easily verify that

$$(\mathbf{F}^{-1})^* = (\mathbf{F}^*)^{-1} = (F^{-1})_a^A \mathbf{e}^a \otimes \mathbf{E}_A \,. \tag{9.11}$$

So we can use $\mathbf{F}^{-*}$ for both $(\mathbf{F}^{-1})^*$ and $(\mathbf{F}^*)^{-1}$ without ambiguity. A result similar to (9.11) can be obtained for the transpose of the inverse of a linear map and the inverse of the transpose of the linear map, i.e., $(\mathbf{F}^{-1})^T = (\mathbf{F}^T)^{-1}$, $\mathbf{F}^{-T}$ can be used for both $(\mathbf{F}^{-1})^T$ and $(\mathbf{F}^T)^{-1}$ without ambiguity.[34]

9.3. Application to Piola-Kirchhoff Stress Tensors

Let $\mathbf{Y}$ be the normal (material covector) to the boundary $\partial\Omega_o$ of the material domain Ω_o, and $\mathbf{y}$ the normal (spatial covector) to the boundary $\partial\Omega_t$ of the spatial domain Ω_t. Also let $\mathbf{P}$, $\mathbf{S}$, and $\boldsymbol{\sigma}$ be respectively the first Piola-Kirchhoff (PK) stress tensor, the second PK stress tensor, and the Cauchy stress tensor. The surface traction on the spatial boundary $\partial\Omega_t$ is written here as $\mathbf{Y}\boldsymbol{\cdot}\mathbf{P}$ (as in Malvern [1969], instead of $\mathbf{P}\boldsymbol{\cdot}\mathbf{Y}$ as in Marsden and Hughes [1983]). The Piola transform is defined as (Marsden and Hughes [1983])

$$\mathbf{y} d(\partial\Omega_t) = J(\mathbf{F}^{-*})\boldsymbol{\cdot}\mathbf{Y} d(\partial\Omega_o) \,, \tag{9.12}$$

where J is the Jacobian determinant of the deformation gradient $\mathbf{F}$, and $d(\partial\Omega_t)$ and $d(\partial\Omega_o)$ are the infinitesimal areas in the deformed configuration and in the undeformed configuration, respectively. Using (9.12) and the following relationship between the first PK stress tensor $\mathbf{P}$ and the Cauchy stress tensor $\boldsymbol{\sigma}$

$$\mathbf{Y}\boldsymbol{\cdot}\mathbf{P} d(\partial\Omega_o) = \mathbf{y}\boldsymbol{\cdot}\boldsymbol{\sigma} d(\partial\Omega_t) \,, \tag{9.13}$$

---

[34] The reader is also referred to Vu-Quoc [1990*a*] for the detail.

one obtains the expression for the first PK stress tensor as

$$\mathbf{P} = J\mathbf{F}^{-1} \bullet \boldsymbol{\sigma} \, , \tag{9.14}$$

which is the same as the result given in Chadwick [1976]. Also using (9.12) and the following relationship between the second PK stress tensor S and the Cauchy stress tensor $\boldsymbol{\sigma}$, one can prove the second equality below (by pulling back to the material configuration the second spatial "leg" of the first PK stress P—Marsden and Hughes [1983])

$$(\mathbf{Y} \bullet \mathbf{S}) \, d\left(\partial\Omega_o\right) := \mathbf{F}^{-1} \bullet (\mathbf{y} \bullet \boldsymbol{\sigma}) \, d\left(\partial\Omega_t\right) = (\mathbf{y} \bullet \boldsymbol{\sigma}) \bullet \mathbf{F}^{-*} d\left(\partial\Omega_t\right) ; \tag{9.15}$$

the second PK stress tensor can be then expressed as

$$\mathbf{S} = J\mathbf{F}^{-1} \bullet \boldsymbol{\sigma} \bullet \mathbf{F}^{-*} \, . \tag{9.16}$$

Also, since $(\mathbf{F}^{-1})^* = (\mathbf{F}^*)^{-1}$ from (9.11), one can express the Cauchy stress tensor $\boldsymbol{\sigma}$ in term of the PK stress tensors easily

$$\boldsymbol{\sigma} = \frac{1}{J} \mathbf{F} \bullet \mathbf{P} = \frac{1}{J} \mathbf{F} \bullet \mathbf{S} \bullet \mathbf{F}^* \, . \tag{9.17}$$

The component form of the first and second PK stress tensors takes very simple form in convected coordinates, which are defined as follows

$$\xi^i = \Phi \circ Z^i \, , \tag{9.18}$$

where Z^i is the Cartesian coordinate in the reference configuration, and ξ^i is the convected coordinate. Let $\left\{\mathbf{E}^A\right\}$ and $\{\mathbf{E}_A\}$ denote respectively the Cartesian basis and its dual basis in the reference configuration, and let $\mathbf{g}_a := \dfrac{\partial \Phi}{\partial Z^a}$ denote the convected basis in the tangent space while $\mathbf{g}^a$ its dual basis in the cotangent space to the deformed configuration. Then the component form of the deformation gradient and its adjoint, respectively, can be expressed in a very simple form as follows

$$\mathbf{F} = \delta^a_A \mathbf{g}_a \otimes \mathbf{E}^A \, , \quad \mathbf{F}^* = \delta^a_A \mathbf{E}^A \otimes \mathbf{g}_a \, , \tag{9.19}$$

while the inverse of the deformation gradient and the adjoint of the inverse of the deformation gradient can be written as

$$\mathbf{F}^{-1} = \delta_a^A \mathbf{E}_A \otimes \mathbf{g}^a \,, \quad \mathbf{F}^{-*} = \delta_a^A \mathbf{g}^a \otimes \mathbf{E}_A \,. \tag{9.20}$$

Also the Jacobian determinant can be simplified as $J = \sqrt{g}$, where g is the determinant of the Riemann metric $\mathbf{g} := g_{ij}\mathbf{g}^i \otimes \mathbf{g}^j$ with $g_{ij} := \mathbf{g}(\mathbf{g}_i, \mathbf{g}_j) = \mathbf{g}_i \cdot \mathbf{g}_j$.

obtain the component form of the first PK stress tensor as

$$P^{Aa} = \sqrt{g}\sigma^{Aa} \,. \tag{9.21}$$

Using (9.16) and (9.20), the component form of the second PK stress tensor can be written as

$$S^{AB} = \sqrt{g}\sigma^{AB} \,, \tag{9.22}$$

which is the same as (9.21) because of the convected coordinate.

CHAPTER 10
KINEMATICS OF DEFORMATION

In this section, we consider the basic kinematics for the geometrically-exact sandwich shell, and derive some important results to be used in the following chapters.

10.1. Basic Kinematic Assumptions and Configurations

Shown in Figure 10.1 are the profile of a sandwich shell in the material configuration, and the definition of the relevant geometric quantities that are crucial in the present theory. The neutral surface (to be defined in (10.31)) of the reference layer (0) in the material configuration is coordinated by the coordinates (ξ^1 , ξ^2). The transverse fiber orthogonal to the reference surface, in the material configuration is coordinated by ξ^3 .

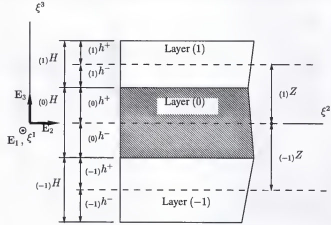

Figure 10.1. *Sandwich shell:* Profile and geometric quantities.

Let $\{ \mathbf{E}_1 , \mathbf{E}_2 , \mathbf{E}_3 \}$ be a set of orthonormal basis vector associated with the Cartesian coordinate (ξ^1 , ξ^2 , ξ^3). The neutral surface of layer (ℓ) with $\ell = \pm 1$ is at the distance ${}_{(\ell)}Z \geq 0$ from the neutral surface of the reference layer (0)(with ${}_{(0)}Z = 0$) and is at the distance ${}_{(\ell)}h^+$ from the top of layer (ℓ), and at ${}_{(\ell)}h^-$ from the bottom of layer (ℓ). Note that ${}_{(\ell)}Z$ is not the ordinate, but the distance, and is thus a positive number, for $\ell = -1, 1$. The thickness of layer (ℓ) is given by

$$ {}_{(\ell)}H := {}_{(\ell)}h^+ + {}_{(\ell)}h^- , \tag{10.1} $$

with ${}_{(\ell)}h^+ \neq {}_{(\ell)}h^-$ in general. The domain of the cross section of layer (ℓ) can be written as

$$ \begin{aligned} {}_{(0)}\mathcal{H} &:= \left[- {}_{(0)}h^- , \; {}_{(0)}h^+ \right] , \\ {}_{(1)}\mathcal{H} &:= \left[\left({}_{(1)}Z - {}_{(1)}h^- \right) , \; \left({}_{(1)}Z + {}_{(1)}h^+ \right) \right] , \\ {}_{(-1)}\mathcal{H} &:= \left[\left(- {}_{(-1)}Z - {}_{(-1)}h^- \right) , \; \left(- {}_{(-1)}Z + {}_{(-1)}h^+ \right) \right] . \end{aligned} \tag{10.2} $$

Remark 10.1. The numbering of the three layers here is $-1, 0, 1$, and is different from that employed in Vu-Quoc and Deng [1995*b*] and Vu-Quoc and Ebcioğlu [1995], which is $1, 2, 3$. ∎

Let $\mathcal{A}$ designate the material surface of the shell and $\mathcal{H} := \bigcup_{\ell=-1}^{1} {}_{(\ell)}\mathcal{H}$ the domain of the sandwich shell in the through-the-thickness direction, then the material domain $\mathcal{B}$ of the sandwich shell can be expressed as

$$ \mathcal{B} := \mathcal{A} \times \mathcal{H} , \tag{10.3} $$

and the material domain ${}_{(\ell)}\mathcal{B}$ of layer (ℓ) as

$$ {}_{(\ell)}\mathcal{B} := \mathcal{A} \times {}_{(\ell)}\mathcal{H} . \tag{10.4} $$

The boundary of $\mathcal{A}$ is denoted by $\partial\mathcal{A}$. The boundary of the surface of layer (ℓ) in the material configuration is denoted by

$$\partial_{(\ell)}\mathcal{A} := \partial\mathcal{A} \times {}_{(\ell)}\mathcal{H} \,. \tag{10.5}$$

Remark 10.2. Since we are focusing on the development of the equations of motion, we will henceforth consider the case where each layer may have different material properties and different thickness, but all layers must have the same surface area in the material configuration. ∎

To simplify the presentation, we use the notation $\boldsymbol{\xi} := \{ \boldsymbol{\xi}^{\underline{\alpha}} , \xi^3 \} \in \mathcal{B}$ to denote the coordinates of a material point, where $\boldsymbol{\xi}^{\underline{\alpha}} := \{ \xi^1 , \xi^2 \} \in \mathcal{A}$ is referred to as the material surface coordinates, and $\xi^3 \in \mathcal{H}$ the material through-the-thickness coordinate.[35]

In the development of the inextensible single-director[36] sandwich shell theory, the unit sphere, denoted by S^2, plays a central role. We set

$$S^2 := \left\{ \boldsymbol{t} \in \mathrm{R}^3 \;\middle|\; \|\boldsymbol{t}\| = 1 \right\} . \tag{10.6}$$

The deformation maps that map the material configuration of each of the shell layers into the corresponding current configuration, as shown in Figure 10.2, are written as[37]

$$\begin{aligned}
{}_{(0)}\boldsymbol{\Phi}\,(\boldsymbol{\xi}, t) &:= {}_{(0)}\boldsymbol{\varphi}\,(\boldsymbol{\xi}^{\underline{\alpha}}, t) + \xi^3\,{}_{(0)}\boldsymbol{t}\,(\boldsymbol{\xi}^{\underline{\alpha}}, t)\,, \\
{}_{(1)}\boldsymbol{\Phi}\,(\boldsymbol{\xi}, t) &:= {}_{(1)}\boldsymbol{\varphi}\,(\boldsymbol{\xi}^{\underline{\alpha}}, t) + \left(\xi^3 - {}_{(1)}Z\right)\,{}_{(1)}\boldsymbol{t}\,(\boldsymbol{\xi}^{\underline{\alpha}}, t)\,, \\
{}_{(-1)}\boldsymbol{\Phi}\,(\boldsymbol{\xi}, t) &:= {}_{(-1)}\boldsymbol{\varphi}\,(\boldsymbol{\xi}^{\underline{\alpha}}, t) + \left(\xi^3 + {}_{(-1)}Z\right)\,{}_{(-1)}\boldsymbol{t}\,(\boldsymbol{\xi}^{\underline{\alpha}}, t)\,,
\end{aligned} \tag{10.7}$$

where ${}_{(\ell)}\boldsymbol{\varphi} : \mathcal{A} \mapsto \mathrm{R}^3$ is the deformation map of the neutral surface of layer (ℓ) of the sandwich shell to be given shortly, and ${}_{(\ell)}\boldsymbol{t} : \mathcal{A} \mapsto S^2$ the unit director to the neutral surface of layer (ℓ), for $\ell = -1, 0, 1$, respectively. The kinematic assumption (10.7) embodies the following basic physical assumption: The deformation of the shell is such that points initially along the initial director ${}_{(\ell)}\boldsymbol{t}_o(\boldsymbol{\xi}^{\underline{\alpha}})$ in the reference configuration remain along the director ${}_{(\ell)}\boldsymbol{t}(\boldsymbol{\xi}^{\underline{\alpha}}, t)$ in the spatial configuration after deformation. The fact that the director field ${}_{(\ell)}\boldsymbol{t}$ is straight, but not necessarily orthogonal to the deformed neutral surface of layer (ℓ) enables us to account for the shear deformation in each layer.

---

[35] The usual convention that Greek indices take values in $\{1, 2\}$ and Latin indices take values in $\{1, 2, 3\}$ is adopted through out this paper.

[36] The director does not rotate about itself, i.e., there is no drill degree of freedom (dof).

[37] A more general formula is given in (Naghdi [1972, p.466]) for the single-layer shell with multiple directors.

In particular, the deformation maps from the material configuration to the reference configuration at time $t = 0$ is obtain from (10.7) as follows

$$ {}_{(\ell)}\boldsymbol{\Phi}_o(\boldsymbol{\xi}) := {}_{(\ell)}\boldsymbol{\Phi}(\boldsymbol{\xi}, 0), \quad \text{for } \ell = -1, 0, 1. \tag{10.8} $$

We now assume that the overall transverse fiber of the deformed sandwich shell is continuous piecewise linear, and thus can be thought of as a chain of rigid links connected by revolute joints. Using this rigid-link assumption, the deformation maps of the neutral surface of the outer layers (1) and (-1) can be related to the deformation map of the neutral surface of the reference layer (0) as

$$ {}_{(1)}\boldsymbol{\varphi}(\boldsymbol{\xi}^{\underline{\alpha}}, t) := {}_{(0)}\boldsymbol{\varphi}(\boldsymbol{\xi}^{\underline{\alpha}}, t) + {}_{(0)}h^{+}\, {}_{(0)}\boldsymbol{t} + {}_{(1)}h^{-}\, {}_{(1)}\boldsymbol{t}, \tag{10.9} $$

$$ {}_{(-1)}\boldsymbol{\varphi}(\boldsymbol{\xi}^{\underline{\alpha}}, t) := {}_{(0)}\boldsymbol{\varphi}(\boldsymbol{\xi}^{\underline{\alpha}}, t) - {}_{(0)}h^{-}\, {}_{(0)}\boldsymbol{t} - {}_{(-1)}h^{+}\, {}_{(-1)}\boldsymbol{t}. \tag{10.10} $$

Remark 10.3. The deformation map for the neutral surface ${}_{(\ell)}\boldsymbol{\varphi}$ and the director field ${}_{(\ell)}\boldsymbol{t}$ are functions of the material surface coordinate $\boldsymbol{\xi}^{\underline{\alpha}}$ and the time t only, not functions of the through-the-thickness variable ξ^3. ∎

Remark 10.4. By virtue of (10.7), (10.9) and (10.10), we note that the continuation of displacements across the layer interfaces is exactly enforced. ∎

The map from the neutral surface of layer (ℓ) in the material configuration to the neutral surface of layer (ℓ) in the reference configuration is defined as

$$ {}_{(\ell)}\boldsymbol{\varphi}_o(\boldsymbol{\xi}^{\underline{\alpha}}) := {}_{(\ell)}\boldsymbol{\varphi}(\boldsymbol{\xi}^{\underline{\alpha}}, 0), \quad \text{for } \ell = -1, 0, 1. \tag{10.11} $$

The reader is referred to Figure 10.2 for the profile of a sandwich shell in the material, reference and spatial configuration and the related deformation maps.

The deformation map for the material neutral surface of the reference layer (0) can be written as

$$ {}_{(0)}\boldsymbol{\varphi}\left(\boldsymbol{\xi}^{\underline{\alpha}}, t\right) := \xi^{\alpha}\, \mathrm{E}_{\alpha} + \tilde{\boldsymbol{u}}\left(\boldsymbol{\xi}^{\underline{\alpha}}, t\right), \tag{10.12} $$

where $\tilde{\boldsymbol{u}}$ is the displacement of the neutral surface from the material configuration to the spatial configuration. The deformation map of the neutral surface of layer (0) from the material configuration to the reference configuration is obtained from (10.12), by restricting the time variable to zero as follows

$$ {}_{(0)}\boldsymbol{\varphi}_{o}\left(\boldsymbol{\xi}^{\underline{\alpha}}, 0\right) := \xi^{\alpha}\, \mathrm{E}_{\alpha} + \tilde{\boldsymbol{u}}_{o}\left(\boldsymbol{\xi}^{\underline{\alpha}}\right), \tag{10.13} $$

where $\tilde{\boldsymbol{u}}_{o}\left(\boldsymbol{\xi}^{\underline{\alpha}}\right) := \tilde{\boldsymbol{u}}\left(\boldsymbol{\xi}^{\underline{\alpha}}, 0\right)$ is the displacement from the material configuration to the reference configuration. The displacement from the reference configuration to the spatial configuration is

$$ \boldsymbol{u} = \tilde{\boldsymbol{u}} - \tilde{\boldsymbol{u}}_{o}\,. \tag{10.14} $$

The principal unknowns in the present geometrically-exact sandwich shell theory are (i) the 3 components of the displacement $\boldsymbol{u}$, (ii) the 3 angles determining the direction of the director ${}_{(\ell)}\boldsymbol{t}$ of layer (ℓ), for $\ell = -1, 0, 1$. There are thus 12 unknown kinematic quantities describing the motion of the shell. However, the inextensibility of the director ${}_{(\ell)}\boldsymbol{t}$, for $\ell = -1, 0, 1$, (which is equivalent to 3 constraint equations relating the 12 unknowns) reduces the total number of unknowns from 12 to 9. We will derive the governing equations of motion relating the 12 unconstrained kinematic unknowns in Section 11.

10.2. Important Kinematic Quantities

For the derivation of the equations of motion in Section 11, the following derivatives of the deformation map ${}_{(\ell)}\boldsymbol{\varphi}$, of layer (ℓ), are needed.

The partial derivatives of ${}_{(\ell)}\boldsymbol{\varphi}$ with respect to the material coordinate ξ^α are as follows

$$\begin{aligned}
{}_{(0)}\boldsymbol{\varphi}_{,\alpha} &= \mathbf{E}_\alpha + \tilde{\boldsymbol{u}}_{,\alpha}\,, \\
{}_{(1)}\boldsymbol{\varphi}_{,\alpha} &= {}_{(0)}\boldsymbol{\varphi}_{,\alpha} + {}_{(0)}h^+\ {}_{(0)}\boldsymbol{t}_{,\alpha} + {}_{(1)}h^-\ {}_{(1)}\boldsymbol{t}_{,\alpha}\,, \\
{}_{(-1)}\boldsymbol{\varphi}_{,\alpha} &= {}_{(0)}\boldsymbol{\varphi}_{,\alpha} - {}_{(0)}h^-\ {}_{(0)}\boldsymbol{t}_{,\alpha} - {}_{(-1)}h^+\ {}_{(-1)}\boldsymbol{t}_{,\alpha}\,.
\end{aligned} \tag{10.15}$$

Noting that the displacement $\tilde{\boldsymbol{u}}_0$ of the neutral surface of layer (0) from the material configuration to the reference configuration is constant in time, and thus by virtue of (10.14)

$$\dot{\boldsymbol{u}} = \dot{\tilde{\boldsymbol{u}}}\,, \quad \ddot{\boldsymbol{u}} = \ddot{\tilde{\boldsymbol{u}}}\,, \tag{10.16}$$

we can use the displacement $\boldsymbol{u}$ from the reference configuration to the spatial configuration to express the first order time rate of ${}_{(\ell)}\boldsymbol{\varphi}$ as

$$\begin{aligned}
{}_{(0)}\dot{\boldsymbol{\varphi}} &= \dot{\boldsymbol{u}}\,, \\
{}_{(1)}\dot{\boldsymbol{\varphi}} &= \dot{\boldsymbol{u}} + {}_{(0)}h^+\ {}_{(0)}\dot{\boldsymbol{t}} + {}_{(1)}h^-\ {}_{(1)}\dot{\boldsymbol{t}}\,, \\
{}_{(-1)}\dot{\boldsymbol{\varphi}} &= \dot{\boldsymbol{u}} - {}_{(0)}h^-\ {}_{(0)}\dot{\boldsymbol{t}} - {}_{(-1)}h^+\ {}_{(-1)}\dot{\boldsymbol{t}}\,,
\end{aligned} \tag{10.17}$$

the second order time rate of ${}_{(\ell)}\boldsymbol{\varphi}$ as

$$\begin{aligned}
{}_{(0)}\ddot{\boldsymbol{\varphi}} &= \ddot{\boldsymbol{u}}\,, \\
{}_{(1)}\ddot{\boldsymbol{\varphi}} &= \ddot{\boldsymbol{u}} + {}_{(0)}h^+\ {}_{(0)}\ddot{\boldsymbol{t}} + {}_{(1)}h^-\ {}_{(1)}\ddot{\boldsymbol{t}}\,, \\
{}_{(-1)}\ddot{\boldsymbol{\varphi}} &= \ddot{\boldsymbol{u}} - {}_{(0)}h^-\ {}_{(0)}\ddot{\boldsymbol{t}} - {}_{(-1)}h^+\ {}_{(-1)}\ddot{\boldsymbol{t}}\,,
\end{aligned} \tag{10.18}$$

and the first order time rate of ${}_{(\ell)}\boldsymbol{\varphi}_{,\alpha}$ as

$${}_{(0)}\dot{\boldsymbol{\varphi}}_{,\alpha} = \dot{\boldsymbol{u}}_{,\alpha}\,,$$

$$\begin{aligned} {}_{(1)}\dot{\boldsymbol{\varphi}}_{,\alpha} &= \dot{\boldsymbol{u}}_{,\alpha} + {}_{(0)}h^{+}\,{}_{(0)}\dot{\boldsymbol{t}}_{,\alpha} + {}_{(1)}h^{-}\,{}_{(1)}\dot{\boldsymbol{t}}_{,\alpha}\,, \\ {}_{(-1)}\dot{\boldsymbol{\varphi}}_{,\alpha} &= \dot{\boldsymbol{u}}_{,\alpha} - {}_{(0)}h^{-}\,{}_{(0)}\dot{\boldsymbol{t}}_{,\alpha} - {}_{(-1)}h^{+}\,{}_{(-1)}\dot{\boldsymbol{t}}_{,\alpha}\,. \end{aligned} \tag{10.19}$$

The spatial convected basis vectors ${}_{(\ell)}\boldsymbol{g}_i$, for layer (ℓ), are defined by differentiating the deformation map ${}_{(\ell)}\boldsymbol{\Phi}$ with respect to the material coordinate ξ^i:

$${}_{(\ell)}\boldsymbol{g}_i\,(\boldsymbol{\xi}\,,\,t) := {}_{(\ell)}\boldsymbol{\Phi}_{,i}\,(\boldsymbol{\xi}\,,\,t) \quad \text{for } \ell = -1, 0, 1. \tag{10.20}$$

Using (10.7), we obtain

$$\begin{aligned} {}_{(0)}\boldsymbol{g}_\alpha\,(\boldsymbol{\xi}\,,\,t) &= {}_{(0)}\boldsymbol{\varphi}_{,\alpha} + \xi^3\,{}_{(0)}\boldsymbol{t}_{,\alpha}\,, \\ {}_{(1)}\boldsymbol{g}_\alpha\,(\boldsymbol{\xi}\,,\,t) &= {}_{(1)}\boldsymbol{\varphi}_{,\alpha} + \left(\xi^3 - {}_{(1)}Z\right)\,{}_{(1)}\boldsymbol{t}_{,\alpha}\,, \\ {}_{(-1)}\boldsymbol{g}_\alpha\,(\boldsymbol{\xi}\,,\,t) &= {}_{(-1)}\boldsymbol{\varphi}_{,\alpha} + \left(\xi^3 + {}_{(-1)}Z\right)\,{}_{(-1)}\boldsymbol{t}_{,\alpha}\,, \\ {}_{(\ell)}\boldsymbol{g}_3\,(\boldsymbol{\xi}\,,\,t) &= {}_{(\ell)}\boldsymbol{t}\,, \quad \text{for } \ell = 1, 2, 3. \end{aligned} \tag{10.21}$$

The reference convected basis vectors ${}_{(\ell)}\boldsymbol{G}_I$ for layer (ℓ) are obtained by particularizing ${}_{(\ell)}\boldsymbol{g}_I$ to $t = 0$ to yield

$${}_{(\ell)}\boldsymbol{G}_I\,(\boldsymbol{\xi}\,) := {}_{(\ell)}\boldsymbol{g}_I\,(\boldsymbol{\xi}\,,\,0) = {}_{(\ell)}\boldsymbol{\Phi}_{,I}\,(\boldsymbol{\xi}\,,\,0) = {}_{(\ell)}\boldsymbol{\Phi}_{o,I}\,(\boldsymbol{\xi}\,)\,. \tag{10.22}$$

The dual basis vectors ${}_{(\ell)}\boldsymbol{g}^i$ and ${}_{(\ell)}\boldsymbol{G}^I$ are defined by the orthogonality condition

$$<\,{}_{(\ell)}\boldsymbol{g}^i\,,\,{}_{(\ell)}\boldsymbol{g}_j\,>= \delta^i_j \quad \text{and} \quad <\,{}_{(\ell)}\boldsymbol{G}^I\,,\,{}_{(\ell)}\boldsymbol{G}_J\,>= \delta^I_J, \tag{10.23}$$

where $<\bullet\,,\,\bullet>$ denotes the inner product, and δ^i_j and δ^I_J the Kronecker deltas.

The deformation gradient ${}_{(\ell)}\boldsymbol{F}$ for layer (ℓ) is, by definition, the tangent map of the deformation map ${}_{(\ell)}\boldsymbol{\chi} = {}_{(\ell)}\boldsymbol{\Phi} \circ {}_{(\ell)}\boldsymbol{\Phi}_o{}^{-1}$ from the reference configuration to the current configuration, thus

$${}_{(\ell)}\boldsymbol{F} := \nabla\,{}_{(\ell)}\boldsymbol{\chi} = \nabla\,{}_{(\ell)}\boldsymbol{\Phi} \circ \left[\nabla\,{}_{(\ell)}\boldsymbol{\Phi}_o\right]^{-1}, \tag{10.24}$$

which when expressed in the convected coordinate, is written as

$$ {}_{(\ell)}\boldsymbol{F} = \delta^i_I \, {}_{(\ell)}\boldsymbol{g}_i \otimes {}_{(\ell)}\boldsymbol{G}^I . \tag{10.25} $$

The component form of the inverse of the deformation gradient ${}_{(\ell)}\boldsymbol{F}^{-1}$ for layer (ℓ) is then

$$ {}_{(\ell)}\boldsymbol{F}^{-1} = \delta^I_i \, {}_{(\ell)}\boldsymbol{G}_I \otimes {}_{(\ell)}\boldsymbol{g}^i . \tag{10.26} $$

The time rate of the deformation gradient, which is crucial for the development of the stress power in Section 11, is given below

$$ {}_{(\ell)}\dot{\boldsymbol{F}} = \delta^i_I \, {}_{(\ell)}\dot{\boldsymbol{g}}_i \otimes {}_{(\ell)}\boldsymbol{G}^I , \tag{10.27} $$

by virtue of (10.25), and by the constancy of ${}_{(\ell)}\boldsymbol{G}^I$ with respect to time.

The Jacobian determinants of the mapping ${}_{(\ell)}\boldsymbol{\Phi}_o$, ${}_{(\ell)}\boldsymbol{\Phi}$ and ${}_{(\ell)}\boldsymbol{\chi}$ are given below

$$ {}_{(\ell)}j_o \;:=\; \det\left[\nabla \, {}_{(\ell)}\boldsymbol{\Phi}_o \left(\boldsymbol{\xi}\right)\right] = \left({}_{(\ell)}\boldsymbol{G}_1 \times {}_{(\ell)}\boldsymbol{G}_2\right) \cdot {}_{(\ell)}\boldsymbol{G}_3 , \tag{10.28} $$

$$ {}_{(\ell)}j_t \;:=\; \det\left[\nabla \, {}_{(\ell)}\boldsymbol{\Phi} \left(\boldsymbol{\xi},\, t\right)\right] = \left({}_{(\ell)}\boldsymbol{g}_1 \times {}_{(\ell)}\boldsymbol{g}_2\right) \cdot {}_{(\ell)}\boldsymbol{g}_3 , \tag{10.29} $$

$$ {}_{(\ell)}J \;:=\; \det\left[\nabla \, {}_{(\ell)}\boldsymbol{\chi} \left(\boldsymbol{\xi},\, t\right)\right] = \frac{{}_{(\ell)}j_t}{{}_{(\ell)}j_o} , \tag{10.30} $$

where (10.30) is obtained by using (10.28)–(10.29) in (10.24).

We now conclude this section by defining the neutral surface of layer (ℓ). Let ${}_{(\ell)}\rho_o$ and ${}_{(\ell)}\rho$ be the mass density in the reference and the spatial configuration, $\mathcal{B}_o$ and $\mathcal{B}_t$, respectively. We select the neutral surface ${}_{(\ell)}\varphi_o$ of layer (ℓ) such that

$$ \int_{{}_{(-1)}\mathcal{H}} \left(\xi^3 + {}_{(-1)}Z\right) {}_{(-1)}j_o \, {}_{(-1)}\rho_o \, d\xi^3 = \int_{{}_{(-1)}\mathcal{H}} \left(\xi^3 + {}_{(-1)}Z\right) {}_{(-1)}j \, {}_{(-1)}\rho \, d\xi^3 = 0, $$

$$ \int_{{}_{(0)}\mathcal{H}} \xi^3 \, {}_{(0)}j_o \, {}_{(0)}\rho_o \, d\xi^3 = \int_{{}_{(0)}\mathcal{H}} \xi^3 \, {}_{(0)}j \, {}_{(0)}\rho \, d\xi^3 = 0, $$

$$ \int_{{}_{(1)}\mathcal{H}} \left(\xi^3 - {}_{(1)}Z\right) {}_{(1)}j_o \, {}_{(1)}\rho_o \, d\xi^3 = \int_{{}_{(1)}\mathcal{H}} \left(\xi^3 - {}_{(1)}Z\right) {}_{(1)}j \, {}_{(1)}\rho \, d\xi^3 = \tag{10,31} $$

which does not necessarily correspond to the geometric center of the cross-section of layer (ℓ).

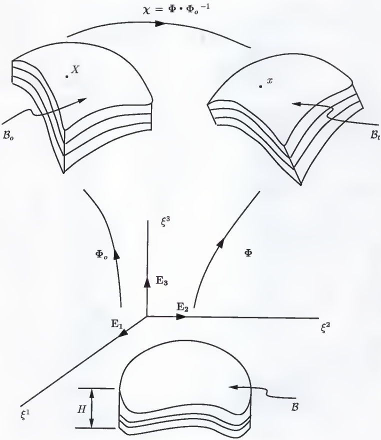

Figure 10.2. *Sandwich shell:* Material configuration $\mathcal{B}$, reference configuration $\mathcal{B}_o$, and spatial configuration $\mathcal{B}_t$.

CHAPTER 11
EQUATIONS OF MOTION

There are several approaches to obtain the equations of motion of geometrically-exact shells. One way is to start from the local balance of linear momentum, (i) which when integrated over the shell thickness yields the resultant balance of linear momentum, and (ii) which when integrated over the shell thickness with the weighting function ξ^3 yields the resultant balance of angular momentum, (see, e.g., Simo and Fox [1989] for the single-layer shell theory). The symmetric condition of the Cauchy stress tensor in terms of stress resultants for the shell serves as the restriction on the constitutive laws relating the shell stress resultants. The kinematic condition of inextensibility of the director in each layer serves as additional constraint that plays a role in the weak form. In the present paper, which deals with sandwich shells, we employ a different approach to derive the equations of motion based on the principle of virtual power, as pioneered for sandwich beams in Vu-Quoc and Ebcioğlu [1995]. The advantage of the adopted approach is that the weak form for the geometrically-exact sandwich shell can be readily obtained from the balance of stress power.

11.1. Power of Contact Forces/Couples

The shell resultant stresses and resultant couples, and their respective conjugate strain measures can be obtained by reducing the expression of the stress power from an integration over a 3-D domain of the shell to an integration over the 2-D domain of its material surface. Let $\boldsymbol{P}$ be the first Piola-Kirchhoff stress tensor, then the stress power of the shell expressed with respect to the reference configuration is

$$\mathcal{P}_c := \int_{\mathcal{B}_o} \boldsymbol{P} \cdot\cdot \dot{\boldsymbol{F}} \, \mathrm{b} \, d\mathcal{V}_o , \tag{11.1}$$

where $d\,\mathcal{V}_o$ is the infinitesimal reference volume.

The first Piola-Kirchhoff stress tensor in layer (ℓ) can be written as (see, e.g., Malvern [1969, p.222])

$$ {}_{(\ell)}\boldsymbol{P} = {}_{(\ell)}J\; {}_{(\ell)}\boldsymbol{F}^{-1} \bullet {}_{(\ell)}\boldsymbol{\sigma}\,, \tag{11.2} $$

where ${}_{(\ell)}J$ is defined in (10.30), ${}_{(\ell)}\boldsymbol{F}^{-1}$ in (10.26), and ${}_{(\ell)}\boldsymbol{\sigma}$ is the Cauchy stress tensor in layer (ℓ). Using the expression for ${}_{(\ell)}\boldsymbol{F}^{-1}$ in (10.26), the first Piola-Kirchhoff stress tensor ${}_{(\ell)}\boldsymbol{P} = {}_{(\ell)}P^{Ij}\; {}_{(\ell)}\boldsymbol{G}_I \otimes {}_{(\ell)}\boldsymbol{g}_j$ can be expressed as

$$ {}_{(\ell)}\boldsymbol{P} = {}_{(\ell)}J\, \delta^I_i\, {}_{(\ell)}\boldsymbol{G}_I \otimes {}_{(\ell)}\boldsymbol{g}^i \bullet {}_{(\ell)}\sigma^{jk}\; {}_{(\ell)}\boldsymbol{g}_j \otimes {}_{(\ell)}\boldsymbol{g}_k = {}_{(\ell)}J\, \delta^I_i\, {}_{(\ell)}\sigma^{ij}\; {}_{(\ell)}\boldsymbol{G}_I \otimes {}_{(\ell)}\boldsymbol{g}_j\,. \tag{11.3} $$

With ${}_{(\ell)}\dot{\boldsymbol{F}}$ given in (10.27), we obtain the following stress power per unit reference volume for layer (ℓ)

$$ \begin{aligned} {}_{(\ell)}\boldsymbol{P} \bullet\bullet\, {}_{(\ell)}\dot{\boldsymbol{F}} &:= {}_{(\ell)}J\, \left[\left(\delta^I_i\, {}_{(\ell)}\boldsymbol{G}_I \otimes {}_{(\ell)}\boldsymbol{g}^i \right) \bullet {}_{(\ell)}\boldsymbol{\sigma} \right] \bullet\bullet \left[\delta^k_J\, {}_{(\ell)}\dot{\boldsymbol{g}}_k \otimes {}_{(\ell)}\boldsymbol{G}^J \right] \\ &= {}_{(\ell)}J\, \delta^I_i \delta^k_J \left({}_{(\ell)}\boldsymbol{G}_I \bullet {}_{(\ell)}\boldsymbol{G}^J \right) {}_{(\ell)}\boldsymbol{g}^i \bullet {}_{(\ell)}\boldsymbol{\sigma} \bullet {}_{(\ell)}\dot{\boldsymbol{g}}_k \\ &= {}_{(\ell)}J\; {}_{(\ell)}\boldsymbol{g}^i \bullet {}_{(\ell)}\boldsymbol{\sigma} \bullet {}_{(\ell)}\dot{\boldsymbol{g}}_i\,, \end{aligned} \tag{11.4} $$

where ${}_{(\ell)}\boldsymbol{G}_I \bullet {}_{(\ell)}\boldsymbol{G}^J = \delta^J_I$. The stress power for the sandwich shell can now be obtained as

$$ \begin{aligned} \mathcal{P}_c &:= \int_{\mathcal{B}_o} \boldsymbol{P} \bullet\bullet\, \dot{\boldsymbol{F}}\, \mathrm{c}d\,\mathcal{V}_o = \sum_{\ell=-1}^{1} \int_{{}_{(\ell)}\mathcal{B}_o} {}_{(\ell)}\boldsymbol{P} \bullet\bullet\, {}_{(\ell)}\dot{\boldsymbol{F}}\, \mathrm{d}d\, {}_{(\ell)}\mathcal{V}_o \\ &= \sum_{\ell=-1}^{1} \int_{{}_{(\ell)}\mathcal{B}_o} {}_{(\ell)}J\; {}_{(\ell)}\boldsymbol{g}^i \bullet {}_{(\ell)}\boldsymbol{\sigma} \bullet {}_{(\ell)}\dot{\boldsymbol{g}}_i\, \mathrm{e}d\, {}_{(\ell)}\mathcal{V}_o\,, \end{aligned} \tag{11.5} $$

where ${}_{(\ell)}\mathcal{B}_o$ designates the reference body for layer (ℓ), and $d\,{}_{(\ell)}\mathcal{V}_o$ the infinitesimal reference volume in layer (ℓ). With the definition of ${}_{(\ell)}J$ and ${}_{(\ell)}j_t$ in (10.30) and (10.29), respectively, and by the conservation of mass, we have

$$ {}_{(\ell)}J\, d\, {}_{(\ell)}\mathcal{V}_o = d\, {}_{(\ell)}\mathcal{V}_t = {}_{(\ell)}j_t\, d\, {}_{(\ell)}\mathcal{V}\,, \tag{11.6} $$

where $d\,{}_{(\ell)}\mathcal{V} \;:=\; d\mathcal{A}d\xi^3$ is the infinitesimal material volume in layer (ℓ). Using the definition (10.4) of the material domain ${}_{(\ell)}\mathcal{B}$ of layer (ℓ), the definition (10.21) of the basis vector ${}_{(\ell)}\boldsymbol{g}_i$, and expression (11.6), the stress power (11.5) is now expressed in the material domain as follows

$$\mathcal{P}_c := \int\int_{\mathrm{f}\mathcal{A}\,\mathrm{g}\,{}_{(1)}\mathcal{H}} {}_{(1)}j_t \left\{ \left({}_{(1)}\boldsymbol{g}^{\alpha} \cdot {}_{(1)}\boldsymbol{\sigma} \right) \cdot \left[{}_{(1)}\dot{\boldsymbol{\varphi}}_{,\alpha} + \left(\xi^3 - {}_{(1)}Z \right) {}_{(1)}\dot{\boldsymbol{t}}_{,\alpha} \right] \right.$$

$$\left. + {}_{(1)}\boldsymbol{t} \cdot {}_{(1)}\boldsymbol{\sigma} \cdot {}_{(1)}\dot{\boldsymbol{t}} \right\} d\mathcal{A}d\xi^3$$

$$+ \int\int_{\mathrm{h}\mathcal{A}\,\mathrm{i}\,{}_{(0)}\mathcal{H}} {}_{(0)}j_t \left\{ \left({}_{(0)}\boldsymbol{g}^{\alpha} \cdot {}_{(0)}\boldsymbol{\sigma} \right) \cdot \left[{}_{(0)}\dot{\boldsymbol{\varphi}}_{,\alpha} + \xi^3\, {}_{(0)}\dot{\boldsymbol{t}}_{,\alpha} \right] + {}_{(0)}\boldsymbol{t} \cdot {}_{(0)}\boldsymbol{\sigma} \cdot {}_{(0)}\dot{\boldsymbol{t}} \right\} d\mathcal{A}d\xi^3$$

$$+ \int\int_{\mathrm{j}\mathcal{A}\,\mathrm{k}\,{}_{(-1)}\mathcal{H}} {}_{(-1)}j_t \left\{ \left({}_{(-1)}\boldsymbol{g}^{\alpha} \cdot {}_{(-1)}\boldsymbol{\sigma} \right) \cdot \left[{}_{(-1)}\dot{\boldsymbol{\varphi}}_{,\alpha} + \left(\xi^3 + {}_{(-1)}Z \right) {}_{(-1)}\dot{\boldsymbol{t}}_{,\alpha} \right] \right.$$

$$\left. + {}_{(-1)}\boldsymbol{t} \cdot {}_{(-1)}\boldsymbol{\sigma} \cdot {}_{(-1)}\dot{\boldsymbol{t}} \right\} d\mathcal{A}d\xi^3 \tag{11.7}$$

Upon defining the resultant forces ${}_{(\ell)}\boldsymbol{n}^{\alpha}$, the resultant couples ${}_{(\ell)}\boldsymbol{m}^{\alpha}$ and the resultant director couple ${}_{(\ell)}\boldsymbol{\ell}$ for layer (ℓ), respectively, as

$${}_{(\ell)}\boldsymbol{n}^{\alpha} \;:=\; \int_{\mathrm{l}\,{}_{(\ell)}\mathcal{H}} {}_{(\ell)}j_t\, {}_{(\ell)}\mathbf{g}^{\alpha} \cdot {}_{(\ell)}\boldsymbol{\sigma}\, d\xi^3, \qquad \text{for } \ell = -1, 0, 1\,, \tag{11.8}$$

$${}_{(0)}\widetilde{\boldsymbol{m}}^{\alpha} \;:=\; \int_{\mathrm{m}\,{}_{(0)}\mathcal{H}} {}_{(0)}j_t\, \xi^3\, {}_{(0)}\mathbf{g}^{\alpha} \cdot {}_{(0)}\boldsymbol{\sigma}\, d\xi^3,$$

$${}_{(1)}\widetilde{\boldsymbol{m}}^{\alpha} \;:=\; \int_{\mathrm{n}\,{}_{(1)}\mathcal{H}} {}_{(1)}j_t \left(\xi^3 - {}_{(1)}Z \right) {}_{(1)}\mathbf{g}^{\alpha} \cdot {}_{(1)}\boldsymbol{\sigma}\, d\xi^3, \tag{11.9}$$

$${}_{(-1)}\widetilde{\boldsymbol{m}}^{\alpha} \;:=\; \int_{\mathrm{o}\,{}_{(-1)}\mathcal{H}} {}_{(-1)}j_t \left(\xi^3 + {}_{(-1)}Z \right) {}_{(-1)}\mathbf{g}^{\alpha} \cdot {}_{(-1)}\boldsymbol{\sigma}\, d\xi^3,$$

$${}_{(\ell)}\boldsymbol{\ell} \;:=\; \int_{\mathrm{p}\,{}_{(\ell)}\mathcal{H}} {}_{(\ell)}j_t\, {}_{(\ell)}\mathbf{g}^{3} \cdot {}_{(\ell)}\boldsymbol{\sigma}\, d\xi^3, \qquad \text{for } \ell = -1, 0, 1, \tag{11.10}$$

the stress power (11.7) can be simplified as

$$\mathcal{P}_c \;=\; \sum_{\ell=-1}^{1} \int_{\mathcal{A}} \Big[{}_{(\ell)}\boldsymbol{n}^{\alpha} \cdot {}_{(\ell)}\dot{\boldsymbol{\varphi}}_{,\alpha} + {}_{(\ell)}\widetilde{\boldsymbol{m}}^{\alpha} \cdot {}_{(\ell)}\dot{\boldsymbol{t}}_{,\alpha} + {}_{(\ell)}\boldsymbol{\ell} \cdot {}_{(\ell)}\dot{\boldsymbol{t}} \Big]\, d\mathcal{A}. \qquad (11.11)$$

Remark 11.1. Our definitions for the resultant forces/couples and the director couples are different from those given in Simo and Fox [1989] by a factor $\dfrac{1}{{}_{(\ell)}\bar{j}_t}$, but are the same as the weighted surface tensors ($N^{\alpha\beta}$, $M^{\alpha\beta}$, and Q^{α}) given in Green and Zerna [1968, p.376] except for the director couple ${}_{(\ell)}\boldsymbol{\ell}$. We note that the definitions employed in Simo and Fox [1989] correspond to the physical resultant forces/couples as explained in Green and Zerna [1968, p.377]. We employ here the weighted surface tensors rather than the physical resultants as in Simo and Fox [1989], because the weighted surface tensors simplify significantly the derivation of the equations of motion. The reason we call ${}_{(\ell)}\boldsymbol{\ell}$ the resultant director couple, rather than "through-the-thickness resultant force" as in Simo and Fox [1989], will be explained later in Remark 11.4. ∎

In order to obtain the equations of motion of the sandwich shell from the balance of power, we reorganize the contact stress power (11.11) with the rate of the displacement $\dot{\boldsymbol{u}}$ and the rate of the director ${}_{(\ell)}\dot{\boldsymbol{t}}$ as the common factors.

Consider the first term in (11.11); using expression (10.19) for ${}_{(\ell)}\dot{\boldsymbol{\varphi}}_{,\alpha}$, we gather first all the terms with factor ${}_{(0)}\dot{\boldsymbol{\varphi}}_{,\alpha} = \dot{\boldsymbol{u}}_{,\alpha}$

$$\int_{\mathcal{A}} \sum_{\ell=-1}^{1} {}_{(\ell)}\boldsymbol{n}^{\alpha} \cdot \dot{\boldsymbol{u}}_{,\alpha}\, d\mathcal{A} = \int_{\mathcal{A}} \hat{\mathbf{n}}^{\alpha} \cdot \dot{\boldsymbol{u}}_{,\alpha}\, d\mathcal{A}, \qquad (11.12)$$

where

$$\hat{\mathbf{n}}^{\alpha} := \sum_{\ell=-1}^{1} {}_{(\ell)}\boldsymbol{n}^{\alpha} . \qquad (11.13)$$

Integrating of (11.12) by parts yields

$$\int_{\mathcal{A}} \sum_{\ell=-1}^{1} {}_{(\ell)}\boldsymbol{n}^{\alpha} \cdot \dot{\boldsymbol{u}}_{,\alpha}\, d\mathcal{A} = \sum_{\ell=-1}^{1} \oint_{\partial\mathcal{A}} {}_{(\ell)}\boldsymbol{n}^{\alpha} \cdot \dot{\boldsymbol{u}}\; {}_{(\ell)}\nu_{\alpha}\, \mathrm{t}d(\partial\mathcal{A}) - \int_{\mathcal{A}} \hat{\boldsymbol{n}}^{\alpha}{}_{,\alpha} \cdot \dot{\boldsymbol{u}}\, d\mathcal{A}, \qquad (11.14)$$

where $\dot{\boldsymbol{u}}$ is the only common vector, and where $d(\partial\mathcal{A})$ is the boundary of the material surface $d\mathcal{A}$, and ${}_{(\ell)}\nu_\alpha$ is the component of the normal ${}_{(\ell)}\boldsymbol{\nu}$ at the boundary of the neutral surface of layer (ℓ) such that

$$ {}_{(\ell)}\boldsymbol{\nu} = {}_{(\ell)}\nu_\alpha \, \mathbf{E}^\alpha . \tag{11.15} $$

Remark 11.2. (11.14) is obtained on the assumption that in the material configuration, we have

$$ {}_{(\ell)}\nu_\alpha = {}_{(0)}\nu_\alpha , \quad \forall\alpha = 1,2, \quad \forall\ell = -1,1. \tag{11.16} $$

This assumption means that the shell in the material configuration is like a straight cylinder. The role of the notation ${}_{(\ell)}\nu_\alpha$ in (11.14) is simply for the symmetry of the formula. Generally, in the reference (initial, stress free) configuration,

$$ {}_{(\ell)}\nu_{o\alpha} \neq {}_{(0)}\nu_{o\alpha} , \quad \forall\alpha = 1,2, \quad \forall\ell = -1,1. \tag{11.17} $$

∎

Next, we gather all terms having ${}_{(0)}\dot{\boldsymbol{t}}$ or ${}_{(0)}\dot{\boldsymbol{t}}_{,\alpha}$ as common factors, coming from the use of $(10.19)_2$–$(10.19)_3$ in the first term of (11.11), and also coming from the second and third terms of (11.11) as follows

$$ \int_{\mathcal{A}} \left[\left({}_{(0)}\widetilde{\boldsymbol{m}}^\alpha \cdot {}_{(0)}\dot{\boldsymbol{t}}_{,\alpha} + {}_{(0)}\boldsymbol{\ell} \cdot {}_{(0)}\dot{\boldsymbol{t}} \right) + \left({}_{(0)}h^+ \, {}_{(1)}\boldsymbol{n}^\alpha - {}_{(0)}h^- \, {}_{(-1)}\boldsymbol{n}^\alpha \right) \cdot {}_{(0)}\dot{\boldsymbol{t}}_{,\alpha} \right] d\mathcal{A} \tag{11.18} $$

Integrating (11.18) over the layer neutral surface by parts, we obtain an expression in which ${}_{(0)}\dot{\boldsymbol{t}}$ is the only common factor:

$$ \begin{aligned} &\int_{\mathcal{A}} \left[\left({}_{(0)}\widetilde{\boldsymbol{m}}^\alpha \cdot {}_{(0)}\dot{\boldsymbol{t}}_{,\alpha} + {}_{(0)}\boldsymbol{\ell} \cdot {}_{(0)}\dot{\boldsymbol{t}} \right) + \left({}_{(0)}h^+ \, {}_{(1)}\boldsymbol{n}^\alpha - {}_{(0)}h^- \, {}_{(-1)}\boldsymbol{n}^\alpha \right) \cdot {}_{(0)}\dot{\boldsymbol{t}}_{,\alpha} \right] d\mathcal{A} \\ &\qquad = \oint_{\partial\mathcal{A}} \left({}_{(0)}\widetilde{\boldsymbol{m}}^\alpha + {}_{(0)}h^+ \, {}_{(1)}\boldsymbol{n}^\alpha - {}_{(0)}h^- \, {}_{(-1)}\boldsymbol{n}^\alpha \right) \cdot {}_{(0)}\dot{\boldsymbol{t}} \; {}_{(0)}\nu_\alpha \, \mathrm{u}d(\partial\mathcal{A}) \\ &\qquad\quad - \int_{\mathcal{A}} \left[\left({}_{(0)}\widetilde{\boldsymbol{m}}^\alpha + {}_{(0)}h^+ \, {}_{(1)}\boldsymbol{n}^\alpha - {}_{(0)}h^- \, {}_{(-1)}\boldsymbol{n}^\alpha \right)_{,\alpha} - {}_{(0)}\boldsymbol{\ell} \right] \cdot {}_{(0)}\dot{\boldsymbol{t}} \, d\mathcal{A}. \end{aligned} \tag{11.19} $$

Next, concerning the top layer (1), we gather all the terms in (11.11) (after the substituting of $(10.19)_2$) that have ${}_{(1)}\dot{\boldsymbol{t}}$ or ${}_{(1)}\dot{\boldsymbol{t}}_{,\alpha}$ as common factors to have

$$\int_{\mathcal{A}} \left({}_{(1)}\widetilde{\boldsymbol{m}}^{\alpha} \bullet {}_{(1)}\dot{\boldsymbol{t}}_{,\alpha} + {}_{(1)}\boldsymbol{\ell} \bullet {}_{(1)}\dot{\boldsymbol{t}} + {}_{(1)}h^{-}\ {}_{(1)}\boldsymbol{n}^{\alpha} \bullet {}_{(1)}\dot{\boldsymbol{t}}_{,\alpha} \right) d\mathcal{A}, \tag{11.20}$$

which after an integration by parts yields an expression having ${}_{(1)}\dot{\boldsymbol{t}}$ as the only common factor:

$$\begin{aligned} &\int_{\mathcal{A}} \left({}_{(1)}\widetilde{\boldsymbol{m}}^{\alpha} \bullet {}_{(1)}\dot{\boldsymbol{t}}_{,\alpha} + {}_{(1)}\boldsymbol{\ell} \bullet {}_{(1)}\dot{\boldsymbol{t}} + {}_{(1)}h^{-}\ {}_{(1)}\boldsymbol{n}^{\alpha} \bullet {}_{(1)}\dot{\boldsymbol{t}}_{,\alpha} \right) d\mathcal{A} \\ &= \oint_{\partial\mathcal{A}} \left({}_{(1)}\widetilde{\boldsymbol{m}}^{\alpha} + {}_{(1)}h^{-}\ {}_{(1)}\boldsymbol{n}^{\alpha} \right) \bullet {}_{(1)}\dot{\boldsymbol{t}}\ {}_{(1)}\nu_{\alpha}\, \mathrm{v}d(\partial\mathcal{A}) \\ &- \int_{\mathcal{A}} \left[\left({}_{(1)}\widetilde{\boldsymbol{m}}^{\alpha} + {}_{(1)}h^{-}\ {}_{(1)}\boldsymbol{n}^{\alpha} \right)_{,\alpha} - {}_{(1)}\boldsymbol{\ell} \right] \bullet {}_{(1)}\dot{\boldsymbol{t}}\, d\mathcal{A}. \end{aligned} \tag{11.21}$$

Finally, concerning the bottom layer (-1), we gather all the terms in (11.11) (after the substituting of $(10.19)_3$) having ${}_{(-1)}\dot{\boldsymbol{t}}$ or ${}_{(-1)}\dot{\boldsymbol{t}}_{,\alpha}$ as common factors to have

$$\int_{\mathcal{A}} \left({}_{(-1)}\widetilde{\boldsymbol{m}}^{\alpha} \bullet {}_{(-1)}\dot{\boldsymbol{t}}_{,\alpha} + {}_{(-1)}\boldsymbol{\ell} \bullet {}_{(-1)}\dot{\boldsymbol{t}} - {}_{(-1)}h^{+}\ {}_{(-1)}\boldsymbol{n}^{\alpha} \bullet {}_{(-1)}\dot{\boldsymbol{t}}_{,\alpha} \right) d\mathcal{A}, \tag{11.22}$$

which after a integration by parts yields an expression having ${}_{(-1)}\dot{\boldsymbol{t}}$ as the only common factor

$$\begin{aligned} &\int_{\mathcal{A}} \left({}_{(-1)}\widetilde{\boldsymbol{m}}^{\alpha} \bullet {}_{(-1)}\dot{\boldsymbol{t}}_{,\alpha} + {}_{(-1)}\boldsymbol{\ell} \bullet {}_{(-1)}\dot{\boldsymbol{t}} - {}_{(-1)}h^{+}\ {}_{(-1)}\boldsymbol{n}^{\alpha} \bullet {}_{(-1)}\dot{\boldsymbol{t}}_{,\alpha} \right) d\mathcal{A} \\ &= \oint_{\partial\mathcal{A}} \left({}_{(-1)}\widetilde{\boldsymbol{m}}^{\alpha} - {}_{(-1)}h^{+}\ {}_{(-1)}\boldsymbol{n}^{\alpha} \right) \bullet {}_{(-1)}\dot{\boldsymbol{t}}\ {}_{(-1)}\nu_{\alpha}\, \mathrm{w}d(\partial\mathcal{A}) \\ &- \int_{\mathcal{A}} \left[\left({}_{(-1)}\widetilde{\boldsymbol{m}}^{\alpha} - {}_{(-1)}h^{+}\ {}_{(-1)}\boldsymbol{n}^{\alpha} \right)_{,\alpha} - {}_{(-1)}\boldsymbol{\ell} \right] \bullet {}_{(-1)}\dot{\boldsymbol{t}}\, d\mathcal{A}. \end{aligned} \tag{11.23}$$

Using (11.14), (11.19), (11.21) and (11.23) the total contact stress power (11.11) can be written as

$$\mathcal{P}_c = \int_{\mathcal{B}_o} \boldsymbol{P} \bullet\bullet \dot{\boldsymbol{F}}\, \mathrm{x}d\mathcal{V}_o = \sum_{\ell=-1}^{1} \int_{\mathcal{A}} \left[{}_{(\ell)}\boldsymbol{n}^{\alpha} \bullet {}_{(\ell)}\dot{\boldsymbol{\varphi}}_{,\alpha} + {}_{(\ell)}\widetilde{\boldsymbol{m}}^{\alpha} \bullet {}_{(\ell)}\dot{\boldsymbol{t}}_{,\alpha} + {}_{(\ell)}\boldsymbol{\ell} \bullet {}_{(\ell)}\dot{\boldsymbol{t}} \right] d\mathcal{A}$$

$$
\begin{aligned}
= & -\int_{\mathcal{A}} \widehat{\boldsymbol{n}}^{\alpha}{}_{,\alpha} \bullet \dot{\boldsymbol{u}}\, d\mathcal{A} - \int_{\mathcal{A}} \left[\left({}_{(1)}\widetilde{\boldsymbol{m}}^{\alpha} + {}_{(1)}h^{-}\; {}_{(1)}\boldsymbol{n}^{\alpha} \right)_{,\alpha} - {}_{(1)}\boldsymbol{\ell} \right] \bullet {}_{(1)}\dot{\boldsymbol{t}}\, d\mathcal{A} \\
- & \int_{\mathcal{A}} \left[\left({}_{(0)}\widetilde{\boldsymbol{m}}^{\alpha} + {}_{(0)}h^{+}\; {}_{(1)}\boldsymbol{n}^{\alpha} - {}_{(0)}h^{-}\; {}_{(-1)}\boldsymbol{n}^{\alpha} \right)_{,\alpha} - {}_{(0)}\boldsymbol{\ell} \right] \bullet {}_{(0)}\dot{\boldsymbol{t}}\, d\mathcal{A} \\
- & \int_{\mathcal{A}} \left[\left({}_{(-1)}\widetilde{\boldsymbol{m}}^{\alpha} - {}_{(-1)}h^{+}\; {}_{(-1)}\boldsymbol{n}^{\alpha} \right)_{,\alpha} - {}_{(-1)}\boldsymbol{\ell} \right] \bullet {}_{(-1)}\dot{\boldsymbol{t}}\, d\mathcal{A} \\
+ & \sum_{\ell=-1}^{1} \oint_{\partial\mathcal{A}} {}_{(\ell)}\boldsymbol{n}^{\alpha} \bullet \dot{\mathbf{u}}\; {}_{(\ell)}\nu_{\alpha}\, \mathrm{y} d(\partial\mathcal{A}) + \oint_{\partial\mathcal{A}} \left({}_{(1)}\widetilde{\boldsymbol{m}}^{\alpha} + {}_{(1)}h^{-}\; {}_{(1)}\boldsymbol{n}^{\alpha} \right) \bullet {}_{(1)}\dot{\boldsymbol{t}}\; {}_{(1)}\nu_{\alpha}\, \mathrm{z} d(\partial\mathcal{A}) \\
+ & \oint_{\partial\mathcal{A}} \left({}_{(0)}\widetilde{\boldsymbol{m}}^{\alpha} + {}_{(0)}h^{+}\; {}_{(1)}\boldsymbol{n}^{\alpha} - {}_{(0)}h^{-}\; {}_{(-1)}\boldsymbol{n}^{\alpha} \right) \bullet {}_{(0)}\dot{\boldsymbol{t}}\; {}_{(0)}\nu_{\alpha} - d(\partial\mathcal{A}) \\
+ & \oint_{\partial\mathcal{A}} \left({}_{(-1)}\widetilde{\boldsymbol{m}}^{\alpha} - {}_{(-1)}h^{+}\; {}_{(-1)}\boldsymbol{n}^{\alpha} \right) \bullet {}_{(-1)}\dot{\boldsymbol{t}}\; {}_{(-1)}\nu_{\alpha} — d(\partial\mathcal{A}). \qquad (11.24)
\end{aligned}
$$

11.2. Power of Assigned Forces/Couples

Let $\boldsymbol{n}^{*}$ denote the distributed assigned force on the neutral surface of the reference layer (0), and ${}_{(\ell)}\widetilde{\boldsymbol{m}}^{*}$ the distributed assigned moment on layer (ℓ). Also let $\boldsymbol{n}^{*\alpha}$ denote the assigned force on the facet with normal ${}_{(0)}\boldsymbol{g}^{\alpha}$ on the boundary $d(\partial\mathcal{A})$ (see the definition of ${}_{(\ell)}\boldsymbol{n}^{\alpha}$ in (11.8)), and ${}_{(\ell)}\widetilde{\boldsymbol{m}}^{*\alpha}$ the assigned couples on the facet with normal ${}_{(\ell)}\boldsymbol{g}^{\alpha}$ on the boundary ${}_{(\ell)}d(\partial\mathcal{A}) := d(\partial\mathcal{A}) \times {}_{(\ell)}\mathcal{H}$ of the neutral surface of layer (ℓ). The power of the assigned forces and couples is written as follows

$$
\begin{aligned}
\mathcal{P}_a = & \int_{\mathcal{A}} \left(\boldsymbol{n}^{*} \bullet \dot{\boldsymbol{u}} + \sum_{\ell=-1}^{1} {}_{(\ell)}\widetilde{\boldsymbol{m}}^{*} \bullet {}_{(\ell)}\dot{\boldsymbol{t}} \right) d\mathcal{A} \\
& + \oint_{\partial\mathcal{A}} \left(\boldsymbol{n}^{*\alpha} \bullet \dot{\boldsymbol{u}}\; {}_{(0)}\nu_{\alpha} + \sum_{\ell=-1}^{1} {}_{(\ell)}\widetilde{\boldsymbol{m}}^{*\alpha} \bullet {}_{(\ell)}\dot{\boldsymbol{t}}\; {}_{(\ell)}\nu_{\alpha} \right) d(\partial\mathcal{A}). \qquad (11.25)
\end{aligned}
$$

11.3. Rate of Kinetic Energy

Let ${}_{(\ell)}\rho$ denote the mass density of layer (ℓ) in the spatial configuration. The kinetic energy $\mathcal{K}$ of the sandwich shell is given by

$$\mathcal{K} = \frac{1}{2} \sum_{\ell=-1}^{1} \int_{{}_{(\ell)}\mathcal{B}_t} {}_{(\ell)}\rho \; {}_{(\ell)}\dot{\mathbf{\Phi}} \cdot {}_{(\ell)}\dot{\mathbf{\Phi}} \, d\left({}_{(\ell)}\mathcal{B}_t\right), \tag{11.26}$$

where ${}_{(\ell)}\mathcal{B}_t = {}_{(\ell)}\mathbf{\Phi}\left({}_{(\ell)}\mathcal{B}\right)$ is the domain of layer (ℓ) in the current configuration.

By the Reynolds transport theorem and the conservation of mass (see, e.g., Malvern [1969, p.210]), we obtain the material time derivative of the kinetic energy $\mathcal{K}$ in (11.26) as

$$\frac{d\mathcal{K}}{dt} = \sum_{\ell=-1}^{1} \int_{{}_{(\ell)}\mathcal{B}_t} {}_{(\ell)}\rho \; {}_{(\ell)}\ddot{\mathbf{\Phi}} \cdot {}_{(\ell)}\dot{\mathbf{\Phi}} \, d\left({}_{(\ell)}\mathcal{B}_t\right), \tag{11.27}$$

which when expressed in the material configuration is given by

$$\frac{d\mathcal{K}}{dt} = \sum_{\ell=-1}^{1} \int_{\mathcal{A}} \int_{{}_{(\ell)}\mathcal{H}} {}_{(\ell)}\rho \; {}_{(\ell)}j_t \; {}_{(\ell)}\ddot{\mathbf{\Phi}} \cdot {}_{(\ell)}\dot{\mathbf{\Phi}} \, d\mathcal{A} \, d\xi^3 . \tag{11.28}$$

To simplify the derivation, we introduce the following notations

$${}_{(0)}\boldsymbol{\psi} := {}_{(0)}\boldsymbol{\varphi} = \xi^\alpha \, \mathbf{E}_\alpha + \tilde{\boldsymbol{u}}\left(\xi^{\underline{\alpha}}, t\right), \tag{11.29}$$

$${}_{(1)}\boldsymbol{\psi} := {}_{(0)}\boldsymbol{\varphi} + {}_{(0)}h^{+}\left({}_{(0)}\boldsymbol{t} - {}_{(1)}\boldsymbol{t}\right), \tag{11.30}$$

$${}_{(-1)}\boldsymbol{\psi} := {}_{(0)}\boldsymbol{\varphi} - {}_{(0)}h^{-}\left({}_{(0)}\boldsymbol{t} - {}_{(-1)}\boldsymbol{t}\right). \tag{11.31}$$

Note that ${}_{(\ell)}\boldsymbol{\psi}$ is not a function of the through-the-thickness coordinate ξ^3, and is introduced to isolate the terms with ξ^3 as a factor from the rest as follows.

$${}_{(\ell)}\mathbf{\Phi} = {}_{(\ell)}\boldsymbol{\psi} + \xi^3 \, {}_{(\ell)}\boldsymbol{t}, \quad \text{for } \ell = -1, 0, 1. \tag{11.32}$$

The term ${}_{(\ell)}\boldsymbol{\psi}$ will play a special role in the integration through the thickness in the following derivation. Define

$${}_{(\ell)}A_\rho^k := \int_{{}_{(\ell)}\mathcal{H}} {}_{(\ell)}\rho \; {}_{(\ell)}j_t \left(\xi^3\right)^k d\xi^3, \qquad \text{for} \quad \left\{ \begin{array}{l} k = 0, 1, 2, \\ \ell = -1, 0, 1, \end{array} \right. \tag{11.33}$$

where ${}_{(\ell)}A^0_\rho$ is the mass per unit underformed area of layer (ℓ), ${}_{(\ell)}A^1_\rho$ is the mass moment per unit underformed area of layer (ℓ), and ${}_{(\ell)}A^2_\rho$ the mass moment of inertia per unit underformed area of layer (ℓ). Since ${}_{(\ell)}\boldsymbol{\psi}$ is not a function of ξ^3, and can therefore be taken out of the integration over the thickness, the time derivative of the kinetic energy (11.28) can be written as

$$\begin{aligned}
\frac{d}{dt}\mathcal{K} &= \sum_{\ell=-1}^{1}\int_{\mathcal{A}}\int_{{}_{(\ell)}\mathcal{H}} {}_{(\ell)}\rho\ {}_{(\ell)}j_t \left({}_{(\ell)}\ddot{\boldsymbol{\psi}} + \xi^3\ {}_{(\ell)}\ddot{\boldsymbol{t}}\right)\cdot\left({}_{(\ell)}\dot{\boldsymbol{\psi}} + \xi^3\ {}_{(\ell)}\dot{\boldsymbol{t}}\right) d\mathcal{A}\, d\xi^3 \\
&= \sum_{\ell=-1}^{1}\int_{\mathcal{A}}\Big\{ {}_{(\ell)}A^0_\rho\ {}_{(\ell)}\ddot{\boldsymbol{\psi}}\cdot{}_{(\ell)}\dot{\boldsymbol{\psi}} + {}_{(\ell)}A^1_\rho \left({}_{(\ell)}\ddot{\boldsymbol{\psi}}\cdot{}_{(\ell)}\dot{\boldsymbol{t}} + {}_{(\ell)}\ddot{\boldsymbol{t}}\cdot{}_{(\ell)}\dot{\boldsymbol{\psi}}\right) \\
&\qquad + {}_{(\ell)}A^2_\rho\ {}_{(\ell)}\ddot{\boldsymbol{t}}\cdot{}_{(\ell)}\dot{\boldsymbol{t}}\Big\} d\mathcal{A} \\
&= \sum_{\ell=-1}^{1}\int_{\mathcal{A}}\left[{}_{(\ell)}\boldsymbol{f}\cdot{}_{(\ell)}\dot{\boldsymbol{\psi}} + {}_{(\ell)}\boldsymbol{q}\cdot{}_{(\ell)}\dot{\boldsymbol{t}}\right] d\mathcal{A}, \qquad (11.34)
\end{aligned}$$

where ${}_{(\ell)}\boldsymbol{f}$ and ${}_{(\ell)}\boldsymbol{q}$ are the inertia force and inertia couple defined as

$$\begin{aligned}
{}_{(\ell)}\boldsymbol{f} &:= \left({}_{(\ell)}A^0_\rho\ {}_{(\ell)}\ddot{\boldsymbol{\psi}} + {}_{(\ell)}A^1_\rho\ {}_{(\ell)}\ddot{\boldsymbol{t}}\right), \\
{}_{(\ell)}\boldsymbol{q} &:= \left({}_{(\ell)}A^1_\rho\ {}_{(\ell)}\ddot{\boldsymbol{\psi}} + {}_{(\ell)}A^2_\rho\ {}_{(\ell)}\ddot{\boldsymbol{t}}\right), \quad \text{for } \ell = -1, 0, 1. \qquad (11.35)
\end{aligned}$$

To obtain the equations of motion for the sandwich shell, we reorganize the rate of kinetic energy according to the 12 principal unknowns (prior to the introduction of the 3 constraints of the inextensibility of the directors), as introduced in Section 10.1. From (11.29), the first and second time derivatives of ${}_{(0)}\boldsymbol{\psi}$ can be written as

$${}_{(0)}\dot{\boldsymbol{\psi}} = {}_{(0)}\dot{\boldsymbol{\varphi}} = \dot{\boldsymbol{u}}, \qquad (11.36)$$

$${}_{(0)}\ddot{\boldsymbol{\psi}} = {}_{(0)}\ddot{\boldsymbol{\varphi}} = \ddot{\boldsymbol{u}}, \qquad (11.37)$$

and thus, from (11.30) and (11.31) the first and second time derivatives of ${}_{(1)}\boldsymbol{\psi}$ and ${}_{(-1)}\boldsymbol{\psi}$ are

$${}_{(1)}\dot{\boldsymbol{\psi}} = \dot{\boldsymbol{u}} + {}_{(0)}h^+\left({}_{(0)}\dot{\boldsymbol{t}} - {}_{(1)}\dot{\boldsymbol{t}}\right), \qquad (11.38)$$

$$
\begin{aligned}
{}_{(-1)}\dot{\boldsymbol{\psi}} &= \dot{\boldsymbol{u}} - {}_{(0)}h^{-}\left({}_{(0)}\dot{\boldsymbol{t}} - {}_{(-1)}\dot{\boldsymbol{t}}\right), &(11.39)\\
{}_{(1)}\ddot{\boldsymbol{\psi}} &= \ddot{\boldsymbol{u}} + {}_{(0)}h^{+}\left({}_{(0)}\ddot{\boldsymbol{t}} - {}_{(1)}\ddot{\boldsymbol{t}}\right), &(11.40)\\
{}_{(-1)}\ddot{\boldsymbol{\psi}} &= \ddot{\boldsymbol{u}} - {}_{(0)}h^{-}\left({}_{(0)}\ddot{\boldsymbol{t}} - {}_{(-1)}\ddot{\boldsymbol{t}}\right). &(11.41)
\end{aligned}
$$

Substitute ${}_{(\ell)}\dot{\boldsymbol{\psi}}$ from (11.36), (11.38) and(11.39) into (11.34), we obtain the alternative form of the rate of the kinetic energy as

$$
\begin{aligned}
\frac{d}{dt}\mathcal{K} &= \sum_{\ell=-1}^{1}\int_{\mathcal{A}}\left[{}_{(\ell)}\boldsymbol{f}\cdot{}_{(\ell)}\dot{\boldsymbol{\psi}} + {}_{(\ell)}\boldsymbol{q}\cdot{}_{(\ell)}\dot{\boldsymbol{t}}\right]d\mathcal{A}\\
&= \int_{\mathcal{A}}\Big\langle\Big\{{}_{(-1)}\boldsymbol{f}\cdot\left[\dot{\boldsymbol{u}} - {}_{(0)}h^{-}\left({}_{(0)}\dot{\boldsymbol{t}} - {}_{(-1)}\dot{\boldsymbol{t}}\right)\right] + {}_{(-1)}\boldsymbol{q}\cdot{}_{(-1)}\dot{\boldsymbol{t}}\Big\}\\
&\quad + \left({}_{(0)}\boldsymbol{f}\cdot\dot{\boldsymbol{u}} + {}_{(0)}\boldsymbol{q}\cdot{}_{(0)}\dot{\boldsymbol{t}}\right) + \Big\{{}_{(1)}\boldsymbol{f}\cdot\left[\dot{\boldsymbol{u}} + {}_{(0)}h^{+}\left({}_{(0)}\dot{\boldsymbol{t}} - {}_{(1)}\dot{\boldsymbol{t}}\right)\right]\\
&\quad + {}_{(1)}\boldsymbol{q}\cdot{}_{(1)}\dot{\boldsymbol{t}}\Big\}\Big\rangle d\mathcal{A}\\
&= \int_{\mathcal{A}}\Big\{\left(\sum_{\ell=-1}^{1}{}_{(\ell)}\boldsymbol{f}\right)\cdot\dot{\boldsymbol{u}} + \left({}_{(-1)}\boldsymbol{q} + {}_{(0)}h^{-}\,{}_{(-1)}\boldsymbol{f}\right)\cdot{}_{(-1)}\dot{\boldsymbol{t}}\\
&\quad + \left[{}_{(0)}\boldsymbol{q} + \left({}_{(0)}h^{+}\,{}_{(1)}\boldsymbol{f} - {}_{(0)}h^{-}\,{}_{(-1)}\boldsymbol{f}\right)\right]\cdot{}_{(0)}\dot{\boldsymbol{t}}\\
&\quad + \left({}_{(1)}\boldsymbol{q} - {}_{(0)}h^{+}\,{}_{(1)}\boldsymbol{f}\right)\cdot{}_{(1)}\dot{\boldsymbol{t}}\Big\}d\mathcal{A}. \qquad (11.42)
\end{aligned}
$$

From (11.42), we define the total inertia force $\widehat{\boldsymbol{f}}$ as

$$
\widehat{\boldsymbol{f}} := \sum_{\ell=-1}^{1}{}_{(\ell)}\boldsymbol{f}\,, \qquad (11.43)
$$

the inertia couple ${}_{(\ell)}\boldsymbol{C}$ for layer (ℓ), with $\ell = 1, 0, -1$, as

$$
\begin{aligned}
{}_{(1)}\boldsymbol{C} &:= {}_{(1)}\boldsymbol{q} - {}_{(0)}h^{+}\,{}_{(1)}\boldsymbol{f}\,,\\
{}_{(0)}\boldsymbol{C} &:= {}_{(0)}\boldsymbol{q} + \left({}_{(0)}h^{+}\,{}_{(1)}\boldsymbol{f} - {}_{(0)}h^{-}\,{}_{(-1)}\boldsymbol{f}\right)\,, \qquad (11.44)\\
{}_{(-1)}\boldsymbol{C} &:= {}_{(-1)}\boldsymbol{q} + {}_{(0)}h^{-}\,{}_{(-1)}\boldsymbol{f}\,.
\end{aligned}
$$

We also define the k*th* mass moment per unit underformed area of all the three layers as

$$\widehat{A}_\rho^k = \sum_{\ell=-1}^{1} {}_{(\ell)}A_\rho^k, \quad \text{for } k = 0, 1, 2. \tag{11.45}$$

From $(11.35)_1$ and (11.43), we obtain the total inertia force as

$$\begin{aligned}
\widehat{\boldsymbol{f}} &= \sum_{\ell=-1}^{1} {}_{(\ell)}\boldsymbol{f} = \sum_{\ell=-1}^{1} \left({}_{(\ell)}A_\rho^0 \, {}_{(\ell)}\ddot{\boldsymbol{\psi}} + {}_{(\ell)}A_\rho^1 \, {}_{(\ell)}\ddot{\boldsymbol{t}} \right) \\
&= \left({}_{(1)}A_\rho^0 \, {}_{(1)}\ddot{\boldsymbol{\psi}} + {}_{(1)}A_\rho^1 \, {}_{(1)}\ddot{\boldsymbol{t}} \right) + \left({}_{(0)}A_\rho^0 \, {}_{(0)}\ddot{\boldsymbol{\psi}} + {}_{(0)}A_\rho^1 \, {}_{(0)}\ddot{\boldsymbol{t}} \right) \\
&\quad + \left({}_{(-1)}A_\rho^0 \, {}_{(-1)}\ddot{\boldsymbol{\psi}} + {}_{(-1)}A_\rho^1 \, {}_{(-1)}\ddot{\boldsymbol{t}} \right) \\
&= {}_{(1)}A_\rho^0 \left[\ddot{\boldsymbol{u}} + {}_{(0)}h^+ \left({}_{(0)}\ddot{\boldsymbol{t}} - {}_{(1)}\ddot{\boldsymbol{t}} \right) \right] + {}_{(1)}A_\rho^1 \, {}_{(1)}\ddot{\boldsymbol{t}} + {}_{(0)}A_\rho^0 \, \ddot{\boldsymbol{u}} + {}_{(0)}A_\rho^1 \, {}_{(0)}\ddot{\boldsymbol{t}} \\
&\quad + {}_{(-1)}A_\rho^0 \left[\ddot{\boldsymbol{u}} - {}_{(0)}h^- \left({}_{(0)}\ddot{\boldsymbol{t}} - {}_{(-1)}\ddot{\boldsymbol{t}} \right) \right] + {}_{(-1)}A_\rho^1 \, {}_{(-1)}\ddot{\boldsymbol{t}} \\
&= \widehat{A}_\rho^0 \, \ddot{\boldsymbol{u}} + \left[- {}_{(0)}h^+ \, {}_{(1)}A_\rho^0 + {}_{(1)}A_\rho^1 \right] {}_{(1)}\ddot{\boldsymbol{t}} \\
&\quad + \left[- {}_{(0)}h^- \, {}_{(-1)}A_\rho^0 + {}_{(0)}A_\rho^1 + {}_{(0)}h^+ \, {}_{(1)}A_\rho^0 \right] {}_{(0)}\ddot{\boldsymbol{t}} \\
&\quad + \left[{}_{(0)}h^- \, {}_{(-1)}A_\rho^0 + {}_{(-1)}A_\rho^1 \right] {}_{(-1)}\ddot{\boldsymbol{t}} ,
\end{aligned} \tag{11.46}$$

and the inertia couple ${}_{(\ell)}\boldsymbol{C}$ for layer (ℓ) as

$$\begin{aligned}
{}_{(1)}\boldsymbol{C} &= \left[- {}_{(1)}A_\rho^0 \, {}_{(0)}h^+ \, {}_{(1)}\ddot{\boldsymbol{\psi}} + {}_{(1)}A_\rho^1 \left({}_{(1)}\ddot{\boldsymbol{\psi}} - {}_{(0)}h^+ \, {}_{(1)}\ddot{\boldsymbol{t}} \right) + {}_{(1)}A_\rho^2 \, {}_{(1)}\ddot{\boldsymbol{t}} \right] \\
&= \Big\{ - {}_{(1)}A_\rho^0 \, {}_{(0)}h^+ \left[\ddot{\boldsymbol{u}} + {}_{(0)}h^+ \left({}_{(0)}\ddot{\boldsymbol{t}} - {}_{(1)}\ddot{\boldsymbol{t}} \right) \right] \\
&\quad + {}_{(1)}A_\rho^1 \left[\ddot{\boldsymbol{u}} + {}_{(0)}h^+ \left({}_{(0)}\ddot{\boldsymbol{t}} - {}_{(1)}\ddot{\boldsymbol{t}} \right) - {}_{(0)}h^+ \, {}_{(1)}\ddot{\boldsymbol{t}} \right] + {}_{(1)}A_\rho^2 \, {}_{(1)}\ddot{\boldsymbol{t}} \Big\} \\
&= \left[{}_{(0)}h^+ \left({}_{(0)}h^+ \, {}_{(1)}A_\rho^0 - 2 \, {}_{(1)}A_\rho^1 \right) + {}_{(1)}A_\rho^2 \right] {}_{(1)}\ddot{\boldsymbol{t}} \\
&\quad + \left(- {}_{(0)}h^+ \, {}_{(1)}A_\rho^0 + {}_{(1)}A_\rho^1 \right) \left(\ddot{\boldsymbol{u}} + {}_{(0)}h^+ \, {}_{(0)}\ddot{\boldsymbol{t}} \right) ,
\end{aligned} \tag{11.47}$$

$$\begin{aligned}
{}_{(0)}\boldsymbol{C} &= \Big[\left(- {}_{(0)}h^- \, {}_{(-1)}A_\rho^0 \, {}_{(-1)}\ddot{\boldsymbol{\psi}} + {}_{(0)}h^+ \, {}_{(1)}A_\rho^0 \, {}_{(1)}\ddot{\boldsymbol{\psi}} \right) \\
&\quad + \left(- {}_{(0)}h^- \, {}_{(-1)}A_\rho^1 \, {}_{(-1)}\ddot{\boldsymbol{t}} + {}_{(0)}A_\rho^1 \, {}_{(0)}\ddot{\boldsymbol{\psi}} \right) + \left({}_{(0)}h^+ \, {}_{(1)}A_\rho^1 \, {}_{(1)}\ddot{\boldsymbol{t}} + {}_{(0)}A_\rho^2 \, {}_{(0)}\ddot{\boldsymbol{t}} \right) \Big]
\end{aligned}$$

$$\begin{aligned}
&= -{}_{(0)}h^{-}\,{}_{(-1)}A_{\rho}^{0}\left[\ddot{\boldsymbol{u}} - {}_{(0)}h^{-}\left({}_{(0)}\ddot{\boldsymbol{t}} - {}_{(-1)}\ddot{\boldsymbol{t}}\right)\right] \\
&\quad + {}_{(0)}h^{+}\,{}_{(1)}A_{\rho}^{0}\left[\ddot{\boldsymbol{u}} + {}_{(0)}h^{+}\left({}_{(0)}\ddot{\boldsymbol{t}} - {}_{(1)}\ddot{\boldsymbol{t}}\right)\right] \\
&\quad + \left(-{}_{(0)}h^{-}\,{}_{(-1)}A_{\rho}^{1}\,{}_{(-1)}\ddot{\boldsymbol{t}} + {}_{(0)}A_{\rho}^{1}\,\ddot{\boldsymbol{u}}\right) + {}_{(0)}h^{+}\,{}_{(1)}A_{\rho}^{1}\,{}_{(1)}\ddot{\boldsymbol{t}} + {}_{(0)}A_{\rho}^{2}\,{}_{(0)}\ddot{\boldsymbol{t}} \\
&= {}_{(0)}h^{+}\left({}_{(1)}A_{\rho}^{1} - {}_{(0)}h^{+}\,{}_{(1)}A_{\rho}^{0}\right){}_{(1)}\ddot{\boldsymbol{t}} \\
&\quad + \left[\left({}_{(0)}h^{-}\right)^{2}\,{}_{(-1)}A_{\rho}^{0} + \left({}_{(0)}h^{+}\right)^{2}\,{}_{(1)}A_{\rho}^{0} + {}_{(0)}A_{\rho}^{2}\right]{}_{(0)}\ddot{\boldsymbol{t}} \\
&\quad + {}_{(0)}h^{-}\left(-{}_{(-1)}A_{\rho}^{1} - {}_{(0)}h^{-}\,{}_{(-1)}A_{\rho}^{0}\right){}_{(-1)}\ddot{\boldsymbol{t}} \\
&\quad + \left(-{}_{(0)}h^{-}\,{}_{(-1)}A_{\rho}^{0} + {}_{(0)}A_{\rho}^{1} + {}_{(0)}h^{+}\,{}_{(1)}A_{\rho}^{0}\right)\ddot{\boldsymbol{u}}\,,
\end{aligned} \tag{11.48}$$

$$\begin{aligned}
{}_{(-1)}\boldsymbol{C} &= \left[{}_{(-1)}A_{\rho}^{0}\,{}_{(0)}h^{-}\,{}_{(-1)}\ddot{\boldsymbol{\psi}} + {}_{(-1)}A_{\rho}^{1}\left({}_{(-1)}\ddot{\boldsymbol{\psi}} + {}_{(0)}h^{-}\,{}_{(-1)}\ddot{\boldsymbol{t}}\right) + {}_{(-1)}A_{\rho}^{2}\,{}_{(-1)}\ddot{\boldsymbol{t}}\right] \\
&= \Big\{{}_{(-1)}A_{\rho}^{0}\,{}_{(0)}h^{-}\left[\ddot{\boldsymbol{u}} - {}_{(0)}h^{-}\left({}_{(0)}\ddot{\boldsymbol{t}} - {}_{(-1)}\ddot{\boldsymbol{t}}\right)\right] \\
&\quad + {}_{(-1)}A_{\rho}^{1}\left[\ddot{\boldsymbol{u}} - {}_{(0)}h^{-}\left({}_{(0)}\ddot{\boldsymbol{t}} - {}_{(-1)}\ddot{\boldsymbol{t}}\right) + {}_{(0)}h^{-}\,{}_{(-1)}\ddot{\boldsymbol{t}}\right] + {}_{(-1)}A_{\rho}^{2}\,{}_{(-1)}\ddot{\boldsymbol{t}}\Big\} \\
&= \left({}_{(0)}h^{-}\,{}_{(-1)}A_{\rho}^{0} + {}_{(-1)}A_{\rho}^{1}\right)\left(\ddot{\boldsymbol{u}} - {}_{(0)}h^{-}\,{}_{(0)}\ddot{\boldsymbol{t}}\right) \\
&\quad + \left[{}_{(0)}h^{-}\left({}_{(0)}h^{-}\,{}_{(-1)}A_{\rho}^{0} + 2\,{}_{(-1)}A_{\rho}^{1}\right) + {}_{(-1)}A_{\rho}^{2}\right]{}_{(-1)}\ddot{\boldsymbol{t}}\,.
\end{aligned} \tag{11.49}$$

The rate of kinetic energy (11.42) of the sandwich shell can finally be written as

$$\frac{d}{dt}\mathcal{K} = \int_{\mathcal{A}}\left[\hat{\boldsymbol{f}}\cdot\dot{\boldsymbol{u}} + \sum_{\ell=-1}^{1}{}_{(\ell)}\boldsymbol{C}\cdot{}_{(\ell)}\dot{\boldsymbol{t}}\right]d\mathcal{A}. \tag{11.50}$$

11.4. Equations of Motion for Sandwich Shells

The balance of the total power of the sandwich shell is given by

$$\frac{d}{dt}\mathcal{K} + \mathcal{P}_c = \mathcal{P}_a\,. \tag{11.51}$$

In deriving the equation of motion, we will not apply the 3 constraints of the inextensibility of the directors; therefore there will be 12 components of virtual velocities, and a total of 12 corresponding scalar equations of motion in component form. The 3 constraints of the inextensibility of the directors will be used in the weak form (see Simo and Fox [1989] for single layer shells, and Vu-Quoc and Deng [1995*c*] for multilayer shells).

Substituting in (11.51) the time rate of the kinetic energy (11.50), the power of the contact forces/couples (11.24), and the power of the assigned forces/couples (11.25), and treating $\dot{\boldsymbol{u}}$ and ${}_{(\ell)}\dot{\boldsymbol{t}}$ as virtual velocities, we obtain the following equations of motion (see also Vu-Quoc and Ebcioğlu [1995] for multilayer beams and 1-D plates).

$$\begin{aligned}
\hat{\mathfrak{n}}^{\alpha}{}_{,\alpha} + \boldsymbol{n}^{*} &= \hat{\boldsymbol{f}}\,, \\
\left({}_{(1)}\widetilde{\boldsymbol{m}}^{\alpha} + {}_{(1)}h^{-}\;{}_{(1)}\boldsymbol{n}^{\alpha}\right)_{,\alpha} - {}_{(1)}\boldsymbol{\ell} + {}_{(1)}\widetilde{\boldsymbol{m}}^{*} &= {}_{(1)}\boldsymbol{C}\,, \\
\left({}_{(0)}\widetilde{\boldsymbol{m}}^{\alpha} + {}_{(0)}h^{+}\;{}_{(1)}\boldsymbol{n}^{\alpha} - {}_{(0)}h^{-}\;{}_{(-1)}\boldsymbol{n}^{\alpha}\right)_{,\alpha} - {}_{(0)}\boldsymbol{\ell} + {}_{(0)}\widetilde{\boldsymbol{m}}^{*} &= {}_{(0)}\boldsymbol{C}\,, \\
\left({}_{(-1)}\widetilde{\boldsymbol{m}}^{\alpha} - {}_{(-1)}h^{+}\;{}_{(-1)}\boldsymbol{n}^{\alpha}\right)_{,\alpha} - {}_{(-1)}\boldsymbol{\ell} + {}_{(-1)}\widetilde{\boldsymbol{m}}^{*} &= {}_{(-1)}\boldsymbol{C}\,, \quad (11.52)
\end{aligned}$$

where $(11.52)_1$ is the balance of linear momentum referred to the neutral surface of the reference layer (0), and $(11.52)_2$–$(11.52)_4$ are the balances of angular momentum of layer (ℓ), for $\ell = -1, 0, 1$, respectively.

The corresponding boundary conditions are obtained from (11.51), after substitution of (11.50), (11.24) and (11.25), as follows

$$\begin{array}{llllr}
\text{either} & \boldsymbol{u} = \boldsymbol{u}^{*} & \text{or} & \hat{\mathfrak{n}}^{\alpha} & = \boldsymbol{n}^{*\alpha}\,, \\
\text{''} & {}_{(1)}\boldsymbol{t} = {}_{(1)}\boldsymbol{t}^{*} & \text{''} & {}_{(1)}\widetilde{\boldsymbol{m}}^{\alpha} + {}_{(1)}h^{-}\;{}_{(1)}\boldsymbol{n}^{\alpha} & = {}_{(1)}\widetilde{\boldsymbol{m}}^{*\alpha}\,, \\
\text{''} & {}_{(0)}\boldsymbol{t} = {}_{(0)}\boldsymbol{t}^{*} & \text{''} & {}_{(0)}\widetilde{\boldsymbol{m}}^{\alpha} - {}_{(0)}h^{-}\;{}_{(-1)}\boldsymbol{n}^{\alpha} + {}_{(0)}h^{+}\;{}_{(1)}\boldsymbol{n}^{\alpha} & = {}_{(0)}\widetilde{\boldsymbol{m}}^{*\alpha}\,, \\
\text{''} & {}_{(-1)}\boldsymbol{t} = {}_{(-1)}\boldsymbol{t}^{*} & \text{''} & {}_{(-1)}\widetilde{\boldsymbol{m}}^{\alpha} - {}_{(-1)}h^{+}\;{}_{(-1)}\boldsymbol{n}^{\alpha} & = {}_{(-1)}\widetilde{\boldsymbol{m}}^{*\alpha}\,.
\end{array} \quad (11.53)$$

Remark 11.3. Note that (11.52) and (11.53) are obtained without the usage of the 3 constraints of inextensibility of the director; there are thus 9 scalar equations of balance of angular momentum, i.e., $(11.52)_2$–$(11.52)_4$, and the corresponding 9 scalar equations in the boundary conditions, i.e., $(11.53)_2$–$(11.53)_4$. The 3 constraints of inextensibility will be introduced in the weak form to reduce the number of equations of balance of angular momentum from 9 to 6 (see Vu-Quoc and Deng [1995*c*]). ∎

Remark 11.4. From the definition (11.10) of the director couple ${}_{(\ell)}\boldsymbol{\ell}$, it can be seen that ${}_{(\ell)}\boldsymbol{\ell}$ has the same dimension as the force ${}_{(\ell)}\boldsymbol{n}^\alpha$ defined in (11.8) thus $\left[{}_{(\ell)}\boldsymbol{\ell}\right] = \left[{}_{(\ell)}\boldsymbol{n}^\alpha\right] = \dfrac{F}{L}$, i.e., force per unit length, where $[\bullet]$ denotes the dimension of the quantity enclosed inside the square bracket. For this reason, the quantities ${}_{(\ell)}\boldsymbol{\ell}$ is sometimes called the "through-the-thickness resultant force" as in Simo and Fox [1989]. However, from the balance of angular momentum equations $(11.52)_2$–$(11.52)_4$, ${}_{(\ell)}\boldsymbol{\ell}$ appears together with the assigned couples ${}_{(\ell)}\widetilde{\boldsymbol{m}}^*$, which has the dimension of couple per unit area, i.e., $\left[{}_{(\ell)}\widetilde{\boldsymbol{m}}^*\right] = \dfrac{FL}{L^2}$. Thus it is better to view ${}_{(\ell)}\boldsymbol{\ell}$ as having the dimension of couple per unit area, i.e., $\left[{}_{(\ell)}\boldsymbol{\ell}\right] = \dfrac{FL}{L^2}$, and therein lies the reason for its name, i.e., director couple per unit (deformed) area (see Naghdi [1972, p.482]). Of course, the other terms in $(11.52)_2$–$(11.52)_4$ also have the same dimension. For example, from the definition (11.9), the resultant couple ${}_{(\ell)}\widetilde{\boldsymbol{m}}^\alpha$ has the dimension of couple per unit length, i.e., $\left[{}_{(\ell)}\widetilde{\boldsymbol{m}}^\alpha\right] = \dfrac{FL}{L}$; thus the terms ${}_{(\ell)}\widetilde{\boldsymbol{m}}^\alpha_{,\alpha}$ in $(11.52)_2$–$(11.52)_4$ have dimension $\left[{}_{(\ell)}\widetilde{\boldsymbol{m}}^\alpha_{,\alpha}\right] = \dfrac{FL}{L^2}$. The terms ${}_{(\ell)}h^\pm\ {}_{(\ell)}\boldsymbol{n}^\alpha_{,\alpha}$ also have dimension $\dfrac{FL}{L^2}$, etc. ∎

The equations of motion (11.52) and their corresponding boundary conditions (11.53) can be simplified if we introduce the following notations

$$\begin{aligned}
{}_{(1)}\mathcal{M}^\alpha &:= {}_{(1)}\widetilde{\boldsymbol{m}}^\alpha + {}_{(1)}h^-\ {}_{(1)}\boldsymbol{n}^\alpha\,, \\
{}_{(0)}\mathcal{M}^\alpha &:= {}_{(0)}\widetilde{\boldsymbol{m}}^\alpha + {}_{(0)}h^+\ {}_{(1)}\boldsymbol{n}^\alpha - {}_{(0)}h^-\ {}_{(-1)}\boldsymbol{n}^\alpha\,, \\
{}_{(-1)}\mathcal{M}^\alpha &:= {}_{(-1)}\widetilde{\boldsymbol{m}}^\alpha - {}_{(-1)}h^+\ {}_{(-1)}\boldsymbol{n}^\alpha\,.
\end{aligned} \qquad (11.54)$$

Then the equations of motion (11.52) take the following alternative form:

$$\begin{aligned} \widehat{\mathbf{n}}^{\alpha}{}_{,\alpha} + \boldsymbol{n}^{*} &= \widehat{\boldsymbol{f}}\,, \\ \left({}_{(1)}\mathcal{M}^{\alpha}\right)_{,\alpha} - {}_{(1)}\boldsymbol{\ell} + {}_{(1)}\widetilde{\boldsymbol{m}}^{*} &= {}_{(1)}\boldsymbol{C}\,, \\ \left({}_{(0)}\mathcal{M}^{\alpha}\right)_{,\alpha} - {}_{(0)}\boldsymbol{\ell} + {}_{(0)}\widetilde{\boldsymbol{m}}^{*} &= {}_{(0)}\boldsymbol{C}\,, \\ \left({}_{(-1)}\mathcal{M}^{\alpha}\right)_{,\alpha} - {}_{(-1)}\boldsymbol{\ell} + {}_{(-1)}\widetilde{\boldsymbol{m}}^{*} &= {}_{(-1)}\boldsymbol{C}\,. \end{aligned} \tag{11.55}$$

The force boundary conditions (11.53) take the following form

$$\begin{aligned} \widehat{\mathbf{n}}^{\alpha} &= \boldsymbol{n}^{*\alpha}\,, \\ {}_{(1)}\mathcal{M}^{\alpha} &= {}_{(1)}\widetilde{\boldsymbol{m}}^{*\alpha}\,, \\ {}_{(0)}\mathcal{M}^{\alpha} &= {}_{(0)}\widetilde{\boldsymbol{m}}^{*\alpha}\,, \\ {}_{(-1)}\mathcal{M}^{\alpha} &= {}_{(-1)}\widetilde{\boldsymbol{m}}^{*\alpha}\,. \end{aligned} \tag{11.56}$$

Remark 11.5. If (i) only the core layer (0) exists without the outer layers, and (ii) the reference surface we chose is the neutral surface for the sandwich shell (see also (3.22) Simo and Fox [1989]), then the equations of motion for sandwich shells (11.52) or (11.55) reduce exactly to those obtained for the single-layer shells in Simo and Fox [1989], keeping in mind the difference in the definition of the resultant forces/couples between the present work and Simo and Fox [1989] (see (11.8)–(11.10)).

The above assertion can be proved via the following procedures: (i) All the items that related to the two outer layers are zero, thus the equation of motion for linear momentum $(11.52)_1$ becomes

$${}_{(0)}\mathbf{n}^{\alpha}{}_{,\alpha} + {}_{(0)}\boldsymbol{n}^{*} = \widehat{\boldsymbol{f}}\,, \tag{11.57}$$

where the resultant force $\widehat{\boldsymbol{f}}$ is obtain from (11.46)

$$\widehat{\boldsymbol{f}} = \widehat{A}^{0}_{\rho}\,\ddot{\boldsymbol{u}} + {}_{(0)}A^{1}_{\rho}\;{}_{(0)}\ddot{\boldsymbol{t}}\,. \tag{11.58}$$

(ii) Omit the layer index and remember the definition of the neutral surface leads to ${}_{(0)}A^1_\rho = 0$, (11.57) can be reduced to

$$\mathbf{n}^\alpha{}_{,\alpha} + \boldsymbol{n}^* = A^0_\rho\, \ddot{\boldsymbol{u}}\,. \tag{11.59}$$

Notice the difference from our definition of the resultant contact force and that in Simo and Fox [1989], we could see that the equation of motion for linear momentum $(11.52)_1$ is exactly the same as that given in Simo and Fox [1989].

If we omit the layer index, then the angular momentum equation for the core layer becomes

$$\widetilde{\boldsymbol{m}}^\alpha{}_{,\alpha} - \boldsymbol{\ell} + \widetilde{\boldsymbol{m}}^* = \boldsymbol{C}\,. \tag{11.60}$$

From (11.48), and use the two assumptions at the beginning of this Remark, we obtain $\boldsymbol{C} = A^2_\rho\, \ddot{\boldsymbol{t}}$. Recalling the difference from our definition of the resultant contact couples and that in Simo and Fox [1989](see Remark (11.1), one sees that the equation of motion for angular momentum $(11.52)_3$ is exactly the same as that given in Simo and Fox [1989].

∎

Remark 11.6. If we assume, on the other hand, that (i) the three layers have the same rotation, i.e.,

$${}_{(-1)}\boldsymbol{t} = {}_{(0)}\boldsymbol{t} = {}_{(1)}\boldsymbol{t} = \boldsymbol{t}\,, \tag{11.61}$$

and that (ii) the reference surface chosen is the neutral surface of the whole sandwich shell i.e.,

$$\sum_{\ell=-1}^{1} \int_{{}_{(\ell)}\mathcal{H}} {}_{(\ell)}\rho\; {}_{(\ell)}j_t\; \xi^3\, d\xi^3 = 0, \tag{11.62}$$

then the equations of motion (11.52) for sandwich shells reduce exactly to the equations of motion (4.19) for single-layer shell in Simo and Fox [1989].

We will first prove that the balance of linear momentum $(11.52)_1$ for sandwich shells will reduce to that of single-layer shells. From (11.8), the total contact force for the sandwich shell (11.13) can be written as

$$\widehat{\mathbf{n}}^\alpha := \sum_{\ell=-1}^{1} {}_{(\ell)}\boldsymbol{n}^\alpha = \sum_{\ell=-1}^{1} \int_{{}_{(\ell)}\mathcal{H}} {}_{(\ell)}j_t \; {}_{(\ell)}\mathbf{g}^\alpha \cdot {}_{(\ell)}\boldsymbol{\sigma} \, d\xi^3 = \int_{\mathcal{H}} j_t \, \mathbf{g}^\alpha \cdot \boldsymbol{\sigma} \, d\xi^3 . \tag{11.63}$$

Using (11.33), (11.45), and (11.62), the inertia force in (11.46) can be written as

$$\begin{aligned} \widehat{\boldsymbol{f}} &= \widehat{A}^0_\rho \, \ddot{\boldsymbol{u}} + \left[{}_{(1)}A^1_\rho + {}_{(0)}A^1_\rho + {}_{(-1)}A^1_\rho \right] \ddot{\boldsymbol{t}} \\ &= \left[\sum_{\ell=-1}^{1} \int_{{}_{(\ell)}\mathcal{H}} {}_{(\ell)}\rho \; {}_{(\ell)}j_t \, d\xi^3 \right] \ddot{\boldsymbol{u}} + \left[\sum_{\ell=-1}^{1} \int_{{}_{(\ell)}\mathcal{H}} {}_{(\ell)}\rho \; {}_{(\ell)}j_t \left(\xi^3\right)^1 d\xi^3 \right] \ddot{\boldsymbol{t}} \\ &= \left(\int_{\text{Ł}\mathcal{H}} \rho \, j_t \, d\xi^3 \right) \ddot{\boldsymbol{u}} . \end{aligned} \tag{11.64}$$

Thus, $(11.52)_1$ reduces to

$$\frac{1}{\bar{j}_t} \left(\int_{\mathcal{H}} j_t \, \mathbf{g}^\alpha \cdot \boldsymbol{\sigma} \, d\xi^3 \right)_{,\alpha} + \frac{1}{\bar{j}_t} \mathbf{n}^* = \frac{1}{\bar{j}_t} \left(\int_{\mathcal{H}} \rho \, j_t \, d\xi^3 \right) \ddot{\boldsymbol{u}} . \tag{11.65}$$

Note that our definition of the applied resultant force $\mathbf{n}^*$ is different, by a factor $\frac{1}{\bar{j}_t}$, from the definition of the applied resultant force per unit length $\overline{\mathbf{n}}$ in equation (A.5) of Simo and Fox [1989]. Using (3.23) and (4.5a) of Simo and Fox [1989] for a definition of the mass per unit length $\overline{\rho}$ and the resultant force $\mathbf{n}^\alpha$, respectively, we can see that (11.65) is exactly the same as (4.19a) of Simo and Fox [1989].

We now check the balance of angular momentum. Sum up $(11.52)_2$–$(11.52)_4$ to obtain

$$\begin{aligned} &\left[\sum_{\ell=-1}^{1} {}_{(\ell)}\widetilde{\boldsymbol{m}}^\alpha + {}_{(1)}h^- \; {}_{(1)}\boldsymbol{n}^\alpha + {}_{(0)}h^+ \; {}_{(1)}\boldsymbol{n}^\alpha - {}_{(0)}h^- \; {}_{(-1)}\boldsymbol{n}^\alpha - {}_{(-1)}h^+ \; {}_{(-1)}\boldsymbol{n}^\alpha \right]_{,\alpha} \\ &\qquad - \sum_{\ell=-1}^{1} {}_{(\ell)}\boldsymbol{\ell} + \sum_{\ell=-1}^{1} {}_{(\ell)}\widetilde{\boldsymbol{m}}^* = \sum_{\ell=-1}^{1} {}_{(\ell)}\mathcal{C} \end{aligned} \tag{11.66}$$

Note that

$${}_{(0)}h^+ + {}_{(1)}h^- = {}_{(1)}Z , \quad {}_{(0)}h^- + {}_{(-1)}h^+ = {}_{(-1)}Z , \tag{11.67}$$

and using the definition (11.8) and (11.9) of resultant forces and couples, the items in the square bracket in (11.66) can be reduced as

$$\begin{aligned}\sum_{\ell=-1}^{1} {}_{(\ell)}\widetilde{\boldsymbol{m}}^{\alpha} \quad &+ \quad {}_{(1)}h^{-}\;{}_{(1)}\boldsymbol{n}^{\alpha} + {}_{(0)}h^{+}\;{}_{(1)}\boldsymbol{n}^{\alpha} - {}_{(0)}h^{-}\;{}_{(-1)}\boldsymbol{n}^{\alpha} - {}_{(-1)}h^{+}\;{}_{(-1)}\boldsymbol{n}^{\alpha} \\ &= \sum_{\ell=-1}^{1} {}_{(\ell)}\widetilde{\boldsymbol{m}}^{\alpha} + {}_{(1)}Z\;{}_{(1)}\boldsymbol{n}^{\alpha} - {}_{(-1)}Z\;{}_{(-1)}\boldsymbol{n}^{\alpha} \\ &= \sum_{\ell=-1}^{1} \int_{{}_{(\ell)}\mathcal{H}} {}_{(\ell)}j_t\;{}_{(\ell)}\mathbf{g}^{\alpha}\;\xi^3 \bullet {}_{(\ell)}\boldsymbol{\sigma}\,d\xi^3 = \int_{\mathcal{H}} j_t\;\mathbf{g}^{\alpha}\;\xi^3 \bullet \boldsymbol{\sigma}\,d\xi^3 . \qquad (11.68)\end{aligned}$$

Using (11.10), the second part in (11.66) can be written as

$$\sum_{\ell=-1}^{1} {}_{(\ell)}\boldsymbol{\ell} = \sum_{\ell=-1}^{1} \int_{{}_{(\ell)}\mathcal{H}} {}_{(\ell)}j_t\;{}_{(\ell)}\mathbf{g}^{3} \bullet {}_{(\ell)}\boldsymbol{\sigma}\;d\xi^3 = \int_{\mathcal{H}} j_t\;\mathbf{g}^{3} \bullet \boldsymbol{\sigma}\;d\xi^3 . \qquad (11.69)$$

With (11.47)–(11.49), (11.61) and (11.62), the total inertia couple can be rewritten as

$$\begin{aligned}\sum_{\ell=-1}^{1} {}_{(\ell)}\boldsymbol{C} &= \left[{}_{(0)}h^{+}\left({}_{(0)}h^{+}\;{}_{(1)}A_{\rho}^{0} - 2\,{}_{(1)}A_{\rho}^{1}\right) + {}_{(1)}A_{\rho}^{2}\right]\,{}_{(1)}\ddot{\boldsymbol{t}} \\ &+ \left(-\,{}_{(0)}h^{+}\;{}_{(1)}A_{\rho}^{0} + {}_{(1)}A_{\rho}^{1}\right)\left(\ddot{\boldsymbol{u}} + {}_{(0)}h^{+}\;{}_{(0)}\ddot{\boldsymbol{t}}\right) + {}_{(0)}h^{+}\left({}_{(1)}A_{\rho}^{1} - {}_{(0)}h^{+}\;{}_{(1)}A_{\rho}^{0}\right)\,{}_{(1)}\ddot{\boldsymbol{t}} \\ &+ \left[\left({}_{(0)}h^{-}\right)^{2}\,{}_{(-1)}A_{\rho}^{0} + \left({}_{(0)}h^{+}\right)^{2}\,{}_{(1)}A_{\rho}^{0} + {}_{(0)}A_{\rho}^{2}\right]\,{}_{(0)}\ddot{\boldsymbol{t}} \\ &+ {}_{(0)}h^{-}\left(-\,{}_{(-1)}A_{\rho}^{1} - {}_{(0)}h^{-}\;{}_{(-1)}A_{\rho}^{0}\right)\,{}_{(-1)}\ddot{\boldsymbol{t}} + \left(-\,{}_{(0)}h^{-}\;{}_{(-1)}A_{\rho}^{0} + {}_{(0)}A_{\rho}^{1} + {}_{(0)}h^{+}\;{}_{(1)}A_{\rho}^{0}\right)\ddot{\boldsymbol{u}} \\ &+ \left({}_{(0)}h^{-}\;{}_{(-1)}A_{\rho}^{0} + {}_{(-1)}A_{\rho}^{1}\right)\left(\ddot{\boldsymbol{u}} - {}_{(0)}h^{-}\;{}_{(0)}\ddot{\boldsymbol{t}}\right) \\ &+ \left[{}_{(0)}h^{-}\left({}_{(0)}h^{-}\;{}_{(-1)}A_{\rho}^{0} + 2\,{}_{(-1)}A_{\rho}^{1}\right) + {}_{(-1)}A_{\rho}^{2}\right]\,{}_{(-1)}\ddot{\boldsymbol{t}} \\ &= \left(\sum_{\ell=-1}^{1} {}_{(\ell)}A_{\rho}^{1}\right)\ddot{\boldsymbol{u}} + \left(\sum_{\ell=-1}^{1} {}_{(\ell)}A_{\rho}^{2}\right)\ddot{\boldsymbol{t}} = \left(\sum_{\ell=-1}^{1} {}_{(\ell)}A_{\rho}^{2}\right)\ddot{\boldsymbol{t}} . \qquad (11.70)\end{aligned}$$

Finally, using (11.68), (11.69) and (11.70), we can write the balance of total angular momentum (11.66) as

$$\left(\int_{\mathcal{H}} j_t\;\mathbf{g}^{\alpha}\;\xi^3 \bullet \boldsymbol{\sigma}\,d\xi^3\right)_{,\alpha} - \int_{\mathcal{H}} j_t\;\mathbf{g}^{3} \bullet \boldsymbol{\sigma}\;d\xi^3 + \sum_{\ell=-1}^{1} {}_{(1)}\widetilde{\boldsymbol{m}}^{*} = \left(\sum_{\ell=-1}^{1} {}_{(\ell)}A_{\rho}^{2}\right)\ddot{\boldsymbol{t}} . \qquad (11.71)$$

Note that our definition of the applied resultant couples $\sum_{\ell=-1}^{1} {}_{(\ell)}\widetilde{\mathbf{m}}^*$ is different from the definition of applied director couple per unit length $\widetilde{\widetilde{\mathbf{m}}}$ in (4.18) of Simo and Fox [1989] by a factor $\frac{1}{\bar{j}_t}$. Employ (3.24), (4.10) and (4.11) of Simo and Fox [1989] for definitions of the mass moment of inertia per unit length $\bar{\mathbf{I}}_\rho$, the across-the-thickness resultant ℓ and the resultant couple $\widetilde{\mathbf{m}}^\alpha$, we can see that (11.71) is exactly the same as (4.19b) of Simo and Fox [1989]. Thus the equations for single-layer shells constitute a particular case of those for sandwich shells. ∎

11.5. Angular Velocity/Acceleration of Director Field

To solve the equations of motion given in (11.52), we need the explicit expression for the first and second time rate of the director field. To this end, we recall some mathematical concepts (Simo and Fox [1989]).

Define the set of rotations whose rotation axis is perpendicular to the vector $\mathbf{E}$ as

$$S_E^2 := \left\{ \Lambda \in SO(3) \;\middle|\; \text{for } \Psi \in \mathrm{R}^3 \text{ such that } \Lambda\,\Psi = \Psi \,, \text{and } \Psi \cdot \mathbf{E} = 0 \right\}, \tag{11.72}$$

where $SO(3)$ is the set of orthogonal transformations. Each rotation operator $\Lambda \in S_E^2$ will apply a drill-free rotation on the vector $\mathbf{E}$, i.e., a rotation of $\mathbf{E}$ such that $\mathbf{E}$ does not rotated about itself; there is thus no drill dof's in the rotations. Let $\mathbf{E} = \mathbf{E}^3 = \mathbf{E}_3$ be the material director field. To each spatial director $t \neq \mathbf{E}$, there exists a unique (Simo and Fox [1989]) rotation operator $\Lambda \in S_E^2$ such that

$${}_{(\ell)}\boldsymbol{t} = {}_{(\ell)}\Lambda\,\mathbf{E}\,. \tag{11.73}$$

The time rate of the spatial director $\boldsymbol{t}$ can be expressed as

$${}_{(\ell)}\dot{\boldsymbol{t}} = {}_{(\ell)}\dot{\Lambda}\,\mathbf{E} = {}_{(\ell)}\Lambda\left({}_{(\ell)}\Lambda^t\,{}_{(\ell)}\dot{\Lambda}\right)\mathbf{E} = {}_{(\ell)}\dot{\Lambda}\,{}_{(\ell)}\Lambda^t\,{}_{(\ell)}\boldsymbol{t}\,. \tag{11.74}$$

Define

$${}_{(\ell)}\widehat{\boldsymbol{\Omega}} := {}_{(\ell)}\Lambda^t\,{}_{(\ell)}\dot{\Lambda}\,, \quad {}_{(\ell)}\widehat{\boldsymbol{\omega}} := {}_{(\ell)}\dot{\Lambda}\,{}_{(\ell)}\Lambda^t\,, \tag{11.75}$$

where ${}_{(\ell)}\widehat{\boldsymbol{\Omega}}$ is the material rotation velocity tensor, and ${}_{(\ell)}\widehat{\boldsymbol{\omega}}$ the spatial rotation velocity tensor. Both ${}_{(\ell)}\widehat{\boldsymbol{\Omega}}$ and ${}_{(\ell)}\widehat{\boldsymbol{\omega}}$ are skew-symmetric (see Simo and Fox [1989]). We also define the axial vector ${}_{(\ell)}\boldsymbol{\omega}$ associated with ${}_{(\ell)}\widehat{\boldsymbol{\omega}}$, (see, e.g., Chadwick [1976, p.29]), as follows

$$\forall \boldsymbol{h} \in \mathrm{R}^3, \quad {}_{(\ell)}\widehat{\boldsymbol{\omega}}\, \boldsymbol{h} = {}_{(\ell)}\boldsymbol{\omega} \times \boldsymbol{h}\,. \tag{11.76}$$

Thus the time rate of the director field (11.74) can be expressed as

$${}_{(\ell)}\dot{\boldsymbol{t}} = {}_{(\ell)}\boldsymbol{\omega} \times {}_{(\ell)}\boldsymbol{t}\,, \quad {}_{(\ell)}\boldsymbol{\omega} \cdot {}_{(\ell)}\boldsymbol{t} = 0, \tag{11.77}$$

which is the requirement of no-drill dof's.

CHAPTER 12
LINEARIZED EQUATIONS OF MOTION

The fully nonlinear stress resultant geometrically-exact sandwich shell equations of motion obtained in Section 11 will be linearized systematically here, based on the small deformation assumption. The reader is referred to Vu-Quoc and Ebcioğlu [1995] for the analogy in the linearization of geometrically-exact sandwich beams and 1-D plates. Here we will verify the proposed theory by comparing a particular case of its linearized version to the linear equations of sandwich plates obtained in Yu [1959*a*]. In this particular case, a symmetric sandwich plate is considered, in which the top layer (1) is identical to the bottom layer (-1), and the core layer (0) is symmetric about its neutral surface. Further, it is assumed that the rotations in layer (1) and in layer (-1) are the same (see Yu [1959*a*]).

12.1. Alternative Equations of Motion

For the subsequent comparison of the linearized equations with those in Yu [1959*a*], we can replace the 3 equations of motion for angular momentum $(11.52)_2$–$(11.52)_4$ by a set of equivalent equations. First, summing up $(11.52)_2$–$(11.52)_4$, we obtain the equations of motion for total angular momentum of geometrically-exact sandwich shells

$$
\begin{aligned}
&\Big[\widehat{\widetilde{\mathbf{m}}}^{\alpha} + \Big({}_{(0)}h^{+}\;{}_{(1)}\boldsymbol{n}^{\alpha} - {}_{(0)}h^{-}\;{}_{(-1)}\boldsymbol{n}^{\alpha}\Big) \\
&\qquad + \Big({}_{(1)}h^{-}\;{}_{(1)}\boldsymbol{n}^{\alpha} - {}_{(-1)}h^{+}\;{}_{(-1)}\boldsymbol{n}^{\alpha}\Big)\Big]_{,\alpha} - \widehat{\boldsymbol{\ell}} + \widehat{\widetilde{\mathbf{m}}}^{*} = \widehat{\boldsymbol{C}}\,, \qquad (12.1)
\end{aligned}
$$

where

$$
\widehat{\widetilde{\mathbf{m}}}^{\alpha} \;:=\; {}_{(1)}\widetilde{\boldsymbol{m}}^{\alpha} + {}_{(0)}\widetilde{\boldsymbol{m}}^{\alpha} + {}_{(-1)}\widetilde{\boldsymbol{m}}^{\alpha}\,, \qquad (12.2)
$$

$$\widehat{\boldsymbol{\ell}} \;:=\; {}_{(1)}\boldsymbol{\ell} + {}_{(0)}\boldsymbol{\ell} + {}_{(-1)}\boldsymbol{\ell}\,, \tag{12.3}$$

$$\widehat{\mathbf{m}}^{*} \;:=\; {}_{(1)}\widetilde{\boldsymbol{m}}^{*} + {}_{(0)}\widetilde{\boldsymbol{m}}^{*} + {}_{(-1)}\widetilde{\boldsymbol{m}}^{*}\,, \tag{12.4}$$

$$\widehat{\boldsymbol{C}} \;:=\; {}_{(1)}\boldsymbol{C} + {}_{(0)}\boldsymbol{C} + {}_{(-1)}\boldsymbol{C}\,, \tag{12.5}$$

with $\widehat{\mathbf{m}}^{\alpha}$ being the total contact couple on the facet with normal ${}_{(\ell)}\boldsymbol{g}^{\alpha}$, $\widehat{\boldsymbol{\ell}}$ the total director couple, $\widehat{\mathbf{m}}^{*}$ the total assigned couple, and $\widehat{\boldsymbol{C}}$ the total inertia couple. The difference between the contact couple ${}_{(1)}\widetilde{\boldsymbol{m}}^{\alpha} - {}_{(-1)}\widetilde{\boldsymbol{m}}^{\alpha}$ is governed by the following equation

$$\begin{aligned}&\left[\left({}_{(1)}\widetilde{\boldsymbol{m}}^{\alpha} - {}_{(-1)}\widetilde{\boldsymbol{m}}^{\alpha}\right) + \left({}_{(1)}h^{-}\;{}_{(1)}\boldsymbol{n}^{\alpha} + {}_{(-1)}h^{+}\;{}_{(-1)}\boldsymbol{n}^{\alpha}\right)\right]_{,\alpha}\\ &\quad - \left({}_{(1)}\boldsymbol{\ell} - {}_{(-1)}\boldsymbol{\ell}\right) + \left({}_{(1)}\widetilde{\boldsymbol{m}}^{*} - {}_{(-1)}\widetilde{\boldsymbol{m}}^{*}\right) = {}_{(1)}\boldsymbol{C} - {}_{(-1)}\boldsymbol{C}\,,\end{aligned} \tag{12.6}$$

obtained by subtracting $(11.52)_2$ from $(11.52)_4$. Thus a set of 3 equations of balance of angular momentum equivalent to $(11.52)_2$–$(11.52)_4$ is (12.1), $(11.52)_3$, and (12.6).

The boundary conditions corresponding to (12.1) and (12.6) are obtained by adding $(11.53)_2$–$(11.53)_4$ and by subtracting $(11.53)_2$ from $(11.53)_4$ to yield

$$\widehat{\mathbf{m}}^{\alpha} - {}_{(-1)}\boldsymbol{n}^{\alpha}\left({}_{(-1)}h^{+} + {}_{(0)}h^{-}\right) + {}_{(1)}\boldsymbol{n}^{\alpha}\left({}_{(0)}h^{+} + {}_{(1)}h^{-}\right) = \widehat{\mathbf{m}}^{*\alpha}\,, \tag{12.7}$$

$$\left({}_{(1)}\widetilde{\boldsymbol{m}}^{\alpha} - {}_{(-1)}\widetilde{\boldsymbol{m}}^{\alpha}\right) + \left({}_{(1)}h^{-}\;{}_{(1)}\boldsymbol{n}^{\alpha} + {}_{(-1)}h^{+}\;{}_{(-1)}\boldsymbol{n}^{\alpha}\right) = {}_{(1)}\widetilde{\boldsymbol{m}}^{*} - {}_{(-1)}\widetilde{\boldsymbol{m}}^{*}\,. \tag{12.8}$$

Thus the boundary conditions for the equations of motion (12.1), $(11.52)_3$, and (12.6) are (12.7), $(11.53)_3$, and (12.8), respectively.

From (11.49)–(11.47), we obtain the total inertia couple $\widehat{\boldsymbol{C}}$ as follows

$$\begin{aligned}\widehat{\boldsymbol{C}} \;=\;& \widehat{A}^{1}_{\rho}\,\ddot{\boldsymbol{u}} + \sum_{\ell=-1}^{1} {}_{(\ell)}A^{2}_{\rho}\;{}_{(\ell)}\ddot{\boldsymbol{t}}\\ &+ {}_{(0)}h^{+}\;{}_{(1)}A^{1}_{\rho}\left({}_{(0)}\ddot{\boldsymbol{t}} - 2\,{}_{(1)}\ddot{\boldsymbol{t}}\right) - {}_{(0)}h^{-}\;{}_{(-1)}A^{1}_{\rho}\left({}_{(0)}\ddot{\boldsymbol{t}} - 2\,{}_{(-1)}\ddot{\boldsymbol{t}}\right)\\ &- \left({}_{(0)}h^{+}\right)^{2}\;{}_{(1)}A^{0}_{\rho}\left({}_{(0)}\ddot{\boldsymbol{t}} - {}_{(1)}\ddot{\boldsymbol{t}}\right) - \left({}_{(0)}h^{-}\right)^{2}\;{}_{(-1)}A^{0}_{\rho}\left({}_{(0)}\ddot{\boldsymbol{t}} - {}_{(-1)}\ddot{\boldsymbol{t}}\right)\end{aligned}$$

$$
\begin{aligned}
&+ \left({}_{(0)}h^{+}\right)^{2} {}_{(1)}A_{\rho}^{0} \left({}_{(0)}\ddot{\boldsymbol{t}} - {}_{(1)}\ddot{\boldsymbol{t}}\right) + \left({}_{(0)}h^{-}\right)^{2} {}_{(-1)}A_{\rho}^{0} \left({}_{(0)}\ddot{\boldsymbol{t}} - {}_{(-1)}\ddot{\boldsymbol{t}}\right) \\
&+ {}_{(0)}h^{+} \, {}_{(1)}A_{\rho}^{1} \, {}_{(1)}\ddot{\boldsymbol{t}} - {}_{(0)}h^{-} \, {}_{(-1)}A_{\rho}^{1} \, {}_{(-1)}\ddot{\boldsymbol{t}} \\
= \; & \widehat{A}_{\rho}^{1} \, \ddot{\boldsymbol{u}} + \sum_{\ell=-1}^{1} {}_{(\ell)}A_{\rho}^{2} \, {}_{(\ell)}\ddot{\boldsymbol{t}} \\
&+ {}_{(0)}h^{+} \, {}_{(1)}A_{\rho}^{1} \left[{}_{(0)}\ddot{\boldsymbol{t}} - {}_{(1)}\ddot{\boldsymbol{t}}\right] - {}_{(0)}h^{-} \, {}_{(-1)}A_{\rho}^{1} \left[{}_{(0)}\ddot{\boldsymbol{t}} - {}_{(-1)}\ddot{\boldsymbol{t}}\right],
\end{aligned}
\tag{12.9}
$$

and the difference $\left({}_{(1)}\boldsymbol{C} - {}_{(-1)}\boldsymbol{C}\right)$ as follows

$$
\begin{aligned}
{}_{(1)}\boldsymbol{C} - {}_{(-1)}\boldsymbol{C} \; = \; & \left(- {}_{(0)}h^{+} \, {}_{(1)}A_{\rho}^{0} - {}_{(0)}h^{-} \, {}_{(-1)}A_{\rho}^{0} + {}_{(1)}A_{\rho}^{1} - {}_{(-1)}A_{\rho}^{1}\right) \ddot{\boldsymbol{u}} \\
&+ {}_{(1)}A_{\rho}^{2} \, {}_{(1)}\ddot{\boldsymbol{t}} - {}_{(-1)}A_{\rho}^{2} \, {}_{(-1)}\ddot{\boldsymbol{t}} + {}_{(0)}h^{+} \, {}_{(1)}A_{\rho}^{1} \left({}_{(0)}\ddot{\boldsymbol{t}} - 2 \, {}_{(1)}\ddot{\boldsymbol{t}}\right) \\
&+ {}_{(0)}h^{-} \, {}_{(-1)}A_{\rho}^{1} \left({}_{(0)}\ddot{\boldsymbol{t}} - 2 \, {}_{(-1)}\ddot{\boldsymbol{t}}\right) \\
&- \left({}_{(0)}h^{+}\right)^{2} {}_{(1)}A_{\rho}^{0} \left({}_{(0)}\ddot{\boldsymbol{t}} - {}_{(1)}\ddot{\boldsymbol{t}}\right) + \left({}_{(0)}h^{-}\right)^{2} {}_{(-1)}A_{\rho}^{0} \left({}_{(0)}\ddot{\boldsymbol{t}} - {}_{(-1)}\ddot{\boldsymbol{t}}\right).
\end{aligned}
\tag{12.10}
$$

12.2. Equations of Motion for Symmetric Sandwich Shells

Now, let us consider the symmetric sandwich shell. We have

$$
{}_{(\ell)}h^{+} = {}_{(\ell)}h^{-} = {}_{(\ell)}h, \quad \forall \ell = -1, 0, 1, \qquad {}_{(1)}h = {}_{(-1)}h, \qquad {}_{(1)}\rho = {}_{(-1)}\rho,
\tag{12.11}
$$

and thus

$$
{}_{(0)}A_{\rho}^{1} = 0, \; {}_{(1)}A_{\rho}^{0} = {}_{(-1)}A_{\rho}^{0}, \; {}_{(1)}A_{\rho}^{1} = - {}_{(-1)}A_{\rho}^{1}, \; {}_{(1)}A_{\rho}^{2} = {}_{(-1)}A_{\rho}^{2}.
\tag{12.12}
$$

From (11.52) and (11.46)–(11.47), we obtain the following nonlinear equations of motion for symmetric sandwich shells

$$
\widehat{\boldsymbol{n}}^{\alpha}{}_{,\alpha} + \boldsymbol{n}^{*} = \left({}_{(0)}h \, {}_{(-1)}A_{\rho}^{0} + {}_{(-1)}A_{\rho}^{1}\right) {}_{(-1)}\ddot{\boldsymbol{t}} + \left(- {}_{(0)}h \, {}_{(1)}A_{\rho}^{0} + {}_{(1)}A_{\rho}^{1}\right) {}_{(1)}\ddot{\boldsymbol{t}} + \widehat{A}_{\rho}^{0} \, \ddot{\boldsymbol{u}}
\tag{12.13}
$$

$$
\begin{aligned}
&\left({}_{(1)}\widetilde{\boldsymbol{m}}^{\alpha} + {}_{(1)}h\ {}_{(1)}\tilde{\boldsymbol{n}}^{\alpha}\right)_{,\alpha} - {}_{(1)}\boldsymbol{\ell} + {}_{(1)}\widetilde{\boldsymbol{m}}^{*} \\
&\qquad = \left(-\,{}_{(0)}h\ {}_{(1)}A^{0}_{\rho} + {}_{(1)}A^{1}_{\rho}\right)\ddot{\boldsymbol{u}} + {}_{(1)}A^{2}_{\rho}\ {}_{(1)}\ddot{\boldsymbol{t}} \\
&\qquad + {}_{(0)}h\ {}_{(1)}A^{1}_{\rho}\left({}_{(0)}\ddot{\boldsymbol{t}} - 2\,{}_{(1)}\ddot{\boldsymbol{t}}\right) - \left({}_{(0)}h\right)^{2}\ {}_{(1)}A^{0}_{\rho}\left({}_{(0)}\ddot{\boldsymbol{t}} - {}_{(1)}\ddot{\boldsymbol{t}}\right), \quad (12.14)
\end{aligned}
$$

$$
\begin{aligned}
&\left({}_{(0)}\widetilde{\boldsymbol{m}}^{\alpha} + {}_{(0)}h\ {}_{(1)}\boldsymbol{n}^{\alpha} - {}_{(0)}h\ {}_{(-1)}\boldsymbol{n}^{\alpha}\right)_{,\alpha} - {}_{(0)}\boldsymbol{\ell} + {}_{(0)}\widetilde{\boldsymbol{m}}^{*} \\
&\qquad = {}_{(0)}h\ {}_{(1)}A^{1}_{\rho}\ {}_{(1)}\ddot{\boldsymbol{t}} - {}_{(0)}h\ {}_{(-1)}A^{1}_{\rho}\ {}_{(-1)}\ddot{\boldsymbol{t}} + {}_{(0)}A^{2}_{\rho}\ {}_{(0)}\ddot{\boldsymbol{t}} \\
&\qquad + \left({}_{(0)}h\right)^{2}\ {}_{(1)}A^{0}_{\rho}\left({}_{(0)}\ddot{\boldsymbol{t}} - {}_{(1)}\ddot{\boldsymbol{t}}\right) + \left({}_{(0)}h\right)^{2}\ {}_{(-1)}A^{0}_{\rho}\left({}_{(0)}\ddot{\boldsymbol{t}} - {}_{(-1)}\ddot{\boldsymbol{t}}\right), (12.15)
\end{aligned}
$$

$$
\begin{aligned}
&\left({}_{(-1)}\widetilde{\boldsymbol{m}}^{\alpha} - {}_{(-1)}h\ {}_{(-1)}\boldsymbol{n}^{\alpha}\right)_{,\alpha} - {}_{(-1)}\boldsymbol{\ell} + {}_{(-1)}\widetilde{\boldsymbol{m}}^{*} \\
&\qquad = \left({}_{(0)}h\ {}_{(-1)}A^{0}_{\rho} + {}_{(-1)}A^{1}_{\rho}\right)\ddot{\boldsymbol{u}} + {}_{(-1)}A^{2}_{\rho}\ {}_{(-1)}\ddot{\boldsymbol{t}} \\
&\qquad - {}_{(0)}h\ {}_{(-1)}A^{1}_{\rho}\left({}_{(0)}\ddot{\boldsymbol{t}} - 2\,{}_{(-1)}\ddot{\boldsymbol{t}}\right) - \left({}_{(0)}h\right)^{2}\ {}_{(-1)}A^{0}_{\rho}\left({}_{(0)}\ddot{\boldsymbol{t}} - {}_{(-1)}\ddot{\boldsymbol{t}}\right). (12.16)
\end{aligned}
$$

Similar to the discussion at the beginning of this section, the balance of angular momentum equations (12.16), (12.15) and (12.14) can be replaced by a set of three equivalent equations: (12.16) is replaced by the sum of (12.16), (12.15) and (12.14); (12.15) remains the same; (12.14) is replaced by subtracting (12.14) from (12.16). Summing up (12.16), (12.15) and (12.14), we obtain

$$
\begin{aligned}
&\left[\widehat{\widetilde{\mathbf{m}}}^{\alpha} + \left({}_{(0)}h + {}_{(1)}h\right)\left({}_{(1)}\boldsymbol{n}^{\alpha} - {}_{(-1)}\boldsymbol{n}^{\alpha}\right)\right]_{,\alpha} - \hat{\boldsymbol{\ell}} + \widehat{\widetilde{\mathbf{m}}}^{*} \\
&\qquad = \widehat{A}^{1}_{\rho}\,\ddot{\boldsymbol{u}} + \sum_{\ell=-1}^{1} {}_{(\ell)}A^{2}_{\rho}\ {}_{(\ell)}\ddot{\boldsymbol{t}} + {}_{(0)}h\ {}_{(1)}A^{1}_{\rho}\left(2\,{}_{(0)}\ddot{\boldsymbol{t}} - {}_{(1)}\ddot{\boldsymbol{t}} - {}_{(-1)}\ddot{\boldsymbol{t}}\right) \\
&\qquad = \sum_{\ell=-1}^{1} {}_{(\ell)}A^{2}_{\rho}\ {}_{(\ell)}\ddot{\boldsymbol{t}} + {}_{(0)}h\ {}_{(1)}A^{1}_{\rho}\left(2\,{}_{(0)}\ddot{\boldsymbol{t}} - {}_{(1)}\ddot{\boldsymbol{t}} - {}_{(-1)}\ddot{\boldsymbol{t}}\right). \qquad (12.17)
\end{aligned}
$$

Subtracting (12.14) from (12.16), we obtain

$$
\left[\left({}_{(1)}\widetilde{\boldsymbol{m}}^{\alpha} - {}_{(-1)}\widetilde{\boldsymbol{m}}^{\alpha}\right) + {}_{(1)}h\left({}_{(1)}\boldsymbol{n}^{\alpha} + {}_{(-1)}\boldsymbol{n}^{\alpha}\right)\right]_{,\alpha}
$$

$$
\begin{aligned}
&-\left({}_{(1)}\boldsymbol{\ell} - {}_{(-1)}\boldsymbol{\ell}\right) + \left({}_{(1)}\widetilde{\boldsymbol{m}}^{*} - {}_{(-1)}\widetilde{\boldsymbol{m}}^{*}\right) \\
&= 2\left(-\,{}_{(0)}h\;{}_{(1)}A_{\rho}^{0} + {}_{(1)}A_{\rho}^{1}\right)\ddot{\boldsymbol{u}} \\
&+ \left[{}_{(1)}A_{\rho}^{2} - 2\,{}_{(0)}h\;{}_{(1)}A_{\rho}^{1} + \left({}_{(0)}h\right)^{2}\,{}_{(1)}A_{\rho}^{0}\right]\left({}_{(1)}\ddot{\boldsymbol{t}} - {}_{(-1)}\ddot{\boldsymbol{t}}\right)
\end{aligned}
\tag{12.18}
$$

The force boundary conditions for (12.17) and (12.18) are obtained from (12.7) and (12.8), by using the symmetric condition (12.11), as follows

$$
\widehat{\widetilde{\mathbf{m}}}^{\alpha} + \left({}_{(0)}h + {}_{(1)}h\right)\left({}_{(1)}\boldsymbol{n}^{\alpha} - {}_{(-1)}\boldsymbol{n}^{\alpha}\right) = \widehat{\widetilde{\mathbf{m}}}^{*}\,, \tag{12.19}
$$

$$
\left({}_{(1)}\widetilde{\boldsymbol{m}}^{\alpha} - {}_{(-1)}\widetilde{\boldsymbol{m}}^{\alpha}\right) + {}_{(1)}h\left({}_{(1)}\boldsymbol{n}^{\alpha} + {}_{(-1)}\boldsymbol{n}^{\alpha}\right) = {}_{(1)}\widetilde{\boldsymbol{m}}^{*} - {}_{(-1)}\widetilde{\boldsymbol{m}}^{*}\,. \tag{12.20}
$$

12.3. Classical Results for Symmetric Sandwich Plates

The equations of motion obtained in the previous section reduce exactly to the classical results for sandwich plate obtained in Yu [1959*a*], provided we make the following assumptions as in Yu [1959*a*]: (i) Only small deformation is considered (this assumption only affects the inertia part of the equations of motion); (ii) the sandwich plate is symmetric with respect to the neutral surface, i.e., (12.11) and (12.12) hold true; (iii) the two outer layers have the same rotation, i.e., ${}_{(-1)}\boldsymbol{t} = {}_{(1)}\boldsymbol{t}$.

A consequence of the assumption (i) above is that ${}_{(\ell)}j_t \approx 1$. From (11.8), and (11.13) we obtain the total resultant stress $\widehat{\mathbf{n}}^{\alpha}$ as

$$
\widehat{\mathbf{n}}^{\alpha} := \sum_{\ell=-1}^{1}\int_{{}_{(\ell)}\mathcal{H}} {}_{(\ell)}\mathbf{g}^{\alpha}\cdot{}_{(\ell)}\boldsymbol{\sigma}\,d\xi^{3}\,. \tag{12.21}
$$

The resultant couple ${}_{(\ell)}\widetilde{\boldsymbol{m}}^{\alpha}$ and the director couple ${}_{(\ell)}\boldsymbol{\ell}$ can be simplified by substituting ${}_{(\ell)}j_t \approx 1$ into (11.9) and (11.10) to yield

$$
{}_{(1)}\widetilde{\boldsymbol{m}}^{\alpha} := \int_{{}_{(1)}\mathcal{H}} \left(\xi^{3} - {}_{(1)}Z\right){}_{(1)}\mathbf{g}^{\alpha}\cdot{}_{(1)}\boldsymbol{\sigma}\,d\xi^{3}\,,
$$

$$
\begin{aligned}
{}_{(0)}\widetilde{\boldsymbol{m}}^{\alpha} &:= \int_{{}_{(0)}\mathcal{H}} \xi^3 \, {}_{(0)}\mathbf{g}^{\alpha} \bullet {}_{(0)}\boldsymbol{\sigma} \, d\xi^3 , \qquad (12.22) \\
{}_{(-1)}\widetilde{\boldsymbol{m}}^{\alpha} &:= \int_{{}_{(-1)}\mathcal{H}} \left(\xi^3 + {}_{(-1)}Z \right) {}_{(-1)}\mathbf{g}^{\alpha} \bullet {}_{(-1)}\boldsymbol{\sigma} \, d\xi^3 ,
\end{aligned}
$$

$$
{}_{(\ell)}\boldsymbol{\ell} := \int_{{}_{(\ell)}\mathcal{H}} {}_{(\ell)}\mathbf{g}^3 \bullet {}_{(\ell)}\boldsymbol{\sigma} \, d\xi^3 , \qquad \text{for } \ell = -1, 0, 1. \qquad (12.23)
$$

The consequences of the assumptions (ii) and (iii) above are

$$
{}_{(1)}\widetilde{\boldsymbol{m}}^{\alpha} = {}_{(-1)}\widetilde{\boldsymbol{m}}^{\alpha} \quad \text{and} \quad {}_{(1)}\boldsymbol{n}^{\alpha} = - {}_{(-1)}\boldsymbol{n}^{\alpha} . \qquad (12.24)
$$

The consequences of the assumptions (ii) and (iii) above also are (12.12) and

$$
{}_{(1)}\ddot{\boldsymbol{t}} = {}_{(-1)}\ddot{\boldsymbol{t}} . \qquad (12.25)
$$

Using (12.12) and (12.25), the balance of linear momentum equations (12.13) becomes

$$
\widehat{\boldsymbol{n}}^{\alpha}{}_{,\alpha} + \boldsymbol{n}^{*} = \widehat{A}^{0}_{\rho} \, \ddot{\boldsymbol{u}} . \qquad (12.26)
$$

The balance of total angular momentum equations (12.17) becomes

$$
\begin{aligned}
&\left[\widehat{\widetilde{\mathbf{m}}}^{\alpha} + \left({}_{(0)}h + {}_{(1)}h \right) \left({}_{(1)}\boldsymbol{n}^{\alpha} - {}_{(-1)}\boldsymbol{n}^{\alpha} \right) \right]_{,\alpha} - \widehat{\boldsymbol{\ell}} + \widehat{\widetilde{\mathbf{m}}}^{*} \\
&\qquad = \sum_{\ell=-1}^{1} {}_{(\ell)}A^{2}_{\rho} \, {}_{(\ell)}\ddot{\boldsymbol{t}} + 2 \, {}_{(0)}h \, {}_{(1)}A^{1}_{\rho} \left({}_{(0)}\ddot{\boldsymbol{t}} - {}_{(1)}\ddot{\boldsymbol{t}} \right) . \qquad (12.27)
\end{aligned}
$$

The balance of angular momentum equations (12.15) becomes

$$
\begin{aligned}
&\left({}_{(0)}\widetilde{\boldsymbol{m}}^{\alpha} + {}_{(0)}h \, {}_{(1)}\boldsymbol{n}^{\alpha} - {}_{(0)}h \, {}_{(-1)}\boldsymbol{n}^{\alpha} \right)_{,\alpha} - {}_{(0)}\boldsymbol{\ell} + {}_{(0)}\widetilde{\boldsymbol{m}}^{*} \\
&\qquad = 2 \, {}_{(0)}h \, {}_{(1)}A^{1}_{\rho} \, {}_{(1)}\ddot{\boldsymbol{t}} + {}_{(0)}A^{2}_{\rho} \, {}_{(0)}\ddot{\boldsymbol{t}} + 2 \left({}_{(0)}h \right)^{2} {}_{(1)}A^{0}_{\rho} \left({}_{(0)}\ddot{\boldsymbol{t}} - {}_{(1)}\ddot{\boldsymbol{t}} \right) (12.28)
\end{aligned}
$$

Due to (12.24), the balance of angular momentum equations (12.18) vanishes identically. Thus the 3 nonlinear equations governing the motion of the symmetric sandwich plate with identical outer layer rotations are (12.26)–(12.28).

The force boundary conditions corresponding to (12.26)–(12.28) are obtained from $(11.53)_1$, (12.7) and $(11.53)_3$, respectively

$$\hat{\boldsymbol{n}}^{\alpha} = \boldsymbol{n}^{*\alpha}, \tag{12.29}$$

$$\widehat{\widetilde{\mathbf{m}}}^{\alpha} + \left({}_{(0)}h + {}_{(1)}h \right) \left({}_{(1)}\boldsymbol{n}^{\alpha} - {}_{(-1)}\boldsymbol{n}^{\alpha} \right) = \widehat{\widetilde{\mathbf{m}}}^{*}, \tag{12.30}$$

$${}_{(0)}\widetilde{\boldsymbol{m}}^{\alpha} + {}_{(0)}h\ {}_{(1)}\boldsymbol{n}^{\alpha} - {}_{(0)}h\ {}_{(-1)}\boldsymbol{n}^{\alpha} = \widetilde{\boldsymbol{m}}^{*\alpha}. \tag{12.31}$$

Now, decompose the displacement $\boldsymbol{u}$ and the director ${}_{(\ell)}\boldsymbol{t}$ in the material Cartesian coordinate as follows

$$\boldsymbol{u} := u\,\mathbf{E}^1 + v\,\mathbf{E}^2 + w\,\mathbf{E}^3, \tag{12.32}$$

$${}_{(\ell)}\boldsymbol{t} := {}_{(\ell)}\psi\,\mathbf{E}^1 + {}_{(\ell)}\varphi\,\mathbf{E}^2 + \left({}_{(\ell)}\beta + 1 \right) \mathbf{E}^3, \tag{12.33}$$

where $\{ \mathbf{E}^i \}$ is the Cartesian basis in the reference configuration. From (12.32) and (12.33), we obtain the second time rate of the displacement $\boldsymbol{u}$ and the director ${}_{(\ell)}\boldsymbol{t}$ as follows

$$\ddot{\boldsymbol{u}} := \ddot{u}\ \mathbf{E}^1 + \ddot{v}\ \mathbf{E}^2 + \ddot{w}\ \mathbf{E}^3, \tag{12.34}$$

$${}_{(\ell)}\ddot{\boldsymbol{t}} := {}_{(\ell)}\ddot{\psi}\ \mathbf{E}^1 + {}_{(\ell)}\ddot{\varphi}\ \mathbf{E}^2 + {}_{(\ell)}\ddot{\beta}\ \mathbf{E}^3. \tag{12.35}$$

Using (12.34) and (12.35), we can easily verify that the component form of the equations of motion (12.26)–(12.28) are the same as equation (9) in Yu [1959*a*]. To simplify the presentation, we now just compare some component equations here.

Shown in Figure 12.1 is the configuration of a symmetric sandwich plate and its corresponding geometric quantities written in the convention as in Yu [1959*a*]. For such sandwich plate, the material properties in the present paper and the corresponding notations used in Yu [1959*a*] are given below

$${}_{(1)}\rho = {}_{(-1)}\rho \rightarrow \rho_2, \quad {}_{(1)}A^1_{\rho} = -\,{}_{(-1)}A^1_{\rho} \rightarrow \frac{1}{2}\rho_2 \left(h^2 - h_1^2 \right),$$

$${}_{(0)}A^1_{\rho} = 0, \quad {}_{(0)}A^0_{\rho} \rightarrow 2\,\rho_1\ h_1, \quad {}_{(1)}A^0_{\rho} = {}_{(-1)}A^0_{\rho} \rightarrow \rho_2\ h_2, \quad {}_{(0)}A^2_{\rho} \rightarrow \frac{2}{3}\rho_1\ h_1^3, \tag{12.36}$$

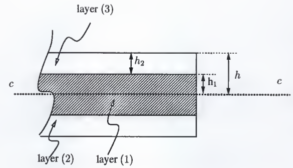

Figure 12.1. *Symmetric Sandwich shell in Y. Y. Yu's convention:* Profile and geometric quantities.

where the arrow "→" is used to designate the correspondence between our notations and Yu's notations, and ρ_1 and ρ_2 designate the mass density of the core layer and outer layers respectively.

We now want to compare the first equation in (12.26), (12.27) and (12.28) with $(9)_1$, $(9)_4$ and $(9)_7$ in Yu [1959*a*], respectively. To this end, we list the equations $(9)_1$, $(9)_4$ and $(9)_7$ in Yu [1959*a*] below.

$$\frac{\partial N_x}{\partial x} + \frac{\partial N_{xy}}{\partial y} + [(\tau_{zx3})|_h - (\tau_{zx2})|_{-h}] = 2(\rho_1 h_1 + \rho_2 h_2)\, \ddot{u} \,, \tag{12.37}$$

$$\begin{aligned} &\underbrace{\frac{\partial}{\partial x}\left[M_x + \left(h_1 + \frac{h_2}{2}\right)(N_{x3} - N_{x2})\right] + \frac{\partial}{\partial y}\left[M_{xy} + \left(h_1 + \frac{h_2}{2}\right)(N_{xy3} - N_{xy2})\right]}_{[1]} \\ &\qquad - Q_x + \underbrace{h\,[(\tau_{zx3})|_h - (\tau_{zx2})|_{-h}]}_{[2]} \\ &\qquad = \underbrace{\rho_1 \frac{2h_1^3}{3} \ddot{\psi}_1 + \rho_2 h_1 \left(h^2 - h_1^2\right)\left(\ddot{\psi}_1 - \ddot{\psi}_2\right) + \rho_2 \frac{2}{3}\left(h^3 - h_1^3\right) \ddot{\psi}_2}_{[3]}, \end{aligned} \tag{12.38}$$

$$\frac{\partial}{\partial x}\left[M_{x1} + h_1\,(N_{x3} - N_{x2})\right] + \frac{\partial}{\partial y}\left[M_{xy1} + h_1\,(N_{xy3} - N_{xy2})\right]$$
$$- Q_{x1} + h_1\left[(\tau_{zx3})\,|_h - (\tau_{zx2})\,|_{-h}\right]$$
$$= \rho_1 \frac{2\,h_1^3}{3}\,\ddot{\psi}_1 + 2\,\rho_2\,h_1^2\,h_2\left(\ddot{\psi}_1 - \ddot{\psi}_2\right) + \rho_2\,h_1\left(h^2 - h_1^2\right)\ddot{\psi}_2 . \tag{12.39}$$

In the above equations, $\ddot{u}$ designates the displacement in *x*-direction of the neutral surface of the shell, and ψ_1 and ψ_2 the rotations about the *x*-axis of the core layer and of the outer layers, respectively. The membrane stress resultants, stress couples and shear stress resultants are defined in the following equations

$$(N_x\,,\,N_{xy}) = \int (\sigma_x\,,\,\tau_{xy})\,dz,\quad (M_x\,,\,M_{xy}) = \int (\sigma_x\,,\,\tau_{xy})\,dz,\quad Q_x = \int (\tau_{zx})\,dz \tag{12.40}$$

where σ_x, τ_{xy}, and τ_{zx} are the components of the Cauchy stress tensor. For the stress resultants and stress couples, the number in the subscript is the layer index, with 1, 2, 3 designate core layer, lower layer and upper layer, respectively. The notation $|_h$ or $|_{-h}$ means that the variable is evaluated at $z = h$ or $z = -h$.

First, let us compare the first component of (12.26) with (12.37), i.e., $(9)_1$ in Yu [1959*a*]. The first component in (12.26) can be written as

$$\widehat{n}^{11}{}_{,1} + \widehat{n}^{12}{}_{,2} + n^{*1} = \widehat{A}^0_\rho\,\ddot{u}^1\,, \tag{12.41}$$

where the term $\widehat{n}^{11}{}_{,1} + \widehat{n}^{12}{}_{,2}$ corresponds to $\dfrac{\partial N_x}{\partial x} + \dfrac{\partial N_{xy}}{\partial y}$ in Yu [1959*a*], whereas the assigned force n^{*1} corresponds to $(\tau_{zx3})|_h - (\tau_{zx2})|_{-h}$ in Yu [1959*a*]. Using (12.36), the inertia force in (12.26) can be written as

$$\widehat{A}^0_\rho\,\ddot{\mathbf{u}} \to 2\,(\rho_1\,h_1 + \rho_2\,h_2)\,\ddot{\mathbf{u}}\,. \tag{12.42}$$

Thus, the first component in (12.26) is exactly the same as (12.37), or $(9)_1$ in Yu [1959*a*].

Second, we compare the equation of total balance of angular moment (12.27) with (12.38)($(9)_4$ in Yu [1959*a*]). Note that

$$_{(0)}\widetilde{\boldsymbol{m}}^\alpha \to \mathbf{M}_{\alpha 1}\,,\quad {}_{(0)}h^+ \to h_1\,,\quad {}_{(0)}h^- = {}_{(1)}h^+ \to \frac{h_2}{2}. \tag{12.43}$$

The first square bracket in (12.27) is the same as part [1] of (12.38). Also, notice that $\widehat{\ell}$ has the same meaning as Q_x, whereas the boundary term $\widehat{\widehat{\mathrm{m}}}^*$ is the same as part [2] of (12.38). Finally, by using assumption (iii), (12.35) and (12.36), the inertia force in (12.27) (left hand term) can reduce to part [3] of (12.38). Thus, the first component of (12.27) is identical to (12.38) i.e., $(9)_4$ in Yu [1959*a*].

Using the same procedure, we can easily show that the first component of the balance of angular momentum (12.28) reduces to (12.39), i.e., $(9)_7$ in Yu [1959*a*]. The other components can also be verified in the same way.

CHAPTER 13
STRAIN MEASURES AND CONSTITUTIVE LAWS

In this Section, we derive the elastic constitutive equations in terms of the stress resultants and conjugate strain measures. To this end, we first introduce the layer effective stress resultants (resultant force ${}_{(\ell)}\tilde{n}^{\beta\alpha}$, and ${}_{(\ell)}\tilde{q}^{\alpha}$, and resultant couple ${}_{(\ell)}\widetilde{m}^{\beta\alpha}$), and then derive their conjugate strain measures. The constitutive laws related to these quantities will be postulated. The reader is referred to Simo and Fox [1989] for further detail on the single layer case.

13.1. Constitutive Restriction

In Section 11, we define the resultant force ${}_{(\ell)}\boldsymbol{n}^{\alpha}$ in (11.8), the resultant couple ${}_{(\ell)}\widetilde{\boldsymbol{m}}^{\alpha}$ in (11.9) and the resultant director couple ${}_{(\ell)}\boldsymbol{\ell}$ in (11.10). These quantities are not independent, but are related to each other by a relation, called the constitutive restriction, arise from the local balance of angular momentum in the three-dimensional continuum, which in turn give rise to the symmetry of the Cauchy stress tensor. One can think of this constitutive restriction as the resultant form of the symmetry of the Cauchy stress tensor.

The local balance of angular momentum is written as

$$ {}_{(\ell)}\boldsymbol{\sigma} = {}_{(\ell)}\boldsymbol{\sigma}^{t}, \quad \text{or} \quad \left({}_{(\ell)}\boldsymbol{g}^{I} \cdot {}_{(\ell)}\boldsymbol{\sigma} \right) \times {}_{(\ell)}\boldsymbol{g}_{I} = 0. \tag{13.1} $$

Multiply $(13.1)_2$ with ${}_{(\ell)}j_t$, integrate the result over the layer thickness ${}_{(\ell)}\mathcal{H}$, and make use of (10.21), we obtain

$$ \int\limits_{{}_{(1)}\mathcal{H}} \left\{ \left({}_{(1)}\boldsymbol{g}^{\alpha} \cdot {}_{(1)}\boldsymbol{\sigma} \right) \times \left[{}_{(1)}\boldsymbol{\varphi}_{,\alpha} + \left(\xi^{3} - {}_{(1)}Z \right) {}_{(1)}\boldsymbol{t}_{,\alpha} \right] + \left({}_{(1)}\boldsymbol{g}^{3} \cdot {}_{(1)}\boldsymbol{\sigma} \right) \times {}_{(1)}\boldsymbol{t} \right\} {}_{(1)}j_t \, d\xi^{3} = 0, $$

$$ \int\limits_{{}_{(0)}\mathcal{H}} \left\{ \left({}_{(0)}\boldsymbol{g}^{\alpha} \cdot {}_{(0)}\boldsymbol{\sigma} \right) \times \left[{}_{(0)}\boldsymbol{\varphi}_{,\alpha} + \xi^{3} \, {}_{(0)}\boldsymbol{t}_{,\alpha} \right] + \left({}_{(0)}\boldsymbol{g}^{3} \cdot {}_{(0)}\boldsymbol{\sigma} \right) \times {}_{(0)}\boldsymbol{t} \right\} {}_{(0)}j_t \, d\xi^{3} = 0, \tag{13.2} $$

$$\int\limits_{{}_{(-1)}\mathcal{H}} \left\{ \left({}_{(-1)}\boldsymbol{g}^{\alpha} \cdot {}_{(-1)}\boldsymbol{\sigma} \right) \times \left[{}_{(-1)}\boldsymbol{\varphi}_{,\alpha} + \left(\xi^{3} + {}_{(-1)}Z \right) {}_{(-1)}\boldsymbol{t}_{,\alpha} \right] + \left({}_{(-1)}\boldsymbol{g}^{3} \cdot {}_{(-1)}\boldsymbol{\sigma} \right) \times {}_{(-1)}\boldsymbol{t} \right\} {}_{(-1)}j_{t}\, d\xi^{3} = 0.$$

Substitute in (13.2) the definition of the resultant force ${}_{(\ell)}\boldsymbol{n}^{\alpha}$ in (11.8), the resultant couple ${}_{(\ell)}\widetilde{\boldsymbol{m}}^{\alpha}$ in (11.9), and the director couple ${}_{(\ell)}\boldsymbol{\ell}$ in (11.10), we obtain the following relation linking these stress resultants:

$${}_{(\ell)}\boldsymbol{n}^{\alpha} \times {}_{(\ell)}\boldsymbol{\varphi}_{,\alpha} + {}_{(\ell)}\widetilde{\boldsymbol{m}}^{\alpha} \times {}_{(\ell)}\boldsymbol{t}_{,\alpha} + {}_{(\ell)}\boldsymbol{\ell} \times {}_{(\ell)}\boldsymbol{t} = 0, \tag{13.3}$$

which represents the restriction placed on the admissible form of the constitutive laws by the balance of angular momentum.

13.2. Alternative Form for the Balance of Angular Momentum

Using the constitutive restriction (13.3), the equations of motion for the balance of angular momentum $(11.52)_2$–$(11.52)_4$ can be recast in an alternative form. Define

$${}_{(\ell)}\boldsymbol{m}^{\alpha} = {}_{(\ell)}\boldsymbol{t} \times {}_{(\ell)}\widetilde{\boldsymbol{m}}^{\alpha}, \quad {}_{(\ell)}\boldsymbol{m}^{*} = {}_{(\ell)}\boldsymbol{t} \times {}_{(\ell)}\widetilde{\boldsymbol{m}}^{*}. \tag{13.4}$$

First by forming the vector product of ${}_{(-1)}\boldsymbol{t}$ and $(11.52)_4$, we obtain

$${}_{(-1)}\boldsymbol{t} \times \left({}_{(-1)}\widetilde{\boldsymbol{m}}^{\alpha} - {}_{(-1)}h^{+}\, {}_{(-1)}\boldsymbol{n}^{\alpha} \right)_{,\alpha} - {}_{(-1)}\boldsymbol{t} \times {}_{(-1)}\boldsymbol{\ell} + {}_{(-1)}\boldsymbol{t} \times {}_{(-1)}\widetilde{\boldsymbol{m}}^{*} = {}_{(-1)}\boldsymbol{t} \times {}_{(-1)}\boldsymbol{C} (13.5)$$

By substituting (13.3) in (13.5) and reorganizing the term in the parenthesis, notice that ${}_{(\ell)}h^{+}$ and ${}_{(\ell)}h^{-}$ are not functions of ξ^{α}, we obtain

$$\left({}_{(-1)}\boldsymbol{t} \times {}_{(-1)}\widetilde{\boldsymbol{m}}^{\alpha} \right)_{,\alpha} - {}_{(-1)}\boldsymbol{t}_{,\alpha} \times {}_{(-1)}\widetilde{\boldsymbol{m}}^{\alpha} - {}_{(-1)}h^{+}\, {}_{(-1)}\boldsymbol{t} \times {}_{(-1)}\boldsymbol{n}^{\alpha}_{,\alpha} + {}_{(-1)}\boldsymbol{\varphi}_{,\alpha} \times {}_{(-1)}\boldsymbol{n}^{\alpha} + {}_{(-1)}\boldsymbol{t}_{,\alpha} \times {}_{(-1)}\widetilde{\boldsymbol{m}}^{\alpha} + {}_{(-1)}\boldsymbol{t} \times {}_{(-1)}\widetilde{\boldsymbol{m}}^{*} = {}_{(-1)}\boldsymbol{t} \times {}_{(-1)}\boldsymbol{C}\,. \tag{13.6}$$

Using (13.4), (13.6) can be rewritten as

$$ {}_{(-1)}\boldsymbol{m}^{\alpha}_{,\alpha} - {}_{(-1)}h^{+}\ {}_{(-1)}\boldsymbol{t} \times {}_{(-1)}\boldsymbol{n}^{\alpha}_{,\alpha} + {}_{(-1)}\boldsymbol{\varphi}_{,\alpha} \times {}_{(-1)}\boldsymbol{n}^{\alpha} + {}_{(-1)}\boldsymbol{m}^{*} = {}_{(-1)}\boldsymbol{t} \times {}_{(-1)}\boldsymbol{C}\,. \quad (13.7) $$

Similarly, we obtain from $(11.52)_3$ and $(11.52)_2$ the following alternative equations of motion for angular momentum

$$ {}_{(0)}\boldsymbol{m}^{\alpha}_{,\alpha} + {}_{(0)}h^{+}\ {}_{(0)}\boldsymbol{t} \times {}_{(1)}\boldsymbol{n}^{\alpha}_{,\alpha} - {}_{(0)}h^{-}\ {}_{(0)}\boldsymbol{t} \times {}_{(-1)}\boldsymbol{n}^{\alpha}_{,\alpha} + {}_{(0)}\boldsymbol{\varphi}_{,\alpha} \times {}_{(0)}\boldsymbol{n}^{\alpha} + {}_{(0)}\boldsymbol{m}^{*} $$

$$ = {}_{(0)}\boldsymbol{t} \times {}_{(0)}\boldsymbol{C}\,. \quad (13.8) $$

$$ {}_{(1)}\boldsymbol{m}^{\alpha}_{,\alpha} + \underbrace{{}_{(1)}h^{-}\ {}_{(1)}\boldsymbol{t} \times {}_{(1)}\boldsymbol{n}^{\alpha}_{,\alpha} + {}_{(1)}\boldsymbol{\varphi}_{,\alpha} \times {}_{(1)}\boldsymbol{n}^{\alpha}} + {}_{(1)}\boldsymbol{m}^{*} = {}_{(1)}\boldsymbol{t} \times {}_{(1)}\boldsymbol{C}\,. \quad (13.9) $$

Remark 13.1. We now proceed to prove that (13.7)–(13.9) can be reduced to (3.37)–(3.39) in Vu-Quoc and Ebcioğlu [1995] for the two-dimensional geometrically-exact sandwich beams. To simplify the verification, we only consider (13.9) for the top layer (1), which corresponds to (3.39) in Vu-Quoc and Ebcioğlu [1995], as an example. To lead the readers through this verification, we recall that (3.39) in Vu-Quoc and Ebcioğlu [1995] reads as follows

$$ {}_{(1)}m_{,S} + \underbrace{\left[{}_{(0)}\boldsymbol{\Phi}_{0,S} \times {}_{(1)}\mathbf{n}\right] \boldsymbol{\cdot} \mathbf{e}_3 - {}_{(0)}h\ {}_{(0)}\theta_{,S}\left({}_{(1)}\mathbf{n} \boldsymbol{\cdot}\ {}_{(0)}\mathbf{t}_2\right)} $$

$$ \underbrace{-\ {}_{(1)}h\left({}_{(1)}\mathbf{n} \boldsymbol{\cdot}\ {}_{(1)}\mathbf{t}_1\right)_{,S}} + {}_{(1)}\bar{\boldsymbol{m}} = {}_{(1)}C, \quad (13.10) $$

where the layer indices have been changed to be consistent with this paper (see Remark 10.1). In (13.10), ${}_{(1)}m_{,S}$, ${}_{(1)}\mathbf{n}$, ${}_{(1)}\bar{\boldsymbol{m}}$ and ${}_{(1)}C$ are respectively the resultant contact couple, the resultant contact force, the resultant assigned couple and the inertia couple associated with layer (1), whereas ${}_{(0)}\boldsymbol{\Phi}_0$, ${}_{(0)}\theta$, ${}_{(\ell)}h$ and ${}_{(\ell)}\mathbf{t}_\alpha$ are respectively the deformation map of the centroidal line of the core layer, the rotation of the centroidal line of the core layer, the half-layer thickness of layer (ℓ), and the basis vector attached to the layer cross-section. The subscript $_{,S}$ denotes the derivative with respect to the spatial coordinate S along the beam axis. By making the projection of (13.9) on the spatial Cartesian basis vector $\boldsymbol{e}_3$, it is easy to verify that the quantities ${}_{(1)}\boldsymbol{m}^{\alpha}_{,\alpha}$, ${}_{(1)}\boldsymbol{m}^{*}$ and ${}_{(1)}\boldsymbol{t} \times {}_{(1)}\boldsymbol{C}$ for shells in (13.9) (i.e., the non-underbraced terms) correspond to the quantities ${}_{(1)}m_{,S}$, ${}_{(1)}\bar{\boldsymbol{n}}$ and ${}_{(1)}C$ for beams in (13.10), respectively. Using (10.9)—i.e., the relation between the deformation map of the neutral surface of layer (1) and that of the core layer (0)—the underbraced terms in (13.9) can be reorganized as follows

$$\begin{aligned} &{}_{(1)}h^{-}\ {}_{(1)}\boldsymbol{t} \times {}_{(1)}\boldsymbol{n}^{\alpha}_{,\alpha} + {}_{(1)}\boldsymbol{\varphi}_{,\alpha} \times {}_{(1)}\boldsymbol{n}^{\alpha} \\ &\qquad = {}_{(0)}\boldsymbol{\varphi}_{,\alpha} \times {}_{(1)}\boldsymbol{n}^{\alpha}_{,\alpha} + {}_{(0)}h^{+}\ {}_{(0)}\boldsymbol{t}_{,\alpha} \times {}_{(1)}\boldsymbol{n}^{\alpha}_{,\alpha} + {}_{(1)}h^{-} \left({}_{(1)}\boldsymbol{t} \times {}_{(1)}\boldsymbol{n}^{\alpha} \right)_{,\alpha} \end{aligned} \tag{13.11}$$

Notice that the director ${}_{(0)}\boldsymbol{t}$ in shell theory corresponds to the basis vector ${}_{(0)}\boldsymbol{t}_2$ in beam theory, and that in the plane beams we have ${}_{(0)}\boldsymbol{t}_{2,S} = -\, {}_{(0)}\theta_{,S}\ {}_{(0)}\mathbf{t}_1$ and ${}_{(0)}\mathbf{t}_1 \times {}_{(0)}\mathbf{t}_2 = \boldsymbol{e}_3$. Thus, by forming the projection of (13.11) on $\boldsymbol{e}_3$, the right-hand-side terms in (13.11) reduce to the underbraced terms in (13.10).

We thus proved that (13.9) can be reduced to (3.39) in Vu-Quoc and Ebcioğlu [1995]. Similarly, we can prove that the angular momentum equations (13.7)–(13.8) for sandwich shells can be reduced to the angular momentum equations (3.37)–(3.38) for sandwich beams in Vu-Quoc and Ebcioğlu [1995]. The computational formulation for the equations of motion in Vu-Quoc and Ebcioğlu [1995] and several numerical simulations are discussed in Vu-Quoc and Deng [1995*b*] and Vu-Quoc and Deng [1995*a*]. ∎

13.3. Effective Stress Resultants

To obtain properly the invariant elastic constitutive laws for geometrically-exact sandwich shell, we make use of the definition of the effective stress resultants ${}_{(\ell)}\tilde{\boldsymbol{n}}^{\beta\alpha}$ and ${}_{(\ell)}\tilde{\boldsymbol{q}}^{\alpha}$ (see Simo and Fox [1989]). To this end, we must make use of the inextensibility of the director, i.e., ${}_{(\ell)}\boldsymbol{t} \in S^2$.

First, we decompose the spatial derivative ${}_{(\ell)}\boldsymbol{t}_{,\alpha}$ of the director ${}_{(\ell)}\boldsymbol{t}$ along the neutral surface convected basis $\left\{ {}_{(\ell)}\boldsymbol{\varphi}_{,\alpha} \, , \, {}_{(\ell)}\boldsymbol{t} \right\}$ as

$$ {}_{(\ell)}\boldsymbol{t}_{,\alpha} \, = \, {}_{(\ell)}\lambda^{\mu}_{.\alpha} \; {}_{(\ell)}\boldsymbol{\varphi}_{,\mu} \, + \, {}_{(\ell)}\lambda^{3}_{.\alpha} \; {}_{(\ell)}\boldsymbol{t} \, . \tag{13.12} $$

Using the constraint ${}_{(\ell)}\boldsymbol{t} \in S^2$, or equivalently ${}_{(\ell)}\boldsymbol{t} \cdot {}_{(\ell)}\boldsymbol{t} \, = 1$, we obtain

$$ {}_{(\ell)}\boldsymbol{t}_{,\alpha} \cdot {}_{(\ell)}\boldsymbol{t} = 0, \quad {}_{(\ell)}\dot{\boldsymbol{t}} \cdot {}_{(\ell)}\boldsymbol{t} = 0, \quad {}_{(\ell)}\boldsymbol{t} \cdot {}_{(\ell)}\dot{\boldsymbol{t}}_{,\alpha} = - \, {}_{(\ell)}\boldsymbol{t}_{,\alpha} \cdot {}_{(\ell)}\dot{\boldsymbol{t}} \, , \quad \text{for } \ell = 1, 2, 3. \tag{13.13} $$

Using $(13.13)_1$, we obtain from (13.12) the expression for ${}_{(\ell)}\lambda^{3}_{.\alpha}$ as

$$ {}_{(\ell)}\lambda^{3}_{.\alpha} \, = - \, {}_{(\ell)}\lambda^{\mu}_{.\alpha} \; {}_{(\ell)}\boldsymbol{\varphi}_{,\mu} \cdot {}_{(\ell)}\boldsymbol{t} \, . \tag{13.14} $$

We now resolve the stress resultants ${}_{(\ell)}\boldsymbol{n}^{\alpha}$ and ${}_{(\ell)}\widetilde{\boldsymbol{m}}^{\alpha}$ along the neutral surface convected basis $\left\{ {}_{(\ell)}\boldsymbol{\varphi}_{,\alpha} \, , \, {}_{(\ell)}\boldsymbol{t} \right\}$ as

$$ {}_{(\ell)}\boldsymbol{n}^{\alpha} \, = \, {}_{(\ell)}n^{\alpha\beta} \; {}_{(\ell)}\boldsymbol{\varphi}_{,\beta} \, + \, {}_{(\ell)}q^{\alpha} \; {}_{(\ell)}\boldsymbol{t} \, , \tag{13.15} $$

$$ {}_{(\ell)}\widetilde{\boldsymbol{m}}^{\alpha} \, = \, {}_{(\ell)}\widetilde{m}^{\alpha\beta} \; {}_{(\ell)}\boldsymbol{\varphi}_{,\beta} \, + \, {}_{(\ell)}\widetilde{m}^{\alpha 3} \; {}_{(\ell)}\boldsymbol{t} \, . \tag{13.16} $$

Substitute (13.15) and (13.16) into the constitutive restriction (13.3) we obtain

$$ \begin{aligned} & \left({}_{(\ell)}n^{\alpha\beta} \; {}_{(\ell)}\boldsymbol{\varphi}_{,\beta} \right) \times \, {}_{(\ell)}\boldsymbol{\varphi}_{,\alpha} + \left({}_{(\ell)}q^{\alpha} \; {}_{(\ell)}\boldsymbol{t} \right) \times \, {}_{(\ell)}\boldsymbol{\varphi}_{,\alpha} \\ & + \left({}_{(\ell)}\widetilde{m}^{\alpha\beta} \; {}_{(\ell)}\boldsymbol{\varphi}_{,\beta} \, + \, {}_{(\ell)}\widetilde{m}^{\alpha 3} \; {}_{(\ell)}\boldsymbol{t} \right) \times \, {}_{(\ell)}\boldsymbol{t}_{,\alpha} \, + \, {}_{(\ell)}\boldsymbol{\ell} \, \times \, {}_{(\ell)}\boldsymbol{t} \, = 0. \end{aligned} \tag{13.17} $$

The projection of (13.17) on ${}_{(\ell)}\boldsymbol{t}$ yields

$$ \left[\left({}_{(\ell)}n^{\alpha\beta} \; {}_{(\ell)}\boldsymbol{\varphi}_{,\beta} \right) \times \, {}_{(\ell)}\boldsymbol{\varphi}_{,\alpha} \right] \cdot {}_{(\ell)}\boldsymbol{t} \, + \left[\left({}_{(\ell)}\widetilde{m}^{\alpha\beta} \; {}_{(\ell)}\boldsymbol{\varphi}_{,\beta} \right) \times \, {}_{(\ell)}\boldsymbol{t}_{,\alpha} \right] \cdot {}_{(\ell)}\boldsymbol{t} \, = 0, \tag{13.18} $$

which, via the use of (13.12), leads to

$$ \left({}_{(\ell)}n^{\alpha\beta} \, + \, {}_{(\ell)}\lambda^{\alpha}_{.\mu} \; {}_{(\ell)}\widetilde{m}^{\mu\beta} \right) \left({}_{(\ell)}\boldsymbol{\varphi}_{,\beta} \, \times \, {}_{(\ell)}\boldsymbol{\varphi}_{,\alpha} \right) \cdot {}_{(\ell)}\boldsymbol{t} \, = 0. \tag{13.19} $$

Furthermore, by interchanging the dummy summation variables, we obtain another form of (13.19)

$$\left({}_{(\ell)}n^{\alpha\beta} - {}_{(\ell)}\lambda^{\beta}_{\cdot\mu} \, {}_{(\ell)}\widetilde{m}^{\mu\alpha} \right) \left({}_{(\ell)}\boldsymbol{\varphi}_{,\beta} \times {}_{(\ell)}\boldsymbol{\varphi}_{,\alpha} \right) \cdot {}_{(\ell)}\boldsymbol{t} = 0. \tag{13.20}$$

Consequently, from (13.19) or (13.20), we define the effective resultant membrane stress

$${}_{(\ell)}\tilde{n}^{\alpha\beta} := {}_{(\ell)}n^{\alpha\beta} + {}_{(\ell)}\lambda^{\alpha}_{\cdot\mu} \, {}_{(\ell)}\widetilde{m}^{\mu\beta} = {}_{(\ell)}n^{\alpha\beta} - {}_{(\ell)}\lambda^{\beta}_{\cdot\mu} \, {}_{(\ell)}\widetilde{m}^{\mu\alpha} . \tag{13.21}$$

It follows from (13.19) or (13.20) that

$$\begin{aligned} {}_{(\ell)}\tilde{n}^{\alpha\beta} \left({}_{(\ell)}\boldsymbol{\varphi}_{,\beta} \times {}_{(\ell)}\boldsymbol{\varphi}_{,\alpha} \right) \cdot {}_{(\ell)}\boldsymbol{t} &= {}_{(\ell)}\tilde{n}^{12} \left({}_{(\ell)}\boldsymbol{\varphi}_{,1} \times {}_{(\ell)}\boldsymbol{\varphi}_{,2} \right) \cdot {}_{(\ell)}\boldsymbol{t} \\ + {}_{(\ell)}\tilde{n}^{21} \left({}_{(\ell)}\boldsymbol{\varphi}_{,2} \times {}_{(\ell)}\boldsymbol{\varphi}_{,1} \right) \cdot {}_{(\ell)}\boldsymbol{t} &= \left({}_{(\ell)}\tilde{n}^{12} - {}_{(\ell)}\tilde{n}^{21} \right) \left({}_{(\ell)}\boldsymbol{\varphi}_{,1} \times {}_{(\ell)}\boldsymbol{\varphi}_{,2} \right) \cdot {}_{(\ell)}\boldsymbol{t} \end{aligned} \tag{13.22}$$

Since $\left({}_{(\ell)}\boldsymbol{\varphi}_{,\beta} \times {}_{(\ell)}\boldsymbol{\varphi}_{,\alpha} \right) \cdot {}_{(\ell)}\boldsymbol{t} \neq 0$ for $\alpha \neq \beta$, we conclude that the effective membrane force tensor ${}_{(\ell)}\tilde{\boldsymbol{n}} = {}_{(\ell)}\tilde{n}^{\alpha\beta} \, {}_{(\ell)}\boldsymbol{\varphi}_{,\alpha} \otimes {}_{(\ell)}\boldsymbol{\varphi}_{,\beta}$ is symmetric.

Remark 13.2. We give (13.21) two possible expressions for the effective membrane force ${}_{(\ell)}\tilde{n}^{\alpha\beta}$. In Simo and Fox [1989], only expression $(13.21)_2$ was obtained. It should also be noted that the convention for the superscripts of the components of the stress tensors employed here follows consistently the convention used in Malvern [1969]), and differs from the convention used in Simo and Fox [1989]; see the definitions (11.8)–(11.10). ∎

The components of the director couple ${}_{(\ell)}\boldsymbol{\ell}$ with respect to the basis vectors $\left\{ {}_{(\ell)}\boldsymbol{\varphi}_{,\alpha} \; {}_{(\ell)}\boldsymbol{t} \right\}$ can be expressed in terms of the stress resultants as follows. Let

$${}_{(\ell)}\boldsymbol{\ell} = {}_{(\ell)}\mathbf{L}^{\alpha} \, {}_{(\ell)}\boldsymbol{\varphi}_{,\alpha} + {}_{(\ell)}\lambda \, {}_{(\ell)}\boldsymbol{t} . \tag{13.23}$$

Forming the dot product of the constitutive restriction (13.17) with the basis vector ${}_{(\ell)}\boldsymbol{\varphi}_{,\gamma}$ and making use of (13.12), we obtain explicitly the expression for the components ${}_{(\ell)}\mathbf{L}^{\alpha}$ as

$${}_{(\ell)}\mathbf{L}^{\alpha} = {}_{(\ell)}q^{\alpha} - {}_{(\ell)}\lambda^{3}_{\cdot\mu} \, {}_{(\ell)}\widetilde{m}^{\mu\alpha} + {}_{(\ell)}\lambda^{\alpha}_{\cdot\mu} \, {}_{(\ell)}\widetilde{m}^{\mu 3} , \tag{13.24}$$

in terms of the stress resultant, and arrive at the following expression for the director couple ${}_{(\ell)}\boldsymbol{\ell}$

$$ {}_{(\ell)}\boldsymbol{\ell} = \left({}_{(\ell)}q^{\alpha} - {}_{(\ell)}\lambda^{3}_{\cdot\mu} \, {}_{(\ell)}\widetilde{m}^{\mu\alpha} + {}_{(\ell)}\lambda^{\alpha}_{\cdot\mu} \, {}_{(\ell)}\widetilde{m}^{\mu 3} \right) {}_{(\ell)}\boldsymbol{\varphi}_{,\alpha} + {}_{(\ell)}\lambda \, {}_{(\ell)}\boldsymbol{t} \, . \tag{13.25} $$

Let the effective resultant shear force ${}_{(\ell)}\widetilde{q}^{\alpha}$ be defined as follows

$$ {}_{(\ell)}\widetilde{q}^{\alpha} := {}_{(\ell)}q^{\alpha} - {}_{(\ell)}\lambda^{3}_{\cdot\mu} \, {}_{(\ell)}\widetilde{m}^{\alpha\mu} \, , \tag{13.26} $$

then the director couple ${}_{(\ell)}\boldsymbol{\ell}$ in (13.25) is now expressed as

$$ {}_{(\ell)}\boldsymbol{\ell} = {}_{(\ell)}\widetilde{q}^{\alpha} \, {}_{(\ell)}\boldsymbol{\varphi}_{,\alpha} + {}_{(\ell)}\lambda^{\alpha}_{\cdot\mu} \, {}_{(\ell)}\widetilde{m}^{\mu 3} \, {}_{(\ell)}\boldsymbol{\varphi}_{,\alpha} + {}_{(\ell)}\lambda \, {}_{(\ell)}\boldsymbol{t} \, . \tag{13.27} $$

The effective stress resultants are crucial in the development of the constitutive equations for sandwich shells in the following section.

13.4. Reduced Stress Power and Conjugate Strain Measures

The convected basis vector at the spatial neutral surface are denoted by $\left\{ {}_{(\ell)}\boldsymbol{a}_{\underline{i}} \right\}$ and are obtained by evaluating the basis vectors $\left\{ {}_{(\ell)}\boldsymbol{g}_{\underline{i}} \right\}$ at $\xi^3 = 0$, i.e.,

$$ \left\{ {}_{(\ell)}\boldsymbol{a}_{\underline{i}} \right\} := \left\{ {}_{(\ell)}\boldsymbol{a}_1 \, , \; {}_{(\ell)}\boldsymbol{a}_2 \, , \; {}_{(\ell)}\boldsymbol{a}_3 \right\} := \left\{ {}_{(\ell)}\boldsymbol{\varphi}_{,1} \, , \; {}_{(\ell)}\boldsymbol{\varphi}_{,2} \, , \; {}_{(\ell)}\boldsymbol{t} \right\} \Big|_{\xi^3 = 0} \, , \quad \text{for } \ell = -1, 0, 1. \tag{13.28} $$

The basis vectors $\left\{ {}_{(\ell)}\boldsymbol{a}^{\underline{j}} \right\}$, dual to $\left\{ {}_{(\ell)}\boldsymbol{a}_{\underline{i}} \right\}$, are defined by the standard orthogonal relation

$$ < {}_{(\ell)}\boldsymbol{a}_{i} \, , \, {}_{(\ell)}\boldsymbol{a}^{j} >= \delta_{i}^{j} \, , \tag{13.29} $$

where δ_i^j is the Kronecker delta. The convected basis in the reference configuration is given by specifying $t = 0$ in the spatial-neutral-surface convected basis to obtain

$$ \left\{ {}_{(\ell)}\boldsymbol{A}_{\underline{I}} \right\} := \left\{ {}_{(\ell)}\boldsymbol{A}_1 \, , \; {}_{(\ell)}\boldsymbol{A}_2 \, , \; {}_{(\ell)}\boldsymbol{A}_3 \right\} := \left\{ {}_{(\ell)}\boldsymbol{a}_1 \, , \; {}_{(\ell)}\boldsymbol{a}_2 \, , \; {}_{(\ell)}\boldsymbol{a}_3 \right\} \Big|_{t=0} \, , \quad \text{for } \ell = -1, 0, 1. \tag{13.30} $$

The basis $\left\{ {}_{(\ell)}\boldsymbol{A}^{\underline{I}} \right\}$, dual to the reference-neutral-surface convected basis $\left\{ {}_{(\ell)}\boldsymbol{A}_{\underline{I}} \right\}$, is defined similar to (13.29).

The membrane strain ${}_{(\ell)}\boldsymbol{\epsilon}$, the bending strain measure ${}_{(\ell)}\boldsymbol{\rho}$ and the transverse shear strain ${}_{(\ell)}\boldsymbol{\delta}$–which, as we will see later, are conjugate to the resultant membrane stress ${}_{(\ell)}\widetilde{n}^{\beta\alpha}$, the resultant couple ${}_{(\ell)}\widetilde{m}^{\beta\alpha}$ and the transverse shear ${}_{(\ell)}\widetilde{q}^{\alpha}$, respectively–can be defined as follows

$$
\begin{aligned}
{}_{(\ell)}\boldsymbol{\epsilon} &:= {}_{(\ell)}\epsilon_{\alpha\beta}\ {}_{(\ell)}\boldsymbol{a}^{\alpha} \otimes {}_{(\ell)}\boldsymbol{a}^{\beta}, && (13.31) \\
{}_{(\ell)}\boldsymbol{\rho} &:= {}_{(\ell)}\rho_{\alpha\beta}\ {}_{(\ell)}\boldsymbol{a}^{\alpha} \otimes {}_{(\ell)}\boldsymbol{a}^{\beta}, && (13.32) \\
{}_{(\ell)}\boldsymbol{\delta} &:= {}_{(\ell)}\delta_{\alpha}\ {}_{(\ell)}\boldsymbol{a}^{\alpha}. && (13.33)
\end{aligned}
$$

The components of the strain tensor ${}_{(\ell)}\boldsymbol{\epsilon}$ are given by

$$
{}_{(\ell)}\epsilon_{\alpha\beta} = \frac{1}{2}\left({}_{(\ell)}a_{\alpha\beta} - {}_{(\ell)}A_{\alpha\beta} \right), \tag{13.34}
$$

where

$$
{}_{(\ell)}a_{\alpha\beta} := {}_{(\ell)}\boldsymbol{a}_{\alpha} \cdot {}_{(\ell)}\boldsymbol{a}_{\beta}, \quad {}_{(\ell)}A_{\alpha\beta} := {}_{(\ell)}\mathbf{A}_{\alpha} \cdot {}_{(\ell)}\mathbf{A}_{\beta} \tag{13.35}
$$

are the component of the Riemann metric tensors of layer (ℓ), ${}_{(\ell)}a_{\alpha\beta}\ {}_{(\ell)}\boldsymbol{a}^{\alpha} \otimes {}_{(\ell)}\boldsymbol{a}^{\beta}$ and ${}_{(\ell)}A_{\alpha\beta}\ {}_{(\ell)}\boldsymbol{A}^{\alpha} \otimes {}_{(\ell)}\boldsymbol{A}^{\beta}$, in the spatial configuration and in the reference configuration, respectively (see, e.g., Naghdi [1972], Marsden and Hughes [1983]).

The components of the bending strain tensor ${}_{(\ell)}\boldsymbol{\rho}$ is given by

$$
{}_{(\ell)}\rho_{\alpha\beta} = {}_{(\ell)}\kappa_{\alpha\beta} - {}_{(\ell)}\kappa^{0}_{\alpha\beta}, \tag{13.36}
$$

where the spatial director (non-symmetric) metric ${}_{(\ell)}\kappa_{\alpha\beta}$ for layer (ℓ) is defined as

$$
{}_{(\ell)}\kappa_{\alpha\beta} := {}_{(\ell)}\boldsymbol{a}_{\alpha} \cdot {}_{(\ell)}\boldsymbol{t}_{,\beta}, \tag{13.37}
$$

and reference director (non-symmetric) metric ${}_{(\ell)}\kappa^{0}_{\alpha\beta}$ for layer (ℓ) is defined as

$$
{}_{(\ell)}\kappa^{0}_{\alpha\beta} := {}_{(\ell)}\boldsymbol{A}_{\alpha} \cdot {}_{(\ell)}\boldsymbol{t}_{0,\beta}. \tag{13.38}
$$

The components of the transverse shear strain ${}_{(\ell)}\boldsymbol{\delta}_\alpha$ are given by

$$ {}_{(\ell)}\delta_\alpha \equiv {}_{(\ell)}\gamma_\alpha - {}_{(\ell)}\gamma^0_\alpha , \tag{13.39} $$

where

$$ {}_{(\ell)}\gamma_\alpha = {}_{(\ell)}\boldsymbol{a}_\alpha \bullet {}_{(\ell)}\boldsymbol{t} , \quad {}_{(\ell)}\gamma^0_\alpha = {}_{(\ell)}\mathbf{A}_\alpha \bullet {}_{(\ell)}\boldsymbol{t}_0 , \tag{13.40} $$

which are measures of how much the director ${}_{(\ell)}\boldsymbol{t}$ and the director ${}_{(\ell)}\boldsymbol{t}_0$ depart from the normal to the neutral surfaces in the spatial configuration and in the reference configuration, respectively.

We have the following relations between the spatial basis ${}_{(\ell)}\boldsymbol{a}_\beta$ and their basis ${}_{(\ell)}\boldsymbol{a}^\alpha$:

$$ {}_{(\ell)}\boldsymbol{a}^\alpha = {}_{(\ell)}a^{\alpha\beta}\, {}_{(\ell)}\boldsymbol{a}_\beta , \quad {}_{(\ell)}a^{\alpha\beta} = {}_{(\ell)}\boldsymbol{a}^\alpha \bullet {}_{(\ell)}\boldsymbol{a}^\beta , \quad {}_{(\ell)}a^{\alpha\gamma} \bullet {}_{(\ell)}a_{\beta\gamma} = \delta^\alpha_\beta . \tag{13.41} $$

From (13.35), (13.37) and (13.40), we have the following time rate

$$ {}_{(\ell)}\dot{a}_{\alpha\beta} = {}_{(\ell)}\dot{\boldsymbol{a}}_\alpha \bullet {}_{(\ell)}\boldsymbol{a}_\beta + {}_{(\ell)}\boldsymbol{a}_\alpha \bullet {}_{(\ell)}\dot{\boldsymbol{a}}_\beta , \tag{13.42} $$

$$ {}_{(\ell)}\dot{\kappa}_{\alpha\beta} = {}_{(\ell)}\dot{\boldsymbol{a}}_\alpha \bullet {}_{(\ell)}\boldsymbol{t}_{,\beta} + {}_{(\ell)}\boldsymbol{a}_\alpha \bullet {}_{(\ell)}\dot{\boldsymbol{t}}_{,\beta} , \tag{13.43} $$

$$ {}_{(\ell)}\dot{\gamma}_\alpha = {}_{(\ell)}\dot{\boldsymbol{a}}_\alpha \bullet {}_{(\ell)}\boldsymbol{t} + {}_{(\ell)}\boldsymbol{a}_\alpha \bullet {}_{(\ell)}\dot{\boldsymbol{t}} . \tag{13.44} $$

Relation (13.42)–(13.44) play an important role in the development of the expression of the contact stress power and to identify the conjugate strain measures.

To this end, substitute (13.15), (13.16), and (13.27) into the integrand ${}_{(\ell)}I$ of the stress power $\mathcal{P}_c$ in (11.11) to arrive at

$$ \begin{aligned} {}_{(\ell)}I &= {}_{(\ell)}\boldsymbol{n}^\alpha \bullet {}_{(\ell)}\dot{\boldsymbol{\varphi}}_{,\alpha} + {}_{(\ell)}\widetilde{\boldsymbol{m}}^\alpha \bullet {}_{(\ell)}\dot{\boldsymbol{t}}_{,\alpha} + {}_{(\ell)}\boldsymbol{\ell} \bullet {}_{(\ell)}\dot{\boldsymbol{t}} \\ &= \underbrace{\left({}_{(\ell)}n^{\alpha\beta}\; {}_{(\ell)}\boldsymbol{a}_\beta + {}_{(\ell)}q^\alpha\; {}_{(\ell)}\boldsymbol{t} \right) \bullet {}_{(\ell)}\dot{\boldsymbol{a}}_\alpha}_{[1]} + \left(\underbrace{{}_{(\ell)}\widetilde{m}^{\alpha\beta}\; {}_{(\ell)}\boldsymbol{a}_\beta}_{[2a]} + \underbrace{{}_{(\ell)}\widetilde{m}^{\alpha 3}\; {}_{(\ell)}\boldsymbol{t}}_{[2b]} \right) \bullet {}_{(\ell)}\dot{\boldsymbol{t}}_{,\alpha} \\ &\quad + \left(\underbrace{{}_{(\ell)}\widetilde{q}^\alpha\; {}_{(\ell)}\boldsymbol{a}_\alpha + {}_{(\ell)}\lambda^\alpha_{.\mu}\; {}_{(\ell)}\widetilde{m}^{\mu 3}\; {}_{(\ell)}\boldsymbol{a}_\alpha}_{[3a]} + \underbrace{{}_{(\ell)}\lambda\; {}_{(\ell)}\boldsymbol{t}}_{[3b]} \right) \bullet {}_{(\ell)}\dot{\boldsymbol{t}} \end{aligned} \tag{13.45} $$

Next, using $(13.21)_2$ and (13.26) in part [1] of (13.45), (13.43) in part [2a] of (13.45), and $(13.13)_2$ in part [3b] of (13.45), we can rewrite ${}_{(\ell)}I$ as follows

$$
\begin{aligned}
{}_{(\ell)}I \;=\; & \left(\underbrace{{}_{(\ell)}\tilde{n}^{\alpha\beta}}_{[1a]} + \underbrace{{}_{(\ell)}\lambda^{\beta}_{\cdot\mu}\;{}_{(\ell)}\widetilde{m}^{\mu\alpha}}_{[1b]} \right) {}_{(\ell)}\boldsymbol{a}_{\beta} \cdot {}_{(\ell)}\dot{\boldsymbol{a}}_{\alpha} + \left(\underbrace{{}_{(\ell)}\tilde{q}^{\alpha}}_{[2a]} + \underbrace{{}_{(\ell)}\lambda^{3}_{\cdot\mu}\;{}_{(\ell)}\widetilde{m}^{\mu\alpha}}_{[2b]} \right) {}_{(\ell)}\boldsymbol{t} \cdot {}_{(\ell)}\dot{\boldsymbol{a}}_{\alpha} \\
& + {}_{(\ell)}\widetilde{m}^{\alpha\beta} \left({}_{(\ell)}\dot{\kappa}_{\alpha\beta} \underbrace{- {}_{(\ell)}\dot{\boldsymbol{a}}_{\beta} \cdot {}_{(\ell)}\boldsymbol{t}_{,\alpha}}_{[3]} \right) - \underbrace{{}_{(\ell)}\widetilde{m}^{\alpha 3}\;{}_{(\ell)}\boldsymbol{t}_{,\alpha} \cdot {}_{(\ell)}\dot{\boldsymbol{t}}}_{[4]} \\
& + \left(\underbrace{{}_{(\ell)}\tilde{q}^{\alpha}}_{[5a]} + \underbrace{{}_{(\ell)}\lambda^{\alpha}_{\cdot\mu}\;{}_{(\ell)}\widetilde{m}^{\mu 3}}_{[5b]} \right) {}_{(\ell)}\boldsymbol{a}_{\alpha} \cdot {}_{(\ell)}\dot{\boldsymbol{t}} \qquad (13.46)
\end{aligned}
$$

By the symmetry of ${}_{(\ell)}\boldsymbol{n}^{\alpha\beta}$ as expressed in (13.22) and by definition (13.42) of ${}_{(\ell)}\dot{a}_{\alpha\beta}$, part $[1a]$ of (13.46) can be written as

$$
{}_{(\ell)}\tilde{n}^{\alpha\beta}\;{}_{(\ell)}\boldsymbol{a}_{\beta} \cdot {}_{(\ell)}\dot{\boldsymbol{a}}_{\alpha} = \frac{1}{2}\,{}_{(\ell)}\tilde{n}^{\alpha\beta} \left[{}_{(\ell)}\dot{\boldsymbol{a}}_{\alpha} \cdot {}_{(\ell)}\boldsymbol{a}_{\beta} + {}_{(\ell)}\boldsymbol{a}_{\alpha} \cdot {}_{(\ell)}\dot{\boldsymbol{a}}_{\beta} \right] = \frac{1}{2}\,{}_{(\ell)}\tilde{n}^{\alpha\beta}\;{}_{(\ell)}\dot{a}_{\alpha\beta} \qquad (13.47)
$$

part $[2a]$ and $[5a]$ of (13.46) can be combined to yield

$$
{}_{(\ell)}\tilde{q}^{\alpha} \left({}_{(\ell)}\dot{\boldsymbol{a}}_{\alpha} \cdot {}_{(\ell)}\boldsymbol{t} + {}_{(\ell)}\boldsymbol{t} \cdot {}_{(\ell)}\dot{\boldsymbol{a}}_{\alpha} \right) = {}_{(\ell)}\tilde{q}^{\alpha}\;{}_{(\ell)}\dot{\gamma}_{\alpha}\,, \qquad (13.48)
$$

by virtue of definition (13.44) of ${}_{(\ell)}\dot{\gamma}_{\alpha}$. part $[1b]$ and $[2b]$ of (13.46) are combined to yield

$$
{}_{(\ell)}\widetilde{m}^{\mu\alpha}\;{}_{(\ell)}\dot{\boldsymbol{a}}_{\alpha} \cdot \left({}_{(\ell)}\lambda^{\beta}_{\cdot\mu}\;{}_{(\ell)}\boldsymbol{a}_{\beta} + {}_{(\ell)}\lambda^{3}_{\cdot\mu}\;{}_{(\ell)}\boldsymbol{t} \right) = {}_{(\ell)}\widetilde{m}^{\mu\alpha}\;{}_{(\ell)}\dot{\boldsymbol{a}}_{\alpha} \cdot {}_{(\ell)}\boldsymbol{t}_{,\mu}\,, \qquad (13.49)
$$

by virtue of (13.12). Clearly, (13.49) cancels part [3] in (13.46); thus parts $[1b]$, $[2b]$, and [3] in (13.46) cancel each other. With the aid of (13.12), and $(13.13)_2$, part [4] in (13.46) can be written as

$$
{}_{(\ell)}\widetilde{m}^{\alpha 3}\;{}_{(\ell)}\dot{\boldsymbol{t}} \cdot \left({}_{(\ell)}\lambda^{\mu}_{\cdot\alpha}\;{}_{(\ell)}\boldsymbol{a}_{\mu} + {}_{(\ell)}\lambda^{3}_{\cdot\alpha}\;{}_{(\ell)}\boldsymbol{t} \right) = {}_{(\ell)}\lambda^{\alpha}_{\cdot\mu}\;{}_{(\ell)}\widetilde{m}^{\mu 3}\;{}_{(\ell)}\boldsymbol{a}_{\alpha} \cdot {}_{(\ell)}\dot{\boldsymbol{t}}\,, \qquad (13.50)
$$

which cancels part $[5b]$ of (13.46); thus parts [4] and $[5b]$ in (13.46) cancels each other. Finally, using (13.47) and (13.48) in expression (13.46) for ${}_{(\ell)}I$, the stress power $\mathcal{P}_c$ in (11.11) of geometrically-exact sandwich shells can now be written as

$$
\mathcal{P}_c \;=\; \sum_{\ell=-1}^{1} \int_{\mathcal{A}} \left[\frac{1}{2}\,{}_{(\ell)}\tilde{n}^{\beta\alpha}\;{}_{(\ell)}\dot{a}_{\alpha\beta} + {}_{(\ell)}\widetilde{m}^{\beta\alpha}\;{}_{(\ell)}\dot{\kappa}_{\alpha\beta} + {}_{(\ell)}\tilde{q}^{\alpha}\;{}_{(\ell)}\dot{\gamma}_{\alpha} \right] d\mathcal{A}. \qquad (13.51)
$$

For layer (ℓ), we employ the constitutive relations

$$ {}_{(\ell)}\widetilde{n}^{\alpha\beta} = \frac{{}_{(\ell)}E\ {}_{(\ell)}H}{1-\left({}_{(\ell)}\nu\right)^2}\,{}_{(\ell)}H^{\beta\alpha\gamma\delta}\ {}_{(\ell)}\epsilon_{\gamma\delta}\,, \tag{13.52} $$

$$ {}_{(\ell)}\widetilde{m}^{\alpha\beta} = \frac{{}_{(\ell)}E\,\left({}_{(\ell)}H\right)^3}{12\left[1-\left({}_{(\ell)}\nu\right)^2\right]}\,{}_{(\ell)}H^{\beta\alpha\gamma\delta}\ {}_{(\ell)}\rho_{\gamma\delta}\,, \tag{13.53} $$

$$ {}_{(\ell)}\widetilde{q}^{\alpha} = K\,{}_{(\ell)}G\ {}_{(\ell)}H\ {}_{(\ell)}A^{\alpha\beta}\ {}_{(\ell)}\delta_{\beta}\,, \tag{13.54} $$

where

$$ {}_{(\ell)}H := {}_{(\ell)}h^{+} + {}_{(\ell)}h^{-}, \qquad {}_{(\ell)}A^{\alpha\beta} := {}_{(\ell)}\boldsymbol{A}^{\alpha}\cdot{}_{(\ell)}\boldsymbol{A}^{\beta} \tag{13.55} $$

is the total thickness of layer (ℓ), and the dual metric tensor of layer (ℓ) in the reference configuration. Wheras ${}_{(\ell)}E$, ${}_{(\ell)}G$, ${}_{(\ell)}\nu$ are the Youngs' modulus, shear modulus and Poisson's ratio for layer (ℓ), respectively. And K is the shear correction coefficient, when $K=\frac{5}{6}$, (13.54) is the same as that given in Naghdi [1972, p.587]. The elastic constant ${}_{(\ell)}H^{\beta\alpha\gamma\delta}$ given as follows

$$ {}_{(\ell)}H^{\beta\alpha\gamma\delta} = {}_{(\ell)}\nu\ {}_{(\ell)}A^{\beta\alpha}\ {}_{(\ell)}A^{\gamma\delta} + \frac{1}{2}\left(1-{}_{(\ell)}\nu\right)\left({}_{(\ell)}A^{\beta\gamma}\ {}_{(\ell)}A^{\alpha\delta} + {}_{(\ell)}A^{\beta\delta}\ {}_{(\ell)}A^{\alpha\gamma}\right), \tag{13.56} $$

is a fourth order elasticity tensor.

CHAPTER 14
CLOSURE

A new theory of geometrically-exact multilayer beams/1-D plates has been presented. In addition to the general fully nonlinear theory, we derive several particular cases, with restrictive assumptions, but with important applications. The case of infinitesimal outer layer rotations superposed onto the finite core layer rotation is of practical importance. The classical linear theory of Yu [1959*a*] is shown to be yet another more particular case. The theory can be applied to a wide class of problems involving multilayer structures undergoing large deformation and/or large overall motion. We have successfully formulated a Galerkin projection of the equations developed herein; this formulation and the numerical results are also presented. As mentioned in the introduction, the present formulation is not restricted to multilayer structures having three layers, but the number of layers can vary between one and three. Further the lengths of the layers need not be equal as in multilayer structures with ply drop-off. The analysis of the important class of structures with variable number of layers and with ply drop-off is discussed in detail here. Examples involving large deformation and large overall motion of sandwich beams, in both static and dynamic cases, have been presented. In the static case, we have presented the roll-up maneuver and the bifurcation phenomenon of sandwich beams with three identical layers, the Saint-Venant principle have also been demonstrated at the tip of the short sandwich beams. In the dynamic case, free vibration of a sandwich frame with ply drop-offs, free flight of sandwich beams, large angle maneuver of sandwich beams have been presented.

In the second part of this dissertation, we have presented a detailed development of the dynamics of the geometrically-exact sandwich shell theory obtained by reduction of the general three-dimensional continuum mechanics theory by means of the one inextensible director assumption, and by using the balance of power of the sandwich shell. The fully nonlinear equations of motion is subsequently linearized systematically, based on the small deformation assumption. In particular, for the symmetric sandwich plate, the linearized equations can be reduced exactly to the classical results as given in Yu [1959*a*]. The equations of motion can also be reduced exactly to the equations of motion for sandwich beams presented in Vu-Quoc and Ebcioğlu [1995], for which the numerical justification is given in Vu-Quoc and Deng [1995*b*]. Our future work will be concentrated on the weak form and the finite element implementation of the equations of motion herein.

REFERENCES

Alberts, T. E. [1993], Dynamic analysis to evaluate viscoelastic passive damping augmentation for the space shuttle remote manipulator system, *ASME Journal of Dynamic Systems, Measurements, and Control* **114**, 468–475.

Bathe, K. J. [1996], *Finite Element Procedures*, Prentice Hall, Englewood Cliffs, New Jersey.

Chadwick, P. [1976], *Continuum Mechanics*, John Wiley & Sons, New York.

Chia, C. [1988], Geometrically nonlinear behavior of composite plates: A review, *Applied Mechanics Review* **41**, 439–450.

Crampin, M. and Pirani, F. [1988], *Applicable Differential Geometry*, Cambridge University Press, New York.

Dökmeci, M. C. [1990], Shell theory for vibrations of piezoceramics under a bias, *IEEE Transactions on Ultrasonics, Ferroelectrics, and Frequency Control* **37**(5), 369–385.

Dubbelday, P. S. [1993], Constrained-layer damping analysis for extensional waves in infinite, fluid-loaded plates, *The Journal of the Acoustical Society of America* **93**, 1927–1935.

Edwards, K. [1991], Sandwich structures, *Engineering* **231**, 37–38.

Evseichik, Y. B. [1989], Equations of vibrations of multilayer piezoceramic shells with tangential polarization, *Soviet Applied Mechanics* **24**(8), 758–763.

Green, A. E. and Naghdi, P. M. [1982], A theory of laminated composite plates, *IMA Journal of Applied Mathematics* **29**, 1–23.

Green, A. E. and Zerna, W. [1968], *Theoretical Elasticity*, Dover Publications, New York.

Heuer, R. [1992], Static and dynamic analysis of transversely isotropic, moderately thick sandwich beams by analogy, *Acta Mechanica* **91**, 1–9.

Hughes, T. J. R. [1987], *The Finite Element Method*, Prentice Hall, New Jersey.

Kamman, J. W. and Huston, R. L. [1984], Dynamics of constrained multibody systems, *ASME Journal of Applied Mechanics* **51**, 889–903.

Kane, T. R., Ryan, R. R. and Bamerjee, A. K. [1987], Dynamics of a cantilever beam attached to a moving base, *AIAA Journal of Guidance, Control, and Dynamics* **10**, 139–151.

Kollmann, F. G. and Hackenberg, H. P. [1993], On the algebra of two-point tensors on manifolds with applications in nonlinear solid mechanics, *Zeitschrift fuer Angewandte Mathematik und Mechanik* **73**(11), 307–314.

Lakes, R. S. [1987], Negative Poisson's ratio materials, *Science* **238**, 551.

Lakes, R. S. and Elms, K. [1993], Indentability of conventional and negative Poisson's ratio foams, *Journal of Composite Materials* **27**(12), 1193–1202.

Lee, C. K. [1990], Theory of laminated piezoelectric plates for the design of distributed sensors/actuators. Part I: Governing equations and reciprocal relationships, *The Journal of the Acoustical Society of America* **87**(3), 1144–1158.

Malvern, L. E. [1969], *Introduction to the Mechanics of a Continuous Medium*, Prentice-Hall, Inc., Englewood Cliffs, New Jersey.

Mantena, P. R. [1991], Optimal constrained viscoelastic tape lengths for maximizing damping in laminated composites, *AIAA Journal* **29**, 1678–1685.

Marsden, J. E. and Hughes, T. J. R. [1983], *Mathematical Foundations of Elasticity*, Prentice Hall, Englewood Cliffs, New Jersey.

Milgrom, M. [1989], A layered-shell model of isotropic composites and exact expressions for the effective properties, *ASME Journal of Applied Mechanics* **66**, 3429–36.

Motovilovets, I. A. [1985], Thermomechanical behavior of multilayered piezoceramic shells with harmonic excitation, *Soviet Applied Mechanics* **21**(7), 661–666.

Naghdi, P. M. [1972], The theory of shells and plates, *in* C. Truesdell, ed., Mechanics of Solids, *Vol.II*, Springer-Verlag, New York, pp. 425–640.

Noor, A. K. and Burton, W. S. [1989], Assessment of shear deformation for multilayered composite plates, *Applied Mechanics Reviews* **42**(1), 1–12.

Noor, A. K., Burton, W. S. and Bert, C. W. [1996], Computational models for sandwich panels and shells, *Applied Mechanics Reviews* **49**(3), 155–199.

Plantema, J. [1966], *Sandwich Construction*, John Wiley & Sons, Inc., New York.

Rao, M. D. [1993], Dynamic analysis and design of laminated composite beams with multiple damping layers, *AIAA Journal* **31**(4), 736–745.

Rao, V. S., Sankar, B. and Sun, C. [1992], Constrained layer damping of initially stressed composite beams using finite elements, *Journal of Composite Materials* **26**(12), 1752–1766.

Reddy, J. [1989], On the generalization of displacement-based laminate theories, *Applied Mechanics Reviews* **42**(11), S213–222. Supplement.

Sayir, M. and Koller, M. G. [1986], Dynamic behaviour of sandwich plates, *Zeitschrift für Angewandte Mathematik und Physik (ZAMP Journal of Applied Mathematics and Physics)* **37**(1), 78–103.

Schreffler, R. [1993], Quiet!!! Japanese automakers increase their use of vibration damping steel, *Automotive Industries* **173**, 19.

Sigmund, O. [1994], 'Materials with prescribed constitutive parameters: An inverse homogenization problem', Talk at the SIAM Conference on *Emerging Issues in Mathematics and Computation from the Materials Sciences*, Pittsburgh, 18-20 April 1994.

Simo, J. C. [1985], A finite strain beam formulation. the three dimensional dynamic problem. Part I, *Computer Methods in Applied Mechanics and Engineering* **49**, 55–70.

Simo, J. C. and Fox, D. D. [1989], On a stress resultant geometrically exact shell model. Part I: Formulation and optimal parametrization, *Computer Methods in Applied Mechanics and Engineering* **72**, 267–304.

Simo, J. C. and Vu-Quoc, L. [1986*a*], On the dynamics of flexible beams under large overall motions—The plane case: Part I, *ASME Journal of Applied Mechanics* **53**(4), 849–854.

Simo, J. C. and Vu-Quoc, L. [1986*b*], On the dynamics of flexible beams under large overall motions—The plane case: Part II, *ASME Journal of Applied Mechanics* **53**(4), 855–863.

Simo, J. C. and Vu-Quoc, L. [1986*c*], A three-dimensional finite-strain rod model. Part II: Computational aspects, *Computer Methods in Applied Mechanics and Engineering* **58**(1), 79–116.

Simo, J. C. and Vu-Quoc, L. [1988], On the dynamics in space of rods undergoing large motions—a geometrically-exact approach, *Computer Methods in Applied Mechanics and Engineering* **66**, 125–161.

Simo, J. C. and Vu-Quoc, L. [1991], A geometrically-exact beam model incorporating torsion shear and torsion warping deformation, *International Journal of Solids and Structures* **27**(3), 371–393.

Simo, J. C., Fox, D. D. and Rifai, M. S. [1989], On a stress resultant geometrically exact shell model. Part II: The linear theory; Computational aspects, *Computer Methods in Applied Mechanics and Engineering* **73**, 53–92.

Simo, J. C., Fox, D. D. and Rifai, M. S. [1990], On a stress resultant geometrically exact shell model. Part III: Computational aspects of the nonlinear theory, *Computer Methods in Applied Mechanics and Engineering* **79**, 21–70.

Simo, J. C., Rifai, M. S. and Fox, D. D. [1990], On a stress resultant geometrically exact shell model. Part IV: Variable thickness shells with through-the-thickness stretching, *Computer Methods in Applied Mechanics and Engineering* **81**, 91–126.

Sirkis, J. S. [1993], Unified approach to phase-strain-temperature models for smart structure interferometric optical fiber sensors: Applications, *Optical Engineering* **32**, 762–773.

Thompson, B. S. [1987], Composite laminate components for robotic and machine systems: Research issues in design, *Applied Mechanics Review* **40**(11), 1545–1552.

Thompson, B. S. and Sung, C. K. [1986], An analytical and experimental investigation of high-speed mechanisms fabricated with composite laminates, *Journal of Sound and Vibration* **111**(3), 399–428.

Toledano, A. and Murakami, H. [1987], A composite plate theory for arbitrary laminate configurations, *ASME Journal of Applied Mechanics* **54**, 181–189.

Tzou, H. S. [1989], Theoretical analysis of a multi-layered thin shell coupled with piezoelectric shell actuators for distributed vibration controls, *Journal of Sound and Vibration* **132**(3), 433–450.

Vu-Quoc, L. [1986], *Dynamics of Flexible Structures Performing Large Overall Motions: A Geometrically-Nonlinear Approach*, PhD thesis, University of California at Berkeley, Berkeley, CA.

Vu-Quoc, L. [1990*a*], *Lecture notes on geometrically-exact shell theory*, University of Florida, Gainesville, FL 32511, USA.

Vu-Quoc, L. [1990*b*], A perturbation method for dynamic analysis using under-integrated shell elements, *Computer Methods in Applied Mechanics and Engineering* **79**, 129–172.

Vu-Quoc, L. and Deng, H. [1995*a*], Dynamics of geometrically-exact multilayer beams: Computational aspects, *Computer Methods in Applied Mechanics and Engineering*. Accepted.

Vu-Quoc, L. and Deng, H. [1995*b*], Galerkin projection for geometrically-exact multilayer beams allowing for ply drop-off, *ASME Journal of Applied Mechanics* **62**, 479–488.

Vu-Quoc, L. and Deng, H. [1995*c*], Geometrically-exact multilayer shells: Computational aspects, *Computer Methods in Applied Mechanics and Engineering*. To be submitted.

Vu-Quoc, L. and Ebcioğlu, I. K. [1995], Dynamic formulation for geometrically-exact sandwich beams and 1-D plates, *ASME Journal of Applied Mechanics* **62**, 756–763.

Vu-Quoc, L. and Ebcioğlu, I. K. [1996], General multilayer geometrically-exact beams/1-D plates with piecewise linear section deformation, *Zeitschrift für Angewandte Mathematik und Mechanik (ZAMM)* **76**(7), 391–409.

Vu-Quoc, L. and Li, S. [1995], Dynamics of sliding geometrically-exact beams: Large angle maneuver and parametric resonance, *Computer Methods in Applied Mechanics and Engineering* **120**(1–2), 65–118.

Vu-Quoc, L. and Mora, J. [1989], A class of simple and efficient degenerated shell elements—analysis of global spurious-mode filtering, *Computer Methods in Applied Mechanics and Engineering* **74**, 117–175.

Yu, Y. Y. [1959*a*], *A new theory of sandwich plates—General case*, Technical Report Contract AF49(638)–455, Air Force Office of Scientific Research .

Yu, Y. Y. [1959*b*], Simple thickness-shear modes of vibration of infinite sandwich plates, *ASME Journal of Applied Mechanics* **26**, 679–681.

Yu, Y. Y. [1989], Dynamics and vibration of layered plates and shells—A perspective from sandwiches to laminated composites, in *AIAA/ASCE/AHS/ASC 30th Structures, Structural Dynamics, and Materials Conference, Mobile, Alabama*, Vol. 4.

Zienkiewicz, O. C. and Taylor, R. L. [1989], *The Finite Element Method. Volume 1: Basic Formulation and Linear Problems*, 4th edn, McGraw-Hill, New York.

Zinno, R. and Barbero, E. J. [1994], A three-dimensional layer-wise constant shear element for general anisotropic shell-type structures, *International Journal for Numerical Methods in Engineering* **37**(14), 2445.

BIOGRAPHICAL SKETCH

Hui Deng was born on June 10, 1964, in Dandong, Liaoning Province, China. He received his secondary education at the Second High school in Dandong, Liaoning, China in July, 1982. After that he entered Beijing University and earned his Bachelor of Science in July, 1986 and Master of Science in July, 1989, from the Department of Mechanics. He came to the Department of Aerospace Engineering, Mechanics and Engineering Science at the University of Florida to pursue his Ph.D degree in January in 1993.

I certify that I have read this study and that in my opinion it conforms to acceptable standards of scholarly presentation and is fully adequate, in scope and quality, as a dissertation for the degree of Doctor of Philosophy.

Vu Quoc Loc

Loc Vu-Quoc, Chairman
Associate Professor of Aerospace Engineering,
Mechanics, and Engineering Science

I certify that I have read this study and that in my opinion it conforms to acceptable standards of scholarly presentation and is fully adequate, in scope and quality, as a dissertation for the degree of Doctor of Philosophy.

Ibrahim K. Ebcioglu

Ibrahim K. Ebcioglu
Professor of Aerospace Engineering,
Mechanics, and Engineering Science

I certify that I have read this study and that in my opinion it conforms to acceptable standards of scholarly presentation and is fully adequate, in scope and quality, as a dissertation for the degree of Doctor of Philosophy.

Nicolaie D. Cristescu
Graduate Research Professor of
Aerospace Engineering,
Mechanics, and Engineering Science

I certify that I have read this study and that in my opinion it conforms to acceptable standards of scholarly presentation and is fully adequate, in scope and quality, as a dissertation for the degree of Doctor of Philosophy.

B Sankar

Bhavani V. Sankar
Professor of Aerospace Engineering,
Mechanics, and Engineering Science

I certify that I have read this study and that in my opinion it conforms to acceptable standards of scholarly presentation and is fully adequate, in scope and quality, as a dissertation for the degree of Doctor of Philosophy.

Marc I. Hoit
Associate Professor of
Civil Engineering

This dissertation was submitted to the Graduate Faculty of the College of Engineering and to the Graduate School and was accepted as partial fulfillment of the requirements for the degree of Doctor of Philosophy.

August 1997

Winfred M. Phillips
Dean, College of Engineering

Karen A. Holbrook
Dean, Graduate School

LD
1780
1997
.D391

UNIVERSITY OF FLORIDA
3 1262 06556 6007